Solid State Structures and Transport Properties of Selenazyl Radicals

by

Craig Miles Robertson

A thesis
presented to the University of Waterloo
in fulfillment of the
thesis requirement for the degree of
Doctor of Philosophy
in
Chemistry

Waterloo, Ontario, Canada, 2008

I hereby declare that I am the sole author of this thesis. This is a true copy of the thesis, including any required final revisions, as accepted by my examiners.

I understand that my thesis may be made electronically available to the public.

Abstract

The synthetic routes to the salts of the 3*H*-naphtho[1,2-*d*][1,2,3]dithiazolylium cation and its three selenium containing variants are described. The most efficient approach involves the condensation of *bis*-acetylated aminoselenolates and aminothiolates with sulfur and selenium halides. Cyclic voltammetry experiments illustrate that the four cations can be reduced to their neutral radical state and are stable in solution. The EPR spectra of all four radicals have been recorded and the spin distributions have been compared with those obtained from DFT calculations. It has been found that the selenium containing radicals are thermally unstable at room temperature, but the all sulfur species has been isolated and characterized by X-ray crystallography. In the solid state, the radicals associate into cofacial dimers and short interdimer S---S′, S---N′ and C---H′ contacts are observed. The all-selenium species has been characterized in its oxidized state by X-ray crystallography.

A series of four challenging crystallographic projects are presented. (1) 8-Phenyl-4-methyl-4*H*-*bis*[1,2,3]thiaselenazolo[4,5-*b*:5′,4′-*e*]pyridinyl has been prepared and its solid-state structure determined by powder X-ray diffraction methods. The radical crystallizes in the space group $P3_121$ and is isostructural with its ethylated derivative and its all-sulfur containing analogue. Variable-temperature magnetic measurements confirm that the radical is an undimerized $S = ½$ system with weak intermolecular antiferromagnetic coupling. Pressed pellet variable-temperature electrical conductivity measurements provide a room-temperature conductivity (σ_{RT}) of 3.3×10^{-5} S cm^{-1} and an activation energy (E_{act}) of 0.29 eV. The results of Extended Hückel Theory (EHT) band structure calculations are presented. (2) Single-crystal and powder X-ray diffraction methods on a family of selenium-containing radicals based the 4-methyl-3*H*,4*H*-*bis*[1,2,3]dithiazolo[4,5-*b*:5′,4′-e]pyridin-3-yl radical are presented. All three radicals (SSN, SSeN and SeSeN) are isostructural, crystallizing in the space group $P2_12_12_1$, and form slipped π-stacks of undimerized radicals with close E---E′ contacts. Pressed pellet variable-temperature electrical conductivity measurements of the systems provide $\sigma_{RT} = 3 \times 10^{-4}$ and 1×10^{-3} S cm^{-1} and E_{act} of 0.24 eV and 0.17 eV for the SSeN and SeSeN radicals respectively. (3) The crystal structures of 4-methyl-4*H*-*bis*[1,2,3]dithiazolo[4,5-b:5′,4′-*e*]pyrazin-3-yl at 298 K, 123 K and 88 K are presented. At 298 K the radicals remain undimerized, crystallizing in the space group *Cmca* and forming evenly-spaced π stacks.

Upon cooling to 123 K the space group symmetry is lowered by loss of *C*-centering to *Pccn* such that the radicals are not evenly spaced within the π-stack. At 88 K a further lowering of space group symmetry to $P2_1/c$ is observed. (4) [1,3,2]Dithiazolo[4,5-*b*]pyridin-2-yl is polymorphic, crystallizing in $P2_1$ and $P2_1/n$. A non-merohedral twin law is required to model the $P2_1$ system. The structures of both crystals are comprised of layers of head-to-head π dimers and the two structures differ in the orientation of the π dimers along the stacks. Variable-temperature magnetic data reveal that both phases are essentially diamagnetic at low temperatures and form weak π dimers at higher temperatures.

Synthetic methods have been developed to generate the complete series of resonance stabilized heterocyclic thia/selenazyl radicals based on 8-chloro-4-ethyl-4*H*-*bis*[1,2,3]dithiazolo[4,5-*b*:5′,4′-e]pyridin-3-yl. X-ray crystallographic studies confirm that all four radicals are isostructural, belonging to the tetragonal space group $P\bar{4}2_1m$. The crystal structures consist of slipped π-stack arrays of undimerized radicals. Variable temperature conductivity measurements reveal an increase in conductivity with increasing selenium content, with σ_{RT} reaching a maximum of 3.0×10^{-4} S cm^{-1} with an E_{act} of 0.19 eV for the all-selenium containing variant. Variable temperature magnetic susceptibility measurements indicate that all four radicals exhibit $S = \frac{1}{2}$ Curie-Weiss behaviour over the temperature range 20 - 300 K. At lower temperatures, the three selenium-based radicals display magnetic ordering. The first radical with selenium positioned at the E_1 site, undergoes a phase transition at 14 K to a weakly spin-canted ($\phi = 0.010°$) antiferromagnetic state. By contrast, the radical containing the apical selenium and the all-selenium variant, which both possess selenium in the E_2 position, order ferromagnetically, with Curie temperatures (T_c) = 12.8 K and 17.0 K respectively and coercive fields H_c at 2 K of 250 Oe and 1370 Oe respectively. The transport properties of the entire series of radicals are discussed in the light of EHT band-structure calculations.

A series of *bis*-thiaselenazolyl radicals (R_2BPTSR_1) based on the *bis*-[1,2,3]-thiaselenazolo[4,5-b:5',4'-*e*]pyridin-3-yl (R_1 = Et, Pr and CF_3CH_2, R_2 = Cl; R_1 = Et, R_2 = Me and Br) have been prepared and characterized by X-ray crystallography. The radicals are formally isostructural, all belonging to the tetragonal space group $P\bar{4}2_1m$. The crystal structures consist of slipped π-stack arrays of undimerized radicals packed about $\bar{4}$ centers. Variations in R_1 (Et, Pr, CF_3CH_2) with R_2 = Cl lead to significant changes in the degree of slippage of the π-stacks and hence the proximity of the Se---Se′ contacts.

By contrast, variations in R_2 (Cl, Br, Me) with R_1 = Et induce very little change in either the slippage angle or the Se---Se′ contacts. Variable temperature conductivity measurements show relatively constant values for σ_{RT} (10^{-5} - 10^{-4} S cm^{-1}) and E_{act} (0.27 - 0.31 eV) across the entire series. Variable temperature magnetic susceptibility measurements indicate major differences in the magnetic behaviour. Radicals with R_1 = Pr, CH_2CF_3, R_2 = Cl behave as weakly antiferromagnetically coupled Curie-Weiss paramagnets, but radicals with R_1 = Et; R_2 = Cl, Me, Br demonstrate ferromagnetic ordering, with T_c values of 12.8 K (R_2 = Cl), 13.6 K (R_2 = Me), and 14.1 K (R_2 = Br).

Acknowledgments

There are many people whom I would like to thank. First and foremost, I would like to thank my supervisor Prof. Richard T. Oakley. Rich, you have been a mentor to me. I have learned so much chemistry and you have allowed me to develop my passion for X-ray crystallography. Thank you so much for your guidance, patience and friendship.

I would like to extend a sincere thank you to Dr. Leanne Beer, Dr. Jackyln Brusso, Dr. Owen Clements, Ms. Kristina Cvrkalj, Ms. Alicea Leitch, Ms. Kristen Matkovich, Dr. Daniel Myles, Dr. Robert Reed, Ms. Maarit Risto, Mr. Doug MacGregor, Ms. Lenora Sawyer and Mr Stephen Winter. It has been a pleasure working with all of you and many great friendships have been developed.

The members of my supervisory committee, Prof. Holger Kleinke, Prof. Sonny Lee and Prof. Kathryn Preuss have been very kind and helpful. Thank you for your guidance and advice.

I would like to extend a special thanks to all of our collaborators. First, Dr. Jim Britten, I wish to thank you for taking me under your wing and teaching me crystallography. You are truly a mentor. As well, thanks to Prof. A. Wallace Cordes (Arkansas), Dr. Paul Dube (McMaster), Prof. Natia Frank (Victoria), Prof. Robert Haddon (UC Riverside), Prof. John Richardson (Louisville) and Prof. Laurence Thompson. Thank you for your contributions and assistance.

I would like to thank my mother and father for all of their support throughout my university life. Mom and dad, I did it!

Finally, I wish to thank the two most important people in my life. First, my beautiful wife Barbara-Anne. Barbie, you have given me your unquestioned support through all of this. You are the most amazing person I know. Thanks so much! Without you, I could not have accomplished this! Second, I want to thank my little boy Jack, who will be turning 4 months old upon submission of this thesis. I can’t wait until the day you come to me and say “ Dad, I want to do a PhD in chemistry.” Just kidding. Go play the guitar.

Dedication

Dedicated to the two most beautiful people I know: Barbara-Anne and Jack.

Table of Contents

Chapter 3 X-ray Crystallography: Structural Problems in Dithiazolyl Materials

Chapter 4 The Isostructural *Eureka*

Chapter 5 Enhanced Conductivity and Magnetic Ordering in Isostructural Heavy-Atom Radicals

Chapter 6 Variations on a Tetragonal Theme

Appendix A

References

List of Tables

List of Captioned Figures

List of Uncaptioned Figures

Figures are numbered sequentially in each chapter. The numerical prefix in the figure label corresponds to the chapter in which the figure may be found. For example, a figure in **Chapter 2** will be assigned the prefix **2-**. The same figure may appear in multiple chapters, having the appropriate prefix.

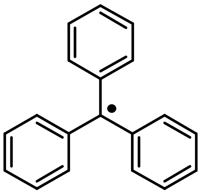

1-1

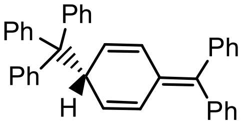

1-2

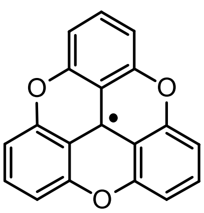

1-3

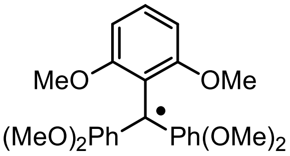

1-4

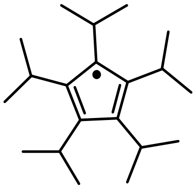

1-5

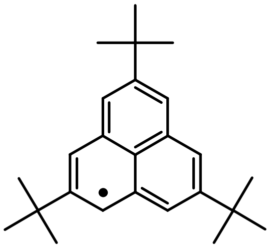

1-6

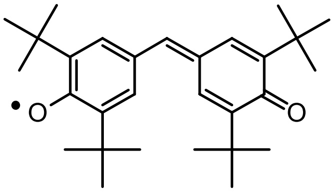

1-7

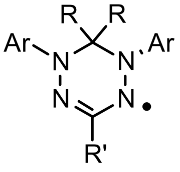

1-8

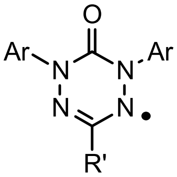

1-9

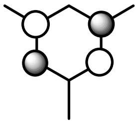

1-10a

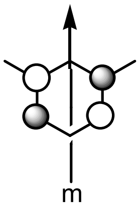

1-10b

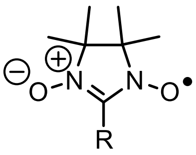

1-11

SN•

1-12

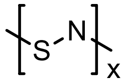

1-13

1-14

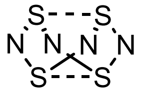

1-15

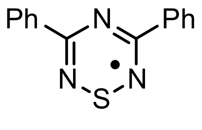

1-16

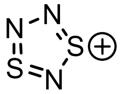

1-17

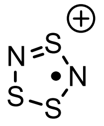

1-18

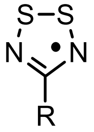

1-19

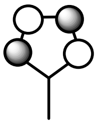

1-20

1-21

1-22

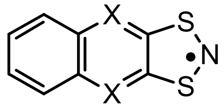

X = N, CH

1-23

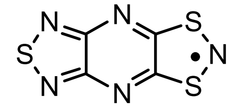

1-24

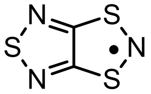

1-25

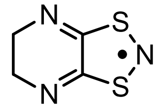

1-26

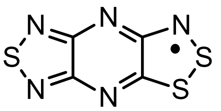

1-27

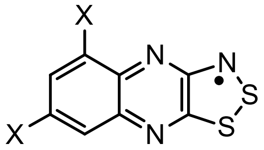

X = H, Cl

1-28

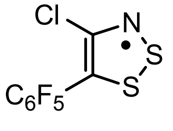

1-29

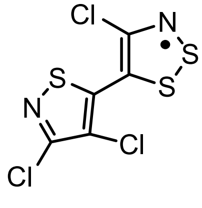

1-30

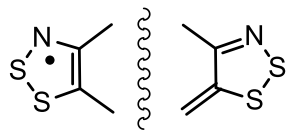

1-31

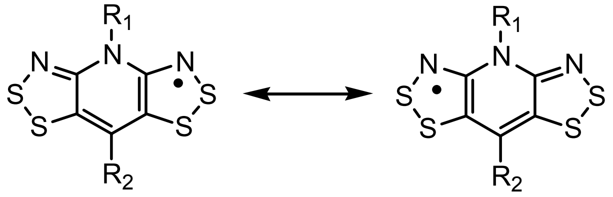

1-32

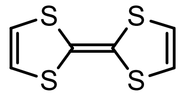

1-34

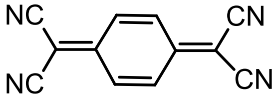

1-35

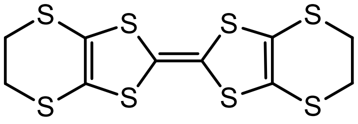

1-36

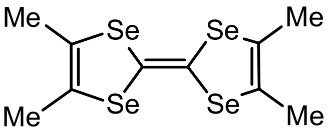

1-37

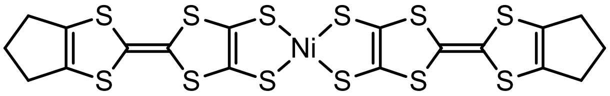

1-38

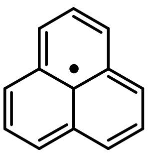

1-39

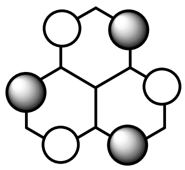

1-40

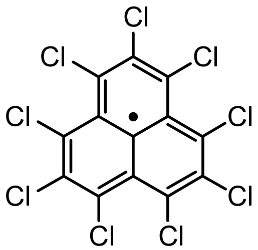

1-41

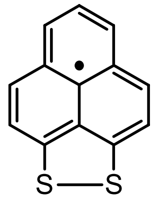

1-42

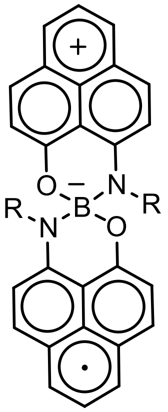

1-43

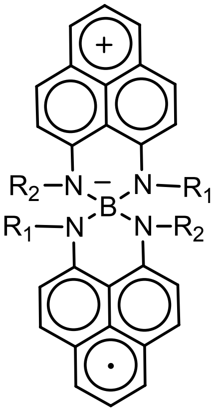

1-44

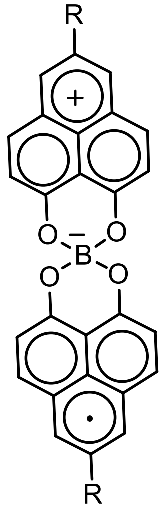

1-45

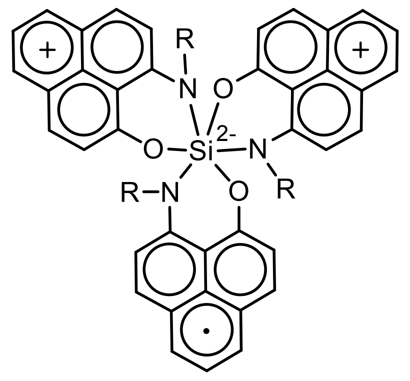

1-46

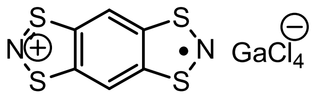

1-47

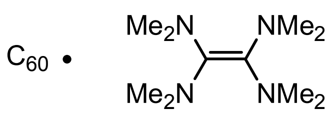

1-48

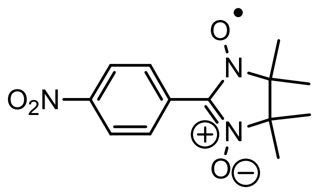

1-49

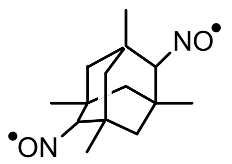

1-50

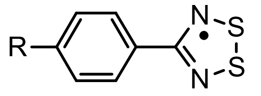

R = NO_2, FM; CN, WF

1-51

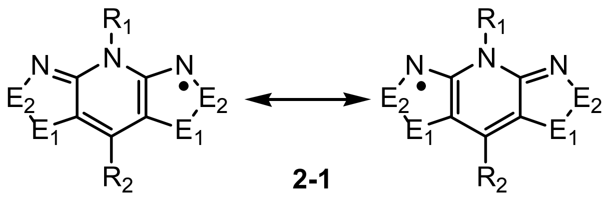

2-1

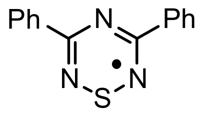

2-2

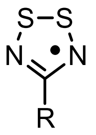

2-3

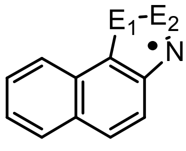

2-4

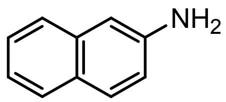

2-5

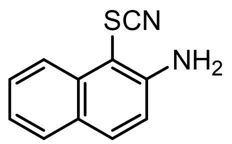

2-6

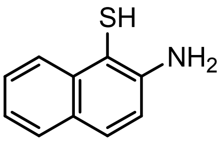

2-7

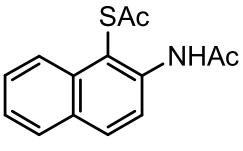

2-8

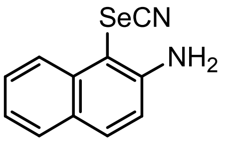

2-9

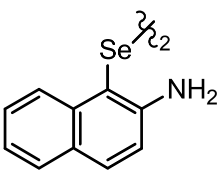

2-10

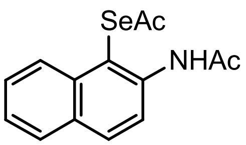

2-11

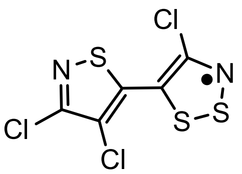

2-12

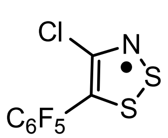

2-13

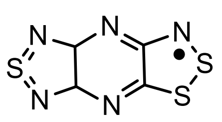

2-14

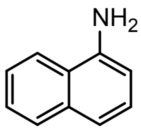

2-12

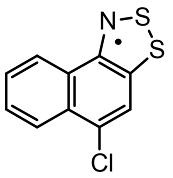

2-13

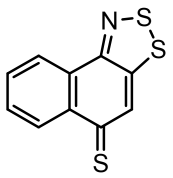

2-14

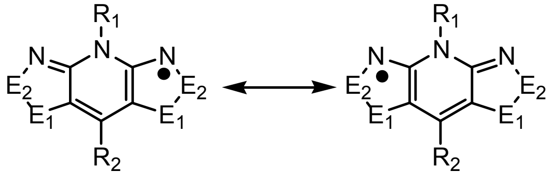

3-1

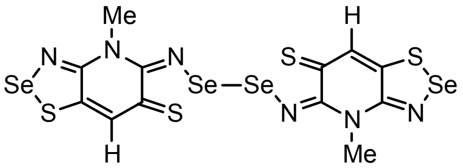

3-2

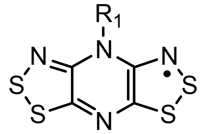

3-3

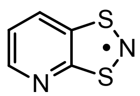

3-4

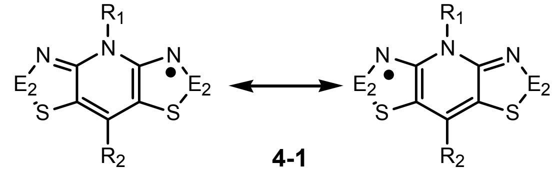

4-1

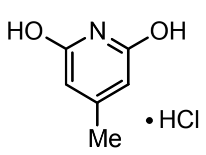

4-2

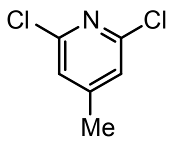

4-3

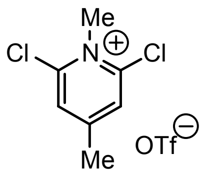

4-4

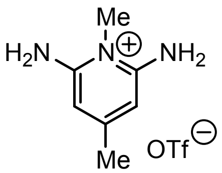

4-5

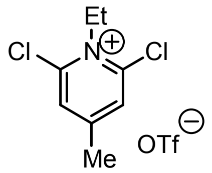

4-6

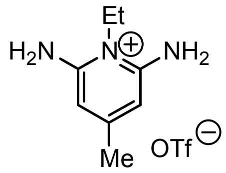

4-7

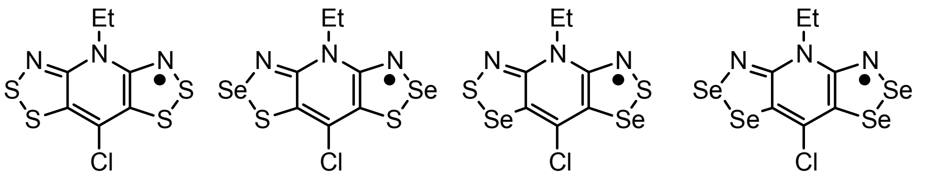

4-8

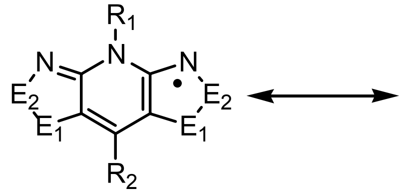

	E_1	E_2
1	S	S
2	S	Se
3	Se	S
4	Se	Se

5-1a, 5-2a, 5-3a, 5-4a: R_1 = Et, R_2 = Cl

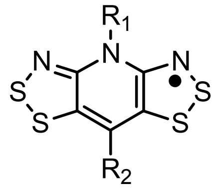

6-1

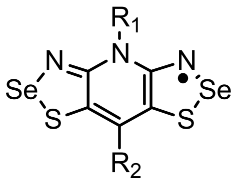

6-2

	6-2a	**6-2b**	**6-2c**	**6-2d**	**6-2e**
R_1	Et	Pr	CH_2CF_3	Et	Et
R_2	Cl	Cl	Cl	Me	Br

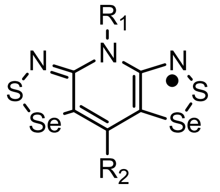

6-3

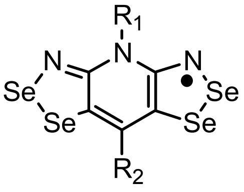

6-4

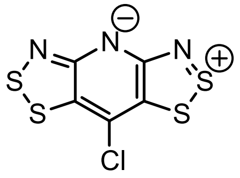

6-5

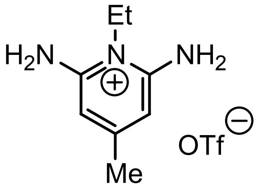

6-6

List of Abbreviations

6-31G(d,p)	a split valence plus polarization basis set
a	crystallographic unit cell axis; hyperfine coupling constatnts
*a**	reciprocal cell axis
A	acceptor
AFM	antiferromagnetism
Å	angstrom
AC	alternating current
Anal.	analysis
b	crystallographic unit cell axis
*b**	reciprocal cell axis
B3LYP	hybrid B3 including an HF exchange term and the LYP correlation functional
BEDT	*bis*(ethylenedithio)
bis-DTA	resonance-stabilized 1,2,3-dithiazolo-1,2,3-dithiazolyl pyridine framework
BPzMe	4-methyl-4*H*-*bis*[1,2,3]dithiazolo[4,5-b:5′,4′-*e*]pyrazin-3-yl
br	broad (IR peak descriptor)
C	Curie constant
ºC	degree centigrade
c	crystallographic unit cell axis
*c**	reciprocal cell axis
calcd.	calculated
cm^{-1}	reciprocal centimeters
CO	crystal orbital
Cp	cyclopentadienyl
Cp^*	pentamethyl cyclopentadienyl
CT	charge transfer
CV	cyclic voltammetry
d	doublet (NMR peak descriptor); interatomic distance

D	donor
DC	direct current
DCE	dichloroethane
DCM	dichloromethane
dec.	decomposition
deg	degrees
DFT	Density Functional Theory
DMFc	*bis*(pentamethylcyclopentadienyl)iron
1,2,3-DTA	1,2,3-dithiazolyl radical
1,3,2-DTA	1,3,2-dithiazolyl radical
DTA	dithiazolyl
1,2,3,5-DTDA	1,2,3,5-dithiadiazolyl radical
DTDA	dithiadiazolyl
E	sulfur or selenium
ΔE	change in energy
$E_{1/2}$	half-wave potential
E_a	activation energy
EA	electron affinity
E_{cell}	peak to peak potential separation
EHT	Extended Hückel Theory
EI	electron impact
emu	electromagnetic unit
E_{pa}	anodic peak potential
E_{pc}	cathodic peak potential
EPR	electron paramagnetic resonance
ET	*bis*(ethylenedithio) tetrathiafulvalene
ESI	electrospray ionization
Et	ethyl

EtOH	ethanol
eV	electron volt
f	fraction of band filled
FC	field cooled
FOM	figure of merit
FOX	Free Objects for Crystallography
fw	formula weight
FM	ferromagnetism
g	gram
g	Landé factor
^{1}H	proton
h	hour
HBPMe	4-methyl-3*H*,4*H*-*bis*[1,2,3]dithiazolo[4,5-*b*:5′,4′-e]pyridin-3-yl
H_c	coercive field
ΔH_{disp}	disproportionation enthalpy
HMFc	*bis*(trimethylcyclopentadienyl)iron
HOAc	acetic acid
HOMO	highest occupied molecular orbital
Hz	Hertz
IP	ionization potential
IR	infrared
J	exchange energy
k_B	Boltzmann constant
K	Kelvin
kHz	kilohertz
kJ	kilojoule
kOe	kiloOersted
L	litre

LT	low temperature
LUMO	lowest unoccupied molecular orbital
LW	linewidth
M	molarity
M^+	base peak (mass spectrometry)
m	minute; medium (IR peak descriptor); multiplet (NMR descriptor); mirror plane
m	mass
m/e	mass to charge ratio
min	minute
Me	methyl
MeCN	acetonitrile
MeOH	methanol
mL	millilitre
mmol	millimole
MO	molecular orbital
mol	mole
mp	melting point
M_{rem}	remanent magnetization
MS	mass spectrometry
M_{sat}	saturation magnetization
M_{sp}	spontaneous magnetization
mT	millitesla
NMR	nuclear magnetic resonance
NRC	neutral radical conductor
OAH	odd alternative hydrocarbon
Oe	Oersted
OMFc	*bis*(tetramethylcyclopentadienyl)iron
OTf	triflate anion

ORTEP	Oak Ridge Thermal Ellipsoid Plot
par.	parameters
Ph	phenyl group
PhBPTSMe	8-Phenyl-4-methyl-4*H*-*bis*[1,2,3]thiaselenazolo[4,5-*b*:5′,4′-*e*]pyridinyl
pH	measure of acidity or basicity of solution
PLY	phenalenyl radical
ppm	parts per million
PXRD	powder X-ray diffraction
PyDTA	[1,3,2]Dithiazolo[4,5-*b*]pyridin-2-yl
R	general substituent group
R	agreement index (crystallography)
R_2BPTSR_1	resonance stabilized *bis*-thiaselanazolyl framework
ref.	referenced
restr.	restraints
RIC	radical ion conductor
ROTf	alkyl triflate
R_p	agreement index- profile (crystallography)
RT	room temperature
RVB	resonance valence bond
R_w	weighted agreement index
s	strong (IR peak descriptor); singlet (NMR peak descriptor); second
S	Siemens
S	spin
SCE	saturated calomel electrode
SCF	self consistent field
SeN	selenazyl
SN	thiazyl
$(SN)_x$	polythiazene

sol.	solution
SOMO	singly occupied molecular orbital
SW	sweep width
t	triplet (NMR peak descriptor)
T	temperature
T_c	Curie temperature
TCNQ	tetracyano-*p*-diquinomethane
TDAE	tetrakisdimethyl-aminoethylene
temp	temperature
TM	transition metal
TMPDA	N,N,N′,N′-tetramethyl-*p*-phenylenediamine
$\mathrm{T_{MI}}$	metal-insulator transition
$\mathrm{T_N}$	Néel temperature
Torr	unit of pressure = mmHg = 133.32 Pa
tmdt	trimethylenetetrathiafulvalenedithiolate
TMS	trimethylsilyl group
TMTSF	tetramethyltetraselenafulvalene
TTF	1,1′,3,3′-tetrathiafulvalene
U	Coulombic barrier to charge transfer
V	Volt
V	volume
vs	very strong (IR peak descriptor)
vs	versus
vw	very weak (IR peak descriptor)
w	weak (IR peak descriptor)
W	bandwidth
wR_p	weighted agreement index - profile (powder crystallography)
X	halogen group

x	Cartesian coordinate
y	Cartesian coordinate
Z	number of asymmetric units per unit cell
z	Cartesian coordinate
ZFC	zero field cooled
$^{\circ}$	degree
α	crystallographic axis angle; coulomb parameter
β	crystallographic axis angle; resonance parameter
γ	crystallographic axis angle
δ	chemical shift in ppm; mean separation of molecules in a slipped stack
μ	absorption correction
μA	microamps
π	orbital symmetry
τ	angle between the mean plane of the heterocyclic backbone and the stacking axis
υ	frequence
ρ	electrical resistivity; spin density
σ	electric conductivity; orbital symmetry
σ_{RT}	room temperature conductivity
λ	wavelength
χ	magnetic susceptibility (molar; corrected for diamagnetic contributions)
χ'	real (in-phase) susceptibility
χ''	imaginary (out-of-phase) susceptibility

Chapter 1

Introduction

1.1 A Radical Concept

What is a radical? Electronically, it is a molecule that contains at least one unpaired electron. However, to an organic chemist, a radical is a reactive intermediate, perhaps from the homolytic cleavage of a bond.[1] To the polymer chemist, it is an initiator used in polymerization reactions.[2] To a biochemist, it may be used in cell signaling or as a defensive species generated by the body to eliminate certain bacteria found within.[3] An organometallic chemist may be interested in seventeen-electron metal-centred radicals.[4] The physical chemist may study radicals in the gas phase or trap them in frozen matrices.[5] Radicals are not only limited to the chemist's vocabulary. Free radicals are discussed in the mainstream media, where topics include the radical induced aging processes,[6a] Parkinson's disease,[5b] and the consumption of antioxidants to stop the formation of free radicals in the body.[5c] All of these constructs suggest that radicals are highly reactive, most times hard to control, a blessing or a curse. Mother Nature points out however, that there is a flip side. Stable radicals, meaning radicals that can be isolated and stored without decomposition[7] are found in nature; the best examples are O_2, NO_2 and NO. If stable radicals are found in nature, then the chemist should be able to generate them in the laboratory.

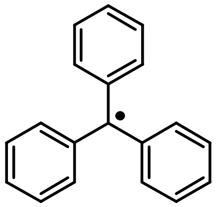

1-1

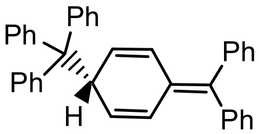

1-2

In 1900 Gomberg isolated the first carbon-based stable radical triphenylmethyl **1-1**.[8] It has been shown by others that this stability arises from the combination of steric effects, supplied by the phenyl groups, and also from resonance effects, where the electron can delocalize onto the phenyl substituents.[9] However, in spite of the electron delocalization and bulky phenyl substituents, the radical forms head-to-tail dimers in the solid state (**1-2**). Elegant studies that probed resonance and steric effects appeared in 1966 with the discussion of the resonance stabilized sesquixanthydryl radical **1-3** which, although having an optimal geometry for delocalization of the unpaired electron, forms an insoluble dimer.[10] When, however, the hexylmethoxy derivative **1-4** was prepared, the large twist angle suppressed dimerization.[11] Further attempts by other groups to incorporate both resonance and steric stabilization into organic radicals have lead to the isolation of the protected cyclopentadienyl **1-5**[12] and phenylenyl **1-6**[13] derivatives, although the latter forms π dimers.

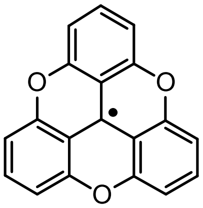

1-3

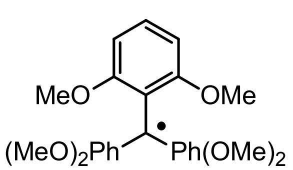

1-4

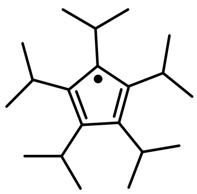

1-5

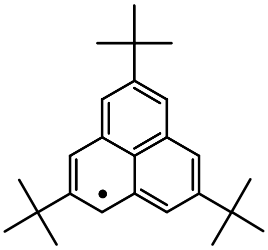

1-6

But what can one learn from Mother Nature? She has shown us that radicals can be resonance stabilized if the unpaired electron is in conjugation with two electron-rich heteroatoms (recall NO and NO_2). In chemistry, many stable radicals contain N, O or a combination of both atoms. In all of the examples of dimerized radicals listed above, dimerization occurred though C centres, as the C-C σ-bond is energetically favourable in many spin-pairing situations. Radical stabilization can occur with the help of both resonance stabilization and electron richness on two atom centers, as this tends to inhibit σ-bond formation. The galvinoxyl radical **1-7** is a prime example, where the combination of spin delocalization throughout the organic backbone and bulky tertbutyl groups lead to a stabilized structure.[14a] Two well-known classes of N- and O-containing stable radicals are verdazyl **1-8**[15] and oxoverdazyl **1-9**[16] radicals. Here, the steric bulk is decreased and the effects of resonance stabilization becomes more pronounced. Some of these materials are stable indefinitely (while others are merely persistent – meaning the radical can be generated and spectroscopically observed but not necessarily isolated).[6] But why are verdazyls and oxoverdazyls stable? One design parameter that is present in both classes is the symmetrical distribution of atoms in the ring system, *i.e.*, the radical contains a mirror plane lying perpendicular to the plane of the ring. Thus, if spin resides on a nitrogen atom on one side of the molecule (**1-10a**), symmetry dictates that it must be found on the other side as well (**1-10b**).

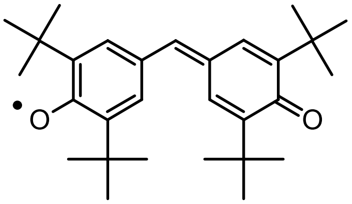

1-7

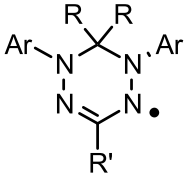

1-8

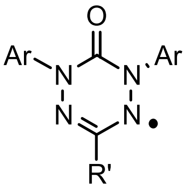

1-9

Finally, nitronyl nitroxides **1-11** , which are extensions of the nitroxide radical,[17] are examples of a resonance stabilized system, where the electron has been shown to be shared between NO units.[18] Many of these radicals display stabilization like that found in verdazyls and oxoverdazyls and form discrete radicals in the solid state, *i.e.*, they do not dimerize, a feature which is the source of interesting magnetic properties. Overall, the radicals discussed above illustrate that electron density must be distributed over many atoms, mainly electron-rich atoms, and under such circumstances innate stability may arise. If this criterion is not met, the radical centre must be sterically blocked or a highly reactive intermediate will result.

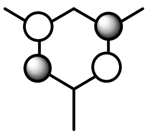

1-10a

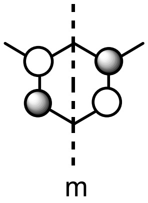

1-10b

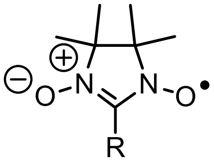

1-11

1.2 Oakley Thiazyl Radicals

Since the early 1980s, the Oakley group has been synthesizing thiazyl (SN) based radicals with a goal to generate and study conductive neutral radicals. In its monomeric form, the SN unit (**1-12**) is a neutral radical with one unpaired electron.[19] Although **1-12** is isoelectronic to NO, thereby fulfilling the electron rich heteroatom pair paradigm, it rapidly polymerizes to the SN_x polymer **1-13**.[20] Further studies have shown that SN can be stabilized by coordination to metals.[17b]

In contrast to NO based compounds, SN gives rise to a large array of cyclic compounds.[21] For example, S_2N_2 **1-14** is a square-planar 6 π-electron system and is an important precursor to **1-13**.[22] S_4N_4 **1-15** can also be prepared, however the molecule adopts a cage-like structure.[23]

SN•

1-12

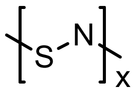

1-13

1-14

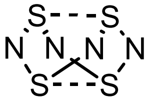

1-15

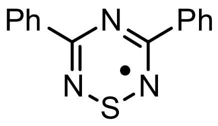

1-16

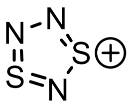

1-17

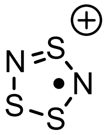

1-18

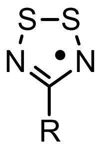

1-19

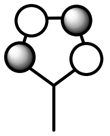

1-20

Initial SN radical studies by Oakley centered on the generation of a 6-membered thiatriazinyl ring **1-16**.[24] These stable radicals were chosen in hope that they might emulate the electronic properties of the $(SN)_x$ polymer **1-13** (*vide infra*) but allow for the inclusion of C into the ring system, forming discrete heterocyclic molecules. Thiatriazinyls are planar ring systems with a series of π-type molecular orbitals in which the electron delocalizes throughout. These materials also exhibit stable cation, radical and anion oxidation states. In the solid state, cofacial π-dimers are formed.

5-Membered rings based on the SN unit have also been well characterized. For example, the cyclic dithiatriazyl cation **1-17** is a 6 π-electron system and is the only example of a nitrogen rich SN binary species.[25] Substitution of S for N gives rise to the planar trithiadiazyl radical cation **1-18** which is prepared by oxidation of **1-15**.[26] Modification of **1-18** generates a planar resonance stabilized class of 1,2,3,5-dithiadiazolyl (DTDA) radical **1-19**,[27] the first example of which was structurally characterized by Banister and coworkers in 1980.[28] These materials are planar, with a π-type SOMO (singly occupied molecular orbital, **1-20**) and like the thiatriazinyl systems, DTDAs exhibit a (rich) diversity of stable oxidation states. In the solid state almost all of the radicals form dimers and display different modes of dimerization which can be explained by the symmetry of the SOMO interactions (**Figure 1.1**).

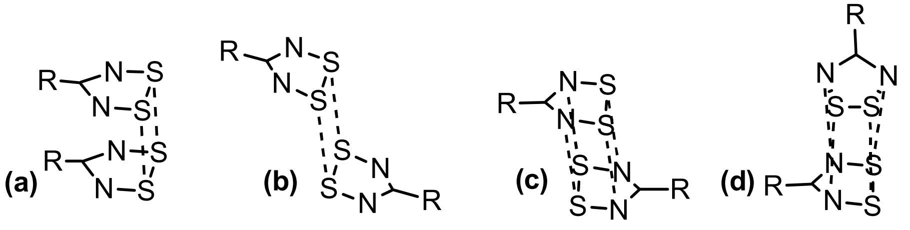

Figure 1.1 Different modes of dimerization in 1,2,3,5-DTDA radicals, (a) *cis*-cofacial, (b) *trans*-antarafacial, (c) *trans*-cofacial, (d) twisted (gauche)

EPR measurements on **1-19** (R = H) demonstrate a radical - dimer equilibrium in solution, with a low dimerization enthalpy $\Delta H_{dim} \sim -35$ kJ mol^{-1}.[29] Furthermore, the R-substituent can be synthetically modified, giving rise to many new materials. The symmetry and distribution of the DTDA SOMO has a direct effect on solid state properties. Here, the MO is spread over the S and N atoms of the DTDA ring and there exists a node at the carbon atom (**1-20**). Thus, the R- substituent will dictate the solid packing of the dimers but has little influence on the electronic properties of the radical.

In attempts to generate heterocyclic SN radicals that allow for the SOMO to develop throughout the whole molecule, the dithiazolyl (DTA) radicals were synthesized. In both isomers, the 1,3,2- and the 1,2,3-DTA (**1-21** and **1-22**) spin density is placed on carbon. Thus, the electronic properties of the radicals can be altered by the attachment of substituents or by the generation of a heterocycle through one or both carbons of the DTA ring. Theoretical calculations and EPR spectroscopy demonstrate that spin density is distributed throughout the DTA radical, but place the large majority of the spin on the S-N-S portion of the 1,3,2-DTA ring. The simple 1,3,2-DTAs form dimers,[30] however the naphthalene and quinoxaline based derivatives **1-23**[31] and the dithiazolopyrazino compound **1-24**[32] are discrete radicals at room temperature in the solid state.

Magnetic susceptibility shows that all 1,3,2-DTAs dimerize at low temperatures, however hysteresis in the magnetic susceptibility associated with the dimer-radical switchover has been observed in **1-24**, Wolmershauser's radical **1-25**[33] and Oakley's pyrazinyl radical **1-26**.[34] The observation of hysteretic behaviour has led to interest in these materials as magneto-thermal switches and for information storage.[35]

1-21

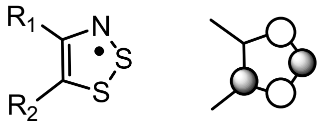

1-22

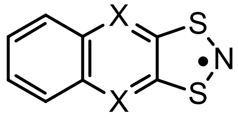

X = N, CH

1-23

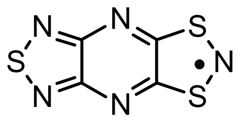

1-24

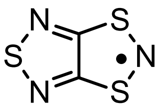

1-25

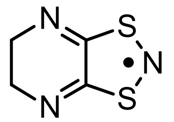

1-26

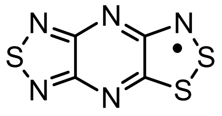

1-27

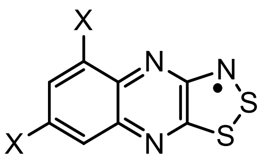

X = H, Cl

1-28

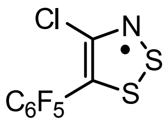

1-29

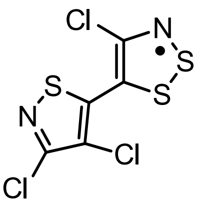

1-30

The 1,2,3-DTA materials **1-22** hold great potential for the delocalization of electron density throughout the molecule. Although these materials have been observed spectroscopically for over twenty years,[36] the first radical (based on the dithiazolopyrazino ring **1-27**) was isolated in 1999.[37] **1-27** forms centrosymmetric π-dimers in the solid state but gives rise to a high room temperature conductivity (σ_{RT}) of 10^{-4} S cm^{-1}, a value that is unprecedented for monofunctional materials of this class (*vide infra*). A second set of fused ring radicals, the quinoxaline series **1-28**, which can be isolated with 0, 1, or 2 Cl-substituents, have been isolated and investigated by EPR spectroscopy.[38] However, the lability of all three quinoxaline radicals did not allow for the isolation of the materials in sufficient quality and quantity to allow single crystal X-ray analysis.

It has been shown that the distribution of the π-SOMO permits electron spin density to reside on the 5-carbon of the 1,2,3-DTA ring (**1-22**) and thus to delocalize from this carbon onto substituents attached at this site; the perfluorophenyl dervative **1-29** illustrates this concept well, as EPR spectroscopy has demonstrated that there is observed spin coupling to the perfluoro- appendages.[39] However, the C_6F_5 substituent has a twisted conformation in the solid, thus decreasing the electron-withdrawing effect of the substituent (*i.e.*, the majority of the spin density resides on the DTA ring). Furthermore, the steric effect of the C_6F_5- group was not enough to inhibit dimerization through sulfur in the DTA ring. In contrast to all 1,2,3-DTA radicals listed above, the thiazole derivative **1-30** is monomeric in the solid state, forming well ordered π-stacks of radicals, even at temperatures below 50 K.[40] The stability of this system, *i.e.*, the propensity to avoid dimerization, is easily rationalized though resonance and steric arguments. EPR spectroscopy has illustrated that there is less electron coupling to the nitrogen atom of the DTA ring compared to **1-29**, suggesting that there is an increase in electron distribution throughout the radical; furthermore, the chloro ligands attached to both heterocycles in **1-30** sterically hinder close approach of the neighbouring radicals.

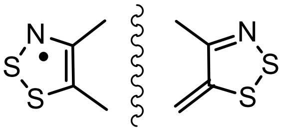

1-31

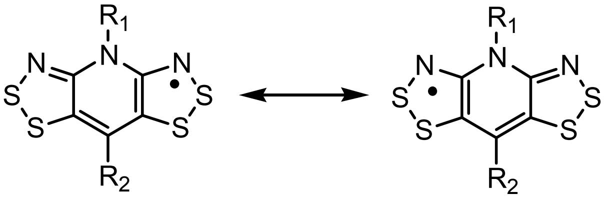

1-32

The generation of 1,2,3- and 1,3,2-DTA radicals represented a major synthetic achievement and delivered encouraging results, *i.e.*, good electron delocalization in the radicals, especially seen in **1-24**, **1-27** and **1-30** through the attachment of highly electron withdrawing substituents. Furthermore, it was demonstrated that removal of electron density from the DTA ring, coupled with the attachment of bulky substituents, could result in the suppression of dimerization in the solid state - a result that had not been observed in previous SN neutral radicals. In attempts to further increase electron delocalization throughout the radical, a new design strategy was developed that targeted the incorporation of two 1,2,3-DTA rings, one carrying a radical and the other a closed shell, which could be fused together by an appropriate bridging heterocycle (**1-31**). This idea resulted in the synthesis and charactization of a new class of neutral radicals - the dithiazolodithiazolyl (*bis*-DTA, **1-32**).[41]

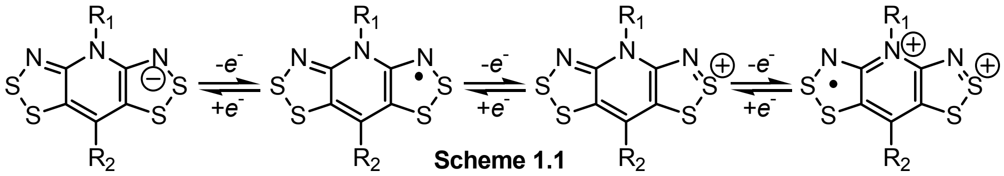

Scheme 1.1

The *bis*-DTA system has a planar fused ring backbone and shows a large range of oxidation states (**Scheme 1.1**) going from a 16 π-electron cation to a 17 π-electron radical to an 18 π-electron anion. Furthermore, there is an accessible 15 π-electron radical dicationic oxidation state in some derivatives, again driving home the electrochemical richness of the material. As seen in other systems, this material has a plane of symmetry passing through the pyridine N and the 4-carbon of the pyridine ring. EPR spectroscopy illustrates the equal distribution of electron density on both DTA rings and, furthermore, spin density is kept off of the central ring, which is in contrast to highly reactive phenazinyl radicals **1-33**.[42]

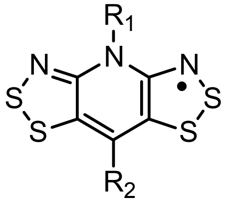

1-32

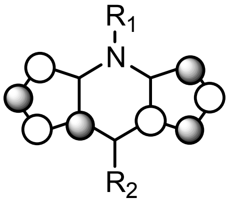

1-32a

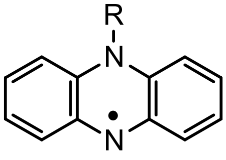

1-33

To date all *bis*-DTA derivatives (save for one radical which dimerizes through C-C or S-S σ bonds)[43] that have been isolated are discrete radicals in the solid state. Furthermore the radicals form π-stacks in the condensed state, an attractive requirement for improved conductivity in crystalline material. An important feature of the *bis*-DTA molecule is the ability to modify R_1 and R_2, which are generally referred to as the "beltline" substituents. Although this feature appears moot, modification of the "beltline" directly influences the crystalline motif, and therefore, alters the bulk properties of the material. In essence, these materials can be "fine-tuned" by synthetic modification of the radical. In the remaining sections, the discussion will centre on the bulk properties of molecular materials as a function of the solid state structure, as it is the way the molecules pack that dictates the observed conductivity (and magnetism) of the material.

1.3 Models of Electrical Conductivity Through Molecular Media[44]

The concept of electrical conduction through molecular media was introduced by McCoy and Moore in 1911,[45] and was followed by Krauss in 1913.[46] However, it was Little in 1964 who discussed the change in bulk conductive properties of a material as a function of synthetic modification to the organic framework.[47] Thereafter, many new classes of molecular conductors emerged, most notable being charge transfer (CT) salts,[48] radical ion conductors[45] and more recently, closed shell conductors.[49]

CT salts have been well studied in the literature. The structural feature most common among this class is the planarity of the organic acceptor (A) and donor (D) molecule. Cocrystallization of D and A results in the oxidation of the donor and reduction of the acceptor molecule *via* electron transfer. The most recognized complex in this class is TTF-TCNQ (TTF = tetrathiafulvalene **1-34**,[50] TCNQ = tetracyanoquinoxaline, **1-35**[51]). TTF- TCNQ co-crystallizes as a 1:1 salt which exhibits maximum metallic conductivities of 10^4 S cm^{-1} at 56 K (**Figure 1.2**)[52]. The crystals adopt segregated π-stack structures, allowing for increased orbital overlap between molecules within each stack. Conductivity is 500 times greater parallel to the stacks than perpendicular to them. TTF-TCNQ is a metal as conductivity increases as temperature decreases down to 54 K, at which point a metal-insulator transition (T$_{MI}$) persists.

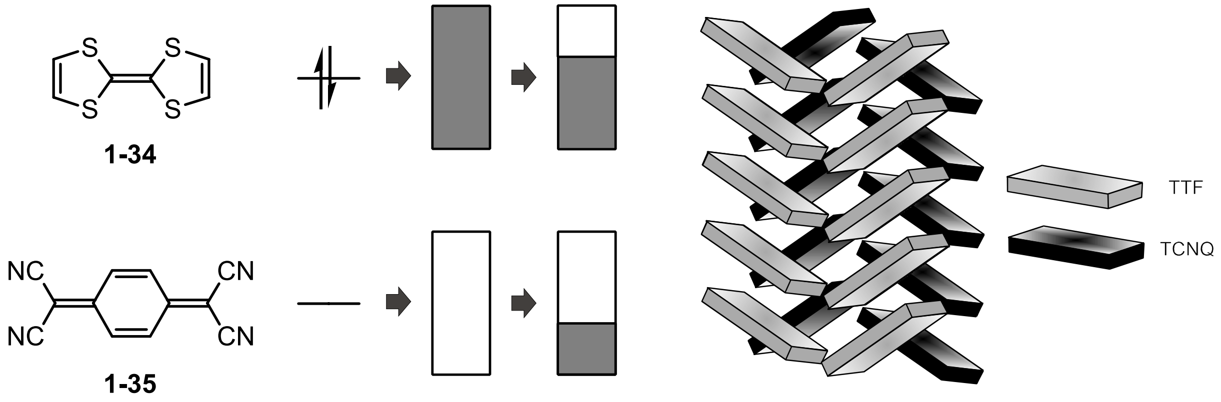

Figure 1.2 (a) Partial charge transfer between TTF and TCNQ, (b) the resulting TTF-TCNQ motif.

Radical ion conductors (RICs) are characterized by the incorporation of inorganic counterions in exchange for an acceptor (or donor) counterpart. The oxidation of the π-molecular donor or reduction of a π-molecular acceptor results in a conductive radical ion salt. The X$^-$ counterion is a spectator and does not participate in charge transfer, *i.e.*, it acts as a charge counterbalance and a means of oxidation or reduction. Significant examples of RICs are salts of BEDT-TTF (*bis*(ethlenedithio) tetrathiafulvalene, or ET, **1-36**)[53] and Bechgaard salts.[54] ET salts generally have a 2:1 stoichiometry, $[ET]_2X$, where X^- is a monovalent inorganic ion such as $IBrI^-$. Bechgaard salts have the formula $[TMTSF]_2X$, where TMTSF is the electron donor tetramethyltetraselenafulvalene (**1-37**); the counter ion is usually a simple tetrahedral or octahedral counterion such as BF_4^- or PF_6^-.

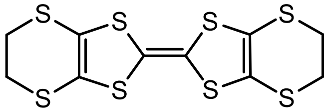

1-36

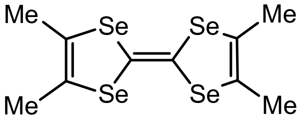

1-37

Of importance to both RICs and CT salts is charge transfer. It must be emphasized that in order for both complexes to exhibit conductive properties, partial charge transfer is needed, as complete charge transfer will result in a poor conductivities. To emphasize this point, the salts [TTF][Br] and $[TTF][Br]_{0.7}$ may be compared. In [TTF]Br, complete electron transfer occurs and the conductivity is 13 orders of magnitude less than $[TTF]Br_{0.7}$, which is partially oxidized.[55]

The previous examples of conductive materials require two components (D and A) to generate charge carriers, and for metallic behaviour to ensue, one must control the crystallization of both components. One way to sidestep cocrystallization of D and A molecules is to incorporate both components into one molecule. For example, the closed shell $[Ni(tmdt)_2]$ complex (tmdt = trimethylenetetrathiafulvalenedithiolate, **1-38**),[56] where tmdt is the electron donor and Ni is the acceptor, exhibits room temperature conductivities of 400 S cm^{-1}, and remains metallic down to 0.6 K. The complex is planar, and packs in a pseudo close-packed arrangement allowing the π-type molecular orbitals to overlap well in the solid state. Gas phase calculations show a HOMO-LUMO energy separation on the order of 0.10 eV, solid-state calculations show that the electronic bands arising from the HOMO and LUMO orbitals cross at the Fermi level, giving rise to a 3-dimensional band structure (**Figure 1.3**).

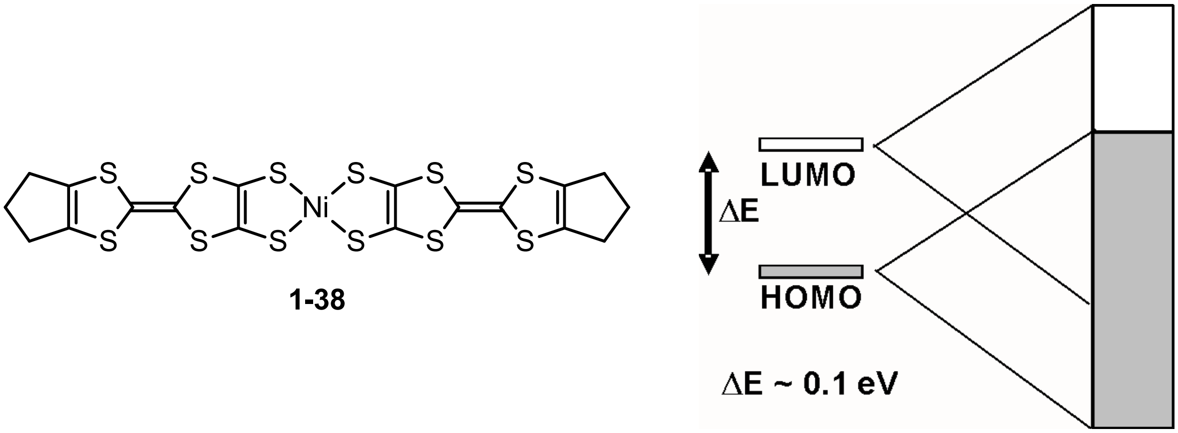

1-38

Figure 1.3 The electronic bands that arise from the HOMO and LUMO MOs of **1-38**.

1.4 Radicals as Charge Carriers

In the previous section, the concept of conduction *via* charge transfer has been presented. This construct has led to the isolation and study of many novel conductive materials, many of which show metallic behaviour. However, this design requires the judicious choice of cation/anion pair. Given the breadth of this multi-component challenge, a different approach would be to generate metallic behaviour without charge transfer, *i.e.*, generate molecular building blocks that give rise to partially filled electronic bands in the solid state, as by definition, these materials are metals. The idea of conductivity without charge transfer in π-type radicals, which has given rise to a class of materials called neutral radical conductors (NRCs), was first described by Haddon in 1975 by using the odd alternate hydrocarbon phenalenyl (PLY, **1-39**) as the model compound.[57] Haddon reasoned that the planar 13-carbon 13 π-electron system would give rise to one electron residing in a non-bonding π-type molecular orbital (or non-bonding SOMO, **1-40**). The structure is planar and therefore such a molecule should form π-stacks in its condensed form (*e.g.*, like stacked plates). Most importantly, there would be few structural changes upon reduction/oxidation of the compound, thus preserving its effective π-stacking. Therefore, radicals containing unpaired electrons in π-type SOMOs will give rise to electronic bands if equally spaced π-stacks are formed in the solid state. Furthermore, if there is one electron per site, the electronic band formed will be half-filled ($f = ½$). By definition, any material containing partially filled bands is a metal and therefore, π- stacks of organic radicals should be metals in the solid state. The degree of overlap between each SOMO in the π-stack will have a direct relationship to the bandwidth (*W*) of the electronic bands, where increased SOMO overlap leads to increased *W*. Alternatively, increasing the space between each radical will decrease *W* (**Figure 1.4**).

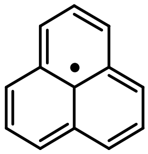

1-39

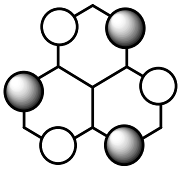

1-40

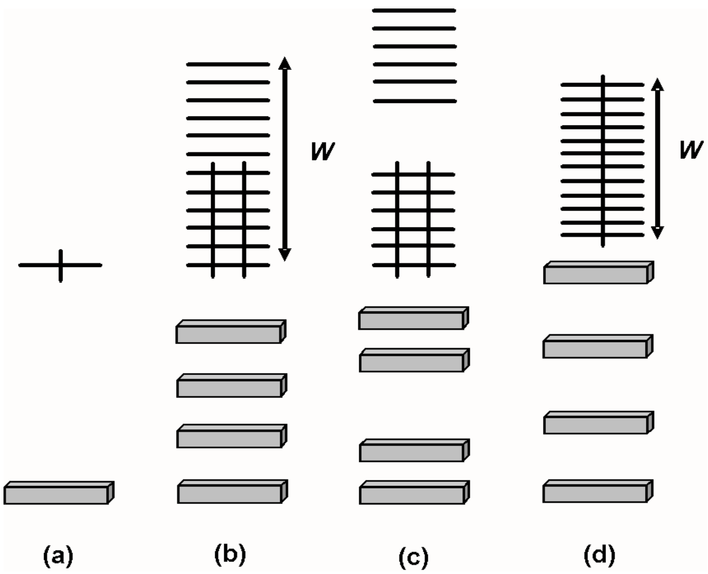

Figure 1.4 Energy levels and bands associated with (a) a single π-radical, (b) an idealized stack of strongly interacting π-radicals possessing a half-filled band, **c**) a Peierls distorted π-radical stack and the resulting band gap, and (d) a weakly interacting array of π-radicals.

Clearly, this is not the only requirement for metallic conduction through π-radicals. It is well known in condensed matter physics that materials possessing partially filled bands of low *W* can exhibit insulating properties; these materials are referred to as a Mott Insulators. First described by Mott[58] and followed up by Hubbard,[59] this phenomenon was shown to occur when *W* is small with respect to the onsite Coulomb repulsion energy *U*. If the bandwidth is large compared to *U*, the electrons will delocalize into the band and behave as metals. If *U* is greater than *W*, the Coulombic repulsion between electrons will lead to electron localization on each molecule, forming a Mott-Hubbard insulator.

The value of U cannot be measured directly and it is therefore difficult to obtain accurate values. Hubbard proposed a simplified methodology to treat electron repulsion within radicals in the solid state, which assumes the only contribution to electron repulsion is from two electrons that occupy the same molecule (**Figure 1.5a**). If a 1-dimensional chain of equally spaced $S = ½$ radicals are considered, as the space between each radical centre is increased, there comes a point where the electrons will localize onto each centre. In order to remove an electron from one site, an ionization energy (*IE*) is required. When the electron is placed onto an adjacent site, there is an energy gained through the electron affinity (EA). Thus, we can express the energy required to move an electron from one site to the next as $U = IP - EA$. *IP* and *EA* values can be probed in solution through cyclic voltammetry (**Figure 1.5b**),and *via* gas phase disproportionation enthaplies (ΔH_{disp}, **Figure 1.5c**) thereby giving us and idea of the magnitude of U.[60]

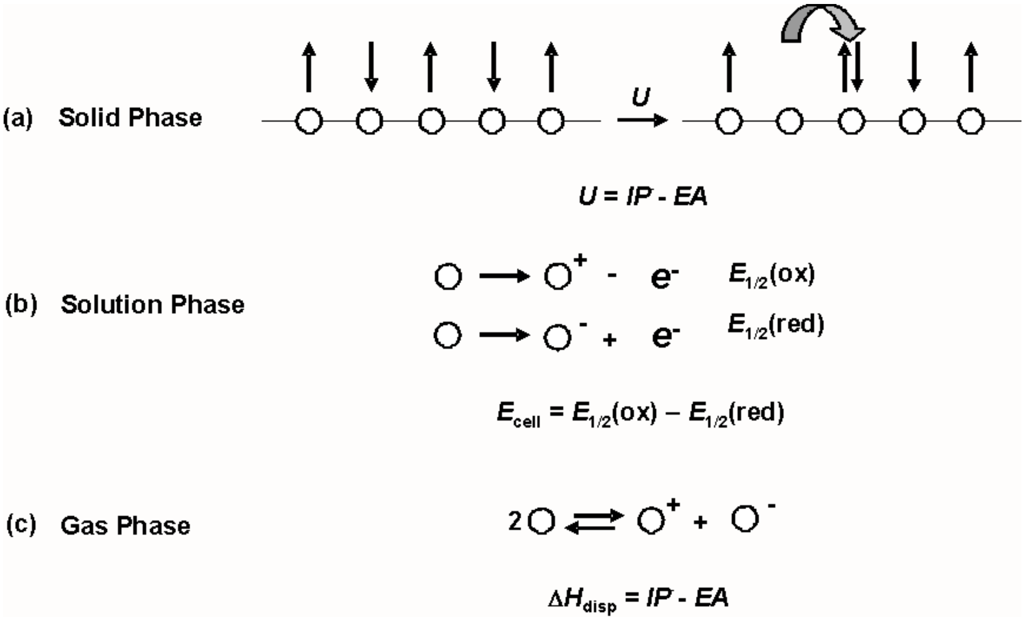

Figure 1.5 Hubbard hopping model of conduction in solids (a), E_{cell} values from the oxidation and reduction of a neutral radical (b), disproportionation enthalpy, ΔH_{disp} (c).

With an understanding of W and U, we can begin to interpret **Figure 1.4**. If the spacing between radicals is small and/or SOMO overlap is maximized, W is large and may exceed U, resulting in metallic behaviour (**Figure 1.4b**). If the spacing between radicals increases and/or SOMO overlap is small, U may be larger than W resulting in electron localization (**Figure 1.4d**). This model requires equal spacing between each radical within the π-stack. However, any partially filled band is susceptible to Peierls instabilities.[61]

In the case of a half filled band, this is manifest as dimer formation, upon which a band gap is opened at the Fermi level and the material is, by definition, an insulator (**Figure 1.4c**).

Haddon's model of conductivity without charge transfer for neutral π-type radicals has given rise to two different research strategies that focus on (i) the synthesis of neutral radicals with decreased values of U, and (ii) the pursuit of radicals with increased W in the solid state.

1.4.1 Minimizing *U*: The Haddon Approach

Haddon's NRC proposal centred on the generation of odd-alternative hydrocarbons, such as PLY (**1-39**). However, the parent PLY structure has not been isolated in the solid state, although it has been characterized by EPR spectroscopy[62] and is thought to form σ-dimers in the solid state.[63] In attempts to isolate derivatives of **1-39**, the *tris*(*tert*-butyl) substituted compound (**1-6**) has been reported,[12] and the steric bulk of the *tert*-butyl groups inhibit σ-dimerization but do not suppress π-dimerization. Dimerization was avoided in the per-chlorinated derivative (**1-41**)[64] in the solid state. However, intramolecular repulsion between the bulky Cl- substituents ruffles the radical, giving rise to a complex mode of crystallization.[65] Overall, the material is a Mott insulator due to the large contact distances between radical units. Modification to the PLY framework has also led to the isolation of the first electron-rich PLY derivative **1-42**. Low electrochemical potentials (E_{cell} = 0.57 V) have been measured and in the solid state **1-42** forms π-dimers, demonstrating that the radical has been stabilized against σ-dimerization by electronic effects, rather than by the presence of bulky substituents.[66]

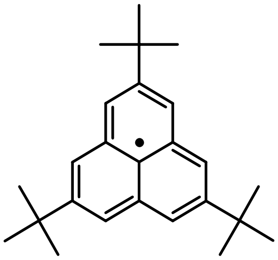

1-16

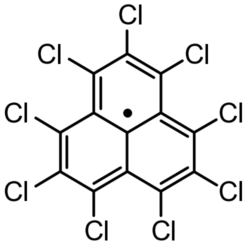

1-41

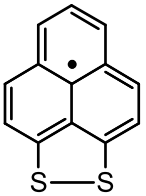

1-42

Haddon's research into PLY-based NRCs with minimal values of U has led to the development of a series of spirobiphenalenyl radicals **1-43**, **1-44** and **1-45**. Unlike conventional neutral radicals, these radicals give rise to a quarter filled ($f = \frac{1}{4}$) electronic band in the solid state, subsequently reducing U. Of the many spirobiphenalenyl derivatives prepared, many do not associate in the solid state, and have C---C′ contact distances greater than the sum of the van der Waals radii.[67] However, π-dimerization has been observed in the ethyl- and butyl- derivatives of **1-43**;[68] σ-dimerization has been also been observed in the octyl system.[69] In contrast, the hexyl and benzyl derivatives of **1-43** exist as discrete radicals in the solid state, and have well characterized semiconducting properties.[70] Derivatives of **1-44**[64] have exhibited antiferromagnetic coupling and good room temperature conductivities. Recently triphenalenyl **1-46**[71] has been reported to form weak π-dimers in the solid state.

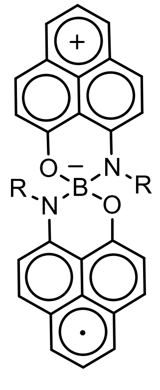

1-43

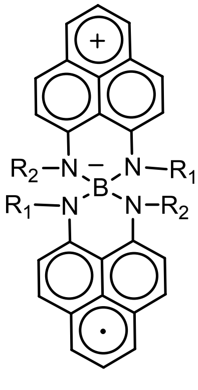

1-44

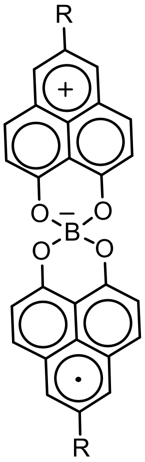

1-45

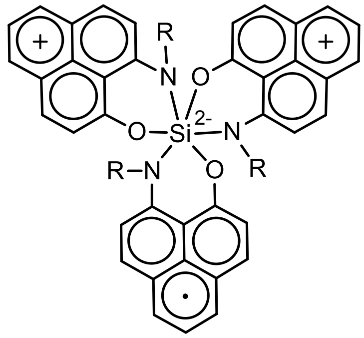

1-46

Of great significance, the cyclohexyl and cycloheptyl derivatives of **1-43**[72] and the methyl and proto derivatives of **1-45**[73] have been shown to consist of a continuous array of π-stacked phenalenyl units exhibiting C---C′ contacts that are shorter than the van der Waals atomic separation. Although the conductivity remains activated (σ(300K) = 0.3 S cm^{-1}), Pauli paramagnetism has been found for these systems and a resonating valence bond ground state has been suggested to describe their conductive properties.[74]

1.4.2 Maximizing Bandwidth

The second approach to generating NRCs, one that is employed by the Oakley group, is to increase the bandwidth *W* of neutral radical solid state materials. This approach utilizes the model proposed by Haddon (**Figure 1.4**), but incorporates electron-rich SN atoms into the radical framework. The idea stems from the discovery of polythiazyl **1-13**, which consists of repeating -S=N- units and has a room temperature conductivity of 2 $\times 10^3$ S cm^{-1} and is superconducting at 0.26 K.[75] This system is the only known metallic polymer that does not require charge transfer in order to generate charge carriers. High electrical conductivity is explained through the electronic configuration, where two π-electrons reside in a bonding π-orbital and the third π-electron resides in a π^* antibonding orbital (**Figure 1.6a**).

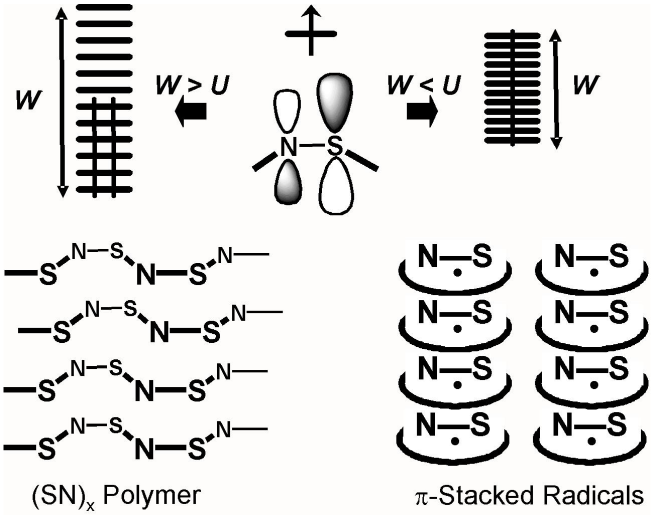

(a) (b)

Figure 1.6 A cartoon representation of the -N=S- fragment, which contains 1 π-electron in an π^* orbital, and which gives rise to (a) chains of **1-13**, a half-filled band and metallic properies as $W > U$, (b) SN neutral radicals that form π-stacks and possess Mott insulating properties as a result of $W < U$.

As a first approximation, polythiazyl may be envisioned as a solid state material with a half-filled band, making this system a perfect candidate for a Peierls-type instability. However, the polymer consists of chains in a close packed arrangement, a configuration which allows for good overlap of SN molecular orbitals, and generates a 3-dimensional network of close contacts that aid in the suppression of Peierls instabilities. Overall, the bandwidth generated by the overlap of the molecular orbitals in **1-13** is greater than

U, hence, a metallic ground state emerges. However, the instability of S_4N_4 (the explosive precursor to polythiazyl) made processing of **1-13** unsafe; furthermore, synthetic modification of the polymer is difficult due to the lack of substituent sites present on the chain.

The discovery of **1-13** prompted investigation into discrete SN-based materials, leading to the π-type radicals researched by the Oakley Group (**Figure 1.6b**). The main theme of this research is to take advantage of the increased orbital overlap afforded by the SN orbital contribution to the overall radical SOMO. Thus, the incorporation of SN heteroatoms into organic π-radicals should lead to better overlap of the SOMOs in the solid state, as compared to purely organic (*i.e.*, C-, N-, and O-containing) π-radicals. Furthermore, the research sought to exploit the recognized tendency of such systems not to undergo irreversible dimerization, compared to their organic-based counterparts.

Efforts by the Oakley group to generate SN-based NRCs began nearly a quarter century ago, where the concern was first to synthetically build a SN radical. The first targets were thia- and selenotriazinyl radicals (**1-16**, **Section 1.2**). In solution the radicals underwent reversible oxidation and reduction but in the solid state they formed strong dimers through sulfur or selenium.[22] Attention turned to synthesis and characterization of 1,2,3,5-DTDA materials (the “first generation” radicals). Many examples of this class of material have been prepared, including mono-, di-, and tri-functional systems.[25] Selenium variants could again be prepared, but all of these radicals suffered the same dimerization fate, having poor conductivities of ~10^{-9} S cm^{-1}. These systems had a large ΔH_{disp} (~7.0 eV) and large E_{cell} potentials (~1.4 V), values that did not depend on the nature of the substituent attached to the DTDA ring. It was demonstrated that at higher temperatures, the weak interdimer S---S′ bonds uncouple, however at these temperatures poor conductivities persisted. Conductivities could be dramatically increased through p-doping, *i.e.*, by moving the level of band filling away form the half-filled level, for which *U* is the largest, and a number of highly conductive charge transfer salts were produced.[25f, 76]

In a search for materials with lower values of *U*, and which could form discrete radicals in the solid state, the 1,3,2- and 1,2,3-DTA materials were generated.[29-38] Calculated disproportionation energies and measured cell potentials were found to be dramatically lower than the 1,2,3,5-DTDA radicals (ΔH_{disp} ~5 eV, E_{cell} ~1.0 V). However, almost all of these “second generation” radicals formed weak dimers in the solid state. Room temperature conductivities in the range of 10^{-9} to 10^{-5} S cm^{-1} have demonstrated that judicious choice of substituent attachment or generation of electron withdrawing heterocyclic backbones will lead to an improvment in gas-phase, solution and solid-state properties over the first generation materials.

The "third generation" of Oakley SN radicals resulted in the isolation of *bis*-DTA radicals with greatly improved ion energetics (ΔH_{disp} < 5.0 eV) and E_{cell} potentials (<0.8 V).[39] Most importantly, the radicals formed stacks of discrete radicals in the solid state. Thus, dimerization has been suppressed and improved *W*s have resulted. Conductivities between 10^{-6} to 10^{-5} S cm^{-1}have been measured, a result that is unprecedented in SN-based NRCs to date. Overall, a large improvement in *W* (0.5 eV) has resulted, however, the conductivity of *bis*-DTAs remain activated suggesting that $W < U$ and the materials are Mott insulators.

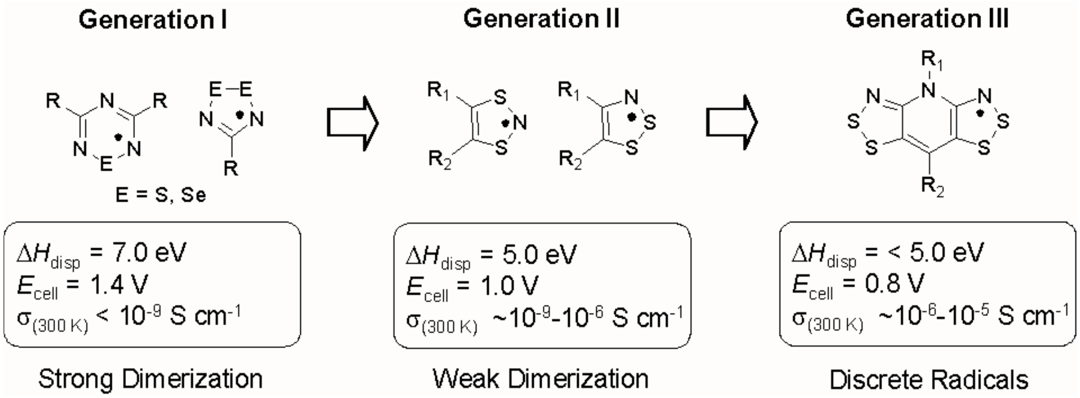

Figure 1.7 An illustration of the three generations of Oakley radicals and their associated physical properies.

1.5 Magnetic Radicals

Because neutral radicals have unpaired electrons, each radical must have an associated magnetic moment. In the solid state, if dimerization occurs, all spins are paired and the material is diamagnetic (its internal magnetic field opposes an applied field). If dimerization can be suppressed, interesting magnetic behaviour will be observed. Generally, neutral radicals are paramagnetic and have Curie or Curie-Weiss behaviour (**Figure 1.8a**).[77] In this system, the spin vector of each unpaired electron is randomly oriented due to the effects of temperature; however, there may be measurable exchange interaction between adjacent spin vectors as the material is cooled in an applied field. Here, the spins either align with one another or oppose one another.

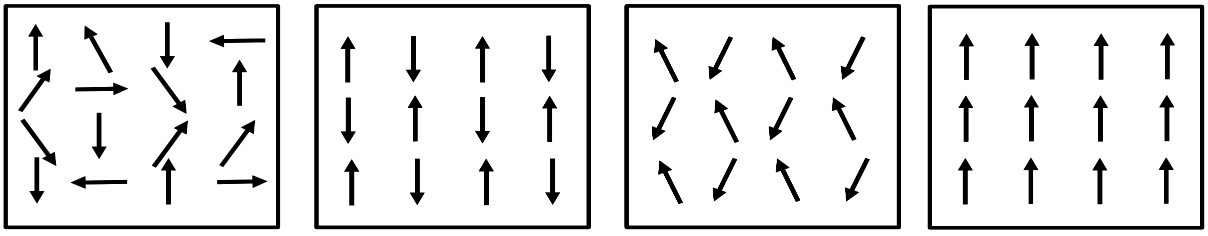
(a) (b) (c) (d)

Figure 1.8 Spin vectors that result in (a) paramagnetism, (b) anitferromagnetism (AFM), (c) weak ferromagnetism (WF), and (d) ferromagnetism (FM).

Below a critical temperature, however, the spin vectors may start to order throughout the bulk material. If spin vectors oppose one another, as in **Figure 1.8b**, antiferromagnetism (AFM) results and the onset of the magnetic transition is indicated by the Néel temperature T_N.[74] If the spins orient in an AFM manner, but do not completely cancel out (**Figure 1.8c**) the material gives rise to a very weak, yet measurable magnetic moment and the material is called a weak ferromagnet WF (or a canted magnet, or a canted antiferromagnet).[74] Unlike AFM, where spin vectors oppose one another, ferromagnetism FM can be regarded as the parallel alignment of each magnetic moment in a material below the Curie temperature, T_c (**Figure 1.8d**).[74]

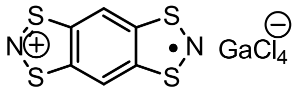
1-47

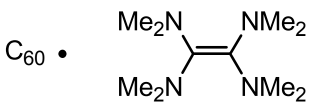
1-48

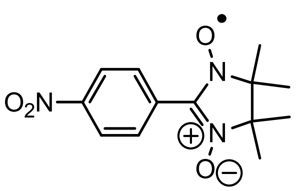
1-49

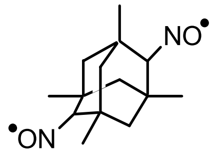
1-50

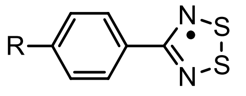
R = NO_2, FM; CN, WF
1-51

To date, molecular-based organic materials with the highest T_cs are those of charge transfer (CT) salts and radical ion conductors (RICs).[78] Most salts contain a transition metal (TM) based counter ion, *e.g.*, $FeCl_4$, to act as the ferromagnetic coupler. However, Awaga demonstrated that TMs could be replaced with counterions containing main group elements when he prepared the benzo-*bis*-dithiazole gallate salt [BBDTA][$GaCl_4$] **1-47**.[79] This material crystallizes with an acetonitrile lattice solvent and is essentially diamagnetic. However, upon gradual desolvation (in *vacuo*), the bulk material orders ferromagnetically at 6.7 K. As Awaga reports, the material has a negligibly small hysteresis loop whose width is less than 10 Oe. Wudl and coworkers have reported the ferromangetic properties of pyrophoric TDAE•C_{60} (the experimentally obtained stoichiometry is $(C_{60})_{1.16}$TDAE, **1-48**).[80] TDAE•C_{60} orders at an impressive 16.1 K (which is the highest T_c of any non-metal ferromagnet to date) and has a room temperature conductivity of ~ 10^{-2} S cm^{-1}. Like **1-47**, this material does not have an associated coersivity (or remanent magnetization).

Ferromagnetism in neutral radicals is rare. There are only a handful of ferromagnets in the literature, furthermore there are only a few examples of ferromagnets that order above 1 K. The first report of a purely organic magnet, *para*-nitrophenyl nitronyl nitroxide (or *p*-NPNN, **1-49**) was reported in 1991 by Kinoshita and coworkers, and orders at 0.6 K.[81] Chiaeilli reported the first example of a ferromagnetically ordered diradical based on an adamantane backbone.[82] The nitroxide biradical, **1-50**, has two NO moieties orthogonally appended to the adamantane unit. In the solid state, the diradical orders ferromagnetically at 1.48 K. In 2003, Rawson reported the first example of a SN-based ferromagnet *para*-$O_2NC_6F_4CNSSN$ (**1-50**, R = NO_2) with a T_c of 1.32 K.[83] Furthermore, Rawson has demonstrated that, by use of functional groups at the *para*- position, crystallization can be altered and a weak ferromagnetic material can be generated (**1-51**, R = CN, T_c = 36 K).[84] To date, there are no known examples of hysteretic behaviour in neutral radical ferromagnetic materials.

1.6 Multifunctional Radicals: Combining Conductivity and Magnetism

Up to this point, this thesis has presented neutral radicals that follow two independent paths, that is, radicals that conduct electricity, and radicals that demonstrate bulk long range magnetic order. It is true that the generation of materials which exhibit high electrical conductivities or ferromagnetism will be a result of major significance. However, generating systems in which both properties are found, *i.e.* multifunctional behaviour, will carry an even greater impact, as such materials offer a host of opportunities in the emerging field of molecular spintronics.[85] Unfortunately, it is far from standard to generate materials which incorporate two novel physical properties. In the emerging field of magnetoelectrics, Coronado has offered one possible solution to this issue by incorporating two molecular networks (*i.e.*, generate a CT complex) where each network contributes one physical property to the multifunctional material.[86] This idea was eloquently illustrated with the combination of the organic π-electon donor BEDT-TTF **1-36** and the metal coordination polymer [$MnCr(C_2O_4)_3$], forming a crystalline metal coordination polymer (the Mn-Cr complex) interleaved with BEDT-TTF (**Figure 1.9**).[87a] The material is both ferromagnetic at 5.5 K and metallic down to 2 K (σ_{RT} = 250 S cm^{-1}); however, there is no apparent interaction between these two properties. The successful approach used by Coronado requires the judicious choice of electron donor and bimetallic complex. Furthermore, it requires the cocrystallizaton of both moieties in a concerted manor, *i.e.*, one component must crystallize in an appropriate way, giving rise to a ferromagnetic lattice, while the other component must form the interpenetrating conductive lattice.

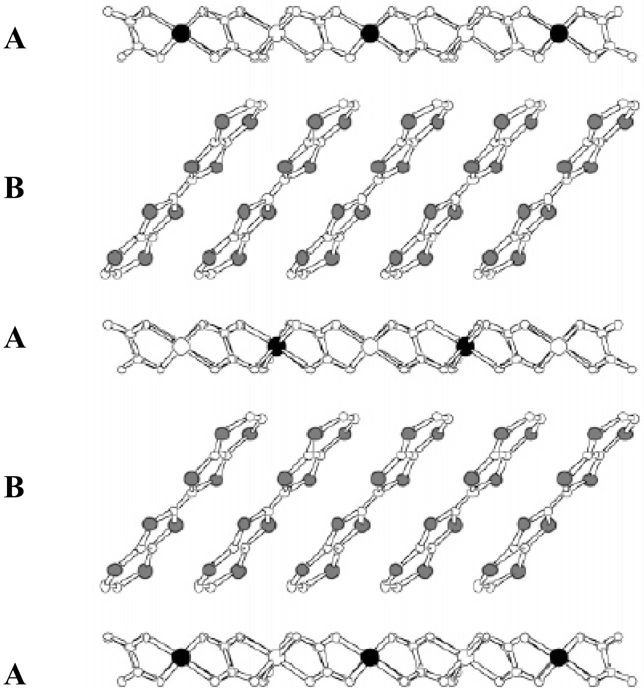

Figure 1.9 Representation of the inorganic (A) and organic (B) layers of (BEDT-TTF)$_3$[$MnCr(C_2O_4)_3$] viewed along the *z*-direction.[84b]

A different approach is to combine both properties into one single component material, eliminating the need for interpenetrating lattices. This approach could be met, in principal, with neutral radicals, where the radical acts as both charge carrier and magnetic coupler. The remaining sections in this chapter serve to introduce the scope of this thesis and will focus on the development of multifunctional radicals based on the *bis*-DTA framework. The main goal of this thesis is to (i) increase the conductivity of *bis*-DTA systems *via* incorporation of Se into the DTA ring system and (ii) observe the effects of Se incorporation on the magnetic properties of the neutral radical.

1.6.1 Conductivity, Magnetism and the Heavy Atom Effect

Presently, all resonance stabilized *bis*-DTA materials generated by the Oakley group have activated conductivities in the range of 10^{-6} to 10^{-5} S cm^{-1}. However, it must be stressed that dimerization has been suppressed in the solid state, even at low temperatures, a feat that has not been realized in all other SN neutral radicals generated to date. In the solid state, the radicals form equally spaced arrays of π-stacked radicals and the resulting crystal lattices demonstrate a rich network of close S---S′ contacts, both within and between the stacks, many of which are well within the van der Waals distances.[88] Furthermore, ΔH_{disp} and E_{cell} parameters for *bis*-DTAs are sufficiently low as compared to early SN radicals, a characteristic attributed to the resonance stabilization afforded by the electron-rich rings. All of these features bode well for the generation of NRCs; however, these materials are all classified as Mott insulators, suggesting that $U > W$. Therefore, U must be further decreased, or alternatively, W must be increased in these systems in order for better conductivities and a metallic ground state to persist. One potential way to reach this goal is to increase W in *bis*-DTAs through the incorporation of heavy atoms into the DTA ring. For example, if Se is introduced, the more spatially diffuse Se atomic orbitals will give rise to a more spatially diffuse π-type SOMO (**Figure 1.10**). Thus, if radical π-stacks are formed in the solid state, orbital overlap may be increased and this will directly increase W, resulting in increased conductivity. Furthermore, the increase in W through Se incorporation may overtake U, giving rise to a metallic ground state.

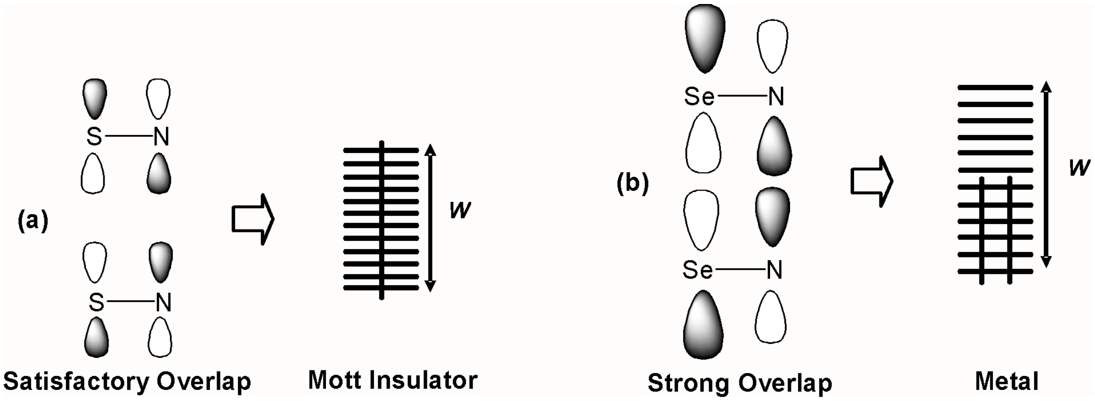

Figure 1.10 The heavy atom effect: (a) *bis*-DTA gives rise to Mott insulators in the solid state, (b) Se-containing *bis*-DTA radicals have more diffuse MOs that overlap to a greater degree, potentially leading to increased conductivity and a metallic ground state.

It has been shown by Rawson that 1,2,3,5-DTDAs (**1-51**) can display interesting magnetic properties such as weak ferromagnetism[81] and ferromagnetism,[80] phenomena that have been attributed to the close intermolecular S---S′ contacts.[89] To date, all *bis*-DTA radicals reported by Oakley have been characterized as Curie-Weiss type paramagnets, where short range magnetic order has been observed for most radicals, but long range order (*i.e.*, antiferromagnetism, ferromagnetism and weak ferromagnetism) has never been observed. Like Rawson's materials, the observation of short range order in Oakley radicals may be due to the short S---S′ contacts in the solid state. However, in contrast to *bis*-DTAs,1,2,3,5-DTDAs require a greater degree of steric bulk in order to suppress dimerization in the solid state. Therefore, *bis*-DTAs (generally) give rise to a greater number of intermolecular contacts that lie within the van der Waals distances, thereby increasing the dimensionality of the material and hence SOMO - SOMO overlap. Consequently, if S is replaced by Se in the DTA ring, the more spatially diffuse SOMO may enhance the magnetic exchange between radical centres. Furthermore, Se incorporation may increase the magnetic anisotropy of the system, as Se orbitals have greater orbital magnetic moments. Therefore, if Se-containing neutral radicals can be generated, the unpaired electron could, in theory, serve as both charge carrier and magnetic coupler, giving rise to magnetic phenomenon other than Curie-Weiss paramagnetism in the solid state (*e.g.*, ferromagnetism and weak ferromagnetism; **Figure 1.11**).

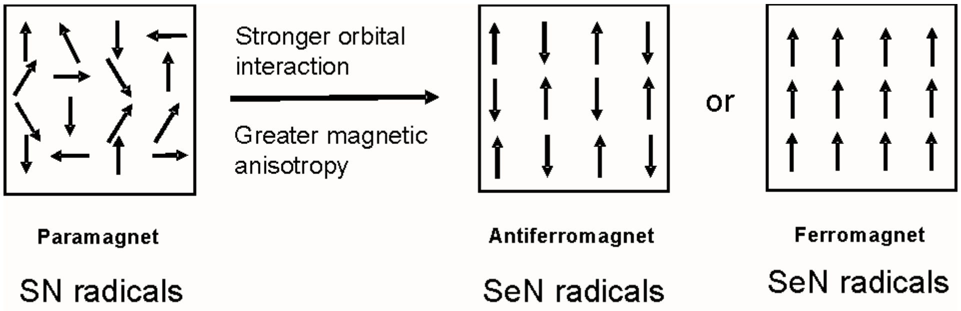

Figure 1.11 Cartoon representation of the potential evolution of paramagnetic properties of *bis*-DTA radicals (left) and the potential for magnetic enhancement of the bulk material upon Se incorporation (right).

1.6.2 Thesis Scope

The preceding discussion has served a twofold purpose: (i) to provide the reader with a basic understanding of the issues surrounding the development of neutral radical conductors and magnetic materials and (ii) to suggest ideas for the generation of new multifunctional materials that demonstrate both conductivity and magnetic ordering in the solid state. Building off of the principles outlined in **Section 1.6**, this thesis will probe the possibility of generating multifunctional materials based on the design and synthesis of Se-containing *bis*-DTA neutral radicals. **Chapter 2** presents early PhD work that focuses on the development of synthetic techniques required to incorporate Se into the DTA ring system. From this work, a naphthalene-based DTA radical and its three Se-containing variants have been isolated. Although it was found that the three Se-containing radicals are thermally unstable at or above room temperature, the radicals could be observed *via* EPR spectroscopy and cyclic voltammetry.

It must be noted that the solid-state structure dictates the bulk properties of our neutral radicals, and in order to understand the properties of solids, one must obtain structural data. Thus, **Chapter 3** shifts focus from the synthesis of Se DTA rings and introduces the reader to the many crystallographic problems associated with S and Se-based DTA radicals. Four examples will be presented where new X-ray crystallographic techniques were required in order to model the solid-state structure of Oakley radicals.

Chapter 4 introduces new synthetic strategies used to generate Se-containing *bis*-DTAs. Furthermore, the chapter serves to develop the idea of isostructural mapping, a concept that gives rise to the first *bis*-DTA based ferromagnet. A family of multifunctional materials, with enhanced conductivity and magnetic interactions is presented in **Chapter 5**. In this chapter, the synthesis and characterization of a complete set of Se-containing radical isomers is reported. Finally, **Chapter 6** brings the thesis to a close with a discussion of the effect of functional group substitution on the magnetic and conductive properties of Se-containing *bis*-DTAs.

Chapter 2

Se Incorporation Into the Monofunctional 1,2,3-Dithiazolyl Framework

2.1 Introduction

As was discussed in the preceding chapter, the generation of resonance stabilized *bis*-DTA neutral radicals **2-1a** is a major advance in the design of single component molecular conductors. In the solid state the bulk conductivity remains activated, *i.e.*, the materials are not metals, although conductivities of 10^{-6} to 10^{-5} S cm^{-1} have been reached, far exceeding all other classes of thiazyl (SN) containing neutral radicals.[1]

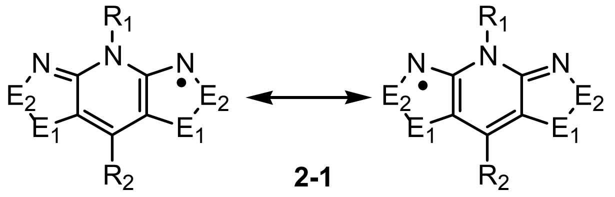

2-1

2-1a: E_1 = S, E_2 = S
2-1b: E_1 = S, E_2 = Se
2-1c: E_1 = Se, E_2 = S
2-1d: E_1 = Se, E_2 = Se

The enhanced conductivity over other SN radicals is attributed to the suppression of dimerization in the solid state, where columns of evenly-spaced radicals are formed (**Figure 2.1**). Each column is further connected by short S---S′ contacts thereby increasing the dimensionality of the electronic band structure. Large electronic bandwidths (on the order of 0.5 eV) arise from SOMO overlap within each column. However, steric interactions between exocyclic ligands R_1 and R_2 in **2-1** inhibit the formation of superimposed radicals within each stack, *i.e.*, the radicals form slipped stacks (**Figure 2.1b**) and this "slippage" decreases the electronic bandwidth (*W*) along the stacking direction to the point where the magnitude of the Coulomb repulsion energy (*U)* overtakes *W*, rendering these materials as Mott insulators.

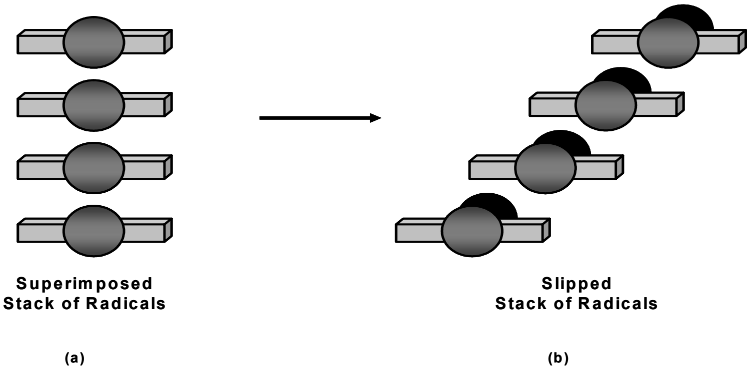

Figure 2.1 A column of *bis*-DTA radicals that crystallize in (a) superimposed π-stacks, (b) slipped π-stacks as a result of the steric interaction of the "bulky beltline" ligands.

Controlling the degree of "slippage" is a challenging task and current work on this topic will be presented in **Section 3.4**. Alternatively, the introduction of Se into the ring system (*i.e.*, the generation of **2-1b**, **2-1c** and **2-1d**) could serve to increase *W* and hence the conductivity of *bis*-DTAs. The Oakley group has demonstrated that Se containing radicals based on 1,2,4,6-thiatriazinyls **2-2**[2] and 1,2,3,5-dithiadiazolyls **2-3**[3] can be synthesized and isolated (as dimers) in the solid state. At the onset of this project, Se had never been synthetically incorporated into any 1,2,3-dithazole ring system. Thus in order to learn more about Se-containing species and particularly methods to effect Se incorporation, we carried out a systematic investigation of the four possible S/Se radicals arising from the naphthalene-based framework **2-4**.[4]

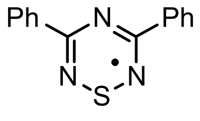

2-2

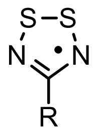

2-3

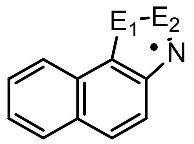

2-4

2-4a: E_1 = S, E_2 = S
2-4b: E_1 = S, E_2 = Se
2-4c: E_1 = Se, E_2 = S
2-4d: E_1 = Se, E_2 = Se

2.2 Preparation of Se-Containing Heterocycles

The preparation of the naphthalene-based 1,2,3-DTA cation [**2-4a**][Cl], radical **2-4a** and the mixed ring system **2-4b** has been reported in my MSc thesis.[5] The preferred method for generating the 1,2,3-dithiazolylium salts is the Herz cyclocondensation[6] of an aromatic amine with sulfur monochloride. In the case of 2-aminonaphthalene **2-5** the reaction under reflux conditions leads exclusively to ring closure at the more reactive 1-position, affording [**2-4a**][Cl] in good yield; chlorination of the naphthalene framework is not observed (**Scheme 2.1**). Access to the mixed ring system [**2-4b**][Cl] required a less direct approach. As a first step, 2-amino-1-thiocyanate **2-6** was prepared by oxidative thiocyanation of 2-aminonaphthalene. Basic hydrolysis and acidification of **2-6** led to the aminothiol **2-7**, which could then be condensed with either sulfur monochloride or thionyl chloride to yield [**2-4a**][Cl], or with selenium tetrachloride to give the mixed S/Se salt [**2-4b**][Cl]. The aminothiol **2-7** is, however, an air sensitive oil and not easily purified. To avoid working with **2-7**, a more convenient and easily handled intermediate was developed by protecting both the amine and thiol functionality of **2-7** with acetyl groups. Thus, when the intermediate thiolate obtained by the hydrolysis of **2-6** was quenched with acetic anhydride rather than acetic acid, the *bis-N,S*-

acetyl derivative **2-8** was produced. This is an air stable crystalline solid which can be crystallized by heptane, thus it is much more easily purified and handled than the aminothiol. It also reacts smoothly under reflux conditions with both $SOCl_2$ and $SeOCl_2$ in acetonitrile to afford [**2-4a**][Cl] and [**2-4b**][Cl] respectively.

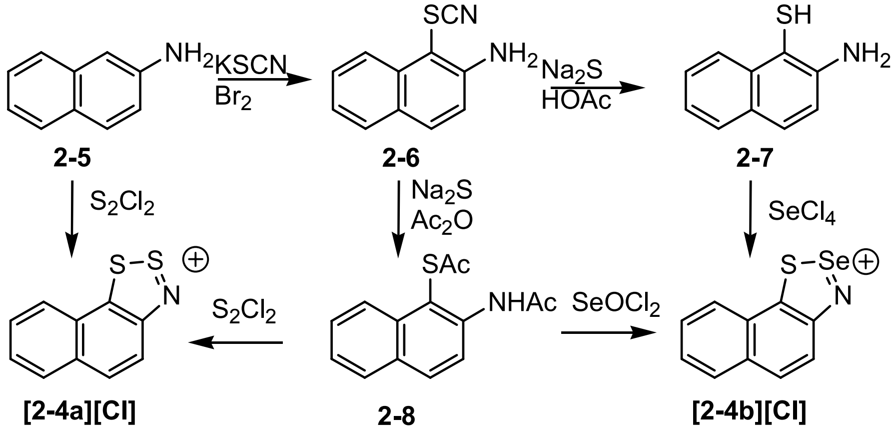

Scheme 2.1

In order to incorporate selenium at the 1-position of the naphthalene ring, and gain access to the frameworks of **2-4c** and **2-4d**, 2-aminonaphthalene-1-selenocyanate **2-9** was prepared by oxidative selenocyanation of 2-aminonaphthalene (**Scheme 2.2**). Based on our experience with the sulfur chemistry, and the success found with the *bis-N,S*-acetyl **2-8**, the selenol derivative was not prepared. Instead, **2-9** was hydrolysed and the resulting selenolate was quenched with a large excess of acetic anhydride, producing the bis-*N,Se*-acetyl derivative **2-11**. Like its sulfur analog **2-8**, compound **2-11** was stable in air and could be recrystallized from heptane. However, when the intermediate selenolate was quenched slowly with acetic anhydride, so that the pH was not allowed go below a value of 7, the *N*-acetyl diselenide **2-10** was produced. As expected the reaction of either **2-10** or **2-11** with excess sulfur monochloride afforded [**2-4c**][Cl] in good yield, and treatment of **2-11** with $SeOCl_2$ at room temperature in MeCN provided the desired diselenazolylium chloride [**2-4d**][Cl] in good yield. A more direct route to generating [**2-4d**][Cl] was found by reflux of 2-aminonaphthalene with $SeCl_4$ and Se, *i.e.*, by generating two equivalents of $SeCl_2$, at reflux. This reaction appears to be the Se analogue of the Herz cyclocondensation,[6] generating [**2-4d**][Cl] in satisfactory yield.

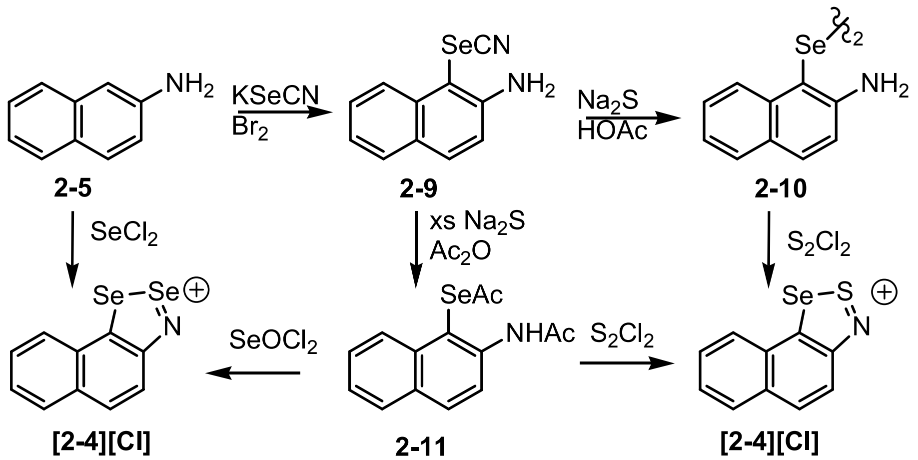

Scheme 2.2

The insoluble chloride salts [**2-4**][Cl] were readily converted, by treatment with $GaCl_3$ in MeCN, into the corresponding tetrachlorogallate salts, all of which were crystallized from chlorobenzene **(Scheme 2.3**). Bulk conversion to the radicals **2-4** was effected by chemical reduction of either the crude chloride salts with triphenylantimony or the tetrachlorogallate salts with decamethylferrocene. In the case of **2-4a** the resulting radical was sufficiently thermally stable and volatile to allow its purification by vacuum sublimation. The selenium containing radicals **2-4b**, **2-4c** and **2-4d**, however, were less thermally stable and purification of these materials by either sublimation or recrystallization methods was unsuccessful. All the radicals were nonetheless fully characterized by EPR spectroscopy and cyclic voltammetry.

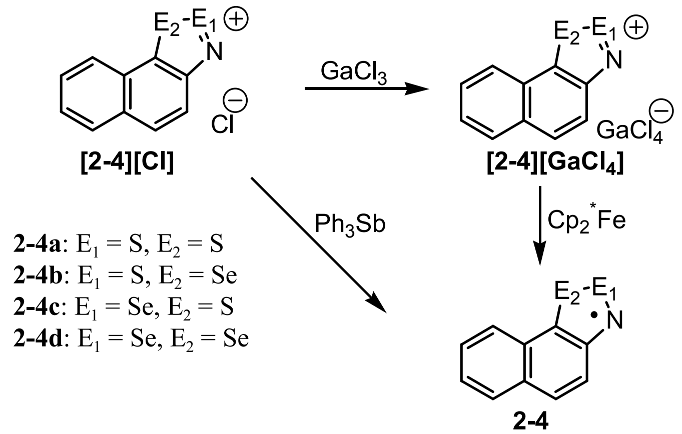

Scheme 2.3

2.3 Cyclic Voltammetry

As part of our ongoing investigations of the spin distributions in 1,2,3-DTA radicals and the effect of spin delocalization on their gas-phase disproportionation enthalpies ΔH_{disp} we have calculated, at the B3LYP/6-31G(d,p) level, the gas phase ionization potentials (*IP*) and electron affinities (*EA*) of **2-4**. We have also measured by cyclic voltammetry the half wave potentials for their oxidation and reduction and the results are summarized in **Table 2.1**. While reduction of the cation to the radical (the +1/0 process) is electrochemically reversible, subsequent reduction of the radical to the anion (the 0/−1 process) is not. This is a common feature of 1,2,3-DTA radicals, and reflects the ease of reductive cleavage of the S-S[7] (or S-N)[8] bond. Overall it is apparent that the naphthalene framework in **2-4** serves as an effective reservoir for spin density. As a result **2-4** is relatively soft, *i.e.*, has a low ΔH_{disp}, a feature which bodes well for this and related radicals in the design of molecular conductors, where a low disproportionation enthalpy and cell potential are critical for promoting a low on-site Coulomb repulsion U,[9,10,11] the energetic barrier to charge transport.

Table 2.1 Gas-Phase Ion Energetics (in eV) and Solution Half-Wave Cell Potentials (V).

Compound	**2-4a**	**2-4b**	**2-4c**	**2-4d**
IP^{a}	6.34	6.31	6.29	6.26
EA^{a}	1.12	1.18	1.15	1.20
$\Delta H_{\mathrm{disp}}{}^{b}$	5.22	5.13	5.15	5.06
$E_{1/2}(0/+1)^{c}$	0.207	0.223	0.214	0.243
$E_{1/2}(-1/0)^{c}$	0.91^{e}	0.86^{e}	0.93^{e}	0.84^{e}
$E_{\mathrm{cell}}{}^{c,d}$	1.09^{f}	1.05^{f}	1.14^{f}	1.05^{f}

[a] ΔSCF values (in eV) from B3LYP/6-31G(d,p) calculations run with full optimization within C_s symmetry. [b] $\Delta H_{disp} = IP - EA$. [c] In MeCN, ref. SCE. [d] $E_{\mathrm{cell}} = E_{½}(+1/0) - E_{½}(0/-1)$. [e] Irreversible behavior, E_{pc} value quoted. [f] E_{cell} estimated as $E_{\mathrm{pc}}(+1/0) - E_{\mathrm{pc}}(0/-1)$.

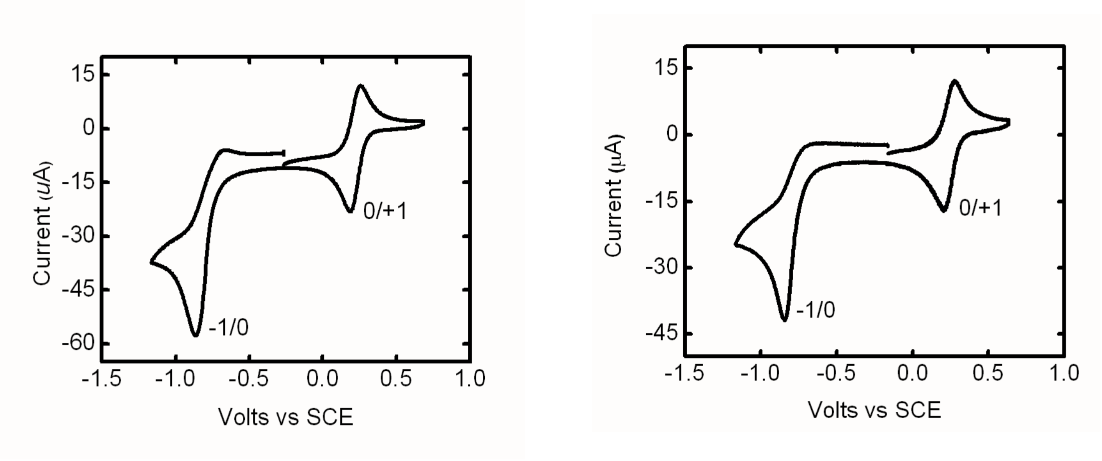

(a) (b)

Figure 2.2 CV scans of **2-4b** (a) and **2-4d** (b) in acetonitrile with [*n*-Bu_4N][PF_6] supporting electrolyte.

2.4 EPR Spectroscopy

The X-band EPR spectra of all four radicals **2-4** have been recorded in CH_2Cl_2 at room temperature. The experimental *g*-values and hyperfine coupling constants derived by simulation are provided in **Table 2.2**, along with those obtained by calculation (B3LYP/6-31G(d,p)). Taken collectively the data reveal a small but steady increase in *g*-value with increasing Se content, as well as a general loss of resolution. Both effects can be attributed to the expected greater spin-orbit contribution of Se. Thus, while the EPR signal of all four radicals is split into a three-line pattern arising from hyperfine coupling to the DTA nitrogen, only in the case of **2-4a** is additional fine structure discernible.

Table 2.2 EPR Data for **2-4**.

Compound	**2-4a**	**2-4b**	**2-4c**	**2-4d**
g-value	2.0081	2.0113	2.0190	2.027
a_N[a]	0.748	0.715	0.731	0.800
	(0.812)	(0.773)	(0.802)	(0.757)
$\rho(N)$[b]	0.414	0.416	0.406	0.407
$\rho(E_1)$[b]	0.139	0.139	0.142	0.144
$\rho(E_2)$[b]	0.216	0.201	0.217	0.206

[a] Experimental values in mT; computed values (in parenthesis) from B3LYP/6-31G(d,p) calculations with full optimization in C_s symmetry. [b] B3LYP/6-31G(d,p) mulliken spin densities ρ over the three-atom sequence E_1E_2N (E = S or Se).

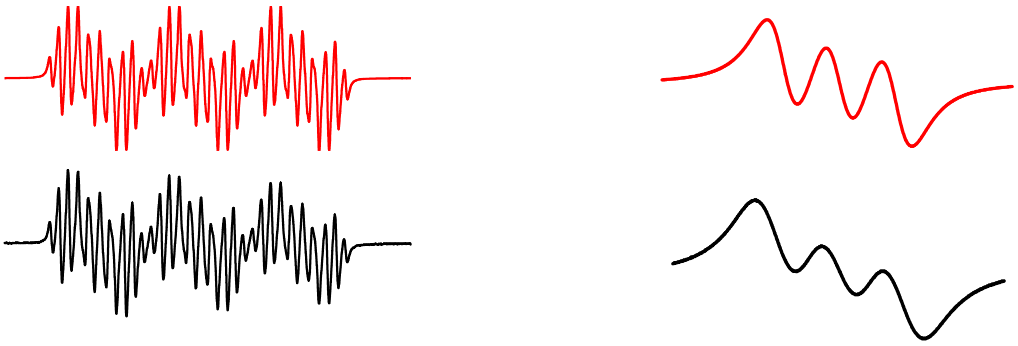

(a) (b)

Figure 2.3 EPR spectrum (SW = 3 mT) in CH_2Cl_2 (below) and simulation (above) for (a) **2-4a**; extracted a_H values: 0.178, 0.158, 0.014, 0.070, 0.069, 0.062 mT, and (b) **2-4d**; a_H values could not be extracted.

As can be seen in **Figure 2.3**, the spectrum of **2-4a** displays a rich overlay of hyperfine structure arising from coupling to the six distinct hydrogens on the naphthalene periphery. All six a_H values have been extracted by simulation, but given the similarity in the various a_H values in **2-4a** we have made no attempt to assign them to particular hydrogens. The value of a_N in **2-4a** is consistent with that seen for aromatic 1,2,3-dithiazolyls,[12] and there is a slight (but not steady) increase with Se incorporation. Similar trends have been observed elsewhere, and have been interpreted in terms of the electronegativity difference between S and Se.[13] In essence, Se, being more electropositive than S, appears to transfer spin density more strongly to nitrogen. These simple ideas are, however, not reflected by the results of spin density calculations, which indicate virtually no variation in the spin distribution as a result of S/Se exchange.

2.5 Crystal Structures

The crystal structures of the S-based radical **2-4a** and the gallate salt of the Se-based cation [**2-4d**][GaCl4] have been determined by single crystal X-ray diffraction at room temperature. Crystal data are compiled in **Table 2.3**, and ORTEP drawings of the molecular units, showing atom numbering, are illustrated in **Figure 2.4**. Summaries of pertinent intra- and intermolecular distances are provided in **Table 2.4**.

The crystal structure of [**2-4d**][$GaCl_4$] belongs to the triclinic space group $P\overline{1}$, and consists of [**2-4d**]$^+$ cations and [$GaCl_4$]$^-$ anions oriented so as to allow a pair of close intermolecular Cl---Se′ contacts. This kind of ion pairing is ubiquitous in related compounds.[14,15,16] At the molecular level the structure holds few surprises; the internal Se-Se and Se-N bond lengths are consistent with those seen in, for example, structures of 1,2,3,5-diselenadiazolylium cations.[3]

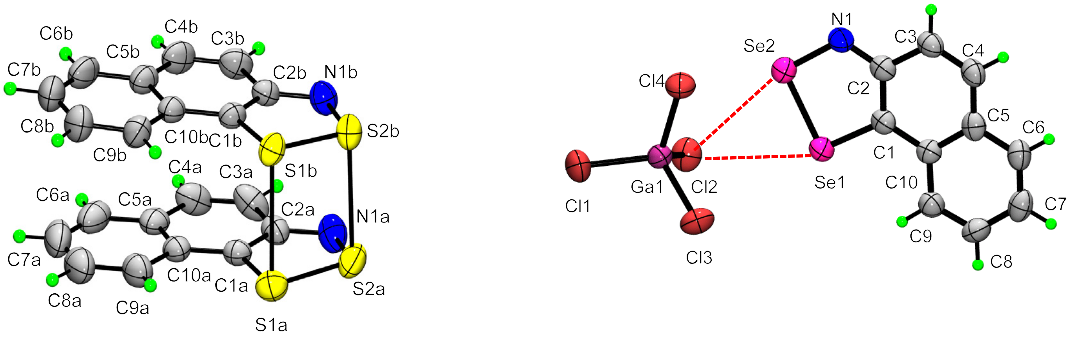

(a)

(b)

Figure 2.4 ORTEP drawings (50% probability ellipsoids) of **2-4a** (a) and [**2-4d**][$GaCl_4$] (b).

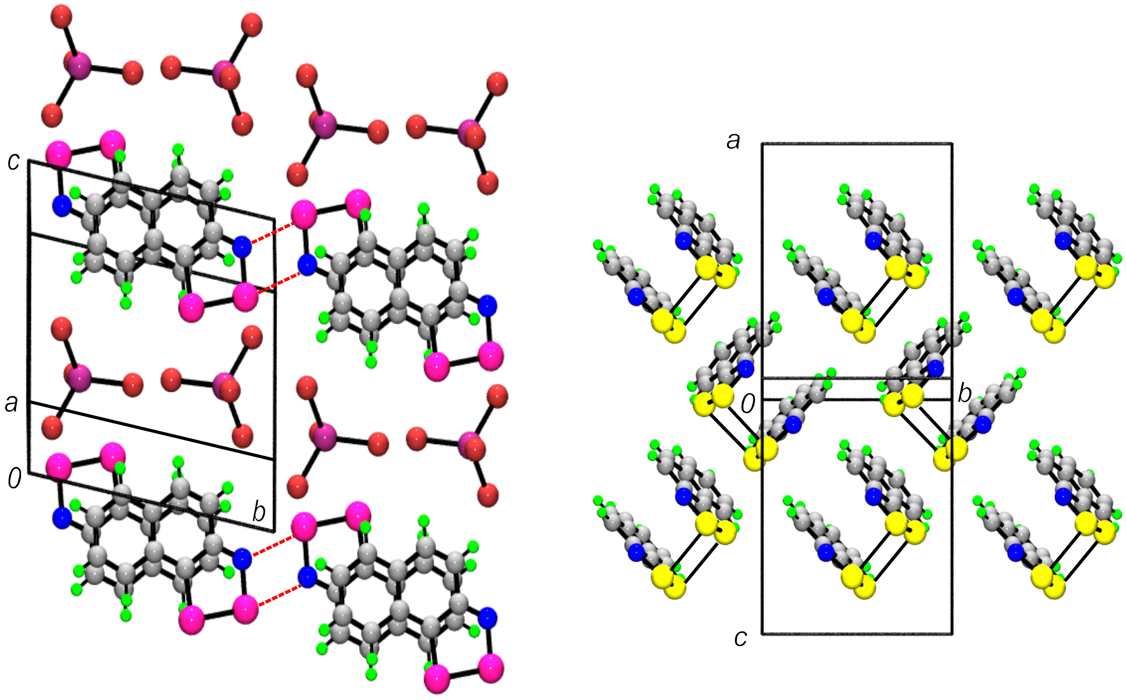

(a)

(b)

Figure 2.5 (a) Packing of [**2-4d**][$GaCl_4$]; (b) herringbone packing of **2-4a**.

Table 2.3 Crystallographic data for **2-4a** and [**2-4d**][$GaCl_4$].

Compound	**2-4a**[a,b]	[**2-4d**][$GaCl_4$][a]
formula	$C_{10}H_6NS_2$	$C_{10}H_6Cl_4GaNSe_2$
fw	204.29	509.60
a, Å	17.841(7)	6.690(4)
b, Å	8.702(3)	10.009(5)
c, Å	11.669(4)	10.109(5)
α, deg	90	100.109(5)
β, deg	104.286(6)	104.778(8)
γ, deg	90	92.760(6)
V, Å^3	1755.6(11)	745.5(6)
ρ (calcd), g cm^{-1}	1.546	2.270
space group	$P2_1/c$	$P\overline{1}$
Z	8	2
temp, K	293(2)	295(2)
μ, mm^{-1}	0.548	7.429
λ, Å	0.71073	0.71073
data/restraints/parameters	4040/0/283	3453/0/163
solution method	direct methods	direct methods
R, R_w (on F^2)	0.0434, 0.0934	0.0444, 0.1002

[a] data from reference 4; [b] data from reference 5.

The crystal packing of [**2-4d**][$GaCl_4$] is illustrated in **Figure 2.5a**. The cations, which are planar to within 0.021(4) Å, adopt a head-to-tail π-stacked arrangement running parallel to the *x*-direction. The interplanar separation within the head-to-tail pairs is 3.513(5) Å, while that between the pairs is 3.383(6) Å. The π-stacked arrays of cations are linked by centrosymmetric pairs of Se2---N1' contacts, thereby generating ribbons running along the *y* direction. These 4-center Se---N′ supramolecular synthons are likely to dominate the solid state structures of reduced materials, where ion pairing effects are no longer present.

The purely S-based radical **2-4a** sublimes at 60 °C/10^{-2} Torr without decomposition to afford highly crystalline bronze blocks belonging to the monoclinic space group $P2_1/c$. The crystals, which are diamagnetic by EPR, consist of cofacial dimers of **2-4a**, with 4 dimers per unit cell linked by two long (3.053(1) and3.309(1) Å) interannular S-S bonds. This mode of association, which is common in 1,2,3,5-DTDA chemistry, has not hitherto been observed for 1,2,3-DTAs. Indeed the propensity for dimerization of 1,2,3-DTAs seems to be less pronounced than it is for 1,2,3,5-DTDAs. For example, in the case of **2-5**[17] the room temperature structure consists of undimerized π-stacks, as do all the resonance stabilized *bis*-DTAs **2-1a**. Dimerization is not, however, without precedent. In **2-6**[18] the sterically bulky C_6F_5-substituent causes the two rings to rotate about their respective midpoints so that only one long S-S linkage (3.299(1) Å) remains, while in **2-7**[19] an unusual head-to-tail mode of association is found. In all cases, however, dimerized or undimerized, the internal S-S, S-N and S-C bonds show little variation, *i.e.*, association by whatever mode has very little effect on the electronic structures of the two halves. They are weakly associated π-radicals.

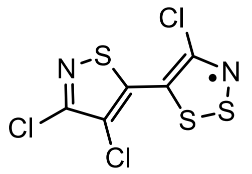

2-5

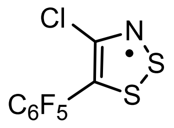

2-6

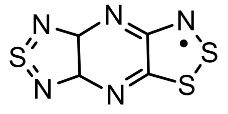

2-7

Dimers of **2-4a** do not form π-stacked arrays. Instead they adopt the closed packed herring-bone arrangement illustrated in **Figure 2.5b**. This structure is reminiscent of that found for the naphthalene based 1,3,2-DTA,[20] although in this latter case the radicals are not dimerized (at room temperature). Many polycyclic aromatics, *e.g.*, naphthalene[21] and anthracene,[22] demonstrate this type of packing, and the preference for it can be attributed to the opportunity that this geometry affords for the development of structure making "tilted T" CH---ring interactions.[23] By contrast, in radicals where the peripheral CH groups are replaced by N atoms, *e.g.*, **2-7**, the preference for close-packing is diminished, and a slipped π-stack structure prevails. The herringbone arrangement also allows for a clustering of the radical heads so as to maximize S---S′ and S---N′ contacts. As shown in **Figure 2.6**, pairs of dimers are linked centrosymmetically by 4-center S---N′ interactions d1and d2 (3.309(1) Å and 3.053(1) Å). Above and below these pairs are located two more dimers, linked by three close d3 - d5 (3.501(1) Å, 3.375(2) Å and 3.549(1) Å) contacts that are well within the van der Waals separation.[24]

Table 2.4 Intra- and Intermolecular Distances (Å) for [**2-4d**][GaCl$_4$] and **2-4a**.

[**2-4d**][GaCl$_4$]			
intramolecular		intermolecular	
Se1—Se	2.2900(12)	Se1---Cl2′	3.534 2)
Se2—N2	1.7667(4)	Se2---Cl3′	3.389(2)
Se1—C1	1.844(5)	Se1---Cl3′	3.578(4)
C1—C2	1.428(7)	Se2---N1′	2.874(4)
2-4a			
intramolecular		intermolecular	
S1a—S2a	2.083(1)	S1a---S1b′	3.309(1)
S1b—S2b	2.081(1)	S2a---S2b′	3.053(1)
S2a—N1a	1.614(3)		
S2b—N1b	1.7617(2)	S2a---N1b′ (d1)	3.162(3)
S1a—C1a	1.740(3)	S2b---N2a′ (d2)	3.113(3)
S1b—C1b	1.732(3)	S2a---S2b′ (d3)	3.501(1)
C1a—C2a	1.410(3)	S2a---S1b′ (d4)	3.375(2)
C1b—C2b	1.402(3)	S1a---S2b′ (d5)	3.549(1)

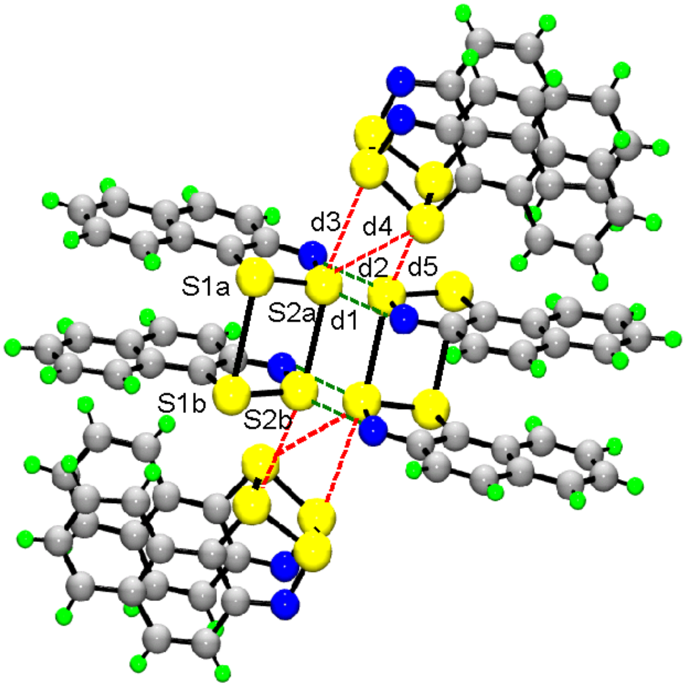

Figure 2.6 Interdimer contacts in **2-4a**. Intermolecular S---N′ and S---S′ contacts (dashed lines) are defined in **Table 2.4**.

2.6 Naphthalene Thione: A Chemical Curiosity

During my synthetic work with 2-aminonaphthalene, I also investigated the Herz chemistry[6] of 1-aminonaphthalene. As reported in my MSc dissertation,[5] the reaction of 1-aminonaphthalene (**2-12**) with sulfur halides[25] is inevitably accompanied by ring chlorination at the 4-position (**Scheme 2.3**). The reduction of [**2-13**][Cl] with triphenylantimony does not produce the corresponding radical **2-13**; instead, the only isolable material is the closed shell naphthalene-thione **2-14**. Furthermore, upon crystallization with DCE, two phases can be isolated (**Figure 2.7**). As part of my PhD work, I attempted to probe the redox behaviour of **2-14**.

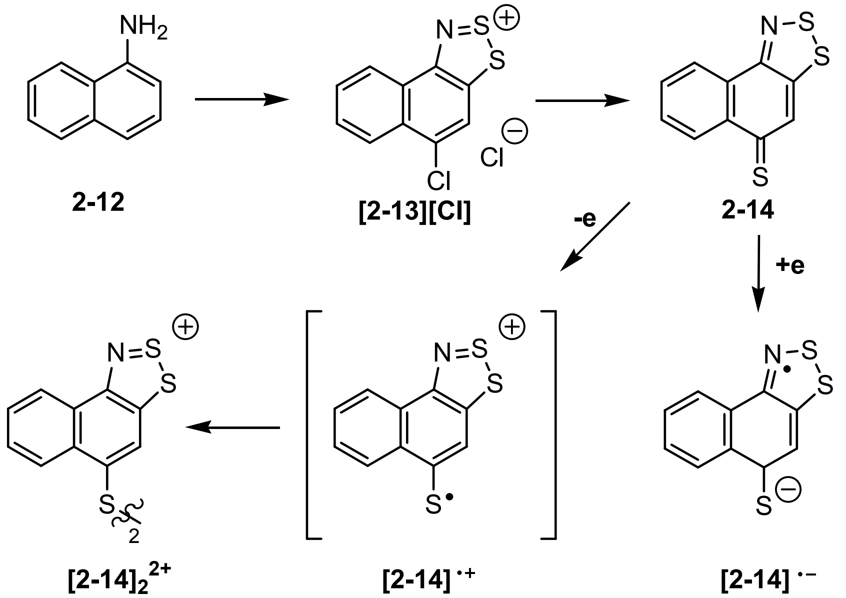

Scheme 2.3

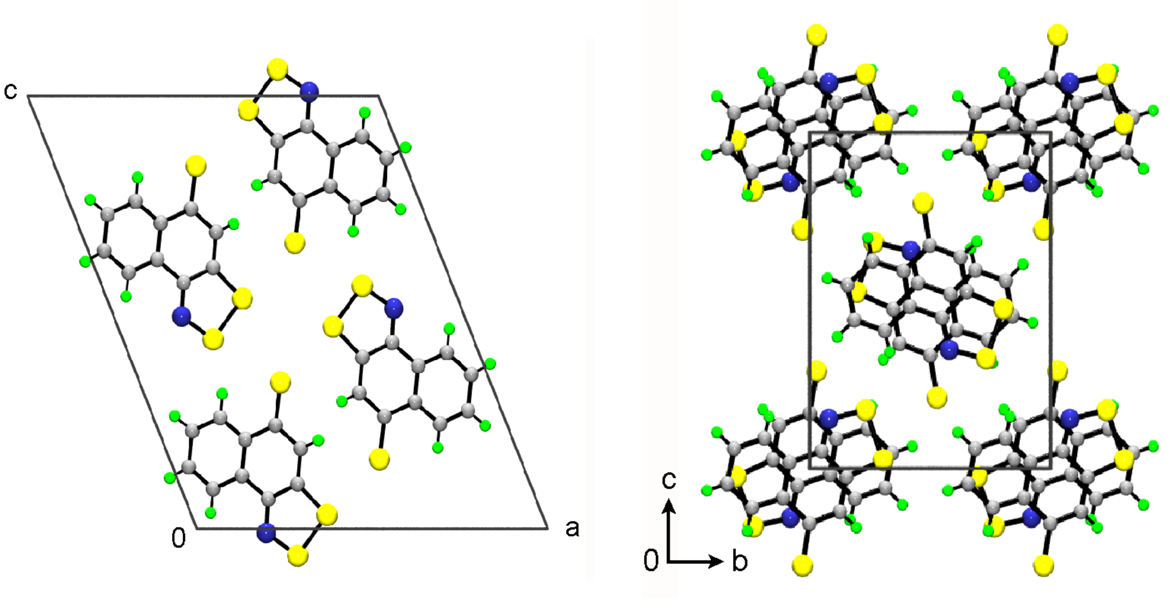

(a) (b)

Figure 2.7 Crystal structures of the α (a) and β phase (b) of **2-14**.

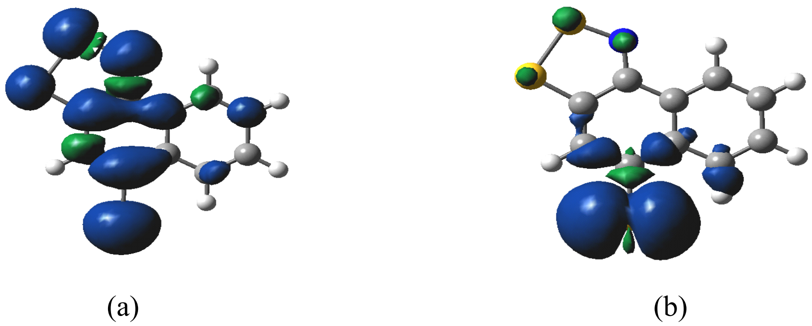
(a) (b)

Figure 2.8 Calculated spin density, at the B3LYP/6-31G(d,p) level, of (a) $[\mathbf{2\text{-}14}]^{\bullet-}$ and (b) $[\mathbf{2\text{-}14}]^{\bullet+}$.

DFT calculations, at the B3LYP/6-31G(d,p) level, on the $[\mathbf{2\text{-}14}]^{\bullet+}$ and $[\mathbf{2\text{-}14}]^{\bullet-}$ were undertaken in order to probe the unpaired electron spin distribution of the thione molecule, following oxidation and reduction of **2-14**. **Figure 2.8** illustrates the calculated spin density of both radical species. These calculations suggest that the reduced thione molecule, *i.e.*, the radical anion, gives rise to a delocalized electron spin distribution over the dithiazole ring (**Figure 2.8a**). Calculated hyperfine electron nuclear coupling ($a_N = 0.70$ mT) to the nitrogen nucleus further suggests that the experimental EPR spectrum would demonstrate a classic three-line pattern. In contrast, calculation of the radical cation $[\mathbf{2\text{-}14}]^{\bullet+}$ suggests that greater than 99% of the unpaired electron density resides on the terminal S of **2-14** (**Figure 2.8b**). Thus, if the radical cation could be generated electrochemically, a fast dimerization process, forming $[\mathbf{2\text{-}14}]_2^{2+}$, will likely follow.

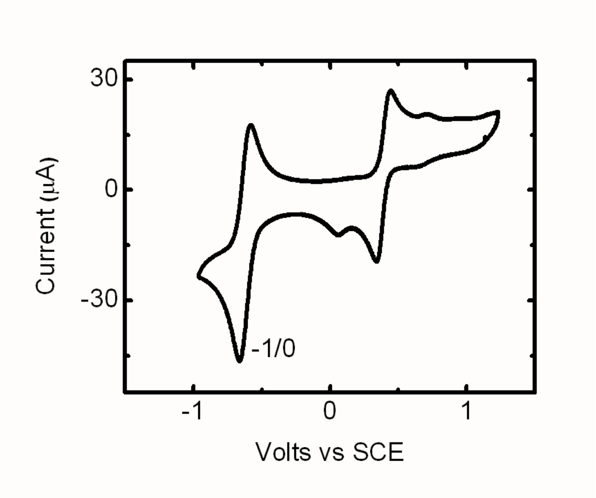

Figure 2.9 CV scans of **2-14** in acetonitrile with $[n\text{-Bu}_4\text{N}][\text{PF}_6]$ supporting electrolyte.

To further probe the redox chemistry of **2-14**, we have measured by cyclic voltammetry the half wave potentials for the oxidation and reduction of the compound (**Figure 2.9**). There is clear evidence of a reversible 0/-1 reduction wave at -0.617 V (vs SCE) indicative of a solution stable radical anion. Although there is a 0/+1 wave at 0.394 V (vs SCE), there appears to be a second species present upon oxidation at the anode, potentially signaling the onset of dimerization to [**2-14**]$_2^{2+}$.

Table 2.5 Calculated Spin Density and EPR Data

	[**2-4**]$^{\bullet-}$	[**2-4**]$^{\bullet+}$
ρ(N)[a]	0.363	-0.007
ρ(S1)[a]	0.051	-0.014
ρ(S2)[a]	0.094	-0.01
ρ(S3)[a]	0.251	0.998
g-value	2.0082	—
a_N[b]	0.679, (0.690)	— , (-0.011)

[a] B3LYP/6-31G(d,p) spin densities ρ over the three-atom sequence S_1S_2N and the thione unit. [b] Experimental values in mT; computed values (in parenthesis) from B3LYP/6-31G(d,p) calculations with full optimization in C_s symmetry.

As molecular modeling (and cyclic voltammetry experiments) suggest the existence of a spin paired dimer upon oxidation, a series of experiments were performed in attempts to isolate a dicationic species, *i.e.*, [**2-14**]$_2^{2+}$. Initially, one equivalent of $NOBF_4$ was added to **2-14** in MeCN, generating a deep red solution (**Scheme 2.3**). The solid formed upon solvent removal could be carefully crystallized in SO_2 affording thin fibrous orange needles. However, the needles were too small for X-ray structural determination. IR spectroscopy performed on the purified material indicated the presence of a BF_4 anion; EI mass spectroscopy was attempted, however the *m*/2 parent ion was not seen, likely due to the instability of the disulfide linker.

No attempt was made to synthesize and isolate the radical anion [**2-14**]$^{\bullet-}$. However, reduction of **2-14** in DCM with Cp_2Co was performed *in situ* in a quartz EPR tube. The resulting spectrum obtained (**Figure 2.10**) as well as the hyperfine coupling constants and *g*-values (acquired from spectral simulation) are listed in **Table 2.5**. As predicted by DFT calculations, a three-line pattern, due to N coupling, was observed and further, hyperfine naphthalene protons were also observed.

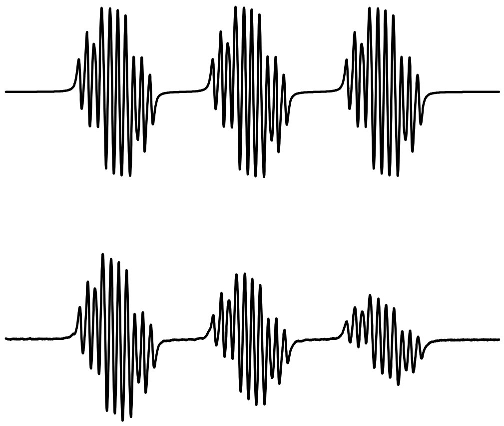

Figure 2.10 EPR spectrum (SW = 3 mT) in CH_2Cl_2 (below) and simulation (above) for [**2-14**]$^{\bullet-}$; extracted a_H values: 0.080, 0.071, 0.038, 0.041 mT.

2.7 Summary

Recent work on the use of resonance stabilized *bis*-DTAs[1] as building blocks for molecular conductors has underscored the need for the development of materials with increased bandwidth, a feature necessary to offset the high on-site Coulomb repulsion energy intrinsic to a neutral radical material.[26] Replacement of S by Se represents an appealing solution to this dilemma, but methods for incorporation of Se are rare.[27] The methodology demonstrated here for the naphthalene based systems, based on the use of acetylated aminothiols and aminoselenols as synthetic intermediates, provides efficient access to all possible combinations of S and Se based cations [**2-4**]$^{+}$. Within this manifold we have been able to isolate and characterize the S-based radical **2-4a**, but the corresponding Se-based variants **2-4b**, **2-4c** and **2-4-d** are less thermally stable.

As reported in my MSc dissertation,[25] the reduction of [**2-13**][Cl] has led to the unexpected isolation of the closed-shell thione **2-14**. Calculations suggest that the electron spin density associated with the radical anion [**2-14**]$^{\bullet-}$ will be distributed over the whole molecule, a feature that has been confirmed by *in situ* reduction of **2-14** with Cp_2Co. Calculations have also suggested that the spin density will primarily reside on the S appendage of **2-14** when oxidized to [**2-14**]$^{\bullet+}$. Attempts to isolate [**2-14**]$^{\bullet+}$ have resulted in the generation of the S-bridged dimer [**2-14**]$_2^{2+}$.

2.8 Experimental

Please see **Appendix A** for general methods and procedures.

Preparation of 2-aminonaphthalene:[28] Sodium bisulfite (5.00 g, 48.0 mmol) and 2-naphthol (5.13 g, 35.6 mmol) were placed in a Parr bomb pressure reactor containing 150 mL of ammonium hydroxide. The solution was heated at 200 °C for 3 h while stirring, at which time the reaction was cooled to room temperature. The following day the bomb reactor was opened and the solid was stirred into *ca.* 400 mL ice/water for 1 h. The white solid was collected by filtration, washed with cold water and dried in air; yield 4.66 g (32.5 mmol, 97%); mp 110 - 111 °C, lit. mp 111 - 113 °C. IR: 3396 (m), 3320 (m), 3205 (m), 3048 (w), 1629 (s), 1599 (m), 1511 (m), 1282 (m), 1224 (m), 1184 (w), 1124 (w), 1015 (w), 956 (w), 855 (m), 840 (m), 814 (s), 742 (s), 689 (w), 619 (w) cm^{-1}.

Preparation of 2-aminonaphthalene-1-thiocyanate 2-6 Liquid bromine (7.77 g, 48.6 mmol) was added dropwise over a period of 20 min to a stirred solution of potassium thiocyanate (17.0 g, 176. mmol) and 2-aminonaphthalene (12.6 g, 88.1 mmol) in 600 mL of degassed methanol at -78 °C (EtOH/dry ice). The resulting pink slurry was stirred for an additional 30 min, and the mixture poured onto 1 L of water. The off-white precipitate was filtered off and dried *in vacuo*. White needles of **2-6** were obtained by recrystallization from EtOH; yield 12.06 g (60.2 mmol, 68%); mp 152 - 154 °C (lit.[29] 150 - 154 °C). IR: 3466 (s), 3363 (s), 3189 (w), 3059 (w), 2154 (vs), 1624 (vs), 1559 (m), 1429 (s), 1398 (m), 1377 (m), 1293 (m), 1250 (m), 1210 (m), 1149 (s), 1031 (w), 978 (w), 867 (w), 821 (vs), 829 (s), 772 (s), 754 (s), 653 (m), 544 (w), 528 (w), 461 (m) cm^{-1}.

Preparation of 2-aminonapthalene-1-thiol 2-7 Thiocyanate **2-6** (5.0 g, 24.9 mmol) was added to solution of sodium sulfide nonahydrate (11.95 g, 50.0 mmol) in 250 mL degassed water, and the slurry heated at reflux for 2 h. The resulting yellow solution was filtered and neutralized with acetic acid to afford a yellow oil. The oil was extracted with 2 × 150 mL DCM, the extracts washed with 2 × 150 mL water and dried over magnesium sulfate. Removal of the solvent *in vacuo* gave a dark yellow air sensitive oil[30] that was not subjected to further purification; yield 3.93 g (22.4 mmol, 90%). IR: 3226 (w), 3061 (m), 2522 (m), 1952 (w), 1829 (w), 1800 (w), 1612 (s), 1566 (s), 1526 (m), 1417 (s), 1339 (m), 1320 (w), 1281 (m), 1235 (w), 1202 (w), 1142 (w), 1123 (w), 1036 (w), 947 (w), 873 (w), 820 (m), 678 (w), 586 (w) cm^{-1}.

Preparation of *S*-[2-(acetylamino)-1-naphthyl]ethanethiolate 2-8: Thiocyanate **2-6** (2.50 g, 12.4 mmol) was added to a solution of sodium sulfide nonahydrate (6.00 g, 24.8 mmol) in 200 mL degassed water, and the mixture gently heated to *ca.* 40 °C for 2 h. The solution was cooled and filtered, and excess acetic anhydride added to the filtrate. The resulting white precipitate was filtered off, washed with water and dried in *vacuo*; crude yield 2.39 g (9.22 mmol, 74%). White needles were grown from heptane; mp 153 - 154 °C. IR: 3336 (m), 1692 (s), 1620 (w), 1595 (w), 1566 (w), 1513 (w), 1497 (s), 1425 (m), 1376 (m), 1364 (w), 1327 (w), 1274 (m), 1229 (w), 1150 (w), 1121 (w), 1018 (w), 948 (m), 860 (w), 820 (m), 771 (w), 743 (m), 667 (w), 656 (w), 620 (m), 591 (w), 538 (w), 509 (w), 427 (w) cm^{-1}. ^1H NMR (δ, $CDCl_3$): 7.4-8.5 (m, 6H, aromatic), 2.49 (s, 3H, $NC(O)CH_3$), 2.23 (s, 3H, $SC(O)CH_3$). Anal. Calcd. for $C_{14}H_{13}NO_2S$: C, 64.84; H, 5.05; N, 5.40%. Found: C, 64.75; H, 5.05; N, 5.27%.

Preparation of 3H-naphtho[1,2-*d*][1,2,3]dithiazolylium chloride [2-4a][Cl] Method 1 Aminothiol **2-7** (4.00 g, 22.8 mmol) and S_2Cl_2 (15.4 g, 0.114 mol) were added to 150 mL of degassed DCE and the mixture heated at reflux for 1 h. The resulting red precipitate of [**7a**][Cl] was filtered off, washed with 2 × 75 mL DCM and dried *in vacuo*; yield 4.10 g (17.1 mmol, 75%). IR: 3069 (w), 1600 (m), 1492 (w), 1426 (w), 1333 (m), 1007 (w), 1150 (w), 1129 (w), 1042 (w), 972 (w), 882 (s), 821 (s), 765 (s), 729 (m), 564 (w), 542 (m), 494 (m), 412 (m) cm^{-1}. **Method 2** Excess of S_2Cl_2 (39.1 g , 0.290 mol) was slowly added to solution of 2-aminonaphthalene (8.30 g, 58.0 mmol) in 150 mL of DCE and the mixture heated at reflux for 4 h. The resulting red precipitate of [**7a**][Cl] was filtered off, washed with 2 × 200 mL DCM and dried *in vacuo*; yield 7.52 g (31.3 mmol, 54%). **Method 3** Excess S_2Cl_2 (1.30 g, 9.63 mmol) was added to a slurry of **2-8** (0.500 g, 1.93 mmol) in 50 mL degassed MeCN. The clear red solution which formed was gently heated (*ca.* 40 °C) for 2 h, and the resulting red precipitate of [**2-4a**][Cl] filtered off, washed with 3 × 50 mL DCM and dried *in vacuo*; yield 0.249 g (1.04 mmol, 54%).

Preparation of 3H-naphtho[1,2-*d*][1,2,3]dithiazolylium tetrachlorogallate [2-4a][$GaCl_4$] Gallium trichloride (1.90 g, 10.8 mmol) was added to a slurry of [**2-4a**][Cl] (2.37 g, 9.90 mmol) in 50 mL MeCN. The resulting orange solution was stirred for 10 min, filtered and the solvent flash distilled to leave an orange solid that was recrystallized from chlorobenzene as dark red platelets of [**2-4a**][$GaCl_4$] ; yield 3.32 g (7.97 mmol, 81%); dec >165 °C. IR: 3069 (w), 2725 (w), 2670 (w), 1602 (s), 1336 (w), 1165 (w), 1130 (w), 983 (w), 885 (s), 822 (s), 777 (m), 760 (m), 666 (m), 566 (w), 538 (m), 498 (w) cm^{-1}. Anal. Calcd. for $C_{10}H_6Cl_4GaNS_2$: C, 28.88; H, 1.45; N, 3.37%. Found: C, 29.07; H, 1.60; N, 3.14%.

Preparation of 3H-naphtho[1,2-*d*][1,2,3]dithiazolyl 2-4a Method 1 Decamethylferrocene (0.393 g, 1.20 mmol) and [**2-4a**][$GaCl_4$] (0.500 g, 1.20 mmol) were added to 15 mL degassed MeCN and the solution cooled to −20 °C overnight. The resulting black precipitate of **2-4a** was filtered off and dried *in vacuo*. The crude radical (0.221g, 1.08 mmol, 90%) was purified by vacuum sublimation in a three-zone temperature gradient furnace (90 - 30 °C /10^{-2} Torr) over a period of 3 days to give bronze blocks of **2-4a**, dec >120 °C. IR: 1603 (m), 1532 (w), 1495 (m), 1421 (m), 1326 (m), 1284 (w), 1250 (m), 1208 (m), 1183 (w), 1136 (m), 1126 (m), 1100 (w), 1081 (w), 1036 (m), 1014 (s), 966 (m), 856 (w), 888 (s), 817 (vs), 805 (s), 761 (m), 733 (s), 661 (s), 501 (m), 535 (m), 511 (m), 500 (s), 466 (s), 412 (m) cm^{-1}. Anal. Calcd. for $C_{10}H_6NS_2$: C, 58.79; H, 2.96; N, 6.86%. Found: C, 59.02; H, 3.15; N, 7.00%. **Method 2** Triphenylantimony (1.55 g, 4.39 mmol) was added to a slurry of [**2-4a**][Cl] (1.41 g, 5.86 mmol) in 15 mL MeCN and the resulting mixture stirred at reflux for 3 h, then filtered and cooled to −20 °C overnight. The resulting black precipitate was filtered off and pumped dried *in vacuo*. The crude radical (0.60 g, 52%) was sublimed as described above.

Preparation of 3H-naphtho[1,2-*d*][1,2,3]thiaselenazolylium chloride [2-4b][Cl] A solution of $SeOCl_2$ was prepared *in situ* by gently warming a slurry of SeO_2 (0.214 g, 1.93 mmol) and $SeCl_4$ (0.426 g, 1.93 mmol) in 40 mL MeCN until all solids dissolved. The mixture was cooled to room temperature and **2-8** (0.500 g, 1.93 mmol) added to give a clear red solution that was gently heated (*ca.* 40 °C) for 2 h. The resulting brown precipitate was filtered off, washed with 3 × 50 mL DCM and dried *in vacuo*; yield 0.400 g (1.40 mmol, 72%). IR: 3064 (w), 3047 (w), 1602 (s), 1593 (m), 1422 (m), 1326 (w), 1294 (w), 1267 (m), 1161 (w), 1140 (m), 1129 (m), 1052 (w), 1021 (w), 968 (w), 951 (w), 870 (m), 814 (s), 783 (w), 748 (s), 703 (m), 662 (m), 537 (s), 412 (m) cm^{-1}.

Preparation of 3H-naphtho[1,2-*d*][1,2,3]thiaselenazolylium tetrachlorogallate [2-4b][$GaCl_4$] Gallium trichloride (2.28 g, 12.9 mmol) was added to a slurry of [**2-4b**][Cl] (3.38 g, 11.8 mmol) in 50 mL MeCN and the resulting solution filtered. The solvent was then flash distilled to leave a dark orange crystalline mass that was recrystallized from chlorobenzene as dark brown needles of [**2-4b**][$GaCl_4$]; yield 4.08 g (8.81 mmol, 74.3%); dec >182 °C. IR: 3065 (w), 3050 (w), 1598 (s), 1592 (s), 1485 (m), 1427 (w), 1343 (m), 1330 (m), 1292 (w), 1264 (m), 1145 (m), 1133 (m), 1046 (w), 1006 (w), 975 (w), 886 (m), 817 (vs), 782 (s), 764 (s), 663 (s), 536 (s), 509 (m), 500 (w), 431 (m), 411 (m) cm^{-1}. Anal. Calcd. for $C_{10}H_6Cl_4GaNSSe$: C, 25.96; H, 1.31; N, 3.03%. Found: C, 25.92; H, 0.96; N, 2.81%.

Preparation of 2-aminonaphthalene-1-selenocyanate 2-9 Bromine (5.34 g, 33.4 mmol) was slowly added to a solution of potassium selenocyanate (9.62 g, 66.8 mmol) in 160 mL of degassed MeOH at -78 °C (EtOH/dry ice). To this mixture was slowly added a solution of 2-aminonaphthalene (4.79 g, 33.4 mmol) in 80 mL cold MeOH. The resulting mixture was warmed to room temperature and quenched with 500 mL water. The red precipitate (9.81 g) was filtered off and dried *in vacuo*. This crude product was extracted into 400 mL EtOH, the extract hot filtered and concentrated to dryness to leave an orange solid that was recrystallized from DCE as orange needles of **2-9**; yield 5.78 g (23.4 mmol, 70%); dec >134 °C. IR: 3464 (s), 3368 (s), 3230 (w), 2149 (vs), 1629 (s), 1499 (s), 1377 (m), 1348 (m), 1293 (m), 1244 (w), 1211 (s), 1161 (m), 1145 (m), 1027 (w), 964 (w), 858 (w), 814 (vs), 643 (w), 545 (w), 501 (w) cm^{-1}. Anal. Calcd. for $C_{11}H_8N_2Se$: C, 53.46; H, 3.26; N, 11.33%. Found: C, 53.54; H, 3.47; N, 11.19%.

Preparation of Se-[2-(acetylamino)-1-naphthyl]ethaneselenolate 2-11 Amino-selenocyanate **2-9** (2.45 g, 10.0 mmol) was added to a solution of sodium sulfide nonhydrate (4.78 g, 19.9 mmol) in 100 mL degassed water and the mixture gently heated at 40 °C for 90 min. The resulting yellow solution was filtered and cooled to 0 °C, whereupon excess acetic anhydride (*ca.* 10 mL) was quickly added. The white precipitate so produced was filtered off and dried in *vacuo*; crude yield 2.79 g (9.11 mmol, 92%). White needles of **2-11** were grown from heptane; mp 116 - 117 °C. IR: 3323 (m), 2724 (w), 1712 (vs), 1696 (m), 1667 (vs), 1618 (m), 1595 (s), 1566 (s), 1515 (m), 1499 (s), 1407 (m), 1326 (s), 1279 (s), 1257 (m), 1227 (w), 1164 (w), 1149 (w), 1135 (w), 1102 (vs), 1032 (w), 1017 (w), 940 (m), 863 (m), 819 (vs), 767 (s), 742 (s), 668 (m), 638 (m), 576 (vs), 529 (m), 503 (m), 467 (w), 418 (m) cm^{-1}. ^1H NMR (δ, $CDCl_3$): 7.4-8.5 (m, 6H, aromatic), 2.49 (s, 3H, $NC(O)CH_3$), 2.23 (s, 3H, $SeC(O)CH_3$). Anal. Calcd. for $C_{12}H_{11}NOSe$: C, 54.56; H, 4.20; N, 5.30%. Found: C, 54.71; H, 4.28; N, 5.34%.

Preparation of *N*-(1-{[2-(acetylamino)-1-naphthyl]diseleno}2-naphthyl)acetamide 2-10 Amino-selenocyanate **2-9** (1.00 g, 0.45 mmol) was added to a solution of sodium sulfide nonhydrate (1.95 g, 8.12

mmol) in 40 mL degassed water and the mixture gently heated at 40 °C for 30 min. The resulting yellow solution was filtered and cooled to 0 °C, whereupon acetic anhydride (*ca.* 1.5 mL) was carefully added until a neutral pH was reached. The orange precipitate was filtered off, washed with water and dried in *vacuo*; crude yield 1.20 g (2.28 mmol, 56%). Orange crystalline blocks of **2-10** were grown from DCE, mp 236 - 238 °C. IR: 3347 (m), 1686 (vs), 1615 (w), 1596 (m), 1561 (s), 1493 (s), 1428 (s), 1327 (s), 1327 (s), 1275 (m), 1253 (m), 1151 (w), 989 (w), 819 (s), 776 (m), 664 (w), 627 (w), 583 (m), 535 (w), 523 (w), 503 (w) cm^{-1}. ^1H NMR (δ, $CDCl_3$): 7.4-8.5 (m, 6H, aromatic), 1.34 (s, br, 3H, $NC(O)CH_3$). Anal. Calcd. for $C_{24}H_{20}N_2O_2Se_2$: C, 54.91; H, 4.28; N, 4.57%. Found: C, 55.14; H, 4.08; N, 4.73%.

Preparation of 3*H*-naphtho[1,2-*d*][1,2,3]selenathiazolylium chloride [2-4c][Cl] Method 1 Sulfur monochloride (2.20 g, 16.3 mmol) was injected into a degassed solution of **2-11** (0.500 g, 1.63 mmol) in 20 mL of DCE, and the mixture gently warmed for 4 h. The dark red precipitate of [**2-4c**][Cl] was filtered off, washed with 2 × 40 mL DCE and dried *in vacuo*; yield 0.235 g (0.820 mmol, 50 %). IR: 1602 (s), 1427 (m), 1339 (m), 1326 (m), 1308 (w), 1263 (m), 1211 (w), 1166 (m), 1123 (m), 964 (m), 884 (s), 804 (s), 771 (m), 751 (m), 667 (w), 650 (w), 558 (w), 526 (m), 480 (m) cm^{-1}. **Method 2** Sulfur monochloride (1.28 g, 9.50 mmol) was injected into a degassed solution of **2-10** (0.500 g, 0.950 mmol) in 30 mL of DCE, and the resulting mixture was gently heated for 4 h. The dark red precipitate of [**2-4c**][Cl] was filtered off and washed with 2 × 40 mL DCE and dried *in vacuo*; yield 0.264 g (0.921 mmol, 49 %).

Preparation of 3*H*-naphtho[1,2-*d*][1,2,3]selenathiazolylium tetrachlorogallate [2-4c][$GaCl_4$]: Gallium trichloride (0.202 g, 1.15 mmol) was added to a slurry of [**2-4c**][Cl] (0.274 g, 0.956 mmol) in 20 mL MeCN, the resulting red solution filtered and the solvent flash distilled from the filtrate to leave an orange crystalline mass. Bright red needles of [**2-4c**][$GaCl_4$] were grown from chlorobenzene; yield 0.265 g (0.574 mmol, 60%); dec > 120 °C. IR: 1601 (s), 1488 (m), 1426 (m), 1329 (m), 1314 (w), 1260 (m), 1214 (w), 1164 (w), 1126 (w), 965 (w), 892 (s), 879 (m), 819 (s), 777 (s), 757 (m), 667 (w), 650 (w), 532 (m), 480 (w) cm^{-1}. Anal. Calcd. for $C_{10}H_6Cl_4GaNSSe$: C, 25.96; H, 1.31; N, 3.03%. Found: C, 26.15; H, 1.12; N, 3.22%.

Preparation of 3*H*-naphtho[1,2-*d*][1,2,3]diselenazolylium chloride [2-4d][Cl] A solution of $SeOCl_2$ was prepared *in situ* by gently warming $SeCl_4$ (1.08 g, 4.90 mmol) and SeO_2 (0.544 g, 4.90 mmol) in 40 mL of degassed MeCN until all solids dissolved. The solution was cooled to room temperature and **2-11** (1.50 g, 4.90 mmol) added. The mixture was then stirred for 2.5 h and the resulting brown precipitate filtered off, washed with 3 × 40 mL DCE and dried *in vacuo*; yield 1.37 g (4.11 mmol, 84%). IR: 1601 (s), 1533 (w), 1420 (m), 1342 (m), 1306 (w), 1261 (m), 1217 (w), 1166 (m), 1145 (w), 1122 (m), 1041 (w), 996 (w), 965 (w), 874 (m), 804 (vs), 786 (m), 772 (m), 750 (m), 698 (m), 668 (w), 659 (w), 648 (w), 526 (m), 494 (w), 463 (m) cm^{-1}.

Preparation of 3*H*-naphtho[1,2-*d*][1,2,3]diselenazolylium tetrachlorogallate [2-4d][GaCl$_4$] Gallium trichloride (0.320 g, 1.82 mmol) was added to a slurry of [**2-4d**][Cl] (0.500 g, 1.52 mmol) in 30 mL MeCN. The resulting clear red solution was filtered, and the filtrate flash distilled to leave a dark brown crystalline mass. Dark purple needles of [**2-4d**][GaCl$_4$] were grown from chlorobenzene; yield 0.526 g (1.03 mmol, 69%); dec > 120 °C. IR: 2002 (w), 1842 (w), 1779 (w), 16.37 (w), 1599 (vs), 1483 (s), 1421 (s), 1410 (w), 1342 (m), 1328 (m), 1286 (w), 1259 (s), 1213 (w), 1167 (w), 1145 (m), 1128 (m), 1044 (w), 1002 (w), 979 (w), 881 (m), 814 (vs), 780 (s), 778 (s), 759 (s), 707 (s), 668 (w), 648 (m), 531 (m), 524 (m), 498 (w), 464 (m) cm^{-1}. Anal. Calcd. for $C_{10}H_6Cl_4GaNSe_2$: C, 23.57; H, 1.19; N, 2.75%. Found: C, 23.70; H, 1.30; N, 2.60%.

Generation of selenium based radicals 2-4b-d Bulk reduction of the gallate salts [**2-4b-d**][GaCl$_4$] with decamethylferrocene, as described above for [**2-4a**][GaCl$_4$], provided precipitates of the corresponding radicals **2-4b-d** in crude form. Attempts to purify these materials by recrystallization or sublimation were ineffective, inevitably leading to the extrusion of varying amounts of elemental selenium. For EPR purposes the radicals were conveniently generated by *in situ* reduction of a slurry of the appropriate chloride salt [**2-4b-d]**[Cl] with triphenylantimony in DCM.

Preparation of [2-13][Cl] Under a nitrogen atmosphere 1-aminonaphthalene (**2-12**; 15.0 g, 105 mmol) was dissolved in 500 mL of MeCN and cooled in an ice bath. Sulfur monochloride (14.1 g , 1.05 mol) was slowly added and the stirred solution was refluxed for 15 h. The resulting red precipitate was filtered, washed with 2 × 400 mL DCE and pumped dry; yield 27.7 g (101 mmol, 96.6%). IR: 3033 (m), 1789 (w), 1651 (w), 1604 (w), 1566 (s), 1524 (s), 1415 (m), 1317 (w), 1235 (s), 1199 (s), 1183 (m), 1161 (s), 1098 (w), 1037 (w), 994 (w), 971 (s), 898 (s), 880 (m), 770 (vs), 758 (s), 686 (s), 646 (w), 595 (w), 557 (m), 515 (m), 466 (w), 441 (w), 414 (m) cm^{-1}.

Preparation of 2-14 Under a nitrogen atmosphere, [**2-13**][Cl] (1.0 g, 3.65 mmol) and triphenylantimony (2.5 g, 7.08 mmol) were added to degassed acetonitrile. The solution was refluxed for 3 h, hot filtered and the filtrate placed in the freezer for 1 hour. The resulting precipitate was filtered off, washed with 10 mL MeCN and dried *in vacuo*. Both α- and β-phases could be grown in chlorobenzene or toluene; yield 217 mg (0.909 mmol, 25.0%); dec. >180 °C. α-phase IR: 3017 (w), 2725 (w), 1604 (w), 1565 (m), 1323 (m), 1297 (m), 1286 (w), 1243 (m), 1168 (m), 1152 (m), 1136 (m), 1082 (m), 1033 (m), 1000 (m), 955 (w), 878 (m), 872 (w), 850 (m), 844 (w), 774 (m), 764 (s), 744 (s), 677 (s), 646 (w), 606 (w), 552 (w), 501 (w), 477 (m) cm^{-1}. β-phase IR: 3017 (w), 2725 (w), 1604 (w), 1565 (m), 1323 (m), 1297 (m), 1286 (w), 1243 (m), 1191 (w), 1168 (m), 1152 (m), 1136 (m), 1082 (m), 1033 (m), 995 (m), 982 (w), 959 (w), 883 (m), 878 (s), 849 (w), 821 (w), 766 (s), 744 (s), 680 (m), 668 (w), 644 (w), 614 (w), 549 (m), 501 (w), 484 (m), 466 (w) cm^{-1}. Anal. Calcd. for $C_{10}H_5NS_3$: C, 50.31; H, 2.11; N, 5.87%. Found: C, 50.22; H, 2.06; N, 5.59%. MS (*m/e*) 235 (M^+, 100%), 191 ($[C_{10}H_7S_2]^+$, 18%), 170 ($[C_{10}H_5NS]^+$, 10%).

Preparation of $[$2-14$]_2[BF_4]_2$ Nitrosonium tetrafluoroborate (0.205 g, 1.76 mmol) was added to a slurry of **2-14** (0.375 g, 1.60 mmol) in 25 mL MeCN, the resulting red solution was stirred for 20 min, filtered and the solvent flash distilled from the filtrate to leave a red powder. Bright orange needles of [**2-14**]$_2[BF_4]_2$ were grown from SO_2; yield 0.120 g (1.00 mmol, 64%); dec > 120 °C. IR: 1567 (s), 1515 (s), 1340 (s), 1239 (m), 1184 (m), 1162 (m), 1114 (w), 965 (s), 891 (m), 862 (w), 766 (w), 735 (m), 684 (m), 646 (w), 592 (w), 565 (w), 548 (w), 533 (w), 512 (w) cm^{-1}.

Chapter 3

X-ray Crystallography: Structural Problems in Dithiazolyl Materials

3.1 Introduction

The previous chapter introduced synthetic methodologies to generate three Se-containing isomers of a naphthalene-based dithazole. Following this work, our research group has synthesized and isolated many resonance stabilized Se-based *bis*-DTA radicals **3-1**. The synthetic projects that I have been involved with are presented in **Chapters 4 - 6** and represent the bulk of my PhD research. However I have also spent a large portion of my time studying X-ray crystallography and I have worked hard to understand and apply advanced crystallographic technologies in order to solve/refine difficult crystallographic data. This chapter presents four projects where "non-standard" techniques were required to elucidate the solid-state structures of our radical materials.

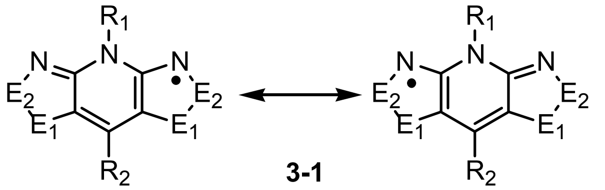

3-1

3-1a: E_1 = S, E_2 = S
3-1b: E_1 = S, E_2 = Se
3-1c: E_1 = Se, E_2 = S
3-1d: E_1 = Se, E_2 = Se

The first two projects employ powder X-ray diffraction (PXRD) methods to model the solid-state structures of **3-1b** (R_1 = Me, R_2 = Ph) and **3-1d** (R_1 = Me, R_2 = H). In both cases we were not able to grow crystals of high enough quality for single crystal X-ray studies. Although the PXRD technique has been used successfully in the determination of closed shell molecular compounds, it is a far from standard methodology for air-sensitive radicals. The third project probes the temperature dependence of a pyrazine-based *bis*-DTA radical. Data was collected at 298 K, 123 K and 88 K in order to elucidate subtle structural changes. The final project discusses the refinement of twinned crystals of a monofunctional DTA radical and demonstrates the outcome of twinned structural data that was solved/refined both with and without a twin law.

3.2 Preparation and Structural Characterization of PhBPTSMe[1]

The first isolated *bis*-thiaselenazolyl was **3-1b** (R_1 = Me, Et, R_2 = H).[2] Reduction of the cation in solution afforded the desired radical; however, the radicals associated into σ-bonded dimers [**3-1b**]$_2$ (R_1 = Me, Et, R_2 = H) in the solid state. At this point it was questioned whether or not all Se radicals would form σ-dimers. One possible solution to this problem was to try and prevent the dimerization through isostructural mapping. For example, if a direct substitution of Se into a S radical could be induced to have the same mode of packing in the solid state (*i.e.*, the same space group and orientation of the radical in the unit cell), then dimerization would be inhibited. This concept was first explored in **3-1a** (R_1 = Et, R_2 = Ph),[3] which crystallizes in the high symmetry space group $P3_121$and contains radicals which congregate about a 3_1 axes. Most importantly, the central S atom is locked into a tight packing arrangement about the 3_1 screw axis, thus prohibiting direct S---S′ lateral contacts like those seen in **3-1a** (R_1 = Me, Et, R_2 = H). In previous work, my coworker was able to show that **3-1b** (R_1 = Et, R_2 = Ph) crystallizes in $P3_221$ and is isostructural with **3-1a** (R_1 = Et, R_2 = Ph),[4,†] and thus, σ-dimer formation was inhibited. In order to make a full comparison of the effects of Se substitution in **3-1b** (R_1 = Me, Et; R_2 = Ph), we made a full investigation of the radical **3-1b** (PhBPTSMe; R_1 = Me, R_2 = Ph), however, we were unable to grow X-ray quality single crystals and in order to elucidate the structure, we turned to the use of powder crystallography.

3.2.1 Synthesis of 3-1b (R_1 = Me, R_2 = Ph)

Synthesis of **3-1b** (R_1 = Me, R_2 = Ph) followed the direct Se substitution route,[5] which will be discussed at length in **Section 4.2.2**. Thus [**3-1a**][OTf] (R_1 = Me, R_2 = Ph)[3] was readily converted into [**3-1b**][OTf] (R_1 = Me, R_2 = Ph, **Scheme 3.1**) by treatment with SeO_2 in HOAc. Bulk powder samples of **3-1b** (R_1 = Me, Et; R_2 = Ph) were generated by reduction of the triflate salt with decamethylferrocene (DMFc) in MeCN. Structural modeling from powder data requires a sample that is free of impurities in order to limit

---

[†] The radical **3-1b** (R_1 = Et, R_2 = Ph) crystallizes in space group $P3_221$ and is the mirror image of **3-1a** (R_1 = Me, R_2 = Ph) which crystallizes in $P3_121$. The radicals are not chiral and presumably, crystallization of both compounds produces a mixture of both enantiomers. By chance, a crystal that crystallizes in $P3_221$ was selected for structural analysis.

unnecessary background noise and/or peaks associated with the impurity. To ensure a high level of purity we reacted pure, degassed solutions of [**3-1b**][OTf] (R_1 = Me, R_2 = Ph) and DMFc, taking care to pass the less soluble cation solution through a filter frit. Particle size (which decreases preferred orientation of the crystallites) was minimized by stirring the solution, thus encouraging nucleation and immediate precipitation.

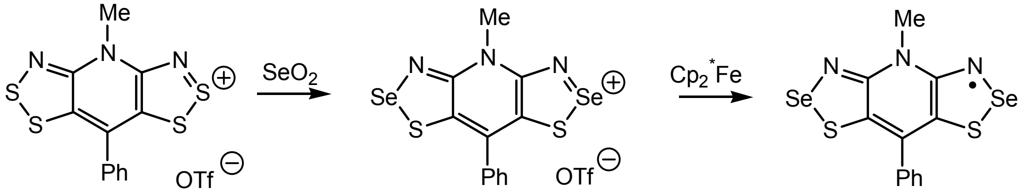

Scheme 3-1

3.2.2 Crystal Structure

A powdered sample **3-1b** (R_1 = Me, R_2 = Ph) was generated by gently grinding 60 mg of sample with a mortar and pestle. The sample was loaded into an aluminum sample holder which was rotated during data collection. The diffraction pattern was collected at ambient temperature and under regular laboratory conditions on a X-ray powder diffractometer with a position sensitive detector using Cu $K_{\alpha 1}$ radiation (λ = 1.54056 Å). The total 2θ range was 0.28 - 112.684° (the limit of the detector), measured in steps of 0.029°. Powder diffractograms were collected at 15 minute intervals so that we could monitor material degradation. It was found that a 3 hour collection was optimal. After 3 hours the material appeared to degrade, *i.e.*, the intensity of the background noise increased dramatically.

The powder data was indexed by the program Taup[6] (as part of the Crysfire software package)[7] to give the following trigonal cell: a = 15.6837 Å, c = 4.6811 Å, with a figure of merit (FOM) of 16.64. Most importantly, when these data were compared to the unit-cell parameters for **3-1a** (R_1 = Me, R_2 = Ph)[3] and **3-1b** (R_1 = Et, R_2 = Ph),[4] it was evident that the three compounds were isostructural (save for chirality), and the space group $P3_121$ was arbitrarily selected. To test the cell metrics and space group assignment, the program FOX[8] was used to obtain a direct space, *ab initio* model (the direct space solution obtained was not used in subsequent steps; it was used for analytical purposes only). The cell parameters (obtained from

Taup), the powder diffraction data, and the (modified) atomic coordinates of **3-1a** (R_1 = Me, R_2 = Ph) were entered into the program. The rigid refinement option was selected (the geometry of the molecule was not optimized; only translations of the rigid body were allowed) and the software gave a satisfactory output, including a well correlated simulation of the experimental powder diffractogram and a convincing real-space orientation of the three radicals in the unit cell. Furthermore, the real-space solution appeared to be isostructural to that of **3-1a** (R_1 = Me, R_2 = Ph) (**Figure 3.1b**). Thus the space group $P3_121$ was assigned to **3-1b** (R_1 = Me, R_2 = Ph). Starting with the atomic coordinates for **3-1a** (R_1 = Me, R_2 = Ph) as the initial model, the structure was refined by Rietveld methods[9] using the GSAS program package.[10] Data were refined from 5.0 to 60.0°, and all atoms, including hydrogens, were used in the refinement. Isotropic displacement parameters were refined for all non-hydrogen atoms, excluding ligand (Me and Ph) carbons, which were assigned a value of 0.025. The final Rietveld refinement gave agreement indices wR_p = 7.79% and R_p = 5.73% (**Figure 3.2**; **Table 3.1**).

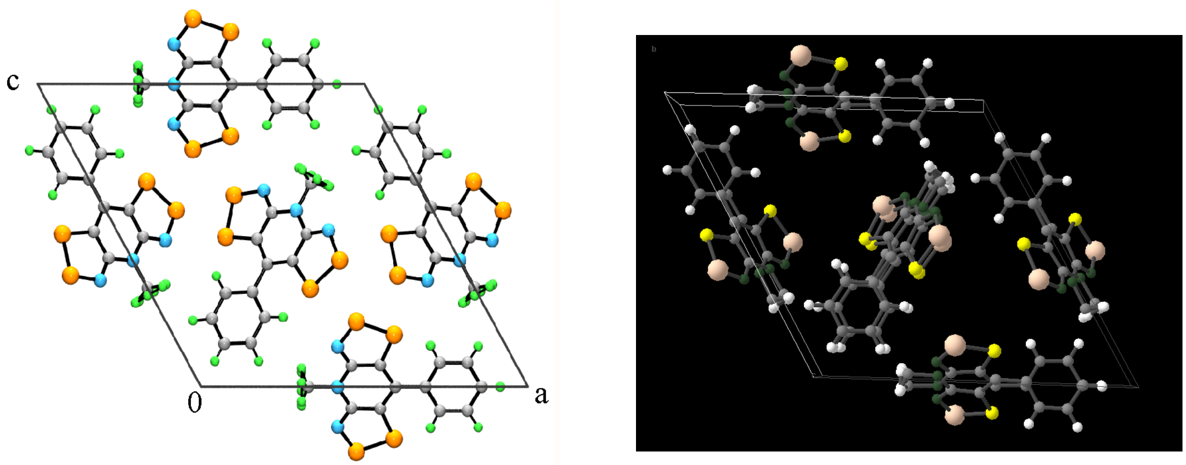

(a) (b)

Figure 3.1 (a) Unit cell drawing of **3-1a** (R_1 = Me, R_2 = Ph) viewed down the *z*-direction and (b) FOX simulation of **3-1b** (R_1 = Me, R_2 = Ph).

Table 3.1 Crystallographic Data for **3-1a** (R_1 = Me, R_2 = Ph) and **3-1b** (R_1 = Me, Et; R_2 = Ph).

Compound[a]	**3-1a** (R_1 = Me)[3]	**3-1b** (R_1 = Et)[4]	**3-1b** (R_1 = Me)[b]
a, Å	16.183(3)	15.733(6)	15.672(1)
c, Å	4.295(1)	4.973(3)	4.689(1)
V, Å^3	974.0(4)	1066.0(9)	997.4(1)
ρ(calcd), g cm^{-1}	1.649	2.011	2.094
space group	$P3_121$	$P3_221$	$P3_121$
Z	3	3	3
temp, K	293(2)	298(2)	293(2)
μ, mm^{-1}	0.718	5.487	—
λ, Å	0.71073	0.71073	1.54059
data/restraints/parameters	1500/0/99	1401/12/106	—
solution method	direct methods	direct methods	powder data[c]
R, R_w (on F^2)	0.0363, 0.0725	0.0605, 0.1242	0.0573, 0.079[d]
d1, Å	3.287(1)	3.397(2)	3.3442(1) [e]
d2, Å	3.507(1)	3.673(2)	3.653(1)
d3, Å	3.467(1)	3.595(3)	3.500(1)
ϕ, deg	12.1	—	12.1

[a] For both **3-1a** and **3-1b** R_2 = Ph. [b] This work. [c] Starting model taken from **3-1a** (R_1 = Me). [d] R_p and wR_p respectively from the Rietveld refinement. [e] These are Se---Se′ contacts; the others listed for this molecule are Se---S′ contacts.

Crystal data and intermolecular contacts are provided in **Table 3.1** and two views of the resulting structure are shown in **Figures 3.3** and **3.4**. The appearance of the unit cell of **3-1b** (R_1 = Me, R_2 = Ph) (**Figure 3.3**) is virtually identical to that previously observed for **3-1b** (R_1 = Et, R_2 = Ph) and **3-1a** (R_1 = Me, R_2 = Ph). Most notable at the molecular level is the fact that neither of the Se-based radicals are dimerized. Furthermore, the steric influence of the ligands, *i.e.*, the nesting effect of the Me/Et (R_1) and Ph (R_2) groups about the three-fold screw axis, produces a pinwheel-like clustering of the radicals (**Figure 3.3**) which militates against the lateral approach of the radicals and consequent formation of a σ-bonded dimer like that seen in **3-1b** (R_1 = Me, Et, R_2 = H). In all three trigonal structures the tricyclic framework of the radicals is not planar. There is a slight ruffling of the terminal five-membered rings to produce a propeller-like distortion about the 2-fold axis on which the molecules are located. Values of the dihedral angle ϕ between the two terminal rings are listed in **Table 3.1**.

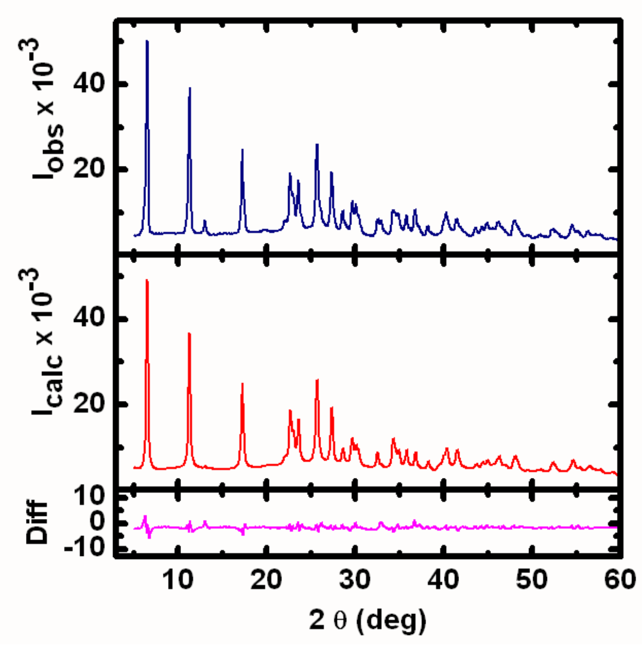

Figure 3.2 Experimental and calculated X-ray powder pattern for **3-1b** (R_1 = Me, R_2 = Ph).

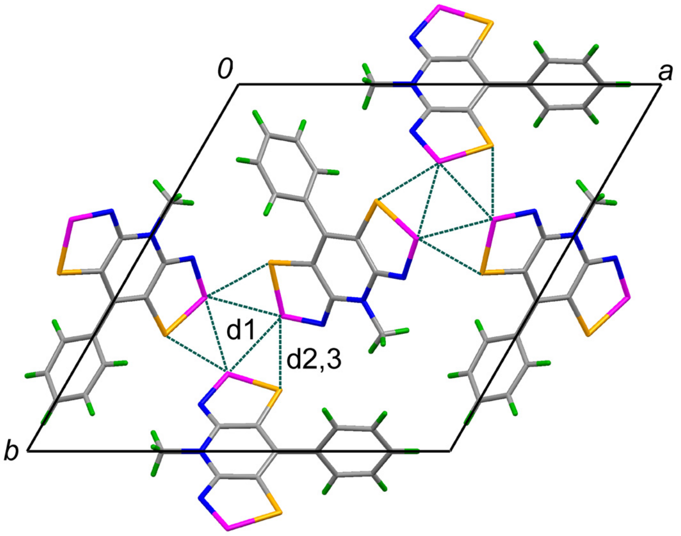

Figure 3.3 Unit cell drawing of **3-1b** (R_1 = Me, R_2 = Ph); intermolecular contacts d1 - d3 are defined in **Table 3.1**.

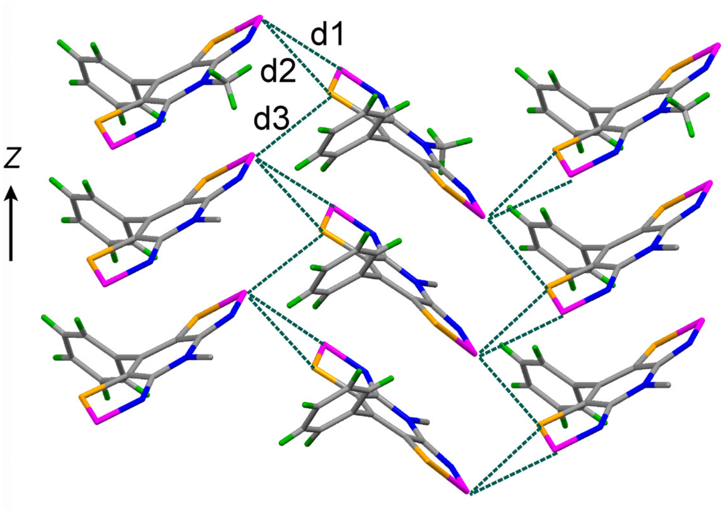

Figure 3.4 Herringbone π-stacking of **3-1b** (R_1 = Me, R_2 = Ph).

Viewed from the side, the π-stacks are locked into herringbone arrays (**Figure 3.4**) interconnected by a series of close intermolecular chalcogen-chalcogen contacts d1 - d3 (defined in **Table 3.1**) that lace the radical termini together about the three-fold screw axis. All of these distances are well within the expected van der Waals separations for S---S′ and S---Se′ and Se---Se′.[17] In addition the contacts found in **3-1b** (R_1 = Me, R_2 = Ph) are significantly shorter than those seen in **3-1a** (R_1 = Me, R_2 = Ph). Collectively, they lead to well developed 2-dimensional network of lattice-wide interactions transverse to the stacking direction. One interesting note is that **3-1a** (R_1 = Et, R_2 = Ph), which was reported with this work,[1] is not isostructural with the others, crystallizing in the $P\overline{1}$ space group.

3.2.3 Band Structure and Conductivity

In order to compare the extent of intermolecular electronic interactions in the three isostructural radicals **3-1a** (R_1 = Me, R_2 = Ph)) and **3-1b** (R_1 = Me, Et; R_2 = Ph) we have performed a series of EHT band structure calculations. The results are summarized in **Figure 3.5**, which shows the dispersion of the crystal orbitals (COs) arising from the three SOMOs in the respective unit cells, plotted from Γ (0, 0, 0) to Z (0, 0, ½) of the reciprocal cell, a direction which can be associated with the interactions along the stacking axis in real space. Also shown in **Figure 3.5** are the bandwidths *W*, estimated in terms of the energetic spread of the crystal orbitals over the range of reciprocal space under consideration.

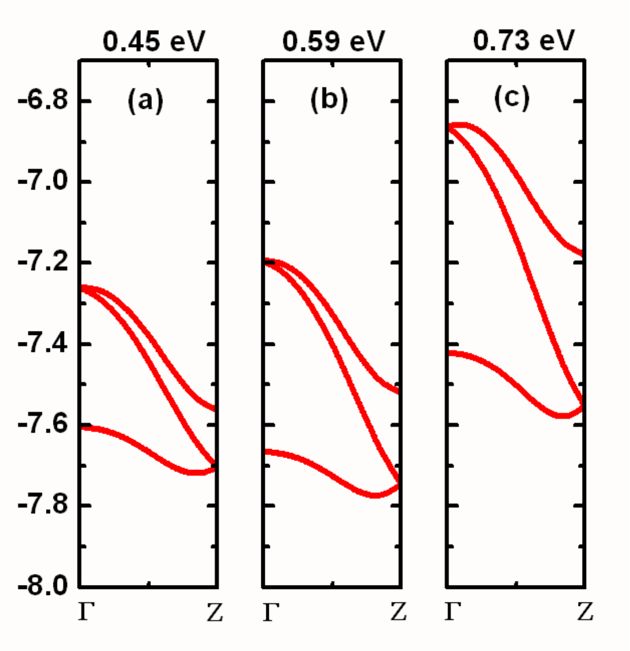

Figure 3.5 EHT band dispersion of SOMO-based crystal orbitals of (a) **3-1a**, (b) **3-1b** (R_1 = Et; R_2 = Ph) and (c) **3-1b** (R_1 = Me; R_2 = Ph). The resultant bandwidths *W* (in eV) are also shown.

The trend of the three isostructural radicals **3-1a** (R_1 = Me, R_2 = Ph) and **3-1b** (R_1 = Me, Et; R_2 = Ph) can be easily rationalized. First, there is an increase in *W* from **3-1a** and **3-1b** (R_1 = Me, R_2 = Ph) of *ca.* 60%, *i.e.*, replacement of S by Se has the desired effect, as the heavier chalcogen affords stronger intermolecular overlap and hence increased *W* along the stacking direction. Second, the difference in *W* between the two Se-based radicals demonstrates the detrimental effect of steric bulk of the organic ligands, *i.e.*, their ability to keep the interacting radicals apart. In this instance the replacement of an ethyl group by a methyl group leads to a 20% increase in *W*.

Preliminary two-probe pressed pellet conductivity measurements on the S-only compound **3-1a** (R_1 = Me, R_2 = Ph) indicated a room temperature conductivity σ_{RT} of *ca.* 10^{-7} S cm^{-1}. More detailed four-probe variable temperature measurements were carried out on the two Se-containing radicals **3-1b** (R_1 = Me, Et; R_2 = Ph), the results of which are illustrated graphically in **Figure 3.6**.[†] The ambient temperature conductivities σ(300 K) of the two compounds are 7.4×10^{-6} S cm^{-1} for R_1 = Et and 3.3×10^{-5} S cm^{-1} for R_1 = Me, indicative of the beneficial effect of Se incorporation. In addition, while the conductivities remain activated, there is a marked decrease in the thermal activation energy E_{act} of 0.32 eV (R_1 = Et) and 0.29 eV (R_1 = Me) relative to all-S based radical **3-1a** (R_1 = Me, R_2 = Ph).

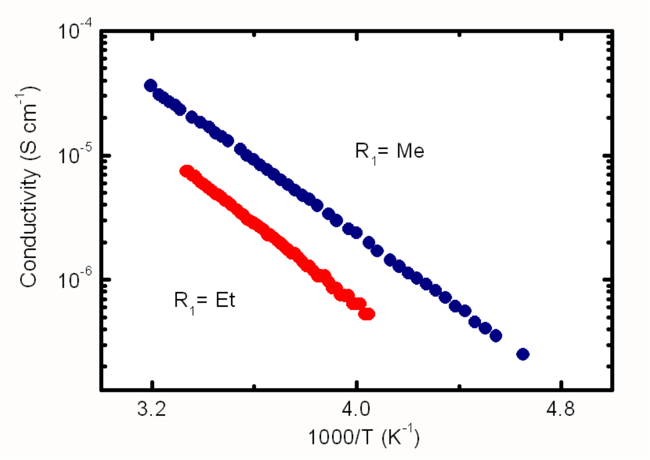

Figure 3.6 Conductivity of **4-1b** (R_1 = Me, Et; R_2 = Ph) as a function of inverse temperature.

Internal comparison of the performance of the two Se radicals reveals a trend heralded in the band calculations described above. The methyl derivative, with its more compact structure and higher electronic bandwidth, displays a higher conductivity and lower activation energy than the ethyl compound, a conclusion that underscores the importance of packing efficiency and close intermolecular interactions on conductivity. The present results illustrate that replacement of the ethyl group by a methyl effects a smaller improvement which may be ascribed to the effect of "chemical pressure", *i.e.*, a more efficient packing occasioned by the removal of steric constraints.

[†] Pressed pellet conductivities are 0.5 orders of magnitude smaller than single crystal conductivities.

3.3 The First Selenazyl Family[11]

With the success of powder crystallography work on **3-1b** (R_1 = Me, R_2 = Ph), we turned to a similar problem, where PXRD was required to elucidate the structure of the all Se-containing analogue of **3-1a** (R_1 = Me, R_2 = H). Se substitution into the DTA rings of **3-1a** (R_1 = Me, R_2 = H)gives rise to four possible isomers, however, as stated above we had recently shown that the generation of Se as in **3-1b** (R_1 = Me, Et; R_2 = H) leads to the σ-dimer **3-2** (R_1 = Me, R_2 = H) and at the time of publication we had not been able to access the other two family members **3-1c** and **3-1d** (R_1 = Me, R_2 = H). Thus our goal was to generate **3-1c** and **3-1d** (R_1 = Me, R_2 = H) as an isostructural set so that we could probe the direct effect of Se incorporation on the electrical conductivity of these materials.

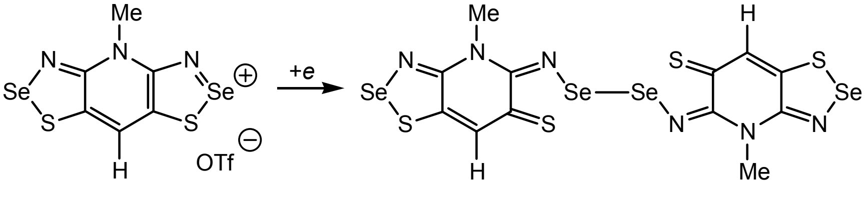

[3-1b][OTF]

3-2

Scheme 3.2

Crystals of **3-1c** (R_1 = Me, R_2 = H) suitable for single crystal X-ray analysis were grown by slow diffusion of a degassed solution of [**3-1c**][OTf] (R_1 = Me, R_2 = H) in MeCN into an equally degassed solution of octamethylferrocene (OMFc) in MeCN. Single crystal data and intermolecular contacts are compiled in **Table 3.2**. In contrast, all attempts to grow single crystals of **3-1d** (R_1 = Me, R_2 = H) failed. However, bulk microcrystalline material could be generated *via* reaction of degassed solutions of **3-1d** (R_1 = Me, R_2 = H) in MeCN and OMFc in MeCN, and once again, we turned to Rietveld methods to model the solid-state structure. The same powder X-ray methods described in **Section 3.2.2** were applied to the structural modeling of **3-1d** (R_1 = Me, R_2 = H). Thus, a powdered sample (*ca.* 60 mg) of **3-1d** (R_1 = Me, R_2 = H) was loaded into an aluminum sample holder and was rotated during data collection. The diffraction pattern was collected on a X-ray powder diffractometer with a position sensitive detector (INEL) at ambient temperature using Cu $K_{\alpha 1}$ radiation (λ = 1.54056 Å). The total 2θ range was 0.279 - 109.812 °, measured in steps of 0.029 ° over a period of 19 h. The powder diffraction pattern (see below) was indexed by the program Treor90[12] to give the following orthorhombic cell: a = 18.500, b = 12.0823, c = 4.16670 Å. When the cell parameters were compared to those of **3-1a** and **3-1c** (R_1 = Me, R_2 = H) it was evident that the three compounds were isostructural, and the space group $P2_12_12_1$ was assigned to **3-1d** (R_1 = Me, R_2 = H). Starting with the coordinates for **3-1a** (R_1 = Me, R_2 = H), the structure was refined by Rietveld methods[9] using the GSAS[10] program package. Data were refined from 5.0 - 62.5 ° and all atoms, including hydrogens, were used in the refinement. Atomic positions and isotropic displacement parameters were refined for all Se atoms. The final Rietveld refinement gave agreement indices $wR_p = 0.0782$ and $R_p = 0.0629$.

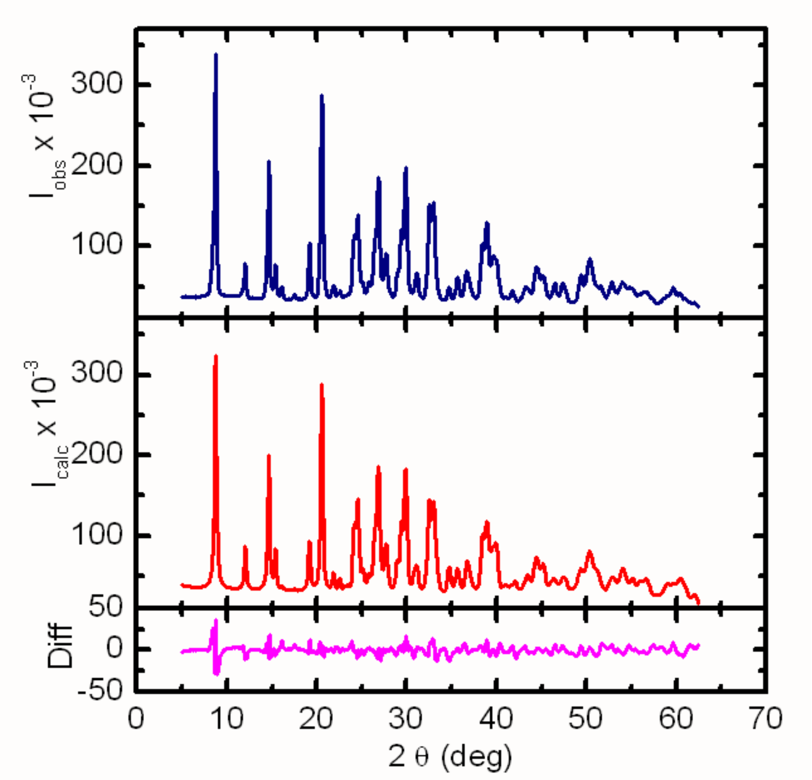

Figure 3.7 Experimental and calculated X-ray powder pattern for **3-1d** (R_1 = Me, R_2 = H).

Table 3.2 Crystal Data for **3-1a**, **3-1c** and **3-1d**.

Compound[a]	**3-1a**[13]	**3-1c**[b]	**3-1d**[b]
a, Å	3.9626(10)	4.1107(1)	4.199(5)
b, Å	11.962(3)	11.795(1)	12.181(13)
c, Å	18.262(5)	18.652(1)	18.64(2)
V, Å^3	865.6(4)	904.40(1)	953.1(18)
ρ(calcd), g cm^{-1}	1.890	2.489	3.024
space group	$P2_12_12_1$	$P2_12_12_1$	$P2_12_12_1$
Z	4	4	4
Temp, K	298(2)	298(2)	298(2)
μ, mm^{-1}	1.044	14.154	—
λ, Å	0.71073	1.54178	1.54056
data/restraints/parameters	977/0/134	1588/0/123	—
solution method	direct methods	direct methods	powder data[c]
R, R_w (on F^2)	0.0338, 0.0597	0.0213, 0.0579	0.0629, 0.0782[d]
d1, Å	3.371(1)	3.494(1)	3.479(3)
d2, Å	3.666(1)	3.604(1)	3.692(3)
d3, Å	3.745(1)	3.790(1)	3.834(3)
d4, Å	3.437(1)	3.473(1)	3.561(3)
d5, Å	3.394(1)	3.314(1)	3.335(3)

[a] For both **3-1a**, **3-1c** and **3-1d** R_1 = Me, R_2 = H. [b] This work. [c] Starting model taken from **3-1a** (R_1 = Me, R_2 = H). [d] R_p and wR_p respectively from the Rietveld refinement.

A drawing of the unit cell of **3-1d** (R_1 = Me, R_2 = H) is shown in **Figure 3.8**. **Table 3.2** provides the unit cell parameters of the three isostructural radicals and also provides a summary of the pertinent intermolecular E---E′ contacts (E = S, Se). In contrast to **3-1b** (R_1 = Me, R_2 = H), which associates in the solid state as laterally Se-Se -bonded dimers (**3-2**), all three radicals **3-1a, 3-1c** and **3-1d** (R_1 = Me, R_2 = H) crystallize in an undimerized fashion, the discrete radicals packing in slipped π-stack arrays along the *x*-direction (**Figure 3.8b**). These arrays are linked into ribbons running parallel to the *z*-direction by a series of close E---E′ contacts d1 - d3. In addition, there are two E---E′ interactions d4 and d5 that bridge neighboring ribbons along the *y*-direction. Collectively, this network of intermolecular interactions generates a closely knit and relatively 3-dimensional electronic structure.

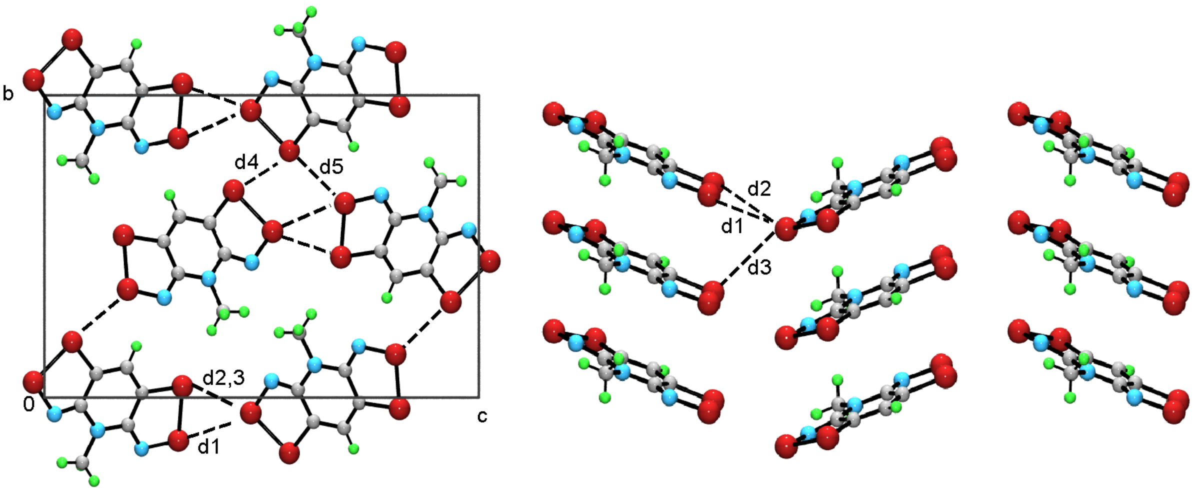

(a) **(b)**

Figure 3.8 Unit cell of **3-1d** (R_1 = Me, R_2 = H) viewed down the *x*-direction (a) and along the *z*-direction (b).

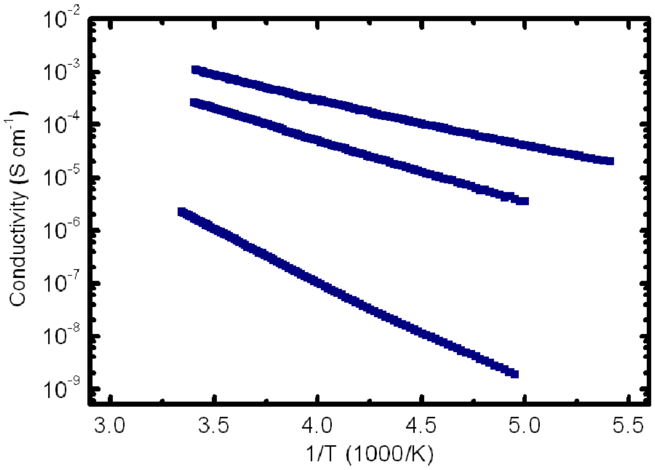

Figure 3.9 Conductivity of **4-1a** (bottom), **4-1c** (middle) and **4-1d** (top; R_1 = Me, Et; R_2 = H) as a function of inverse temperature.

Previous four-probe single-crystal conductivity (σ) measurements on **3-1a** (R_1 = Me, R_2 = H) as a function of temperature indicated Mott insulator behaviour, with a room-temperature conductivity (σ_{RT}) =

2×10^{-6} S cm^{-1} and thermal activation energy E_{act} = 0.41 eV. The results of four-probe pressed pellet measurements on **3-1c** and **3-1d** (R_1 = Me, R_2 = H) are illustrated in **Figure 3.9.** Sequential incorporation of Se leads to progressive improvement in the conductivity, with (295 K) = 3×10^{-4} and 1×10^{-3} S cm^{-1} for **3-1c** and **3-1d** (R_1 = Me, R_2 = H) respectively. At the same time, the value of E_{act} is reduced to 0.24 eV and 0.17 eV for **3-1c** and **3-1d** (R_1 = Me, R_2 = H) .

Upon completion of this project, it was apparent that Se incorporation into all positions of a *bis*-DTA ring was possible. Although early work showed that **3-1b** (R_1 = Me, R_2 = H) forms the dimer **3-2**, we were later able to demonstrate that **3-1a**, **3-1c** and **3-1d** (R_1 = Me, R_2 = H) belong to an isostructural set in which dimerization is inhibited. This allowed a direct comparison of the changes in conductivity occasioned by the direct replacement of S by Se. From this study we have observed a drastic increase in σ_{RT} and a decrease in thermal E_{act} as compared to the all-S *bis*-DTA material.[13]

3.4 BPzMe: Temperature-Dependent Crystallography[14]

As mentioned in **Chapter 1**, all *bis*-DTA radicals based on **3-1a** form slipped π-stacks in the solid state. This is due to the steric effects of the exocyclic R_1 and R_2 ligands which militate against the formation of superimposed π-stacks (**Figure 3.10a**). Overall, the slippage causes a decrease in the bandwidth (*W*) of the material. Increased *W* may be realized through (i) the incorporation of Se into the *bis*-DTA framework (see **Section 1.7**), or (ii) the removal of one bulky ligand, *i.e.* the generation of **3-3**, thus decreasing the steric interaction of the radicals. Through this latter strategy, the hope is to generate an ABABAB π-stack[15] (**Figure 3.10b**), potentially maximizing the orbital interactions of the radicals, hence increasing *W*.

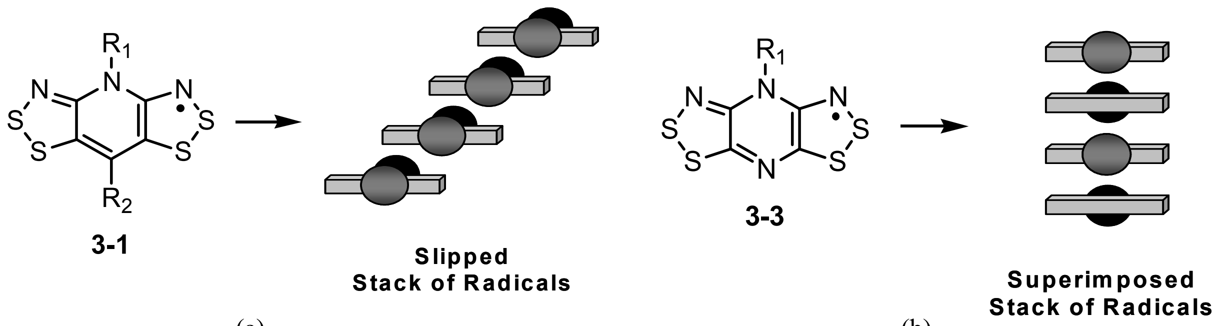

(a) (b)

Figure 3.10 Slipped π-stack of *bis*-DTA radicals (a) and a π-stack of pyrizine-based DTA radicals (b).

Recently my colleagues isolated a *bis*-DTA radical based on a pyrazine backbone (BPzMe; **3-3**, R_1 = Me) and single crystal structural data were collected at 295 K and 123 K. The structure, which contains discrete radicals in a ABABAB π-stack motif, could be solved and satisfactorily refined in the space group *Cmca* at *both* temperatures. However, variable temperature magnetic data obtained for this compound conflicted with the structural data.

A plot of χ_P versus temperature (after correction for diamagnetic contributions)[16] for compound **3-3** is presented in **Figure 3.11**. At 300 K, $\chi_p = 277 \times 10^{-6}$ emu K mol^{-1} suggesting the onset of weak paramagnetism. However, upon cooling the susceptibility slowly decreases, reaching a minimum value of 101×10^{-6} emu K mol^{-1}. Further cooling leads to a rapid increase in χ_p, indicative of paramagnetic lattice defects.[†] Also illustrated in **Figure 3.11** is a plot of χT versus temperature. At 300 K, the value of χT reaches 0.09 emu K mol^{-1}, corresponding to a spin defect concentration of approximately 25% of that expected (0.375 emu K mol^{-1}) for a Curie paramagnet with $S = ½$ and $g = 2$. Upon cooling, χT gradually decreases, reaching a constant of 2 % below 100 K. This residual paramagnetism amounts to the contribution of the defect electrons to the total moment.

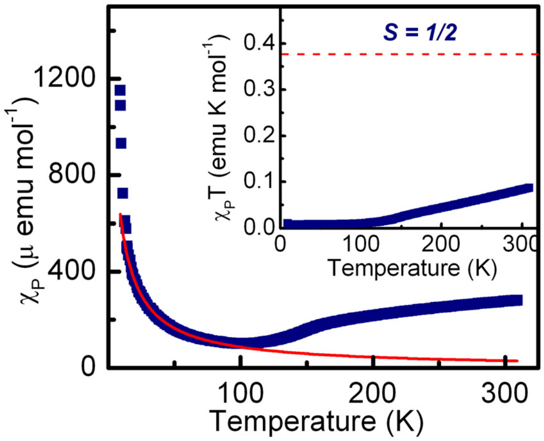

Figure 3.11 Plots of χ_P and χ_PT (inset) versus T for **3-3** (R = Me).

[†] Between 12 - 81 K, the paramagnetism due to lattice defects can be adequately fitted by a Curie-Weiss function affording $C = 0.0091$ emu K mol^{-1} and $\theta = -5.1$ K.

The magnetic susceptibility data for **3-3** suggests a dimerized radical array below 100 K that, upon heating, slowly uncouples affording a 25% spin defect concentration. However, it appears that the initial structural refinements in *Cmca* at 295 K and 123 K for **3-3** (R_1 = Me) do not adequately describe the charge transport properties of the bulk material, *i.e.*, the low temperature structure does not demonstrate a radical dimerization mode, and thus an in-depth investigation of the structural properties of **3-3** was required.

3.4.2 Crystallography

With the magnetic measurements in hand, we began to probe carefully the structural data to determine if a phase transition was present at low temperatures. To help identify the presence of a phase transition, a third data set was collected at 88 K, a temperature that gives rise to a minimum value for χT. The crystal data is presented in **Table 3.3** and ORTEP drawings are reported in **Figure 3.12.**

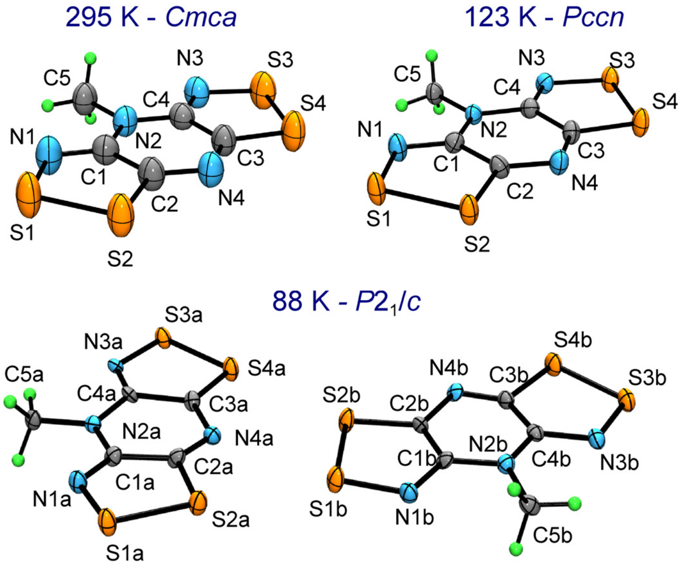

Figure 3.12 ORTEP drawings (50% probability ellipsoids) of the asymmetric units of **3-3** (R_1 = Me) at 295 K, 123 K and 88 K, showing atom numbering schemes.

At 295 K the crystal structure of **3-3** (R = Me) belongs to the orthorhombic space group *Cmca*, and is based on arrays of evenly spaced radicals π-stacked along the *x*-direction. Within the molecular units, bond distances and angles are typical of a *bis*-DTA radical.[13] Two views of the crystal structure, showing the unit cell packing and the lateral S---S′ and S---N′ interactions (**Table 3.4**) between neighbouring molecules, are provided in **Figure 3.13**. There are eight radicals in the unit cell, all of which lie on crystallographic mirror planes at $x = 0$ and ½, with consecutive plates along the x-direction related by the a-glide at $z = ¼$ and ¾ so as to produce superimposed ABABAB arrays with an interplanar separation of $a/2$, or 3.347(2) Å. This arrangement (**Figure 3.14**) affords a series of intracolumnar S---S′ contacts (**Table 3.4**) up and down the π-stack which, although outside of the normal van der Waals range,[17] are well oriented for strong π-overlap. The c-glide operation at $y = ¼$ and ¾ generates pairs of dovetailed arrays of these stacks, the two halves of which are laced together by a network (**Figure 3.13** and **Table 3.4**) of ladder-like intercolumnar π-type S---S′ contacts (S1---S2′, S3---S3′ and S4---S4′) that extend lattice-wide along both the x- and z-directions. The packing of the radicals into double rows of interconnected π-stacks running parallel to the z-direction gives rise to the dovetailed motif shown in **Figure 3.13**. These double rows are then locked together by the 4-center σ-type centrosymmetric S3---N3′ interactions noted earlier. As a result of the absence of intermolecular S---S′ contacts, electronic communication in the y-direction is minimal.

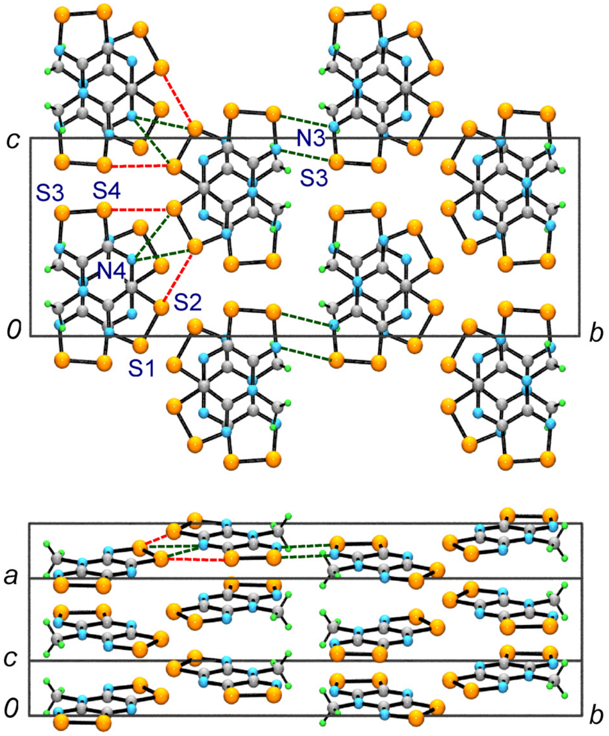

Figure 3.13 Two views of the *Cmca* unit cell of **3-3** (R_1 = Me) at 295 K. Lateral intermolecular S---S′contacts (in red) and S---N′ contacts (in green) are defined in **Table 3.4**.

Table 3.3 Crystal Data for **3-3** (R = Me).

Formula	$C_5H_3N_4S_4$	$C_5H_3N_4S_4$	$C_5H_3N_4S_4$
M	247.35	247.35	247.35
a, Å	9.244(2)	6.5456(6)	6.6488(2)
b, Å	6.5344(17)	9.2558(8)	27.2177(5)
c, Å	27.035(7)	27.040(2)	9.2797(2)
β, deg	90.004(4)	—	—
V, Å^3	1633.0(7)	1638.2(2)	1679.30(7)
ρ(calcd), g cm^{-1}	2.012	2.006	1.957
Space group	$P2_1/c$	*Pccn*	*Cmca*
Z	8	8	8
Temp, K	88(2)	123(2)	295(2)
μ, mm^{-1}	1.11	10.266	10.015
λ, Å	0.71073	1.54178	1.54178
Data/restraints/parameters	4040/182/236	1399/0/130	829/0/79
Solution Method	direct methods	direct methods	direct methods
R, R_w (on F^2)	0.0720, 0.1398	0.0570, 0.1617	0.0387, 0.1105

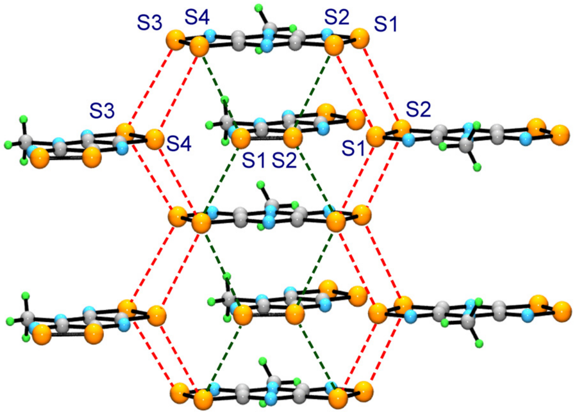

Figure 3.14 Alternating ABABAB π-stacks of **3-3** (R_1 = Me) at 295 K. Intrastack S---S′ contacts (in green) and interstack S---S′ contacts (in red) are defined in **Table 3.4**.

Table 3.4 Summary of Contacts and Angles in **3-3** (R_1 = Me).

Contacts[a]	88 K - $P2_1/c$	123 K - *Pccn*	295 K - *Cmca*
Lateral (σ)			
S1---S2′	3.270(7), 3.294(7)	3.281(2)	3.305(1)
S2---S4′	3.418(8), 3.449(7)	3.435(2)	3.466(1)
S1---N4′	3.179(14), 3.155(13)	3.166(5)	3.192(3)
S2---N4′	3.099(12), 3.193(11)	3.152(5)	3.179(3)
S3---N3′	3.023(13), 2.939(14)	2.989(4)	3.059(3)
Intrastack (π)			
S1---S4′	3.727(6), 3.928(6)	3.760(2)	3.865(1)
S4---S1′	3.750(6), 3.841(6)	3.874(2)	3.865(1)
S2---S2′	3.627(4), 4.001(4)	3.662(3), 3.966(3)	3.851(1)
Interstack (π)			
S1---S2′	3.667(7), 3.844(6)	3.697(2)	3.831(1)
S2---S1′	3.828(7), 3.684(6)	3.831(2)	3.831(1)
S3---S3′	4.120(3), 3.948(3)	3.964(3), 4.121(3)	4.093(1)
S4---S4′	4.079(4), 3.690(4)	3.723(3), 4.056(3)	3.936(1)
δ[b]	0.026(8), 0.024(8)	0.018(3)	0
ϕ[c]	2.6(3), 2.8(3)	2.17(10)	0

[a] Distances in Å. [b] Maximum deviation from the mean molecular plane. [c] Tilt angle of the perpendicular to mean plane from the stacking axis.[17]

Cooling crystals of **3-3** (R = Me) leads to small contractions in unit cell dimensions and intramolecular bond lengths. A second data set, collected at 123 K, could be solved and refined in the original space group (*Cmca*), but the asymmetry of the thermal ellipsoids (elongation along the stacking direction) apparent in the 295 K structure (**Figure 3.12**) was more serious, and a symmetry lowering distortion was considered. A full search over all observed reflections at 123 K revealed several violations of *C*-centering, and a change in Bravais lattice from *C* to *P*. In order to establish the temperature range for this transition, the evolution of the (4, 1, -1) reflection as a function of temperature (**Figure 3.15**) was monitored. At 153 K, this peak was absent, as expected ((h + k) odd) for a *C*-lattice. However, near 143 K, the reflection emerged from the background, thereby signaling the transition to a *P*-lattice. Further cooling to 123 K led to an increase in intensity of this peak. Subsequent evaluation of the systematic absences of the 123 K data in a primitive orthorhombic setting allowed us to conclude that the correct space group is *Pccn*, and the structure reported here is based on that assignment.

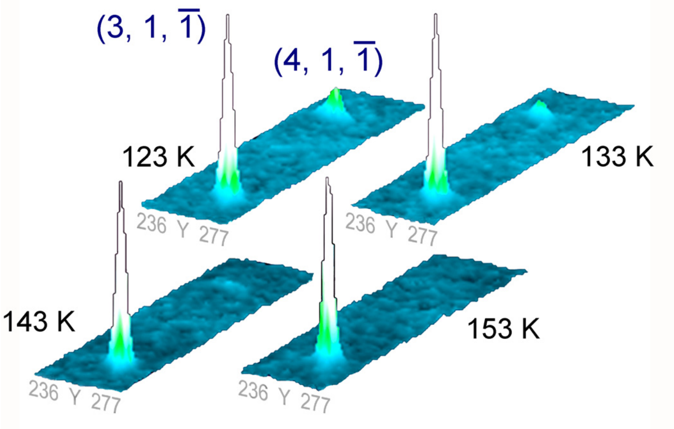

Figure 3.15 Appearance of the (4, 1 $\overline{1}$) reflection below 143 K, heralding the loss of *C*-centering. The strong (3, 1, $\overline{1}$) reflection is allowed in both *P*- and *C*-lattices.

Concomitant with loss of *C*-centering is a crossover in the definition of the *b* and *c* axes, as may be seen in **Table 3.3**. More importantly, the molecular plates along the ABABAB π-stacks are free to move away from their otherwise fixed positions at $x = 0$ and ½. The resulting deviations (**Table 3.4**) are, however, small. The molecules remain essentially planar (δ = 0.018 Å) and tilt very slightly (ϕ = 2.2 Å) away from perpendicularity with respect to the stacking direction (**Figure 3.16**) Consecutive molecules along the π-stack in the new unit cell are related by symmetry (a 2-fold rotation about *c*) but are not equally spaced up and down the π-stacks. As a result the four previously equivalent S1---S4′ contacts associated with a given molecule separate into two pairs, at 3.760(2) Å and 3. 874(2) Å, above and below the molecule respectively, to produce a small but significant alternation in the plate-to-plate separation. The four ladderlike S1---S2′ contacts which were identical in *Cmca* evolve into equivalent pairs above and below the molecule. Finally, the S3---S3′ and S4---S4′ interactions separate into four distinct contacts (two long and two short).

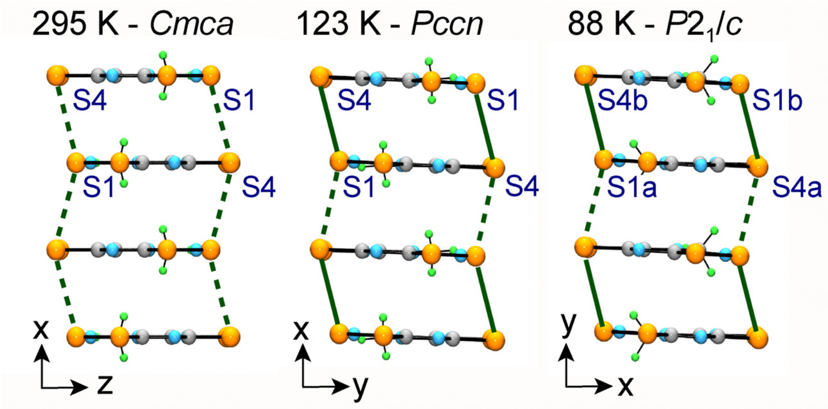

Figure 3.16 Transformation of evenly spaced radical π-stacks to π-dimer stacks as a function of temperature. Intermolecular S1---S4′ contacts (**Table 3.4**) are shown in green.

A third data set was collected at 88 K, and inspection of the systematic absences indicated a loss of two of the three glide planes of *Pccn* and a further reduction in space group symmetry to primitive monoclinic. The presence of the remaining glide plane established the setting to be $P2_1/c$, and the structure was solved and refined in this space group. The slight increase in the R-value (**Table 3.3**) can be ascribed to the need to refine a greater number of weak reflections, and a merohedral twinning arising from the pseudo-orthorhombic nature of the lattice. There is a switchover in unit cell vectors (a ↔b) from the *Pccn* settings (**Table 3.3**), but the cell constants remain close to those seen at 123 K. The symmetry lowering leads to two crystallographically independent molecules per asymmetric unit, so that consecutive molecules along the ABABAB π-stacks are no longer equivalent. The two molecules are nonetheless closely related, being nearly planar (δ = 0.026 Å and 0.024 Å), and the tilt angle ϕ for both increases only slightly (ϕ of 2.6Å and 2.8Å) relative to that seen at 123 K. The four possible S1---S4′ contacts (**Table 3.4** and **Figure**

3.16) are now completely independent, but fall into two groups (long and short), as seen at 123 K, and indicative of a slight but continued migration towards a bond-alternating π-dimer stack.

In summary, the initial X-ray measurements suggested that **3-3** (R_1 = Me) crystallizes as discrete radicals in the space group *Cmca* at room temperature and 123 K. However, upon further examination of the data, a symmetry lowering from a *C*-centred orthorhombic lattice to a primitive orthorhombic lattice was found. As the material is cooled from room temperature to 123 K, the radicals, which appeared to be locked onto crystallographic mirror planes, are free to move above/below the mirror plane leading to a lengthening and shortening of the S---S′ contacts. A third data set collected at 88 K indicated a further lowering of symmetry to a primitive monoclinic cell. At this temperature, the degree of S---S′ lengthening and shortening is more pronounced. Finally, the magnetic behaviour of **3-3** (R_1 = Me), as seen in the susceptibility measurements, is adequately explained by virtue of a temperature dependant symmetry lowering in the crystal structure.

3.5 Twinned Crystals: PyDTA[18]

Twinned crystals are commonly found in crystalline samples and are problematic for the crystallographer. A twinned crystal may be defined as an aggregate that contains crystalline domains of the same lattice, but which have different orientations relative to one another.[19] The boundaries of the various domains are joined together in a way that is described by a twin law. Because the twinned diffraction pattern contains contributions from all domains, the corresponding reflections from each domain may all overlap, (merohedral twinning), or partially overlap (non-merohedral twinning). In the former case the crystal lattice belongs to a higher point group than the crystal structure. In the latter case, multiple domains are (usually) related by a symmetry operation belonging to a higher symmetry supercell.[19] Overall, two key pieces of information are required to satisfactorily model twinned structures, namely the twin law and the fractional contribution of each component. If the collected reflections suggest merohedral twinning, the SHELXTL software package[20] allows one to directly enter the twin law and the fractional contribution into the instruction file. In contrast, the ideal way to model a non-merohedral twin is to use different software packages that utilize algorithms to find the twin law in a more efficient way. In this section, an interesting project where a data set was solved and refined two different ways, that is with and without the use of a non-merohedral twin law, is described.

The compound PyDTA, **3-4**, is a monofunctional 1,3,2-DTA radical that can be generated by the treatment of *bis*(sulphenyl chloride) pyridine with trimethylsiloazide, yielding[**3-4**][Cl] which can then be converted to [**3-4**][GaCl$_4$] and reduced to **3-4** with DiMFc (**Scheme 3.2**).

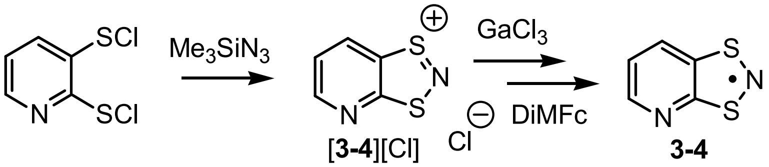

Scheme 3.2

In the hands of my coworkers, crystals of **3-4** suitable for X-ray work were grown by vacuum sublimation, yielding a mixture of green-black shards, purple blocks and purple rods. All three crystal morphologies were examined by single crystal X-ray diffraction, and cell dimensions for the purple blocks and rods (hereafter **β 3-4**) indicated that they were identical, differing only in the preferred direction of crystal growth. It was further determined by X-ray diffraction that the green-black shards (hereafter **α 3-4**) consisted of a different morphology. Initially, full data sets were collected on both **α 3-4** (at 100 K) and **β 3-4** (at 298 K) phases. However, upon investigation of the refined structure and data belonging to **α 3-4**, it was evident that a new data set was required.

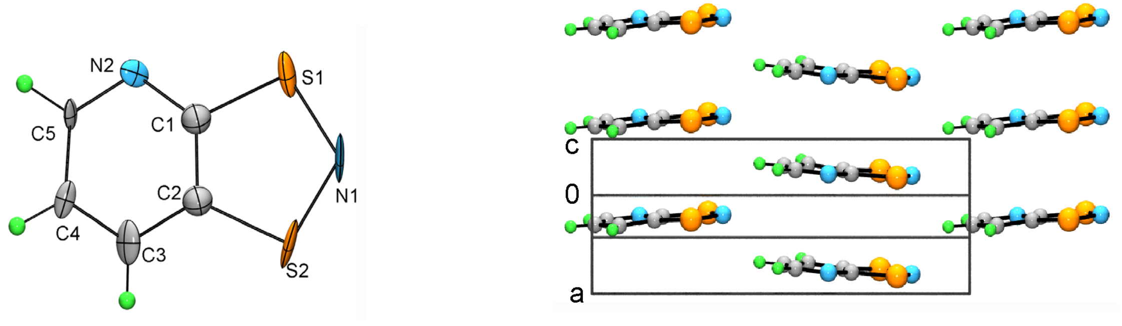

(a)

(b)

Figure 3.17 (a) ORTEP drawings (50 % probability ellipsoids) and atom labeling of **α 3-4** resulting from the original data set/refinement at 100 K. C1 and C2 are non-positive definite (isotropic parameters have been applied); (b) undimerized radical π stacks as viewed along the *x*-direction.

3.5.1 Crystallography

The initial refinement of **α 3-4** data at 100 K was conducted by my colleague and suggested a unit cell containing undimerized radicals belonging to the polar space group $P2_1$ (**Figure 3.17**), thereby having one radical in the asymmetric unit. The discrete radicals form π-stacks along the *x*-direction; the 2_1 screw axis translates each stack along *y*-direction, generating long N---H′ intercolumnar contacts (**Figure 3.17b**). However, upon further inspection of the refinement indices *R* and R_w it was quickly realized that the refinement was incomplete. The raw data (the individual frames) also indicated that there was a non-merohedral twin present. Finally, variable temperature magnetic susceptibility measurements on **α 3-4** (collected some time later) indicated that the material was essentially diamagnetic between 5 and 250 K (*vide infra*), suggesting that the radicals likely associated as dimers at 100 K (the collection temperature of the data set) and not as discrete radicals, as the initial structural refinement had indicated. Evaluation of the original p4p file (the p4p file contains the selected reflections used to determine the unit cell) with RLATT illustrated that a limited number of weak reflections were used to determine the unit cell (**Figure 3.18a**); furthermore, there were several reflections at $a = ½$, indicative of a doubling of the *a* axis, that were dismissed (**Figure 3.18b**). Because (i) the original data set was poor, *i.e.*, the majority of the data consisted of weak, low angle reflections and (ii) the refinement was incomplete, the decision was made to collect new data.

Freshly sublimed **α 3-4** radical was prepared and a total of 15 crystals (over 3 batches) were selected and screened. All 15 crystals showed signs of non-merohedral twinning and the “best” crystal was selected based on reflection intensities and scattering angle. Unit cell data was collected, and the position of the reflections clearly indicated the presence of a non-merohedral twin. The collected reflections were imported into the Cell Now software package and a suitable unit cell, as well as a second cell orientation, both with cell metrics $a = 6.122$, $b = 14.486$, $c = 7.228$ Å and $\beta = 111.19°$ was found (*i.e.*, the twin law; **Figure 3.19**). Finally, a full data set was collected at room temperature. Crystal data for **α 3-4**, along with the data for **β 3-4** is listed in **Table 3.5** and ORTEP drawings of asymmetric unit, showing atom numbering, are illustrated in **Figure 3.20**.

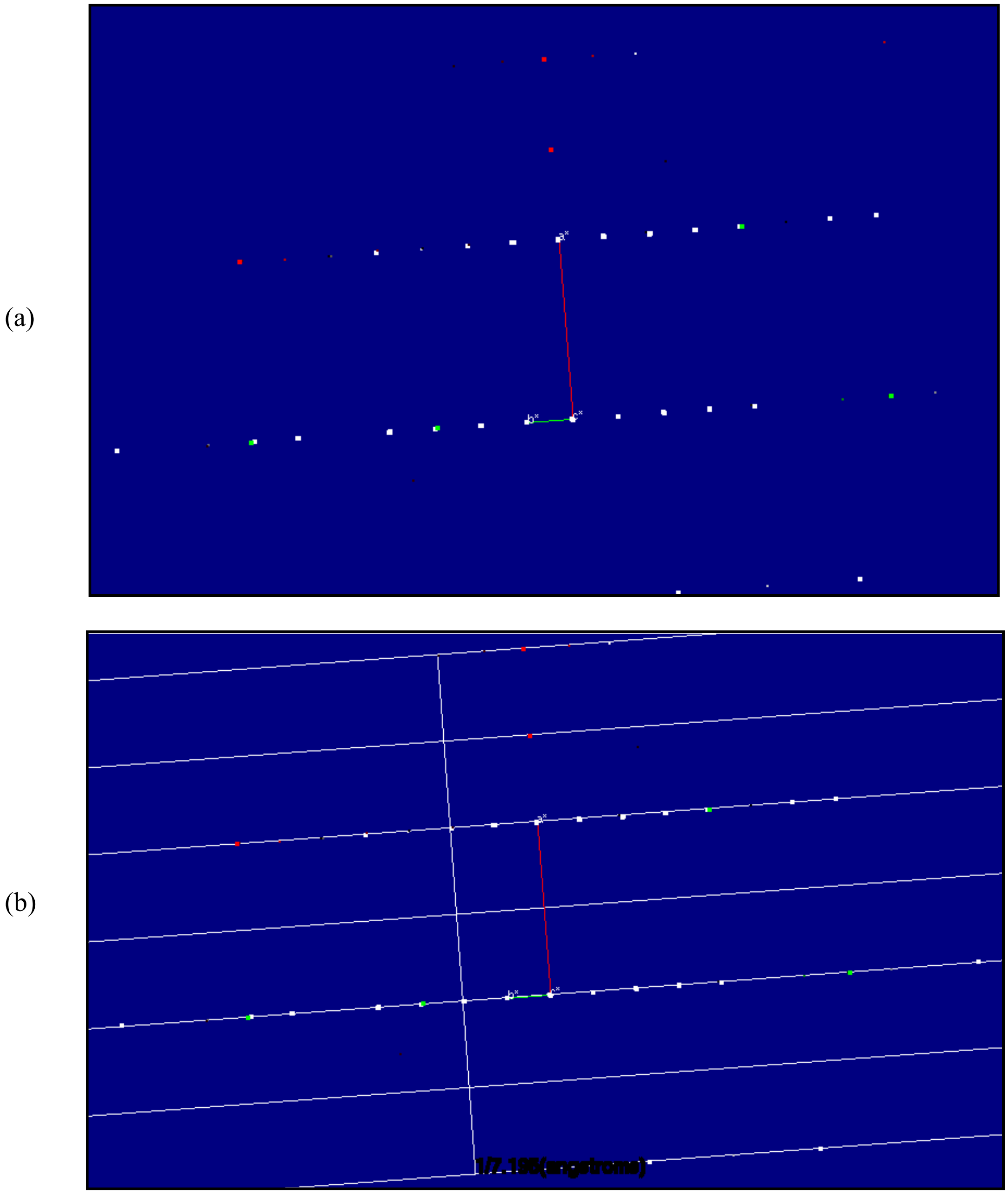

Figure 3.18 Screen capture of RLATT output for **α 3-4** (a) illustrating the reflections selected for the unit cell determination (white) and the rejected reflections (red, green) and (b) the same drawing as above but with a lattice overlay at *a* = ½.

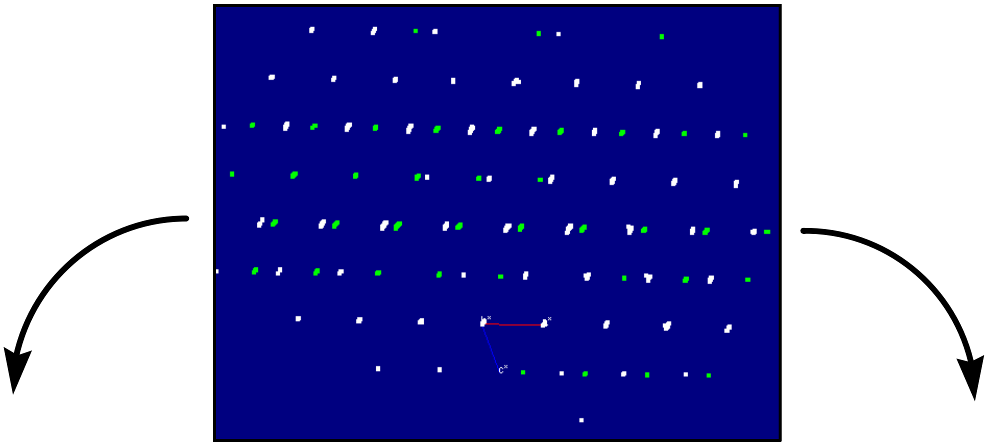

twinned unit cell data

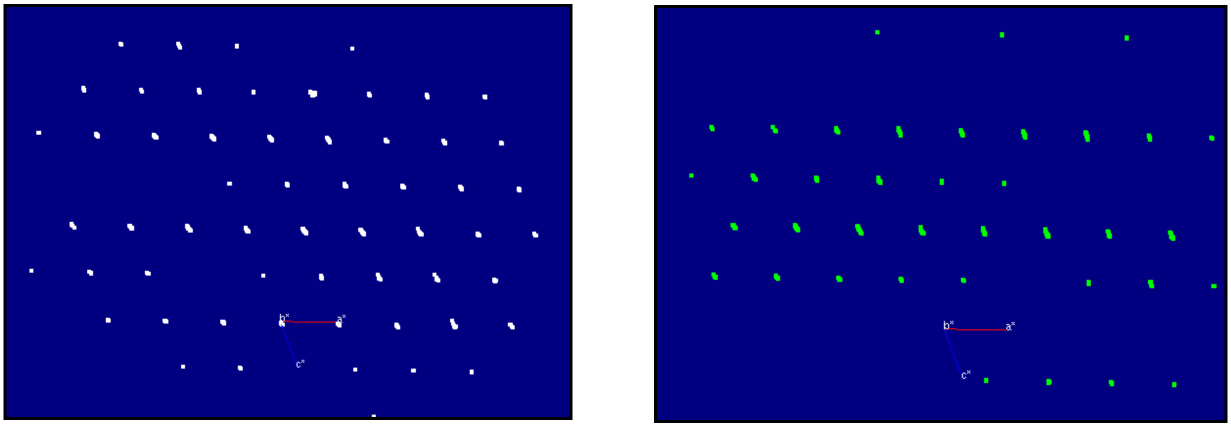

orientation 1

orientation 2

Figure 3.19 Screen capture of RLATT output for recollected **α 3-4** unit cell data illustrating reflection resulting from a non-merohedral twin (top) and the reflections belonging to the two new cell orientations (bottom).

Table 3.6 provides a listing of pertinent intermolecular S---S′ contacts to be discussed below. Crystals of **α 3-4** belong to the polar monoclinic space group $P2_1$ with two molecules in the asymmetric unit. These two radicals form a π*-π* dimer with intradimer S---S′ contacts of 3.373(2) and 3.320(2) Å. This refinement is in stark contrast to the original refinement which suggested the existence of undimerized radicals at 100 K (**Figure 3.17**).

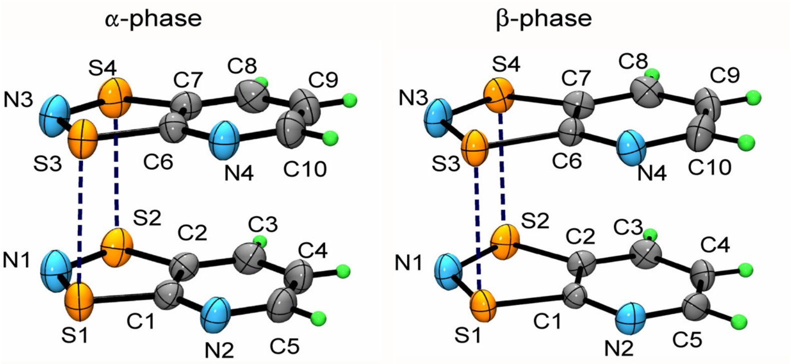

(a) (b)

Figure 3.20 ORTEP drawings (50 % probability ellipsoids) and atom labeling of (a) **α 3-4** from new data collected at 298 K and (b) **β 3-4** collected at 298 K.

Table 3.5 Crystallographic Data.

Polymorph	**α 3-4** (original)	**α 3-4** (final)	**β 3-4**
a, Å	3.5454(15)	6.1262(3)	6.062(4)
b, Å	14.4174(62)	14.4772(6)	14.537(9)
c, Å	5.8224(26)	7.2157(3)	13.716(9)
β, deg	103.153(7)	111.217(3)	100.052(10)
V, Å	289.81(90)	596.58(5)	1190.2(13)
ρ (calcd), g cm-1	1.779	1.728	1.732
space group	$P2_1$	$P2_1$	$P2_1/n$
Z	2	4	8
T, K	100(2)	296(2)	298(2)
μ, mm-1	0.800	0.779	0.781
λ, Å	0.71073	0.71073	0.71073
Flack Parameter	-0.019 (473)	0.470 (174)	—
data/restr./parameters	2065/1/178	1556/1/164	2464/0/163
solution method	direct methods	direct methods	direct methods
R, R_w (on F^2)	0.1015, 0.1601	0.0378, 0.0872	0.0637, 0.1434

Crystals of **β 3-4** crystallize in the space group $P2_1/n$ and also possess two molecules in the asymmetric unit. In this phase the two independent radicals form a π*- π* dimer with intradimer S---S′ distances of 3.253(2) and 3.260(3) Å, that is, similar to the intradimer contacts found in **α 3-4** . The packing of the dimers in the two phases, when viewed from a direction perpendicular to the molecular planes, is virtually identical, with dimers locked head-to tail to produce the layered arrays shown in **Figure 3.21**.

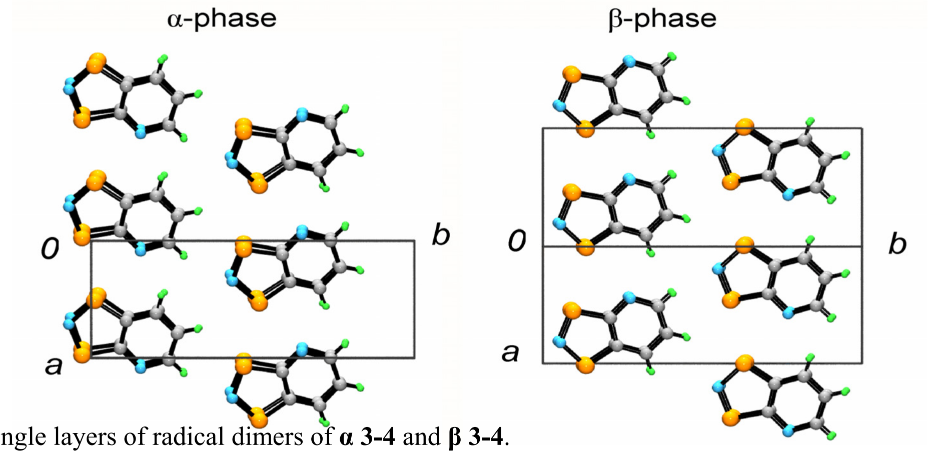

Figure 3.21 Single layers of radical dimers of **α 3-4** and **β 3-4**.

The difference in the two structures of **3-4** stems from the relative orientations of successive layers. In the α-phase successive layers are related simply by a translation along the *z*-direction, as illustrated in **Figure 3.22**, an operation which produces a classical slipped π-dimer structure. The inter-dimer S---S′ contacts (**Table 3.6**) along this π-stacking direction are 3.871(2) and 3.923(2) Å. These interactions are comparable to those observed in other distorted π-stacked structures of dithiazolyl radicals. In addition to the S---S′ contacts along the π-stacks, there are lateral S1---S2′ (3.575(2) Å) and S3---S4′ (3.545(2) Å) contacts that link dimers in the same layers. These latter interactions are illustrated in **Figure 3.23** which shows views of the π-stacked arrays down the *y*-direction. By contrast, in the β-phase, dimers in successive layers are related by an *n*-glide plane, the symmetry element which leads to the doubling of the unit cell dimension and the formation of a head-over-tail or alternating π-dimer stacked assembly. This arrangement precludes interdimer S---S′ contacts directly along the stacking direction (**Figure 3.22**). As in the α-phase, lateral intermolecular contacts S3---S4′ (3.583(3) Å), S1---S2′ (3.591(3) Å) and S2---S3′ (3.533(2) Å) between dimers in adjacent layers are observed, as well as an additional S1---S1′ interaction (3.483(3) Å) across an inversion centre.

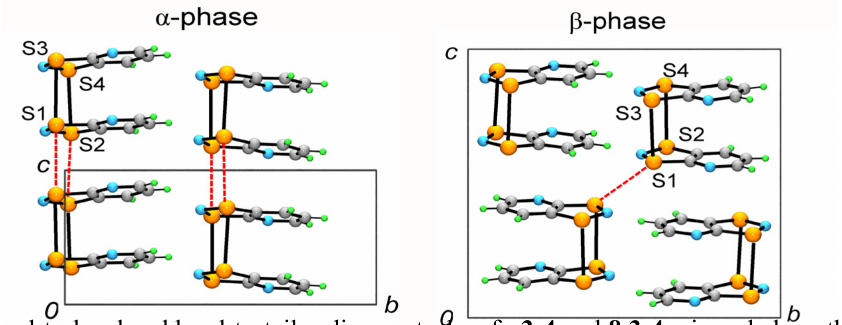

Figure 3.22 Head-to-head and head-to-tail π-dimers stacks of **α3-4** and **β 3-4**, viewed along the *x* direction. Intermolecular S---S′ interactions are shown with dashed red lines.

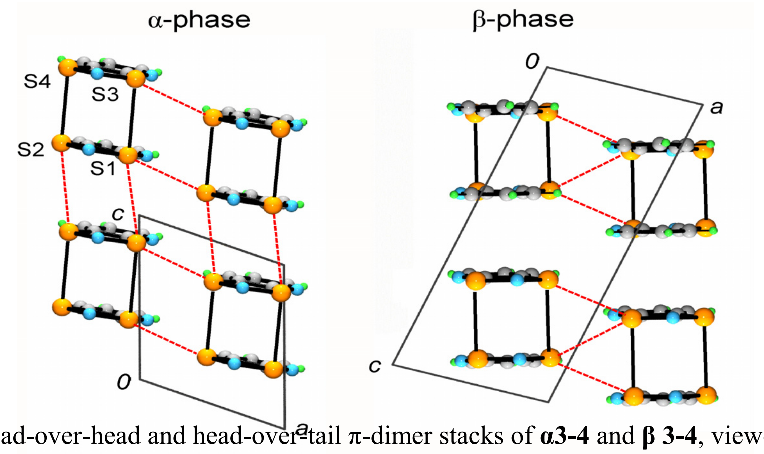

Figure 3.23 Head-over-head and head-over-tail π-dimer stacks of **α3-4** and **β 3-4**, viewed along the *y* direction. Intermolecular S---S′ interactions are shown with dashed red lines.

Table 3.6 Intra- and Interdimer S---S′ Contacts.

Polymorph	**α 3-4**	**β 3-4**
Intradimer S---S′, Å	3.374(2), 3.321(2)	3.870(2), 3.921(2)
Interdimer S---S′, Å	3.253(2), 3.260(3)	—

3.5.2 Magnetic Measurements

We have measured the temperature dependence of the magnetic susceptibility (χ_p), corrected for diamagnetic contributions, of both phases of **3-4** between 5 K and 350 K on a Quantum Design SQUID magnetometer operating at an applied field of 1000 Oe. Data were collected in both warming and cooling modes with heating/cooling rates of 5 K min^{-1}. The results are displayed in **Figure 3.24**, in the form of plots of the nominal free Curie count (= 8/3 χT) as a function of temperature (T).

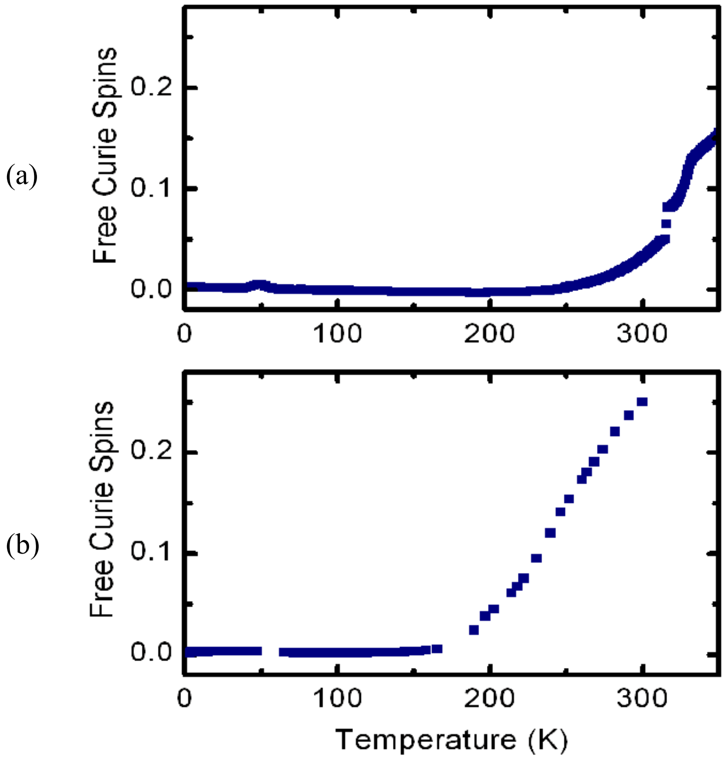

Figure 3.24 Temperature dependence of the free Curie spin count of **α 3-4** (a) and **β 3-4** (b).

As may be seen, at low temperatures both phases are essentially diamagnetic, with Curie spin counts near zero. Above 180 K in the β-phase, and above 250 K in the α-phase, the spin count gradually increases, an effect observed in many other thiazyl and other radical dimer structures, and an indication of the gradual expansion of the intra-dimer interactions and the breakdown of the closed-shell $S = 0$ dimer. Nonetheless, the relatively low spin counts at room temperature in both phases are consistent with the dimeric structures observed crystallographically. Despite the increase in paramagnetism on heating, there is no evidence for hysteretic behaviour; susceptibility/temperature dependancies upon heating and cooling are identical in both cases. Thermal hysteresis has previously been observed in a range of π-stacked dithiazolyl radicals.[21]

3.5.3 Discussion

In this section, structural and magnetic data have been obtained for the polymorphic monofunctional 1,3,2-DTA radical **3-4**. In the **β 3-4** phase, the radical crystallizes in the space group $P2_1/n$, and consists of alternating π-dimer stacks. Magnetic susceptibility data demonstrates a system which is essentially diamagnetic below 180 K, with an increasing spin count as the sample is further heated to room temperature. Initial X-ray data for **α 3-4** suggested a system composed of discrete radicals that crystallize in the space group $P2_1$, and which avoid dimerization down to at least 100 K. However, magnetic susceptibility data opposed this open shell model and upon further inspection it was evident that the data was twinned and incorrectly indexed. A new data refinement that accounts for the merohedral twinning of the isolated crystal illustrates the existence of dimers at room temperature, a model that is supported by the magnetic data. Clearly, **α 3-4** is an example which illustrates the importance of proper crystallographic work - one must always question the computer-generated data and, at times, carefully examine the raw data (reflections) for inconsistencies in the indexing/space group assignments. Furthermore, one must carefully interpret the structure-property relationship of the material.

This discussion would not be complete without addressing the reasons for twinning in DTA-based crystals (as we routinely observe twinning in our compounds). Put simply, a twin occurs when there are intermolecular interactions across a twin boundary that compete energetically with the interactions that would otherwise be formed in the single crystal.[22,23] This interpretation is clearly seen in **3-3** (**Section 3.4.2**) where upon cooling the single crystal from 123 K to 88 K, there is a gradual phase transition from *Pccn* to $P2_1/c$. The monoclinic crystal belonging to **3-3** has the angle $\beta \approx 90.0°$ and although the crystal structure has the point group $2/m$, the crystal lattice has the point group *mmm*. Twinning in this situation occurs when twinned domains are related by a symmetry element belonging to that of *mmm*. Thus, a symmetry operation that is allowed in *Pccn* (in this case, a 2-fold rotation about c^*) is forbidden in $P2_1/c$ (only 2-fold rotations about b^* are permitted). However, the favourable intermolecular interactions formed due to the 2-fold rotation about c^* in the *Pccn* structure are still energetically competitive in the $P2_1/c$ structure, resulting in the observed merohedral twin. This type of twin is commonly seen in materials that undergo a phase transition to a lower symmetry structure upon a change in temperature (or pressure). Finally, due to the lattice point group (*mmm*), a 2-fold rotation about c^* will result in a complete overlap of the diffraction pattern in reciprocal space.

Returning to **α 3-4**, the radical belongs to the monoclinic space group $P2_1$ with $\beta \approx 111.2°$. In contrast to **3-3** (at 88 K), the crystal lattice does not have the point group *mmm* (*i.e.*, $\beta \neq 90°$), and the observed twin must be non-merohedral. Here, the twinned domains give rise to some reflections that overlap and some that do not overlap. Two of the most common non-merohedral twins that occur in the monoclinic cell are that of 2-fold rotations about the unit cell a^* or c^* axes.[19] In the case of **α 3-4**, the rotation is about the a^* axis (as determined by Cell Now), and the real space rotation about the a axis is described by the matrix:

$$\begin{bmatrix} 1 & 0 & 0 \\ 0 & -1 & 0 \\ (2c\cos\beta)/a & 0 & -1 \end{bmatrix}.$$

This corresponds to a 180° rotation about the [1 0 0.306] axis in real space.

Finally, it is well known that layered structures are susceptible to twinning if the interactions between the layers are weak.[22,24] The crystal structure of **α 3-4** consists of head-to-head π-dimer stacks that have short S---S′ contacts within the π-dimer stacks (along the z-direction; **Figure 3.22**), and longer S---S′contacts between the π-dimer stacks (along the x-direction; **Figure 3.23**). However, no strong intermolecular contacts between the radical stacks in the y-direction exist. Thus, a 2-fold rotation about the [1 0 0.306] axis would likely serve to break the weakly interacting layers of π-dimer stacks along the y-direction, potentially forming an energetically competitive interaction across the twin boundary.

Chapter 4

The Isostructural *Eureka*

4.1 Introduction

The previous chapter investigated different powder and single crystal X-ray crystallography techniques that have been used to solve various structural problems in the Oakley group. All of these methods have been used for decades; however it is the very recent advance in computing power and the sensitivity of area detectors that have allowed the bench-top chemist to solve structural problems that were once reserved for the experimenting X-ray crystallographer. These methods have allowed us to (i) model solid-state structures from powder samples,[1,2] (ii) refine twinned data[3] and (iii) detect subtle reflections that signal the onset of phase transitions.[4] These various methods have been developed for our Oakley radicals when routine structural data cannot be collected. In this chapter a synthetic project that was initially designed to incorporate Se into **4-1a** ($R_1 = R_2 =$ Me), generating **4-1b** ($R_1 = R_2 =$ Me) is presented. However, due to the poor solubility of the radical in organic solvents, all attempts to grow suitable single crystals of **4-1b** ($R_1 = R_2 =$ Me) failed. Once again powder X-ray diffraction (PXRD) methods were used to model the solid-state structure.

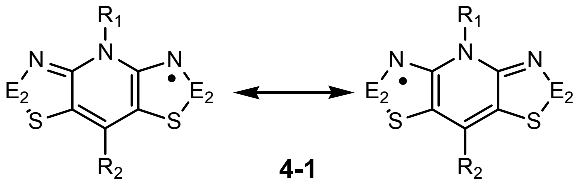

4-1

4-1a: $E_2 = S$
4-1b: $E_2 = Se$

The idea for this project stemmed from the successful isolation and structural characterization of the discrete radical **4-1b** ($R_1 =$ Me, Et, $R_2 =$ Ph),[5] which is isostructural to its S-analogue **4-1a** ($R_1 =$ Me, $R_2 =$ Ph).[6] Building off of this success, we wanted to reduce the size of the bulky Ph substituent which, as we had hoped, inhibited close lateral Se---Se′ contacts, but which limited the bandwidth of the material. We targeted **4-1b** ($R_1 = R_2 =$ Me) because the S-analogue **4-1a** ($R_1 = R_2 =$ Me) gives rise to a π-stacked material consisting of chain-like arrays in the solid state with close S ---S′ contacts of 3.368(2) Å (**Figure 4.1**),[6] and hence the material has a 2-dimensional band structure (unlike **4-1b** ($R_1 =$ Me, $R_2 =$ Ph)). We therefore surmised that if the Se-analogue were isostructural, it should give rise to better electrical conductivities than

4-1b (R_1 = Me, R_2 = Ph). However, upon chemical reduction of [**4-1b**][OTf] (R_1 = Me, R_2 = Me), the radical rapidly precipitated out of solution, generating dendritic crystals that could not be used in single crystal X-ray studies. Structural modeling by powder techniques was not successful, likely as a result of a mixed phase material (*i.e.*, the sample likely contained a mixture of σ-dimers and π-stacked radicals; *vide infra*) and focus therefore shifted to the ethyl derivative **4-1b** (R_1 = Et, R_2 = Me) in hopes that the larger R_1 group would help to solubilize the radical, thereby slowing down nucleation and crystal growth. Single crystals of **4-1b** (R_1 = Et, R_2 = Me) could not be grown and once again we had to rely on powder diffraction studies. However, the S-analogue **4-1a** (R_1 = Et, R_2 = Me) had never been synthesized and we were not able to predict the space group based on the generation of an isostructural set. Indexing of PXRD data suggested that the crystal lattice was tetragonal and it was quickly surmised that **4-1b** (R_1 = Et, R_2 = Me) was likely isostructural with **4-1a** (R_1 = Et, R_2 = Cl), where the radicals pack in the tetragonal space group $P\overline{4}2_1m$.[7] This realization, which we refer to as the "*isostructural eureka*" allowed us to assign the correct space group and refine the structure of **4-1b** (R_1 = Et, R_2 = Me) . Herein the preparation of **4-1b** (R_1 = Me, Et; R_2 = Me) radicals is described. The X-ray crystallography is discussed at length and both conductivity and magnetic measurements on **4-1b** (R_1 = Et, R_2 = Me) are reported. Of major significance are the magnetic measurements, which establish that **4-1a** (R_1 = Et, R_2 = Me) orders as a bulk ferromagnet at 13.6 K. This major discovery has led to the development of all S/Se permutations possible for the **4-1** (R_1 = Et, R_2 = Cl) framework and will be discussed in **Chapter 5.**

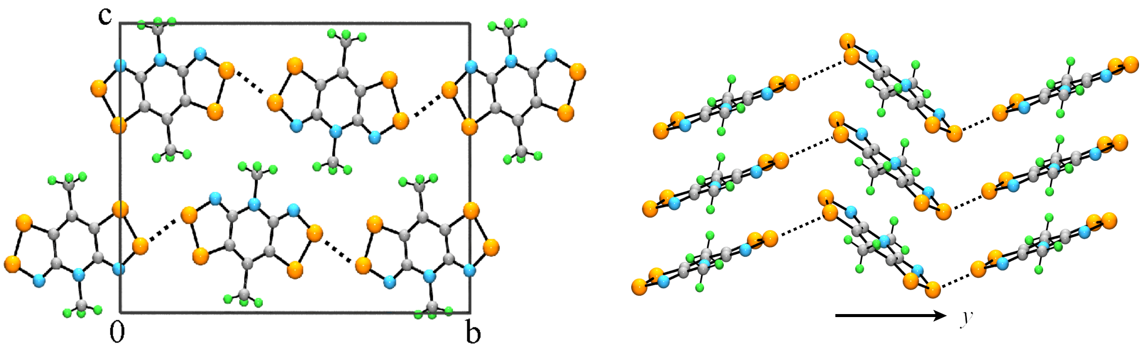

(a) (b)

Figure 4.1 Packing diagram of **4-1a** (R_1 = R_2 = Me) viewed along the *x*-direction (a), and along the *c*-direction (b).

4.2 Preparation of [4-1a][OTf] (R_1 = Me, R_2 = Me)

The preparation of [**4-1a**][OTf] (R_1 = Me, R_2 = Me) follows the synthetic procedures published elsewhere.[6] Thus the conversion of 2,6-dihydroxy-4-methylpyridine hydrochloride (**4-2**)[8] to the dichloro derivative **4-3** progressed smoothly when combined with $POCl_3$ in a Parr bomb reactor (**Scheme 4.1**). The mixture was heated to 180 °C for 5 h, then cooled and poured over ice. DCM extractions, followed by crystallization from hexanes gave **4-3** in good yield. Further treatment of **4-3** with MeOTf in DCE produced the *N*-methyl derivative [**4-4**][OTf], which could be recrystallized from hot DCE. We were then able to aminate both chlorine positions by bubbling NH_3 through a solution of [**4-4**][OTf] and MeCN in a glass bomb.[9] The bomb was then sealed and heated to 80 °C overnight, after which the (cooled) contents of the bomb were filtered to remove NH_4Cl. The filtrate, which contained [**4-5**][OTf] was concentrated to yellow oil. Finally, a double Herz condensation,[7] *i.e.*, the reaction of [**4-5**][OTf] with S_2Cl_2, produced [**4-1a**][OTf] (R_1 = Me, R_2 = Me) in yields of 50 - 60%; the reaction time was minimized in order to prevent chlorination of the methyl group. [**4-1a**][OTf] (R_1 = Me, R_2 = Me) can be recrystallized from hot MeCN, and several recrystallizations were performed in order to purify the material for the next step.

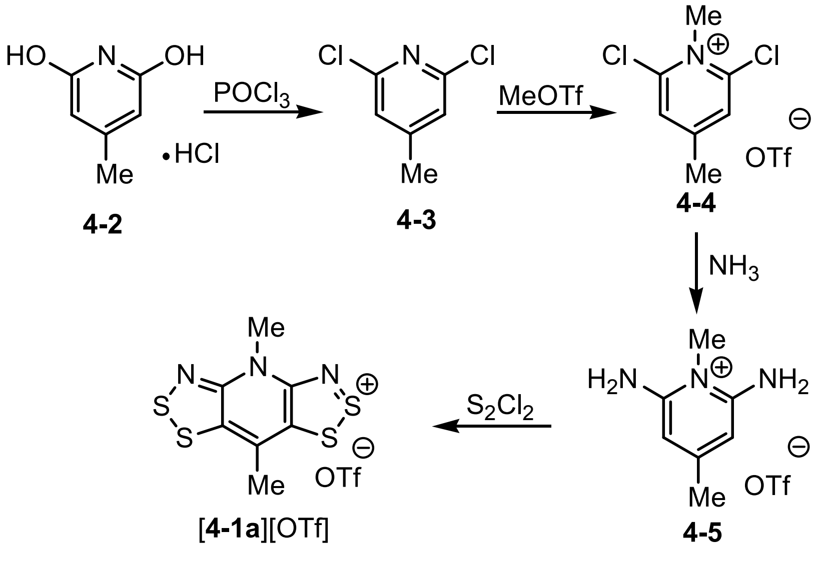

Scheme 4.1

4.2.1 Preparation of [4-1a][OTf] (R_1 = Et, R_2 = Me)

Starting with **4-3**, ethylation with EtOTf in DCE generates [**4-6**][OTf] in excess of 90% yield (**Scheme 4.2**). This material is easily recrystallized in a EtOAc/DCE mixture. As described above, amination of [**4-6**][OTf] affords [**4-7**][OTf] as a yellow oil. The diamine was then reacted with 3 equivalents of S_2Cl_2 and refluxed for 5 h, producing crude [**4-1a**][OTf] (R_1 = Et, R_2 = Me) at 50% yield. Multiple recrystallizations were performed in order to ensure purity of the cation.

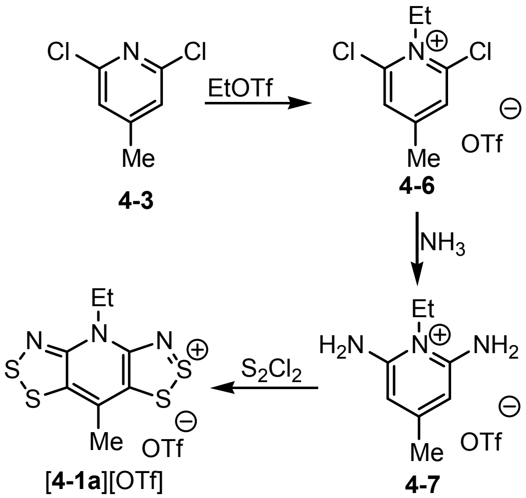

Scheme 4.2

4.2.2 Selenium Insertion

Se insertion, generating [**4-1b**][OTf] (R_1 = R_2 = Me) is a modification to the procedure outlined in **Section 3.2** of the thesis.[10] Thus, three equivalents of ground SeO_2 was added to a solution of [**4-1a**][OTf] (R_1 = R_2 = Me) in MeCN/HOAc, and refluxed overnight (**Scheme 4-3**). The solution was then filtered and concentrated, yielding deep red needles of [**4-1b**][OTf] (R_1 = R_2 = Me).

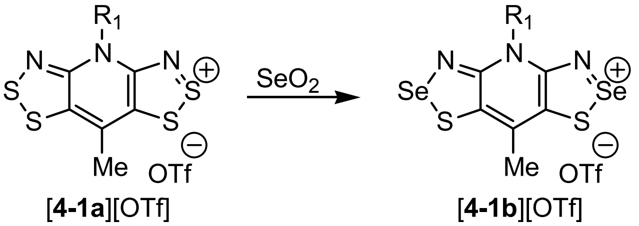

Scheme 4.3

However, a series of recrystallizations were required to ensure the purity of the material. The level of purity could be monitored through ESI MS, where the parent ion, accompanied with small amounts of Se_1, Se_3, and Se_4 containing material (see side reactions in **Figure 4.2**) was observed. It was discovered that through dissolution of crude [**4-1b**][OTf] ($R_1 = R_2 =$ Me) in hot MeCN, followed by hot filtration and concentration of the filtrate, the more soluble Se_1 material remained in solution, and the Se_2, Se_3 and Se_4 material precipitated out. It was further realized that hot filtration of a solution of [**4-1b**][OTf] ($R_1 = R_2 =$ Me) removed the less soluble Se_3 and Se_4 material. Thus, after repetitive hot filtrations, ESI MS demonstrated almost complete removal of the unwanted Se variants.

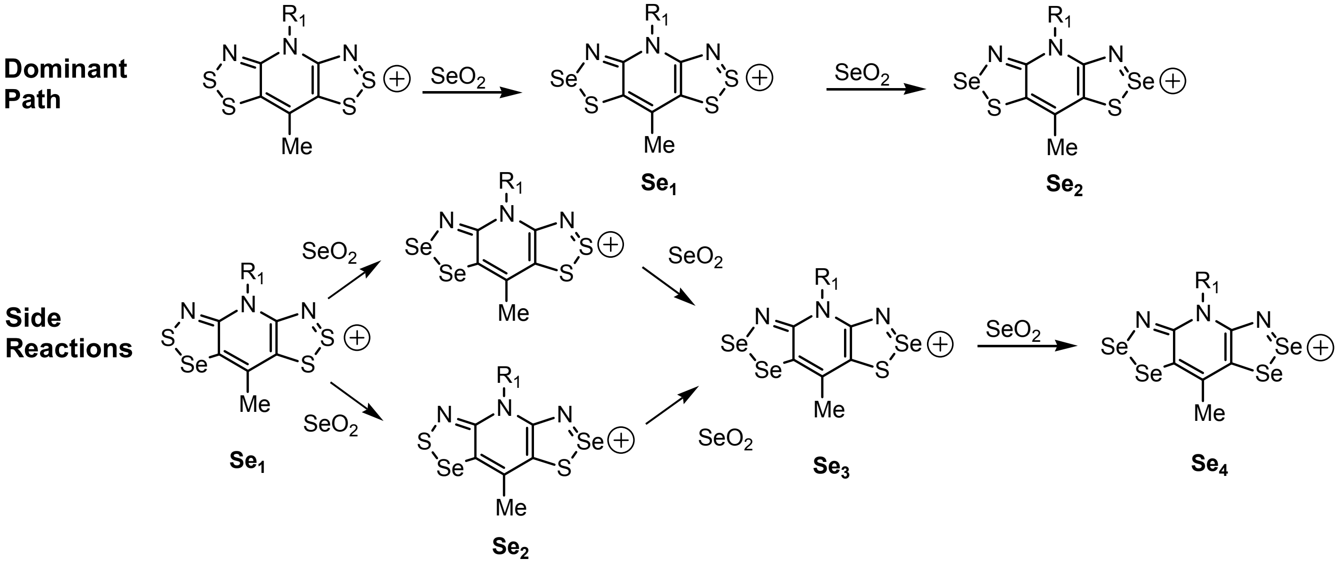

Figure 4.2 The dominant path (above) and the side reactions (below) that produce the Se_1 - Se_4 variations in the Se insertion reactions.

Se insertion into [**4-1a**][OTf] (R_1 = Et, R_2 = Me) presented some challenges at first. Initially, treatment of the triflate salt with 3 equivalents of ground SeO_2 in a 1:1 mixture of MeCN/HOAc at 16 h reflux afforded [**4-1b**][OTf] (R_1 = Et, R_2 = Me) in good yield. Again, ESI MS measurements on the product revealed small amounts of Se_1, Se_3 and Se_4 variants in the crude sample. The same technique described for [**4-1b**][OTf] ($R_1 = R_2 =$ Me) was used to remove the other Se variants; however, the R_1 = Et substituent proved to increase the solubility of [**4-1b**][OTf] (R_1 = Et, R_2 = Me) and all its Se-containing variants. A large number of hot filtrations decreased the levels of Se_1, Se_3 and Se_4 material, but not to the same degree seen in the preparation of [**4-1b**][OTf] ($R_1 = R_2 =$ Me). Luckily, it was later found (by my colleague) that refluxing [**4-1a**][OTf] ($R_1 =$ Et, $R_2 =$ Me) with 3 equivalents of SeO_2 in HOAc for 70 min, produced a crude material which was nearly free of Se_1, Se_3 and Se_4 material. Thus multiple recrystallizations of the crude product afforded a product which was acceptable for subsequent reactions.

4.3 Cyclic Voltammetry

We have probed the redox chemistry of [**4-1b**][OTf] ($R_1 = R_2 =$ Me) and [**4-1b**][OTf] ($R_1 =$ Et, $R_2 =$ Me) by cyclic voltammetry, starting from solutions of the corresponding cations in dry acetonitrile using 0.1 M tetrabutylammonium hexafluorophosphate as the supporting electrolyte and platinum working electrodes. The potentials were referenced to internal ferrocene at 0.38 V vs the SCE couple and reported relative to SCE.[11] The results of the experiments are summarized in **Table 4.1**.

Table 4.1 Solution Half-Wave Cell Potentials (V).

	[**4-1a**][OTf] ($R_1 =$ Me, $R_2 =$ Me)	[**4-1a**][OTf] ($R_1 =$ Et, $R_2 =$ Me)	[**4-1b**][OTf] ($R_1 =$ Me, $R_2 =$ Me)	[**4-1b**][OTf] ($R_1 =$ Et, $R_2 =$ Me)
$E_{1/2}$(+1/+2)[a]	1.278	1.272	1.224	1.219
$E_{1/2}$(0/+1)[a]	-0.136	-0.146	-0.104	-0.127
$E_{1/2}$(-1/0)[a]	-0.940[c]	-0.950	-0.832[c]	-0.830[c]
E_{cell}[a,b]	0.860[d]	0.806	—	0.703[d]

[a] In MeCN, ref. SCE. [b] $E_{\text{cell}} = E_{½}(+1/0) - E_{½}(0/-1)$. [c] Irreversible behavior, E_{pc} value quoted. [d] E_{cell} estimated as $E_{\text{pc}}(+1/0) - E_{\text{pc}}(0/-1)$.

The previously characterized S-based radical [**4-1a**][OTf] ($R_1 = R_2 =$ Me)[6] shows a series of waves corresponding to the -1/0, 0/+1 and +1/+2 processes. The more anodic process, *i.e.*, the 0/+1 and +1/+2 couple are reversible, whereas the -1/0 couple is irreversible. We attribute the irreversibility to a weakening of the S-S[12] (or S-N)[13] bond in the reduced state. In contrast, the ethylated compound [**4-1a**][OTf] ($R_1 =$ Et,

R_2 = Me) shows reversible waves for all three processes and has a cell potential of 0.81 V, which is in line with other *bis*-DTAs (**Figure 4.3a**).[7,14] The Se-containing [**4-1b**][OTf] (R_1 = R_2 = Me) radical gives rise to a reversible +1/+2 and 0/+1couple and an irreversible -1/0 wave, like that observed in its S analogue. Furthermore, a secondary anodic process, perhaps due to a species plating out on the electrode, is observed. Finally, ethylated [**4-1b**][OTf] (R_1 = Et, R_2 = Me) shows a set of 2 reversible waves and a pseudo-reversible wave (the -1/0 process, **Figure 4.3b**). Furthermore, a small anodic shift and a decreased E_{cell} of 0.703 V with respect to its S-analogue is observed.

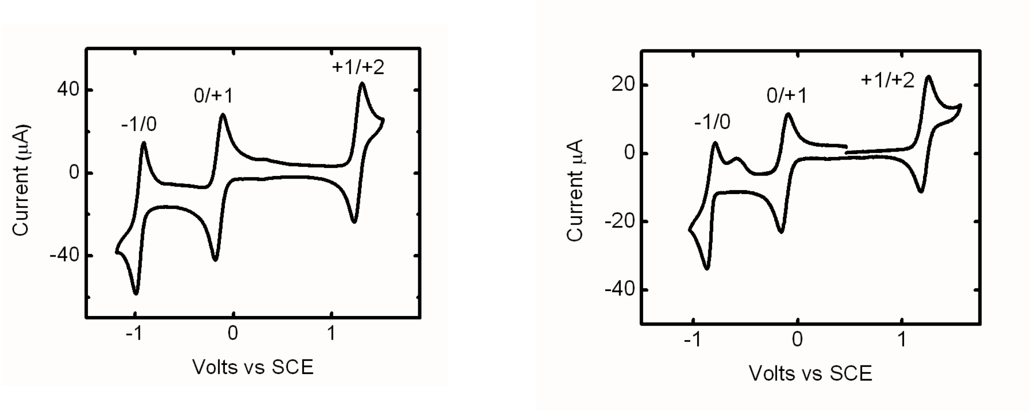

(a) (b)

Figure 4.3 CV scans of (a) [**4-1a**][OTf] (R_1 = Et, R_2 = Me) and (b) [**4-1b**][OTf] (R_1 = Et, R_2 = Me) in acetonitrile with [*n*-Bu_4N][PF_6] supporting electrolyte.

4.4 Reduction Chemistry

The reduction of [**4-1b**][OTf] (R_1 = R_2 = Me) required a judicious choice of reducing agents; a table of reducing agents and their measured redox couples used by the Oakley group may be found in **Appendix A**. Since the 0/+1 couple for the R_1 = Me and R_1 = Et derivatives are -0.104 and -0.127 V respectively, the reducing agents DMFc (0/+1 = -0.131V) and OMFc (0/+1 = -0.038 V) were selected. Bulk reduction of [**4-1b**][OTf] (R_1 = R_2 = Me) was easily achieved by reaction with DMFc in degassed acetonitrile; OMFc bulk reductions were not attempted. The bulk material was of high purity (and used in PXRD analysis, *vide infra*), but the overall solubility of the crude radical was poor and insufficient for recrystallization. We turned to H-cell techniques in attempts to grow single crystals, however all attempts to produce crystals suitable for single crystal X-ray diffraction studies failed.

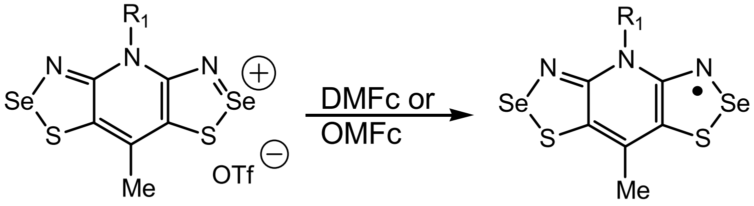

Scheme 4-4

Bulk [**4-1b**][OTf] (R_1 = Et, R_2 = Me) material was generated *via* reduction of the corresponding triflate salt in MeCN using DMFc and OMFc as reducing agents. The resulting crude materials from both reducing agents gave identical results (by FTIR) and all subsequent bulk reductions were carried out with DMFc. Multiple H-cells experiments were attempted and while the replacement of R_1 = Me with R_2 = Et slightly increased the solubility of the radical, the diffusion of solutions of [**4-1b**][OTf] (R_1 = Et, R_2 = Me) and DMFc (or OMFc) afforded thin needles that were not suitable for single crystal analysis. Not willing to give up, one final attempt was made to generate crystals from H-cells; success was found using highly purified cation (*i.e.*, [**4-1b**][OTf] (R_1 = Et, R_2 = Me) that was free of Se_1, Se_3 and Se_4 cation (as measured by ESI MS) and 4 equivalents of OMFc. These experimental conditions resulted in the generation of high quality needles that were suitable for single crystal X-ray studies.

4.5 Crystal Structure Determination

As mentioned in the section above, high quality single crystals of **4-1b** (R_1 = R_2 = Me) could not be grown by recrystallization of the bulk material or by H-cell diffusion techniques, and once again, we turned to powder methods to model the structure. Unfortunately, all attempts failed. Although clean material (by FTIR spectroscopy) was used, we were not able to index the unit cell. When the powder diffractogram of the bulk radical was compared with the powder pattern generated from the all S-containing **4-1a** (R_1 = R_2 = Me) single crystal structure, there was no evidence of correlation, *i.e.*, the two materials are not isostructural. Thus, if microcrystals of discrete **4-1b** (R_1 = R_2 = Me) radicals were generated, they packed in a different space group than the S-analogue. Furthermore, the failure to index the material suggests that there may be two phases present in the sample (*e.g.*, a mixture of σ-dimers and radicals may be generated). Finally, it is possible that the molecules generated, either as discrete radicals or dimers, crystallize in a low symmetry space group such as $P1$ or $P\overline{1}$, as these triclinic crystal systems are difficult to index.

Initially, we could not grow quality single crystals of **4-1b** (R_1 = Et, R_2 = Me), and once again we turned to powder methods. A powdered sample **4-1b** (R_1 = Et, R_2 = Me) was generated by gently grinding ~60 mg of sample with a mortar and pestle. The sample was loaded into an aluminum sample holder which was rotated during data collection. The diffraction pattern was collected at ambient temperature on an X-ray powder diffractometer with a position sensitive detector using Cu $K\alpha_1$ radiation (λ = 1.54056 Å). The total 2θ range was 0.28-112.684 ° (the limit of the detector), measured in steps of 0.029 °. Powder diffractograms were collected at 1 h intervals so that we could monitor material degradation. It was found that an overnight data collection was optimal, as the sample did not appear to degrade within this timeframe. The powder data was indexed with the program Dicvol91[15] (as part of the Crysfire suite)[16] and indicated a tetragonal crystal system (a = 16.0713 and c = 4.1602) with a high figure of merit (FOM = 44.9). Looking at our library of known *bis*-DTA radicals, we realized that **4-1a** (R_1 = Et, R_2 = Cl) crystallizes in the tetragonal space group $P\overline{4}2_1m$ and has similar cell parameters.[7] Because the van der Waals radius for Cl is similar to that of a methyl group (Cl = 1.75, -Me = 1.70),[17] it seemed plausible that **4-1b** (R_1 = Et, R_2 = Me) could be isostructural with **4-1a** (R_1 = Et, R_2 = Cl). The software FOX[18] was used to obtain a direct space, *ab initio* model (the direct space solution obtained was not used in subsequent steps, it was used for analytical purposes only); the resulting structure and simulation are illustrated in **Figure 4.4.** The results suggest that **4-1b** (R_1 = Et, R_2 = Me) is isostructural with that of **4-1a** (R_1 = Et, R_2 = Cl) , and to verify this, a detailed Rietveld analysis was performed using modified atomic coordinates from the single crystal structure of **4-1a** (R_1 = Et, R_2 = Cl) . The results of the refinement are illustrated in **Figure 4.5** and data is tallied in **Table 4.2.** The crystal structure, as refined by Rietveld methods[19] using the GSAS program package,[20] illustrates the desire for **4-1b** (R_1 = Et, R_2 = Me) to form well defined π-stacks which pack around a central $\overline{4}$ axis. Although the radicals are locked onto the {220} mirror plane that slices the *a* and *b* axis by ½, they are free to tilt on the plane. This tilting gives rise to slipped π-stacks.

Very recently, the crystal structure of **4-1b** (R_1 = Et, R_2 = Me) has been determined by single crystal X-ray diffraction at room temperature and 100 K, and both data sets agree with the assigned space group (by powder data) of $P\overline{4}2_1m$. Crystal data are compiled in **Table 4.2** and ORTEP drawings of the asymmetric units of the room temperature structure is presented in **Figure 4.6**.

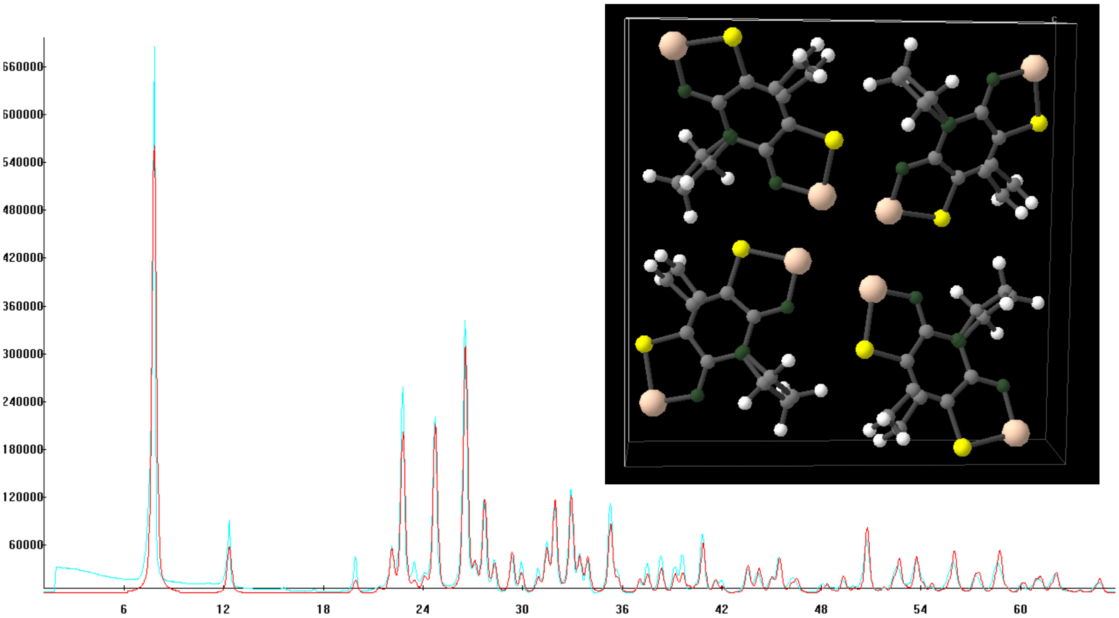

Figure 4.4 FOX output of the powder diffractogram profile (experimental data in blue, simulation in red) and direct space *ab initio* structural solution (insert) of **4-1b** (R_1 = Et, R_2 = Me).

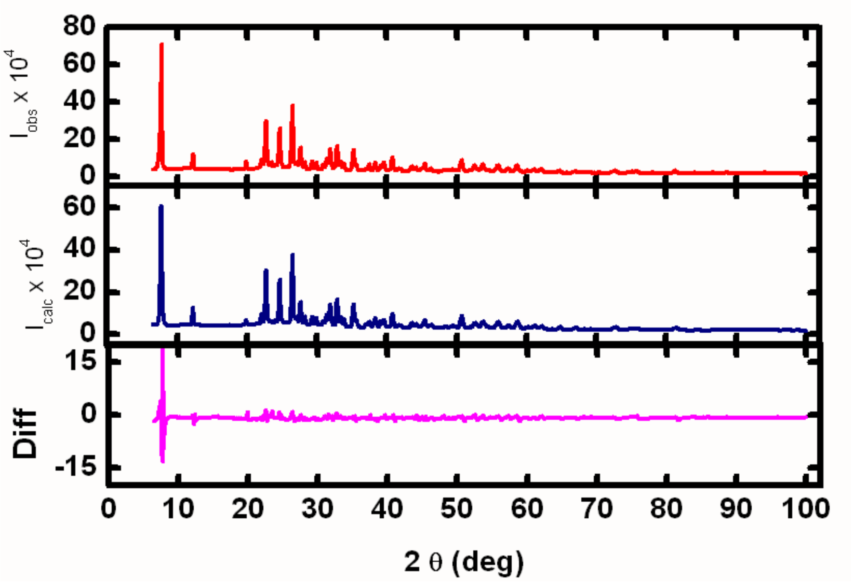

Figure 4.5 Rietveld refinement of **4-1b** (R_1 = Et, R_2 = Me).

Table 4.2 Crystal Data and Metrics for **4-1a** (R_1 = Et, R_2 = Cl) and **4-1b** (R_1 = Et, R_2 = Me).

Compound	**4-1a**[a] R_1 = Et, R_2 = Cl	**4-1b** R_1 = Et, R_2 = Me	**4-1b** R_1 = Et, R_2 = Me	**4-1b** R_1 = Et, R_2 = Me
M	294.83	368.21	368.21	368.21
a, Å	15.886(11)	16.0713(11)	16.0088(17)	16.0276(12)
c, Å	4.1088(4)	4.1602(5)	4.1385(9)	4.0830(7)
V, Å^3	1036.9(5)	1074.5(3)	1060.6(3)	1048.9(2)
ρ (calc), g cm^{-1}	1.889	2.334	2.306	2.332
space group	$P\overline{4}2_1m$	$P\overline{4}2_1m$	$P\overline{4}2_1m$	$P\overline{4}2_1m$
Z	4	4	4	4
temp, K	298(2)	298	298(2)	100(1)
μ, mm^{-1}	1.137	—	7.331	7.414
λ, Å	0.7107	1.54056	0.7107	0.7107
data/restr./par.	1067/0/87	—	1161/5/81	1111/0/77
solution method	direct methods	powder methods[b]	direct methods	direct methods
R, R_w (on F^2)	0.0279, 0.0571	0.0625, 0.1320[c]	0.0337, 0.0793	0.0327, 0.0667
S—E, Å	2.0981(15)	2.195(3)	2.2325(13)	2.2480(13)
E—N, Å	1.657(3)	1.820(4)	1.8138(41)	1.8278(43)
S—C, Å	1.727(4)	1.753(4)	1.7350(45)	1.7542(50)
d1, Å	3.401(2)	3.384[d]	3.343(1)	3.306(1)
d2, Å	3.560(2)	3.435[d]	3.470(1)	3.444(1)
d3, Å	3.573(2)	3.713[d]	3.655(1)	3.648(1)
δ, Å	3.483(12)	3.5801(3)	3.508(5)	3.442(2)
τ, deg	57.9(3)	59.4 (1)	57.95(1)	57.5(1)
dev from pln, Å	0.0663	0.0471	0.0891	0.0919

[a] Data from Reference 7. [b] Starting model taken from 4-1a (R1 = Et, R2 = Cl). [c] R_p and wR_p respectively from Rietveld refinement. [d] ESDs were not calculated for d1 - d3.

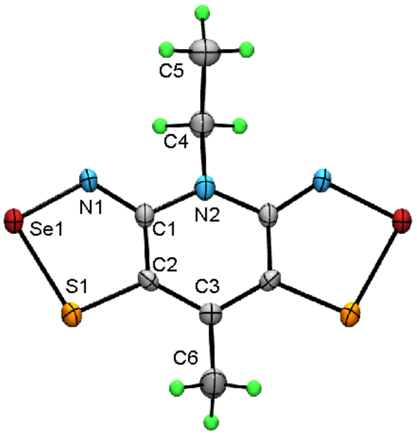

Figure 4.6 ORTEP drawings (50% probability ellipsoids) of **4-1b** (R_1 = Et, R_2 = Me) at 298 K.

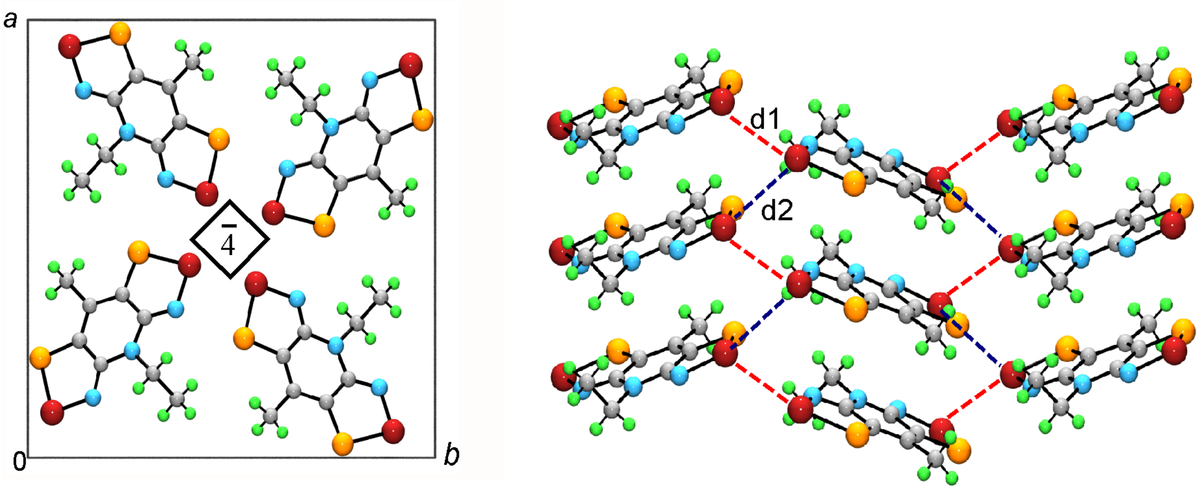

(a)

(b)

Figure 4.7 Crystal packing of **4-1b** (R_1 = Et, R_2 = Me) viewed along the *z*-direction (a), and viewed along the *x*-direction (b).

At room temperature and 100 K, the undimerized radicals cluster about the central $\overline{4}$ axis, forming slipped π-stacked arrays that run along the *z*-direction (**Figure 4.7**). Interplanar separation δ of the radical planes and their inclination angle τ with respect to the packing axis[14] for both data sets is given in **Table 4.2**. The room temperature single crystal structure is nearly identical to the powder refinement save for a small change in contact distances and cell parameters. Discrepancy between room temperature cell constants from powder and single crystal refinements may arise from the fitting of asymmetric low angle powder peaks.[21] As can be seen in **Figure 4.8**, the packing of the room temperature radicals give rise to extensive intermolecular contacts well within the sum of the van derWaals radii for S (3.6 Å) and Se (3.8 Å).[17] These close contacts lace the radicals together, both along and perpendicular to the stacking axis. Furthermore, the S---Se′ d1 and d2 contacts are shorter than that of the S---S′ contacts in **4-1a** (R_1 = Et, R_2 = Cl) and this contraction has been seen in other heavy atom systems.[22] Overall, the contractions give rise to increased intermolecular overlap, thus having a drastic effect on both the bandwidth and magnetism of the radical material (*vide infra*).

Finally, the molecular packing of the 100 K structure is strikingly similar to that of the room temperature structure. However, the contact distances d1 –d3 decrease upon cooling (**Table 4.2**), and as expected, the cell volume decreases (although, only by ~1%).

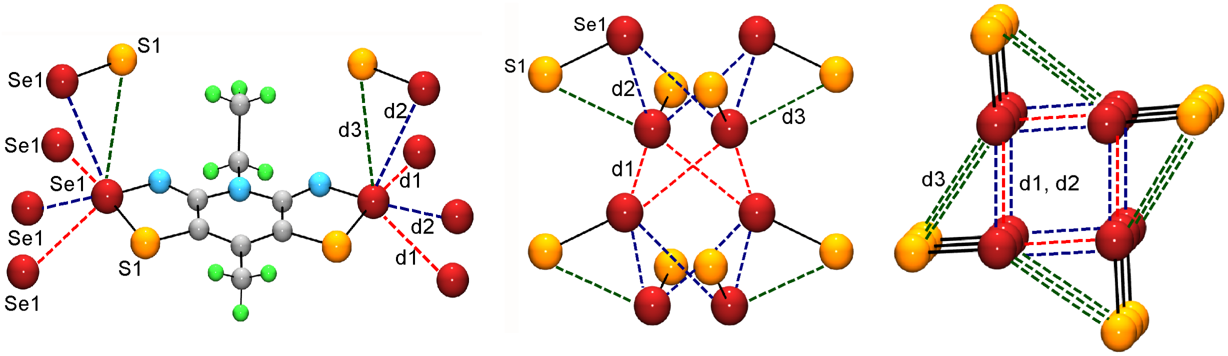

(a) (b) (c)

Figure 4.8 Intermolecular Se---Se′ contacts d1 - d3 to a single molecule of **4-1b** (R_1 = Et, R_2 = Me) (a), and about the $\overline{4}$ centers, viewed perpendicular (b) and parallel (c) to the *z* direction.

4.6 Electronic Band Structure and Conductivity Measurements

In order to compare the extent of intermolecular electronic interactions in **4-1b** (R_1 = Et, R_2 = Me) we performed a series of EHT band structure calculations based on the 298 K and 100 K structural data. The results are summarized in **Figure 4.9**, which shows the dispersion of the COs arising from the four SOMOs in the respective unit cells, plotted along the reciprocal space direction Γ (0, 0, 0) to Z (0, 0, ½). By virtue of the tetragonal symmetry, CO trends along this reciprocal space vector can be associated precisely with orbital interactions along the stacking axis in real space. The band structure of **4-1a** (R_1 = Et, R_2 = Cl), which should be a good representation of the S-analogue of **4-1b** (R_1 = Et, R_2 = Me) has been added for comparison.

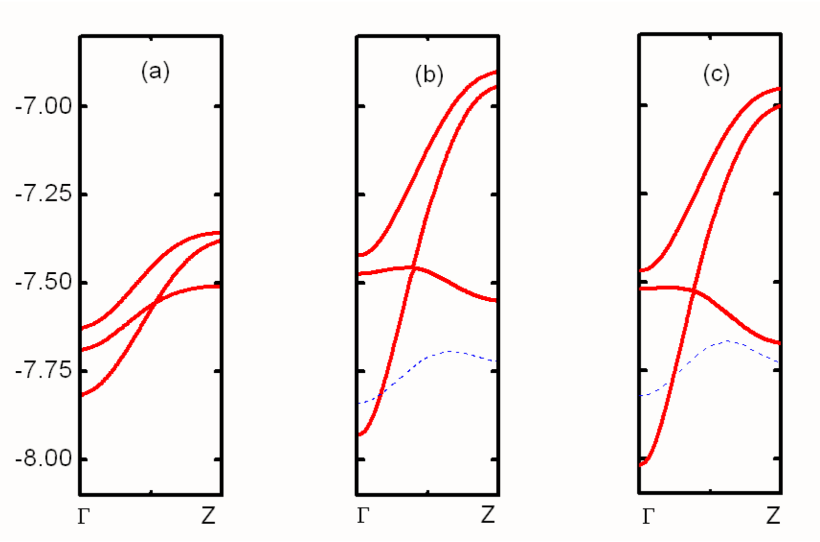

Figure 4.9 CO dispersion curves from Γ (0, 0, 0) to Z (0, 0, ½) for (a) **4-1a** (R_1 = Et, R_2 = Cl), (b) **4-1b** (R_1 = Et, R_2 = Me) at 298 K and (c) 100 K. Dashed lines are intruder bands.

The increase in bandwidth upon incorporation of Se into the radical, from a *W* near 0.5 eV to over 1.0 eV (**Table 4.3**), is quite dramatic, the latter values being significantly larger than in any slipped π-stack thiazyl or selenazyl radical we have ever seen. The increased CO dispersion which leads to this enhancement in *W* is, we believe, attributed to the increased overlap of the COs when S is replaced by Se and also by the much tighter d1 and d2 contacts (**Table 4.2** and **Figure 4.8**) about the $\overline{4}$ centre. There is little change in *W* between the room temperature and 100 K **4-1b** (R_1 = Et, R_2 = Me) structure, which we attribute to the slight decrease in volume (~ 1%) when the crystal is cooled from RT to 100 K.

The results of the band structure calculations described above, especially the large *W* estimated for **4-1b** (R_1 = Et, R_2 = Me), led us to anticipate an increased conductivity (σ) in these systems. Variable temperature, four-probe pressed pellet conductivity measurements on **4-1b** (R_1 = Et, R_2 = Me) confirm these expectations; the results are presented in **Figure 4.10** in the form of plots of log σ versus 1/T. Despite the apparently large *W*s, which for **4-1b** (R_1 = Et, R_2 = Me) are comparable to *U* (arbitrarily estimated as $U \sim E_{cell}$), the material is not metallic and the conductivity remains activated. However, there is an increase in room temperature conductivity (σ_{RT}) by 2 orders of magnitude and large decrease of thermal activation E_{act} when Se is incorporated into the isostructural material (**Table 4.3**). These measurements appear to be in accord with the tighter d1,d2 contacts and the resulting improvement in *W*.

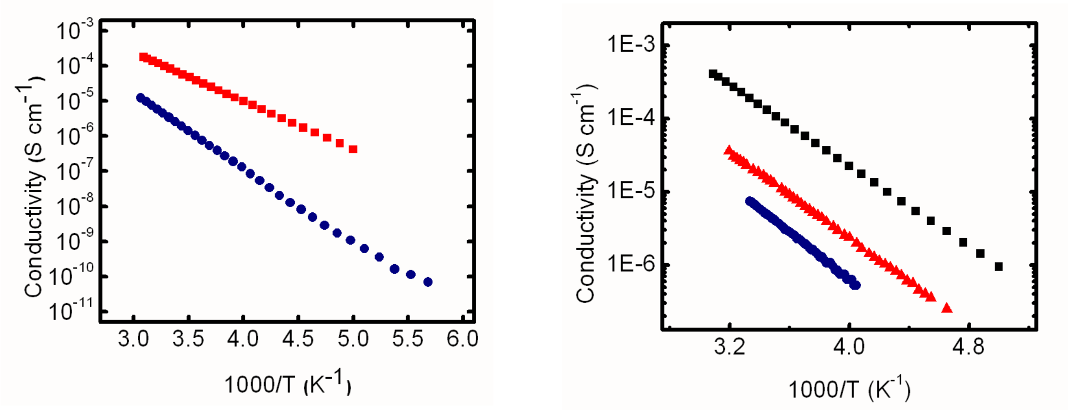

(a) (b)

Figure 4.10 Log σ versus 1/*T* plots for (a) **4-1a** (R_1 = Et, R_2 = Cl) (bottom) and **4-1b** (R_1 = Et, R_2 = Me) (top) and (b) for the Se-containing series **4-1b** (R_1 = Et, R_2 = Me) (top), **4-1b** (R_1 = Me, R_2 = Ph) (middle), and **4-1b** (R_1 = Et, R_2 = Ph) (bottom).

Table 4.3 Bandwidth, Conductivity and Magnetic Parameters.

	4-1a (R_1 = Et, R_2 = Cl)	**4-1b** (R_1 = Et, R_2 = Me)
W (eV)	0.46	1.03, 1.07 [b]
σ (300 K) (S cm^{-1})	3.3×10^{-6} [a]	1.9×10^{-4}
E_{act} (eV)	0.43 [a]	0.24
C (emu K mol^{-1})	0.373	0.391
θ (K)	3.6	18.6
T_c (K)	—	13.6
M_{sat} (Nβ) at 2 K	—	0.98
M_{rem} (Nβ) at 2 K	—	0.374
H_c (Oe) at 2 K	—	240

[a]Data from reference 7; [b]from structural data collected at 100 K.

In accordance with the "chemical pressure" discussion presented in **Section 3.2.4**, when the variable temperature conductivity data for **4-1b** (R_1 = Me, Et, R_2 = Ph) is plotted against **4-1b** (R_1 = Et, R_2 = Me), the concept of chemical pressure is more pronounced. As seen in **Figure 4.10b**, when the R_1 = Et ligand is exchanged for R_1 = Me in **4-1b** (R_1 = Me, Et, R_2 = Ph), the decrease in the steric bulk of the R_1 ligand results in increased conductivity. When the bulky R_2 = Ph substituent is replaced with a R_2 = Me substituent, a further increase in conductivity, greater than 1 order of magnitude, is observed. Thus a "chemical pressure" is applied when the size of substituent is decreased, as this allows the radicals to form shorter intermolecular contacts.

4.7 Magnetic Measurements

Magnetic susceptibility measurements have been performed on **4-1b** (R_1 = Et, R_2 = Me) over the temperature range 2 - 300 K at 100 Oe. At temperatures above 50 K, the susceptibility χ_p (corrected for diamagnetic contributions)[23] follows paramagnetic behaviour with values of $C = 0.391$ emu K mol^{-1}, and θ = 18.4 K, and with a χT (300 K) of 0.417 emu K mol^{-1}, which is near the value expected (0.375 emu K mol^{-1}) for a S = ½ system with g nominally equal to 2. Below 50 K a dramatic increase in susceptibility is observed, followed by a surge in χ just below 20 K, which reaches a maximum value of 181 emu K mol^{-1} at 10.5 K. This magnetic response was unexpected, as we originally predicted Curie-Weiss behaviour over the entire temperature range of the experiment. Consequently, the measured susceptibility of **4-1b** (R_1 = Et, R_2 = Me) is consistent with a phase transition to a ferromagnetically ordered state.

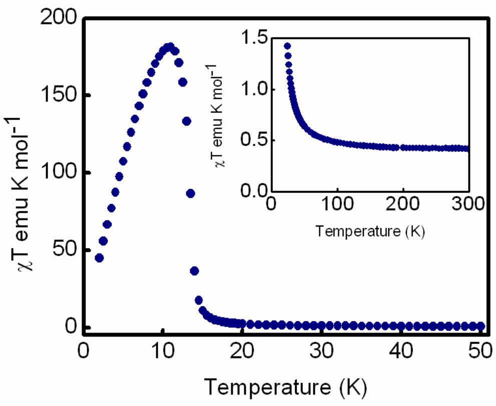

Figure 4.11 Plots of χT (field-cooled) versus temperature for **4-1b** (R_1 = Et, R_2 = Me) at 100 Oe. The inserts show an expansion of the high T region.

In order to probe the validity of the magnetic response, measurements of the field independent magnetization M_{sp} of **4-1b** (R_1 = Et, R_2 = Me) were conducted and provided further evidence for the existence of a ferromagnetically ordered state. As illustrated in **Figure 4.12a**, M_{sp} is strongly temperature dependent and decreases to zero near 13.5 K, in accord with the point of maximum slope in the χT versus T plots described above. Variable AC susceptibility measurements at different frequencies on **4-1b** (R_1 = Et, R_2 = Me) have allowed us to pinpoint the ordering temperature T_c of the radical. As shown in **Figure 4.12b**, there is a sharp maxima in the real (in-phase) χ' and imaginary (out-of-phase) χ' components at 13.6 K. The invariance of T_c with changes in the cycling frequency (from 50 Hz to 5 kHz) establishes that this material is not a spin glass.

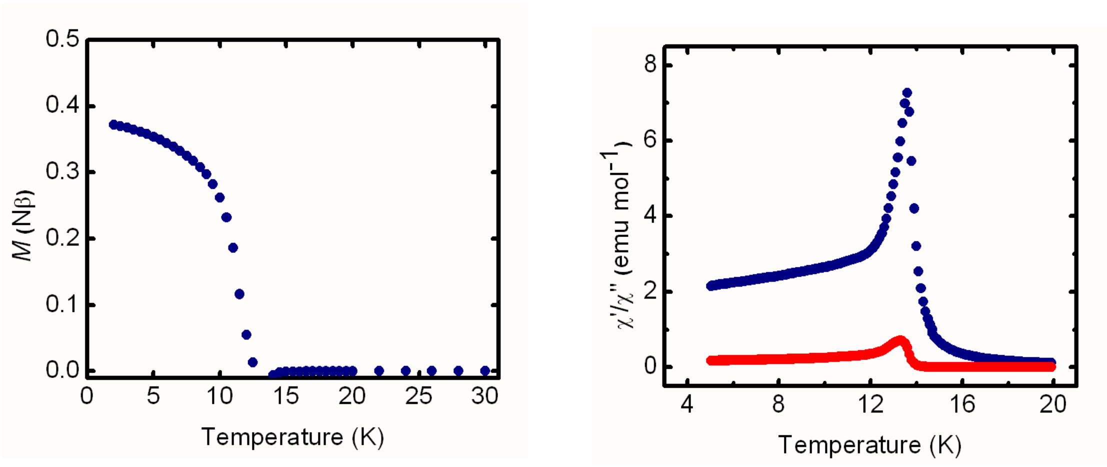

(a) **(b)**

Figure 4.12 Field independent magnetization as a function of temperature (a), and in-phase χ' and out-of-phase χ'' AC magnetic susceptibility (at 1 KHz) as a function of temperature (b) for **4-1b** (R_1 = Et, R_2 = Me).

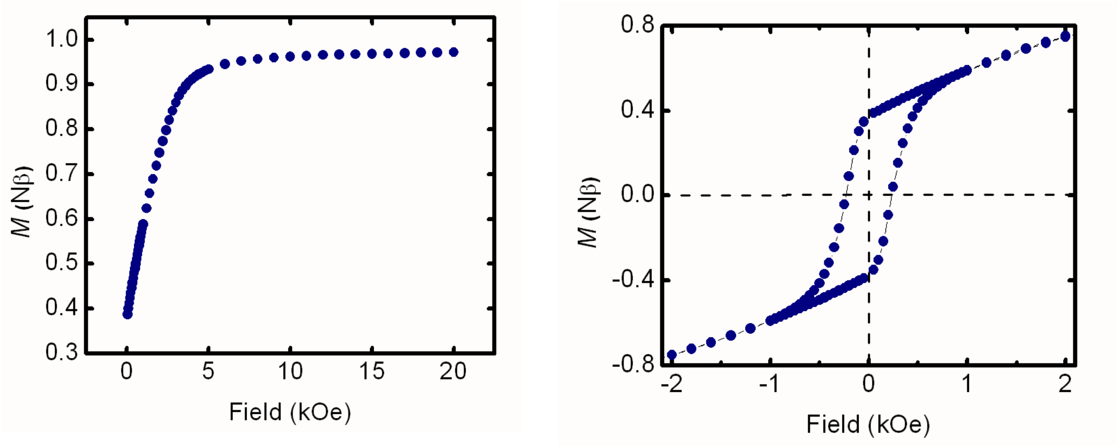

(a) **(b)**

Figure 4.13 Saturation magnetization (a) and hysteresis in magnetization (b) of **4-1b** (R_1 = Et, R_2 = Me) as a function of magnetic field at 2 K.

Magnetization experiments as a function of field have also been performed on **4-1b** (R_1 = Et, R_2 = Me). In **Figure 4.13a**, it can be seen that M rises sharply with H, reaching (at 2 K) a maximum at H = 20 kOe. The corresponding saturation magnetization values M_{sat} is 0.98 Nβ, which is in line with the predicted saturation of S = ½ system with g = 2. Reversal and cycling of the field sweep leads to hysteresis in the magnetization. A plot of M versus H from measurements taken at 2 K are presented in **Figure 4.13b**. From the plot, the remnant magnetization M_{rem} is 0.374 and the coercive field H_c is 240 Oe at 2 K.

4.8 Summary and Research Direction

In this chapter the synthetic development of *N*-methyl and *N*-ethyl radicals **4-1b** (R_1 = Me, Et, R_2 = Me) has been presented; the *N*-methyl radical could be generated, however its structure was not determined. For the purpose of controlling the crystal growth (*i.e.*, by increasing the solubility of the **4-1b** (R_1 = Me, R_2 = Me) radical), the *N*-Et derivative was synthesized. The structure, as determined by both single crystal and PXRD methods, crystallizes in the high symmetry space group $P\overline{4}2_1m$. A significant increase in measured conductivity and calculated bandwidth of **4-1b** (R_1 = Et, R_2 = Me) was found, as compared to the isostructural all S-containing **4-1a** (R_1 = Et, R_2 = Cl). Furthermore, magnetic measurements on **4-1b** (R_1 = Et, R_2 = Me) demonstrate a ferromagnetic phase transition at 13.6 K. These measurements are in stark contrast to those of the all S isostructural partner **4-1a** (R_1 = Et, R_2 = Cl), where the material was essentially paramagnetic, with short range ferromagnetic interactions at low temperature (magnetic data on this compound was originally collected in 2002 and repeated in 2006; the measurements will be presented in **Section 5.6**). The radical also shows magnetic hysteresis below the magnetic ordering temperature T_c, and gives rise to a temperature dependant coersitivity of 240 Oe at 2 K.

These finding are *unprecedented* in thiazyl (SN) based radicals and lead us to believe that the incorporation of the heavier chalcogen Se into **4-1a** (R_1 = Et, R_2 = Me) is responsible for the bulk ferromagnetic ordering described above. In an effort to probe this theory, we have undertaken a systematic investigation of the radical family **4-8**; this work is presented in **Chapter 5**.

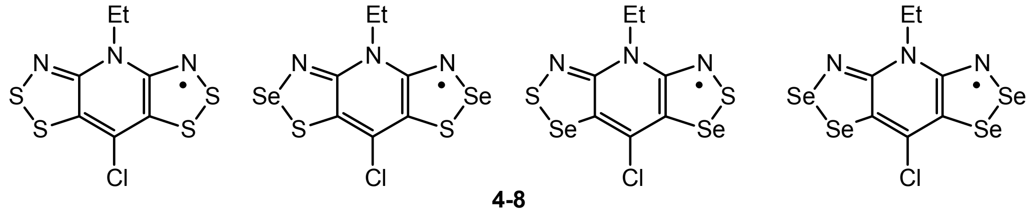

4-8

4.9 Experimental Section

Please see **Appendix A** for general methods and procedures.

Synthesis of *N*-ethyl-2,6-dichloro-4-methylpyridinium triflate, [4-6][OTf]: Ethyl triflate (8.04 mL, 0.0622 mol) was added to a colourless solution of 4-methyl-2,6-dichloropyridine (8.40 g, 0.0518 mol) in 20 mL DCE and the reaction mixture was stirred for 16 h to afford a heavy white precipitate, to which 40 mL diethyl ether was added. After 5 min, the mixture was cooled to -20 ºC for 1 h, at which time the resulting white solid was collected on a fine (E porosity) glass frit, washed with 2 x 30 mL cold diethyl ether and dried *in vacuo*. Recrystallization from a 3:1 solution of ethyl acetate/DCE afforded white needles of [**4-6**][OTf]; yield 11.2 g (0.0329 mol, 64%); mp 146 - 147 ºC. IR: 3070 (w), 1615 (s), 1264 (vs), 1245 (s), 1227 (m), 1159 (m), 1144 (s), 1034 (s), 841 (w), 640 (s), 517 (w) cm^{-1}. ^{1}H NMR (δ, CD_3CN): 7.92 (s, 2H), 4.86 (q, 2H, J = 7.25 Hz), 2.55 (s, 3H), 1.51 (t, 3H, J = 7.27 Hz). Anal. Calcd. for $C_9H_{10}Cl_2F_3NO_3S$: C, 31.78; H, 2.96; N, 4.12 %. Found: C, 31.88; H, 3.10; N, 3.96 %.

Preparation of *N*-ethyl-2,6-diamino-4-methylpyridinium triflate, [4-7][OTf]: Ammonia gas was bubbled through a cooled mixture of [**4-6**][OTf] (9.27 g, 0.0273 mol) in 150 mL MeCN in a large glass pressure vessel. The vessel was then sealed and heated at 80 ºC for 18 h. After the mixture was cooled to room temperature and the reaction vessel vented, the mixture was heated at 90 ºC for 3 h to release excess ammonia. The yellow/orange solid was removed by filtering on a Büchner funnel and the filtrate was evaporated to give a light orange oil of [**4-7**][OTf], which was used in the next step without purification; yield 8.23 g (0.0273 mol, 100 %). ^{1}H NMR (δ, CD_3CN): 6.02 (s, 2H), 3.91 (q, 2H, J = 7.37), 2.15 (s, 3H), 1.30 (t, 3H, J = 7.34).

Synthesis of 4-ethyl-8-methyl-4*H-bis*[1,2,3]dithiazolo[4,5-b:5',4'-e]pyridin-2-ium triflate [4-1a][OTf] (R_1 = Et, R_2 = Me): Sulfur monochloride (6.55 mL, 0.0818 mol) was added to a solution of [**4-7**][OTf] (7.49 g, 0.0249) in 45 mL of a 2:1 solution of DCE/MeCN. The initially green solution gently refluxed for 5 h and the resulting blue solution cooled to room temperature. The mixture was further cooled at -20 ºC for 1 h before the red microcrystalline precipitate of crude [**4-1a**][OTf] (R_1 = Et, R_2 = Me) was collected on a fine (E porosity) glass frit, washed with 2 x 40 mL DCM and dried *in vacuo*; yield 6.67 g (0.0157 mol, 64 %). The crude material was further washed with 75 mL CS_2 and 150 mL hot DCE before being recrystallized from 100 mL MeCN to give [**4-1a**][OTf] (R_1 = Et, R_2 = Me) as red needles; yield 3.76 g (56 % from crude); m.p. 227 - 228 ºC. IR: 1366 (s), 1279 (m), 1251 (m), 1224 (w), 1159 (w), 1031 (m), 740 (m), 638 (m) cm^{-1}. Anal. Calcd. for $C_9H_8F_3N_3O_3S_5$: C, 25.52; H, 1.90; N, 9.92 %. Found: C, 25.50; H, 1.81; N, 9.79 %.

Synthesis of 4,8-dimethyl-4*H-bis*[1,2,3]thiaselenazolo[4,5-b:5',4'-e]pyridin-2-ium triflate [4-1b][OTf] (R_1 = R_2 = Me): Crushed selenium dioxide (0.298 g, 2.69 mmol) was added to a solution of [**4-1a**][OTf] (R_1 = Me, R_2 = Me) (0.50 g, 1.22 mmol) in 100 mL of a 1:1 mixture of MeCN/HOAc. The mixture was heated at reflux for 24 h, after which the green solution was cooled to room temperature. The resulting crystals of [**4-1b**][OTf] (R_1 = R_2 = Me) were filtered off and washed with 20 mL HOAc and 20 mL DCM. The crude product (550 mg, 1.09 mmol, 89%) was recrystallized 3 times from 80 mL MeCN to give red needles; yield 232 mg (0.046 mmol, 38 %); m.p. 243-244 ºC. IR: 1410 (m), 1361 (m), 1270 (m), 1242 (s), 1228 (m), 1165 (m), 1154 (m), 1030 (s), 1011 (m), 777 (w), 760 (w), 641 (s), 627 (m), 595 (s), 540 (w), 517 (w), 481 (w) cm^{-1}. Anal. Calcd for $C_8H_6F_3N_3O_3S_3Se_2$: C, 20.90; H, 1.56; N, 8.12 %. Found: C, 21.17; H, 1.51; N, 7.95 %.

Synthesis of 4-ethyl-8-methyl-4*H-bis*[1,2,3]thiaselenazolo[4,5-b:5',4'-e]pyridin-2-ium triflate, [4-1b][OTf] (R_1 = Et, R_2 = Me): Crushed selenium dioxide (1.22 g, 11.0 mmol) was added to a hot blue solution of [**4-1a**][OTf] (R_1 = Et, R_2 = Me) (1.55 g, 3.66 mmol) in 40 mL HOAc. The mixture was heated at reflux for 70 min, after which the green solution was cooled to room temperature. The resulting orange crystals of [**4-1b**][OTf] (R_1 = Et, R_2 = Me) were filtered off and washed with 20 mL HOAc and 20 mL DCM. The product was recrystallized from 100 mL MeCN to give red needles; yield 990 mg (1.91 mmol, 52 %); m.p. 233 -234 ºC. IR: 1277 (m), 1238 (s), 1174 (w), 1024 (m), 722 (m), 633 (m), 594 (w) cm^{-1}. Anal. Calcd. for $C_9H_8F_3N_3O_3S_3Se_2$: C, 20.90; H, 1.56; N, 8.12 %. Found: C, 21.17; H, 1.51; N, 7.95 %.

Synthesis of 4,8-dimethyl-4*H-bis*[1,2,3]thiaselenazolo[4,5-b:5',4'-e]pyridin-3-yl, 4-1b (R_1 = R_2 = Me): Degassed solutions (3 freeze-pump-thaw cycles) of DMFc (0.230 g, 0.71 mmol) in 15 mL MeCN and [**4-1b**][OTf] (R_1 = R_2 = Me) (0.355 g, 0.71 mmol) in 15 mL MeCN were combined and after 20 min the black microcrystals were filtered off and washed with 4 x 10 mL MeCN, yield 229 mg (0.647 mmol, 91 %), m.p. > 152 ºC dec. IR: 1505 (s), 1435 (s,b), 1419 (s,b), 1344 (s), 1307 (m), 1264 (m), 1197 (w), 1174 (w), 1062 (w), 1009 (s), 842 (w), 816 (w), 693 (w), 606 (m), 659 (m), 569 (m), 522 (m), 464 (w) cm^{-1}.

Synthesis of 4-ethyl-8-methyl-4*H-bis*[1,2,3]thiaselenazolo[4,5-b:5',4'-e]pyridin-3-yl, 4-1c (R_1 = Et, R_2 = Me): **Method 1.** *Bulk material for conductivity and magnetic measurements*. Before use, all glassware was soaked overnight in dilute HNO_3, then washed with dionized water, then distilled water and finally oven dried at 100 °C overnight. Magnetic stirbars were glass-covered. Degassed solutions (3 freeze-pump-thaw cycles) of DMFc (0.199 g, 0.610 mmol) in 125 mL MeCN and [**4-1b**][OTf] (R_1 = Et, R_2 = Me) (0.300 g, 0.580 mmol) in 125 mL MeCN were combined and after 20 min the green crystals were filtered off and washed with 4 x 10 mL MeCN; yield 190 mg (0.516 mmol, 89 %); dec > 150 ºC. IR: 1319 (m), 1233 (s), 1178 (w), 1085 (w), 1006 (w), 978 (w), 837 (m), 702 (s), 613 (s), 539 (w), 461 (w) cm^{-1}. Anal. Calcd for $C_8H_8N_3S_2Se_2$: C, 26.09; H, 2.19; N, 11.41 %. Found: C, 26.42; H, 2.48; 11.62 %.

Method 2. *Diffusion H-cells for single crystal growth*. Degassed solutions (3 freeze-pump-thaw cycles) of OMFc (35.0 mg, 0.155 mol) in 15 mL MeCN and [**4-1b**][OTf] (R_1 = Et, R_2 = Me) (20 mg, 0.0387 mol) in 10 mL MeCN were allowed to diffuse together slowly at room temperature over a period of 16 h. The solvent was decanted to leave metallic green needles of **4-1b** suitable for X-ray work.

Chapter 5

Enhanced Conductivity and Magnetic Ordering in Isostructural Heavy-Atom Radicals

5.1 Introduction

The previous chapter presented the synthesis and solid state properties of **5-2** (R_1 = Et, R_2 = Me). The radical was shown to crystallize in the space group $P\bar{4}2_1m$, forming undimerized π-radical stacks along the *z*-axis; short Se---Se′ intermolecular contacts tightly lace the π-columns together around the central $\bar{4}$ axis. Variable temperature conductivity measurements demonstrate an increase in conductivity when Se is inserted into the E_2 position of the heterocyclic frame (σ(300 K) = 1.9 $\times 10^{-4}$ S cm^{-1}). The radical also demonstrates typical Curie-Weiss behaviour in the 300 - 50 K range, however it is the ferromagnetic ordering of **5-2** (R_1 = Et, R_2 = Me) at 13.6 K and magnetic hysteresis that separates this material from all other thiazyl (SN) radicals characterized to date. At the onset of this work, it was questioned whether or not the incorporation of Se into the E_2 ring position was responsible for the observed magnetic properties. In order to provide the answer to this critical question, the synthetic insertion of Se into **5-1a** (R_1 = Et, R_2 = Cl), which is isostructural to **5-1b** (R_1 = Et, R_2 = Me), was investigated.

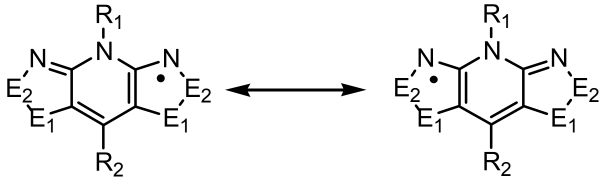

	E_1	**E_2**
1	S	S
2	S	Se
3	Se	S
4	Se	Se

5-1a, 5-2a, 5-3a, 5-4a: R_1 = Et, R_2 = Cl

Scheme 5.1

In this chapter, a full account of the synthesis, spectroscopic, electrochemical and structural (at 100 K and 295 K) characterization of the family of S/Se-based radicals **5-1a** - **5-4a** is presented. These four compounds constitute a complete isostructural set, all belonging to the tetragonal space group $P\bar{4}2_1m$. Variable temperature (AC and DC) magnetic susceptibility and four-probe conductivity measurements have been performed on the Se-based radicals **5-2a**, **5-3a** and **5-4a**. The results provide a pleasing and dramatic display of the effect of the placement (E_1 versus E_2) of Se on transport properties. Conductivities increase and thermal activation energies decrease with Se content along the series **5-1a**, **5-3a**, **5-2a**, **5-4a**, in accord with trends in bandwidth (*W*) estimated from Extended Hückel Theory (EHT) band structure calculations. Magnetic exchange interactions also vary along the series where it has been observed that **5-2a** (E_2 = Se) orders ferromagnetically at 12.6 K and radical **5-3a** (E_1 = Se) behaves as a spin-canted antiferromagnet, ordering near 14 K. Bulk ferromagnetic ordering returns in radical **5-4a**, and the Curie temperature increases to T_c = 17 K.

5.2 Synthesis

Preparative routes to salts of the all-S framework **5-1a**, using the double Herz cyclization of an *N*-alkylated diaminopyridinium salt with sulfur halides, have been reported previously.[1] Our initial approach for the generation of derivatives of **5-2a**, with Se in the E_2-position, was based on the condensation of S-acetylated pyridinedithiols with Se halides, which provided an effective but somewhat lengthy preparative procedure.[2] More recently we have taken advantage of chemistry developed thirty years ago[3] for the direct incorporation of Se into the 2-position of monofunctional 1,2,3-dithiazolylium salts using SeO_2.[4] The method is readily applicable to the present *bis*-DTA systems, and allows for the direct conversion of [**5-1a**]$^+$ into [**5-2a**]$^+$ in a single step.[5] Thus, [**5-1a**][OTf] was treated with SeO_2 in a sealed glass pressure vessel in MeCN (**Scheme 5.2a**). The Se insertion process was monitored by ESI mass spectroscopy, and it was determined that after 48 h of heating at 110 °C a complete transformation of [**5-1a**]$^+$ to [**5-2a**]$^+$ occurred. The vessel was cooled and the solution was filtered through a glass frit, removing a small amount of black precipitate. The filtrate was then concentrated to ~30 mL and placed in the freezer. After 2 hours, there were lustrous red needles, which could be recrystallized from MeCN.

The preparation of salts of [**5-3a**]$^+$ and [**5-4a**]$^+$, which possess Se in the E_1-position, required a different strategy, which utilized the previously synthesized [**5-3**][OTf] (R_1 = Et, R_2 = H) (**Scheme 5.2b**).[6] Thus *N*-ethyl triflate [**5-3**][OTf] (R_1 = Et, R_2 = H) was chlorinated with iodobenzene dichloride under gentle reflux for 1 h and then hot filtered and concentrated, yielding the desired salt [**5-3a**][OTf] as red needles that could be recrystallized in MeCN (**Scheme 5.2b**). Conversion of [**5-3a**][OTf] to [**5-4a**][OTf] utilized the SeO_2 insertion method described above, however, it was later found that treatment of [**5-3a**][OTf] with SeO_2 in HOAc under reflux for 90 min in a sealed glass vessel was a more convenient route, as it gave rise to a solution of [**5-4a**][OTf], as verified by ESI mass spectroscopy. The resulting material was concentrated, precipitating red/purple needles, which could be recrystallized in MeCN and HOAc.

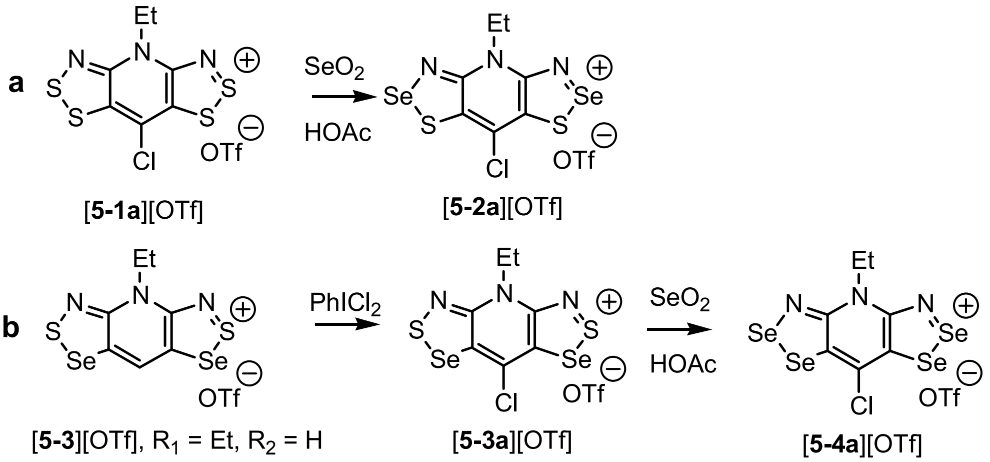

Scheme 5.2

Reduction of the triflate salts of [**5-2a**]$^+$, [**5-3a**]$^+$ and [**5-4a**]$^+$ to afford crystals of the corresponding radicals can be effected chemically and, in one case, electrochemically. We have explored a variety of chemical reducing agents, including deca-, octa- and hexamethylferrocene (DMFc, OMFc and HMFc respectively), tetrakisdimethyl-aminoethylene (TDAE) and N,N,N′,N′-tetramethyl-*p*-phenylenediamine (TMPDA).[7] The eventual choice of reagent was dictated in part by the reduction potentials of the cations (*vide infra*), and partly by concerns about potential contamination of the resulting radicals by paramagnetic by-products, notably ferrocenium salts. Thus, while OMFc performed admirably, and provided single crystals of **5-2a** and **5-3a** suitable for X-ray work, we moved to TDAE in order to eliminate the possibility of metal contamination of samples used for magnetic measurements. TDAE is, however, a more potent reductant, and while it provided analytically pure material, magnetic measurements (*vide infra*) indicated the production of small amounts of diamagnetic material, possibly dimers. Eventually, we turned to TMPDA, a much milder reagent which afforded clean, defect-free, microcrystalline material. The magnetic data reported in this work refer to samples of the radicals generated in this way. Crystals of **5-4a** of sufficient size for X-ray data collection could not be grown by chemical reduction. Satisfyingly, however, the conductivity of this material was such that high quality needles could be grown by electrocrystallization.

This is, to our knowledge, the first instance where this technique has been applied to the growth of a neutral radical.

5.3 Cyclic Voltammetry and EPR Spectroscopy

Electron paramagnetic resonance (EPR) studies on **5-1a** provided confirmation of a highly delocalized spin distribution, the characteristic five-line hyperfine pattern arising from spin coupling to two equivalent ^{14}N nuclei on the two dithiazolyl (DTA) rings.[1] As expected, the observed a_N values (**Table 5.1**) are about one-half those seen in monofunctional DTAs.[8] There are also smaller couplings to the central pyridine nitrogen which can be extracted by spectral simulation. The Se-based radicals **5-2a** - **5-4a** are less soluble than **5-1a**, and solution-based spectra were more difficult to obtain. Good signal-to-noise ratios were eventually achieved by dissolving the radicals in hot degassed toluene. The X-band EPR spectra of the complete series **5-1a** - **5-4a** (recorded at ambient temperature) are shown in **Figure 5.1**. The same five-line appearance is seen in all cases, but the incorporation of Se leads to a progressive line-broadening caused by spin-orbit coupling. For the same reason, there is also a slight increase in the *g*-value (**Table 5.1**), but otherwise the similarity in the spectra confirm the same basic spin distribution, a conclusion predicted by theoretical calculations.[2b]

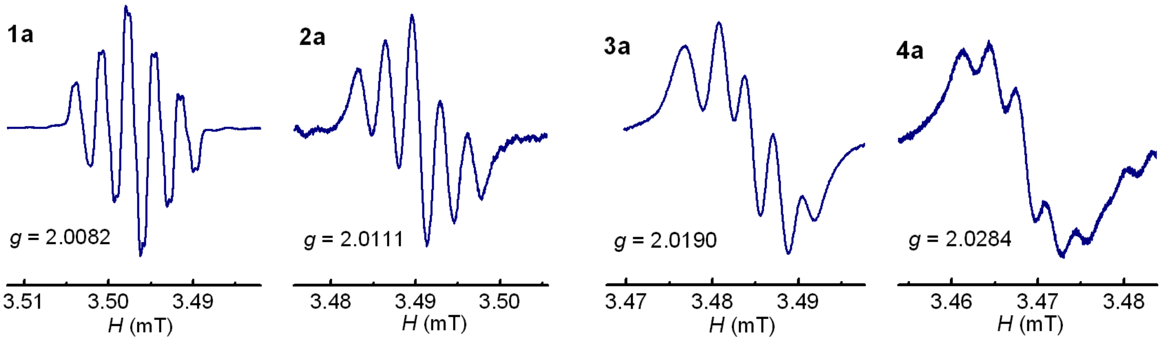

Figure 5.1 X-band EPR spectra of **5-1a** - **5-4a** in toluene, SW = 30 mT. Derived hyperfine coupling constants (for N1 and N2) and *g*-values are listed in **Table 5.1**; extracted a_{Cl} values (corresponding to the $^{35/37}$Cl isotope) for **5-1a** are 0.030, 0.024 mT.

Table 5.1 Hyperfine Coupling Constants (in mT), *g*-Values and Half-Wave Potentials (in V).

	5-1a	**5-2a**	**5-3a**	**5-4a**
a_{N}	0.310 (2N) 0.060 (1N)	0.310 (2N) 0.060 (1N)	0.32 (2N) 0.05 (1N)	0.32 (2N) 0.05 (1N)
g-value	2.0082	2.0111	2.0190	2.0284
$E_{1/2}$ (−1/0)[a]	−0.845	−0.731	−0.813	---[c]
$E_{1/2}$ (0/+1)[a]	−0.018	0.013	0.026	0.053[d]
$E_{1/2}$ (+1/+2)[a]	1.390	1.343	1.311	1.267
E_{cell}[a,b]	0.827	0.744	0.839	---

[a] $E_{1/2}$ values (V) in MeCN, ref. SCE. [b] $E_{cell} = E_{1/2}(0/+1) - E_{1/2}(-1/0)$. [c] No wave observed. [d] Reversible wave at 45 °C and 1000 mV s^{-1}.

The electrochemical behaviour of **5-1a** - **5-4a** has been probed by cyclic voltammetry on solutions of the triflate salts [**5-1a** - **5-4a**][OTf] in MeCN (with [*n*-Bu_4][NPF_6] as supporting electrolyte). The results are presented in the form of half-wave potentials $E_{1/2}$ in **Table 5.1**, and a representative scan (for **5-3a**) is illustrated in **Figure 5.2**. Compounds **5-1a**, **5-2a** and **5-3a** all show three reversible waves, corresponding to the -1/0, 0/+1, and +1/+2 processes. In the case of **5-4a**, the two more positive waves are reversible, but the -1/0 wave collapses completely; the 0/+1 couple also becomes strongly irreversible if the scan range is taken to potentials significantly more cathodic than that of the 0/+1 process. Although the E_{cell} data do not form a complete set (the $E_{1/2}(-1/0)$ value for **5-4a** is not available), some observations can be made about electronic changes along the series **5-1a** to **5-4a**. First, there is a slight anodic shift in the $E_{1/2}(0/+1)$ value with increasing Se content. This change is in accord with the results of calculated (B3LYP/6-31G(d,p)) ionization potentials,[2b] but not sufficiently large to influence the choice of chemical reducing agent for the generation of the radicals. Likewise the slight decrease in cell potential E_{cell} between **5-1a** and **5-2a** parallels the changes in computed gas phase disproportionation energies on model structures,[2b] and augurs well for a slight decrease in the on-site Coulomb repulsion term *U* with increasing Se content in the E_2 position.

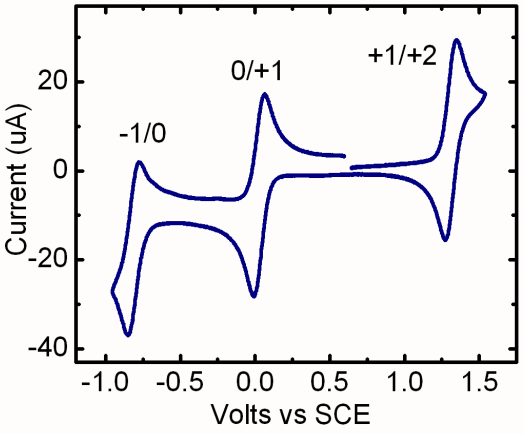

Figure 5.2 Cyclic voltammetry on [**5-3a**][OTf] in acetonitrile with [*n*-Bu_4N][PF_6] supporting electrolyte.

5.4 Crystal Structures

Unit cell information and selected distances on **5-1a** - **5-4a**, derived from X-ray data collected at ambient temperature, are presented in **Table 5.2**. We have also collected full data sets at 100 K, and structural summaries from these refinements are catalogued in **Table 5.3**. The results establish that the four compounds are isostructural, all crystallizing in the tetragonal space group $P\overline{4}2_1m$. As anticipated, dimerization is suppressed across the entire series, even at low temperatures (100 K). At the molecular level the intramolecular distances and angles are typical for this class of heterocyclic radical, the internal E_1-E_2, E_2-N and E_1-C bonds being slightly longer than in the corresponding cations. The difference can be ascribed to the antibonding nature of the radical SOMO, which is not occupied in the cation.[1]

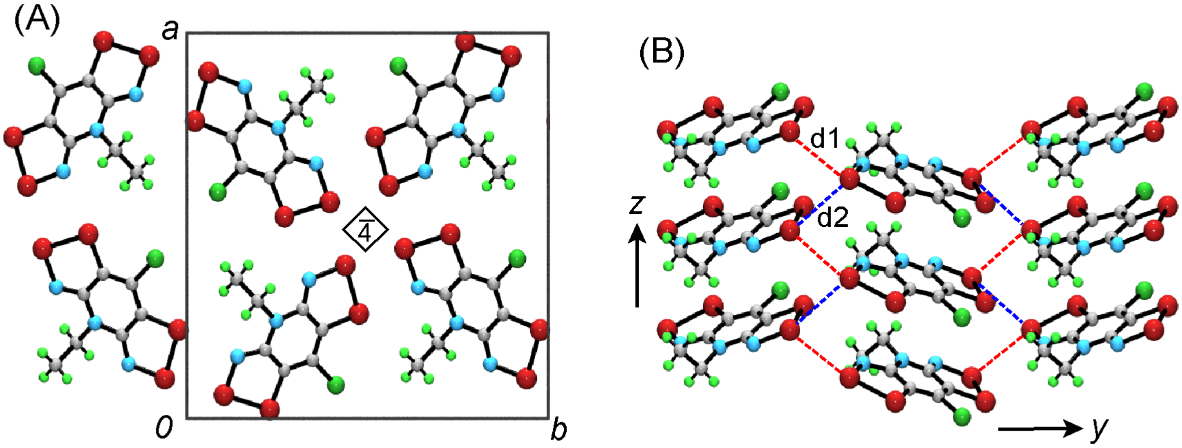

Figure 5.3 Crystal packing of **5-4a** at 298 K, viewed along the *z*- (a) and *x*- (b) directions.

The crystal structures consist of undimerized radicals bisected by mirror planes which generate four-fold pinwheel-like clusters about the $\overline{4}$ centers. The radicals pack in slipped π-stack arrays running along the *z*-direction. The mean interplanar separations δ and the inclination angle τ of the mean molecular plane with respect to the stacking axis are listed in **Table 5.2**[1c] and **Table 5.3**. Representative views of the packing of **5-4a**, along directions parallel and perpendicular to the stacking axis, are shown in **Figure 5.3**. While the radicals are not dimerized, there is an extensive lattice-wide network of intermolecular interactions which lace the radicals together along the stacking direction and perpendicular to it in both the *x*- and *y*-directions. The E---E′contacts d1 - d3 to/from a single radical are shown in **Figure 5.4**, using **5-4a** at 298 K as an example, along with the weblike patterns that these generate along and about the $\overline{4}$ centers. All these contacts are well within the nominal van der Waals separation for S (3.6 Å) and Se (3.8 Å).[9] Of particular note is the contraction in d1 and d2 in **5-2a** and **5-4a** relative to **5-1a** and **5-3a** respectively (**Figure 5.5**). The closer interactions found when Se occupies the E_2 site are reminiscent of the contractions in intermolecular contacts seen in other heavy chalcogen heterocycles.[10] As described below, the four-center Se clusters in **2a** and **4a** play a major role in increasing intermolecular overlap and hence W. They also give rise to interesting magnetic properties.

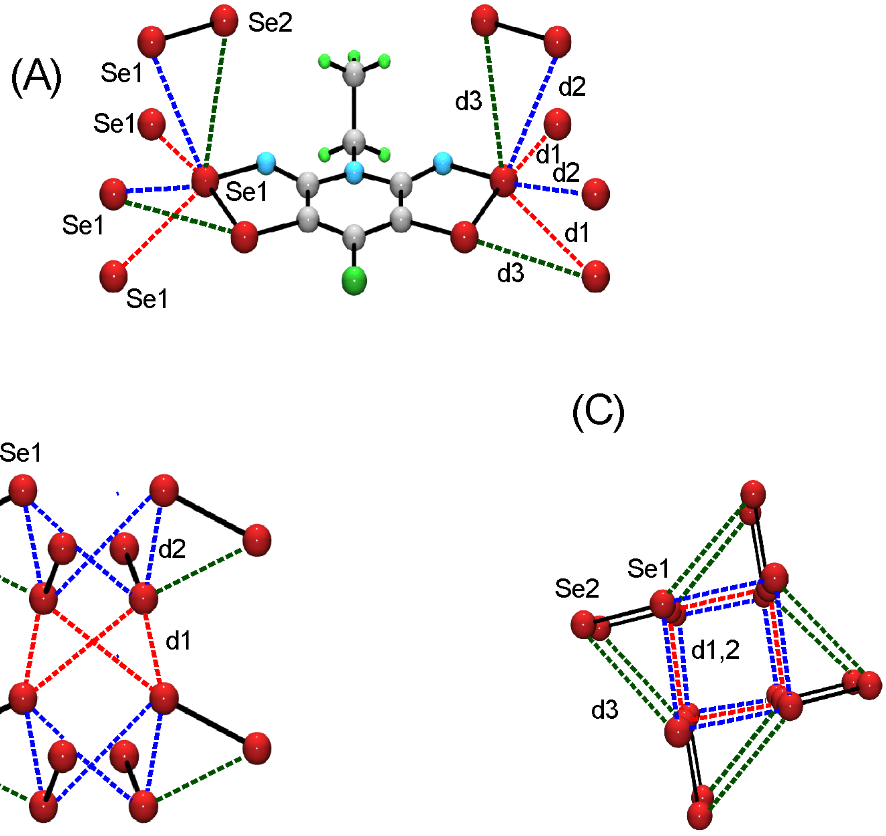

Figure 5.4 Intermolecular Se---Se′ contacts d1 - d3 to a single molecule of **5-4a** at 298 K (a), and about the $\overline{4}$ centers, viewed perpendicular (b) and parallel (c) to the *z*-direction.

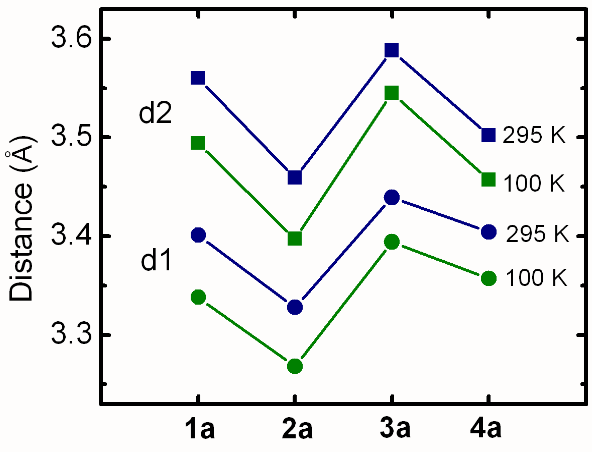

Figure 5.5 Variations in intermolecular E_2---E_2' contacts d1 and d2 in **5-1a** - **5-4a**.

Table 5.2 Crystal Data and Metrics for **5-1a** - **5-4a** at *ca.* 298 K.

	5-1a [a]	**5-2a**	**5-3a**	**5-4a**
Formula	$C_7H_5ClN_3S_4$	$C_7H_5ClN_3S_2Se_2$	$C_7H_5ClN_3S_2Se_2$	$C_7H_5ClN_3Se_4$
M	294.83	388.63	388.63	482.43
a, Å	15.886(4)	16.0334(8)	16.0565(4)	16.2708(5)
c, Å	4.1088(11)	4.1090(4)	4.1599(2)	4.1720(3)
V, Å^3	1036.9(5)	1056.30(13)	1072.47(6)	1104.49(9)
ρ(calcd), g cm^{-1}	1.889	2.444	2.407	2.901
space group	$P\bar{4}2_1m$	$P\bar{4}2_1m$	$P\bar{4}2_1m$	$P\bar{4}2_1m$
Z	4	4	4	4
temp, K	293(2)	298(2)	295(2)	296(2)
μ, mm^{-1}	1.137	7.613	7.498	13.494
λ, Å	0.71073	0.71073	0.71073	0.71073
data/restr./parameters	1064/0/87	1150/0/76	2150/0/76	1209/0/76
solution method	direct methods	direct methods	direct methods	direct methods
R, R_w (on F^2)	0.0279, 0.0571	0.0447, 0.1003	0.0402, 0.0822	0.0374, 0.0635
E_1-E_2, Å	2.1049(12)	2.249(2)	2.2325(9)	2.3614(10)
E_2-N, Å	1.663(3)	1.805(6)	1.660(3)	1.829(5)
E_1-C, Å	1.728(3)	1.733(7)	1.863(3)	1.868(6)
d_1, Å	3.401(1)	3.328(1)	3.439(2)	3.404(1)
d_2, Å	3.560(1)	3.459(1)	3.588(2)	3.502(1)
d_3, Å	3.573(1)	3.655(2)	3.467(1)	3.618(1)
δ, Å	3.483(12)	3.516(7)	3.511(3)	3.545(6)
τ, deg	57.9(3)	58.83(1)	57.57(1)	58.18(2)
deviation from plane, Å	0.0663	0.087	0.0790	0.0843

[a] Data from reference 1a.

Table 5.3 Crystal Data and Metrics for **5-1a** - **5-4a** at 100 K.

	5-1a	**5-2a**	**5-3a**	**5-4a**
Formula	$C_7H_5ClN_3S_4$	$C_7H_5ClN_3S_2Se_2$	$C_7H_5ClN_3S_2Se_2$	$C_7H_5ClN_3Se_4$
M	294.83	388.63	388.63	482.43
a, Å	15.7927(3)	15.9040(10)	16.0331(6)	16.1801(12)
c, Å	4.0310(2)	4.0161(5)	4.0920(3)	4.1264(6)
V, Å^3	1005.37(6)	1015.49(16)	1051.89(6)	1080.27(8)
ρ(calcd), g cm^{-1}	1.948	2.542	2.454	2.966
space group	$P\overline{4}2_1m$	$P\overline{4}2_1m$	$P\overline{4}2_1m$	$P\overline{4}2_1m$
Z	4	4	4	4
temp, K	100(2)	100(2)	100(2)	100(2)
μ, mm^{-1}	1.173	7.920	7.650	13.80
λ, Å	0.71073	0.71073	0.71073	0.71073
data/restr./parameters	1149/0/88	1077/12/76	1350/0/76	1175/0/77
solution method	direct methods	direct methods	direct methods	direct methods
R, R_w (on F^2)	0.0177,0.0387	0.0371,0.0717	0.0197,0.0495	0.0376,0.0813
E_1-E_2, Å	2.1102(6)	2.2391(17)	2.2422(7)	2.3633(11)
E_2-N, Å	1.6647(15)	1.8104(54)	1.6696(22)	1.8190(65)
E_1-C, Å	1.7322(17)	1.7290(60)	1.8711(24)	1.8702(77)
d_1, Å	3.338(1)	3.266(1)	3.394(1)	3.357(1)
d_2, Å	3.494(1)	3.397(1)	3.545(1)	3.457(1)
d_3, Å	3.524(1)	3.613(2)	3.446(1)	3.585(1)
δ, Å	3.455(1)	3.450(2)	3.487(1)	3.492(3)
τ, deg	59.0(1)	59.2(1)	58.5(1)	57.82(1)
deviation from plane, Å	0.105	0.096	0.101	0.103

5.5 Band Structures

In order to compare the extent of intermolecular electronic interactions in the four isostructural radicals **5-1a** - **5-4a** we performed a series of EHT band structure calculations on structural data collected at 298 K. The results must be viewed with caution, as the tight-binding model is inadequate for strongly correlated systems such as these. Nonetheless, within a closely related series of structures, as in the present case, the EHT method gives a qualitative insight into trends in orbital interactions, and hence bandwidth *W*, estimated here in terms of the energetic spread (dispersion) of the crystal orbitals (COs) under consideration. The results are summarized in **Figure 5.6**, which shows the dispersion of the COs arising from the four singly occupied molecular orbitals (SOMOs) in the respective unit cells, plotted along the reciprocal space direction Γ (0, 0, 0) to Z (0, 0, ½,). By virtue of the tetragonal symmetry, CO trends along this reciprocal space vector can be associated precisely with orbital interactions along the stacking axis in real space. The tetragonal symmetry also leads to the degeneracy (coincidence) of two of the COs, and in the case of **5-2a** and **5-4a** there is an intruder orbital that falls in the same energy range.

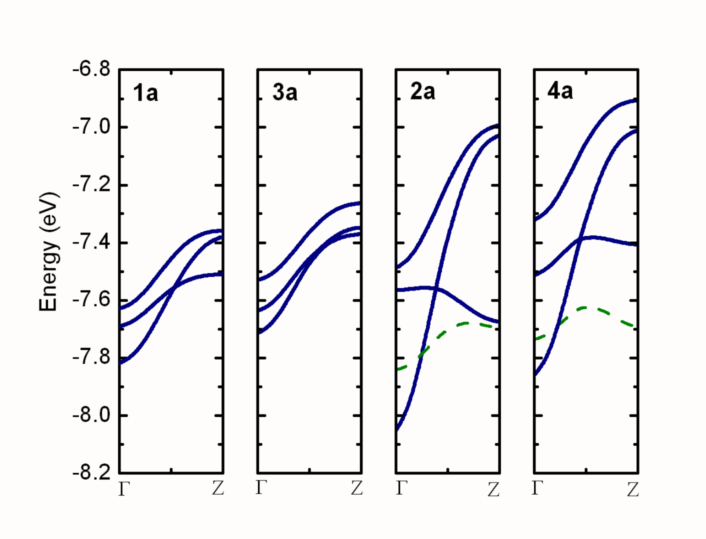

Figure 5.6 CO dispersion curves from Γ (0, 0, 0) to Z (0, 0, ½). Dashed green lines are intruder bands.

From the spread of the dispersion curves across the series **5-1a** - **5-4a** it is readily apparent that the four compounds can be separated into two pairs, that is, those with sulfur (**5-1a**/**5-3a**) and those with Se (**5-2a**/**5-4a**) in the E_2-position. The increase in bandwidth between the two groups, from *W* near 0.5 eV to near

1.0 eV (**Table 5.4**), is quite dramatic, the latter values being significantly larger than in any slipped π-stack thiazyl radical and equivalent to **5-2** (R_1 = Et, R_2 = Me; presented in **Chapter 4**) . The increased CO dispersion which leads to this enhancement in *W* can, we believe, be attributed to the much tighter d1 and d2 contacts (**Table 5.2**, **Table 5.3** and **Figure 5.5**) about the $\overline{4}$ centers in **5-2a**/**5-4a**. Similarly, the slight decrease in *W* within the two pairs **5-1a**/**5-3a** and **5-2a**/**5-4a** can be related to the slight expansion in the contacts d1 and d2 occasioned by the replacement of sulfur by Se in the E_1 position.

Table 5.4 Bandwidth, Conductivity and Magnetic[a] Parameters.

	5-1a	**5-2a**	**5-3a**	**5-4a**
W (eV)	0.46	1.06	0.45	0.95
σ(300 K) (S cm^{-1})	3.2 ×10^{-6} [b]	1.0 × 10^{-4}	2.2 ×10^{-5}	3.0 × 10^{-4}
E_{act} (eV)	0.43 [b]	0.27	0.31	0.19
C (emu K mol^{-1})	0.373	0.369	0.396	0.392
θ (K)	3.6	20.3	-2.3	22.9
T_c (K)	---	12.8	14	17.0
M_{sat} (Nβ) at 2 K	---	1.00	---	1.03
M_{rem} (Nβ) at 2 K	---	0.41	0.15 ×10^{-3}	0.43
H_c (Oe) at 2 K	---	250	66	1370

[a] Data for **5-2a** - **5-4a** from samples prepared using TMPDA as reducing agent. [b] Data from reference 1a.

5.6 Conductivity and Magnetism

The results of the band structure calculations described above, especially the large bandwidths estimated for **5-2a** and **5-4a**, led us to anticipate an increased conductivity in these systems. Variable temperature, four-probe pressed pellet conductivity measurements on the four compounds confirmed these expectations. The results are presented in **Figure 5.7** in the form of plots of log σ versus 1/*T*. Despite the apparently large *W*, which for **5-2a** and **5-4a** are energetically comparable to *U* (arbitrarily estimated as *U* ~ E_{cell}), the materials are not metallic. Instead, the conductivity remains activated. There is, nonetheless, a satisfying correlation between the estimated (EHT) bandwidth, the observed conductivity and the derived thermal activation energy E_{act} (**Table 5.4**). Over the complete series, σ(300 K) increases by two orders of magnitude, and E_{act} decreases with increasing Se content from a maximum of 0.43 eV in **5-1a** to 0.19 eV in **5-4a**. Within the mixed S/Se systems **5-2a** and **5-3a** the former has the higher conductivity and lower activation energy, in accord with the tighter d1,2 contacts and the resulting improvement in *W*.

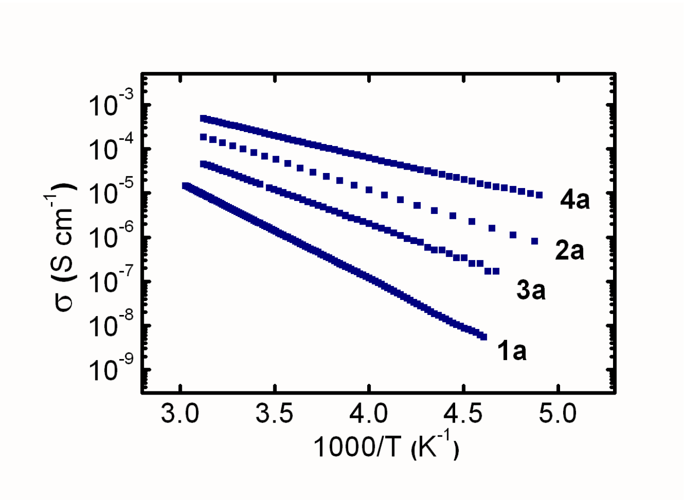

Figure 5.7 Log σ versus 1/*T* plots for **5-1a** - **5-4a**. Derived activation energies are in **Table 5.4**.

Magnetic susceptibility measurements have been performed on **5-1a** - **5-4a** over the temperature range 2 - 300 K. At temperatures above 50 K, the static susceptibility χ (corrected for diamagnetic contributions)[11] of all four compounds follows paramagnetic behaviour; values of *C* and *θ* derived from Curie-Weiss fits to the high temperature data are listed in **Table 5.4**. Below 50 K, however, there are some dramatic changes. For presentation and discussion purposes, results on the four compounds can be separated into two groups, that is, **5-1a** and **5-3a**, which contain S in the E_2 position, and **5-2a** and **5-4a**, which have Se at this site.

Figure 5.8 shows plots of the function χ*T* versus *T* for the first group (**5-1a** and **5-3a**), measured in field-cooled mode at a field strength *H* = 100 Oe. In accord with its small positive *θ*-value, χ*T* for **5-1a** rises slowly upon cooling from room temperature, indicative of weak local ferromagnetic interactions. It reaches a maximum (0.46 emu K mol^{-1}) at about 15 K, then drops rapidly as a result of weaker antiferromagnetic effects. Compound **5-3a** has a small but negative *θ*-value, indicative of weak antiferromagnetic coupling, and accordingly χT decreases rapidly at lower temperatures. Careful examination of the data below 20 K suggested a slight discontinuity, which became more apparent in a χ versus T plot. We therefore performed a series of zero-field-cooled (ZFC) and field-cooled (FC) experiments at different fields. The ZFC and FC curves of χ versus T are virtually coincident at 10 kOe, but when the field is reduced to 100 Oe, there is a separation in the two plots (**Figure 5.8** insert), with a bifurcation or blocking temperature of 14 K. We have seen similar behaviour for **5-3** (and **5-4**) with R_1 = Et, R_2 = H,[12] and, as for those systems, we believe the results here are a manifestation of a phase transition to a spin-canted antiferromagnetic state.

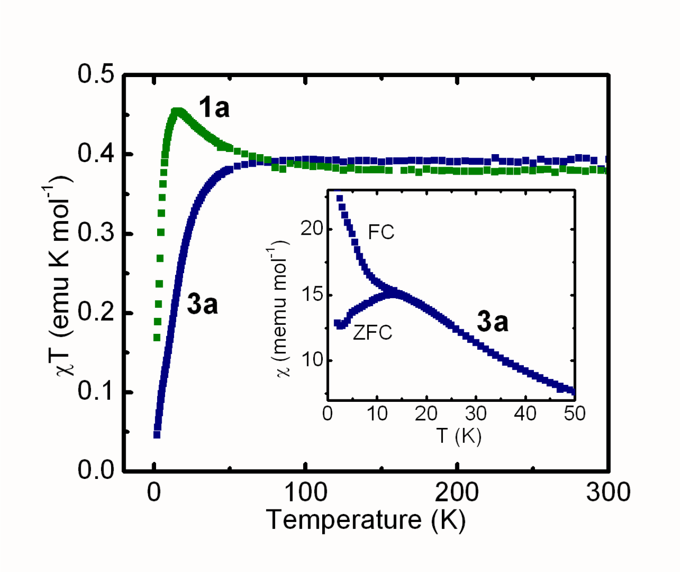

Figure 5.8 Plots of χT (field-cooled) versus temperature for **5-1a** and **5-3a** at 100 Oe. The insert shows ZFC-FC plots of χ versus T for **3a** at 100 Oe.

Further evidence in favour of this interpretation is provided by a measurement of the field-independent or spontaneous magnetization M_{sp} as a function of temperature. As shown in **Figure 5.9**, M_{sp} decays rapidly, approaching a plateau near zero at about T = 14 K, in accord with the blocking temperature noted in the ZFC-FC experiment. When extrapolated to T = 0 K, M_{sp} reaches a value of 0.18 mNβ, which can be used to estimate a spin canting angle $\phi = 0.010°$ by using the formula $\phi = \sin^{-1}(M_{\mathrm{sp}}/M_{\mathrm{sat}})$, where M_{sat} is approximated at 1 Nβ, that is, the saturation value ($M_{\mathrm{sat}} = gS\mathrm{N}\beta$) of magnetization for a ferromagnetic material with $S = \frac{1}{2}$ and $g = 2$. Magnetization experiments at 2 K as a function of field (H = 0 to 50 kOe) reveal a very weak, linear response with increasing field. The magnetization is slightly hysteretic (**Figure**

5.9 insert), as expected, giving rise to a coercive field H_c = 66 Oe (at 2 K) and remanent magnetization M_{rem} of 0.15 mNβ.

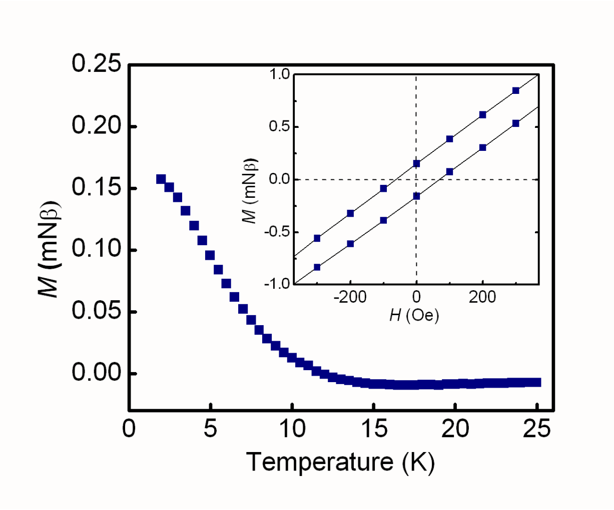

Figure 5.9 Field independent magnetization versus temperature for **5-3a**. The insert shows M versus H at 2 K.

Plots of the product χT (field cooled) versus temperature for **5-2a** and **5-4a** at a field of H = 100 Oe (**Figure 5.10**) confirm that both compounds behave as paramagnets between 50 K and 300 K, with χT(300 K) values of 0.392 emu K mol^{-1} (**5-2a**) and 0.432 emu K mol^{-1} (**5-4a**). Curie-Weiss fits to the data afford Curie constants C of 0.369 emu K mol^{-1} and 0.392 emu K mol^{-1} respectively, that is, near the value expected (0.375 emu K mol^{-1}) for an S = ½ system with g nominally equal to 2. The large positive Weiss constants of 20.3 K (**5-2a**) and 22.9 K(**5-4a**) herald strong local ferromagnetic exchange interactions. Upon cooling both compounds there is a slow rise in χT, in keeping with the positive θ-values. A dramatic surge takes place just below 15 K for **5-2a** and 20 K for **5-4a**, with χT reaching a maximum value of 182 emu K mol^{-1} at 10 K for **5-2a** and of 244 emu K mol^{-1} at 14 K for **5-4a**. This response is consistent with a phase transition to a ferromagnetically ordered state. At temperatures below these maxima there is a steady drop-off in χT for both compounds, as would be expected from low temperature magnetization saturation.

Measurements of the field independent magnetization M_{sp} of **5-2a** and **5-4a** provided further evidence for the existence of a ferromagnetically ordered state, and also afforded a more accurate assessment of the ordering temperatures. As illustrated in **Figure 5.11**, M_{sp} is strongly temperature dependent for both compounds, decaying to zero near 12.5 K and 17 K respectively, in accord with the point of maximum slope in the χT versus T plots described above. Back-extrapolation to T = 0 K afforded values of M_{sp}, the spontaneous magnetization at 0 K near 0.41 Nβ (**5-2a**) and 0.43 Nβ (**5-4a**), that is, three orders of magnitude greater than that seen for the spin-canted antiferromagnet **5-3a**. Variable AC susceptibility measurements at different frequencies on **5-2a** and **5-4a** allowed us to pinpoint the ordering temperatures T_c of the two compounds. As shown in **Figure 5.12**, both radicals show sharp, well-defined maxima in the real (in-phase) χ' and imaginary (out-of-phase) χ'' components at 12.8 K and 17.0 K respectively. The invariance of T_c with changes in the cycling frequency (from 50 Hz to 5 kHz) establishes that these materials are not spin glasses.

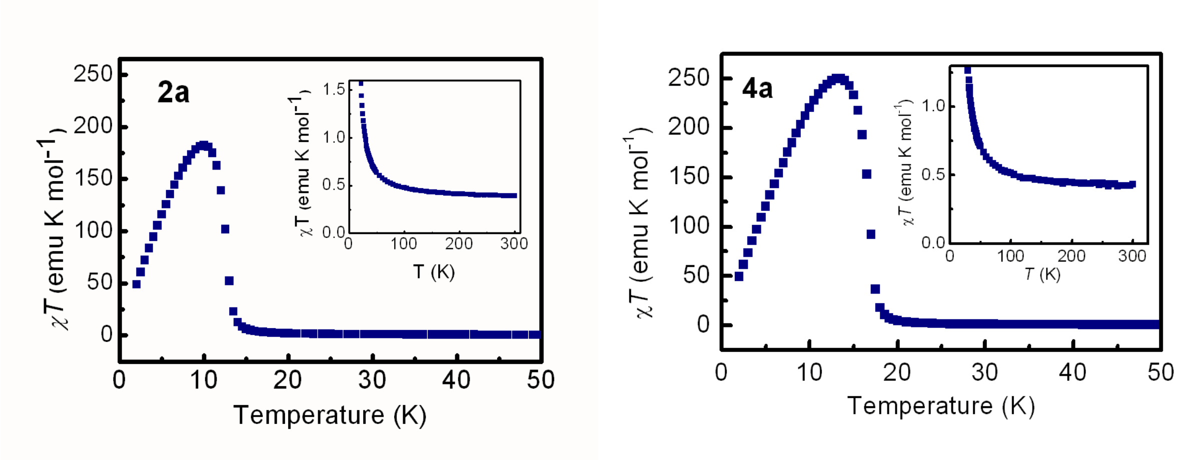

Figure 5.10 Plots of χT (field-cooled) versus temperature for **5-2a** and **5-4a** at 100 Oe. The inserts show an expansion of the high T region.

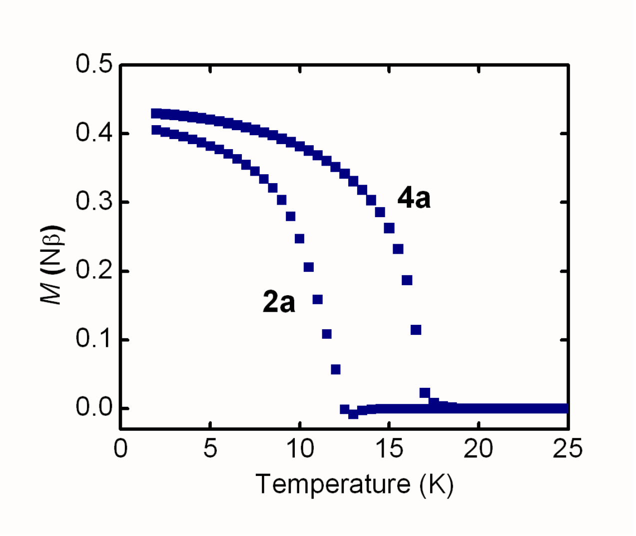

Figure 5.11 Field independent magnetization as a function of temperature for **5-2a** and **5-4a**.

Magnetization experiments as a function of field have also been performed on **5-2a** and **5-4a**. In both cases M rises sharply with H, reaching (at 2 K) a maximum at $H = 10$ kOe, after which there is no further change in M with H (up to 55 kOe). The corresponding saturation magnetization values M_{sat} are 1.00 Nβ for **5-2a** and 1.03 Nβ for **5-4a**.[13] Reversal and cycling of the field sweep leads to hysteresis in the magnetization, the magnitude of which increases with increasing Se content. Plots of M versus H, from measurements taken at 2 K on samples of the two compounds are shown in **Figure 5.13**. While the remanent magnetization M_{rem} of the two compounds is virtually the same, the coercive field H_c of **5-4a** (1370 Oe) is significantly greater than found for **5-2a** (250 Oe).

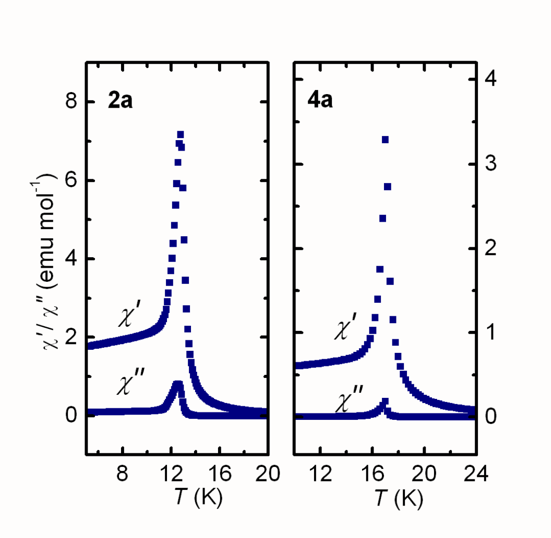

Figure 5.12 In-phase χ′ and out-of-phase χ″ AC magnetic susceptibility (at 1 KHz) of **5-2a** and **5-4a** as a function of temperature.

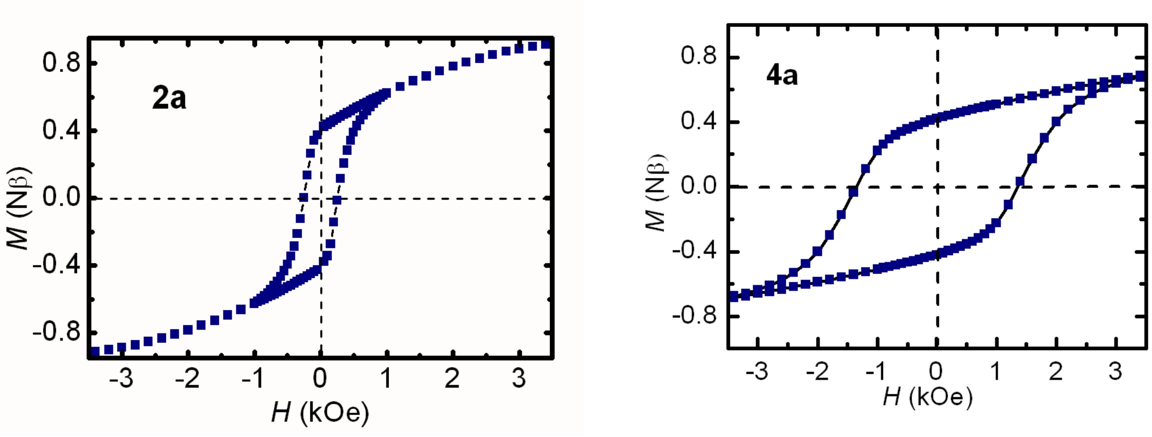

Figure 5.13 Magnetization of **5-2a** and **5-4a** as a function of magnetic field at 2 K.

5.7 Discussion

Our long-standing interest in the use of heterocyclic thiazyl (SN) radicals as building blocks for single component molecular conductors has been predicated on the idea that intermolecular overlap and hence *W* can be enhanced by the presence of a spatially extensive heteroatom.[14] However, these materials suffered from (i) a propensity to dimerize and (ii) high on-site Coulomb repulsion barriers. With the development of resonance stabilized systems such as **5-1a** these two problems were partly alleviated, but loss in *W* arising from π-stack slippage undermined attempts to achieve major improvements in conductivity.[15] The previous chapter sought to probe the effects of Se incorporation into **5-1** (R_1 = Et, R_2 = Me), with the goal being to improve upon the *W* and hence, conductivity of the radical system. The work resulted in the generation of a neutral radical that is isostructural to **5-1a**. However, of greater importance, it was shown that the Se-containing radical gives rise to greatly improved *W*, conductivity and bulk ferromagnetism (at 13.6 K) in the solid state. With these results in hand, we explored the incorporation of Se into **5-1a**, affording the series of S/Se-based materials **5-1a** - **5-4a**. In these series of experiments, our intent was to (i) probe the effects of Se incorporation on the bulk conductivity of the radical, and (ii) investigate the magnetic properties of the Se-containing radicals; both points will be addressed below.

This work was driven by our belief that the heavier heteroatom would provide stronger intermolecular interactions and hence increased *W* and the results on **5-1a** - **5-4a** demonstrate, at several levels, that replacement of S by Se works. We have shown, for the first time, that spin-pairing dimerization can be avoided across an entire series of mixed S/Se-based radicals. We have also achieved an isomorphous mapping across all four compounds, thereby allowing a detailed correlation of structure and transport properties. From a structural perspective, the major difference within the family **5-1a** - **5-4a** is the proximity of chalcogens about the $\overline{4}$ centers. The tightness of the d1 and d2 contacts when Se occupies the E_2-position, that is, in **5-2a** and **5-4a**, leads to increased *W* in these compounds, and a concomitant improvement in their conductivity relative to **5-1a** and **5-3a**. While the conductivity remains activated across the series, thermal activation energies are markedly reduced by heavy atom incorporation, especially so in **5-2a** and **5-4a**.

The magnetic properties of the Se-based radicals described here can also be related, at least phenomenologically, to the presence of the heavy heteroatom. Almost all previous work on radical-based magnetic materials has focused on the use of light heteroatom (N, O) radicals. This approach has yielded a few magnetically ordered materials,[16] but the Curie temperatures and coercive fields have always been low.[17] The discovery of ordering, albeit spin-canted antiferromagnetism, in a dithiadiazolyl at 36 K[18] represented a major step forward, partly for the increase in T_c, but more importantly as a proof of the concept that heavier heteroatoms, that is, S, could afford stronger magnetic exchange interactions. Subsequent work has demonstrated bulk ferromagnetic ordering (at 1.3 K) in a dithiadiazolyl,[16d] but progress with these systems has been limited because the steric protection needed to avoid dimerization also reduces magnetic exchange *via* direct through-space interactions. Attempted extension of the heavy atom logic, by replacing S in a sterically protected dithiadiazolyl radical with Se, led to dimerization.[19]

With the development of highly delocalized Se-based radicals of the general type **5-2**, **5-3** and **5-4**, in which association can be suppressed without the need for steric bulk, the door is opened to the pursuit of other[20] heavy atom radicals capable of strong through-space magnetic interactions, be they ferromagnetic or antiferromagnetic. The variations in behaviour along the series of compounds **5-2a** , **5-3a** and **5-4a** attest to the critical importance of the location of the heavy atom on the sign of exchange coupling. Thus, only when Se atoms are directly in contact about the $\overline{4}$ centers, as in **5-2a** and **5-4a**, is ferromagnetic ordering observed. In **3a**, the ordering is antiferromagnetic, although there is sufficient magnetic anisotropy, arising from spin-orbit contributions[21] from Se and/or the polar space group, to afford some spin canting.

While the ordering temperatures for **5-2a** and **5-4a** are no match for conventional inorganic ferromagnetic materials, they are an order of magnitude higher than those seen in light heteroatom ferromagnetic radicals. Indeed they are comparable to, and in one case (**5-4a**) greater than, the highest T_c values seen in non-metal CT ferromagnets, that is, in materials such as TDAE•C_{60} (T_c = 16.1 K)[22] or [BBDTA][$GaCl_4$] (T_c = 8 K).[23] Perhaps more striking than the ordering temperatures are the coercive fields observed for **5-2a** and **5-4a**, which are at least two orders of magnitude larger than those seen in light atom ferromagnets. While the origin of the magnetic response in these materials is far from understood, the T_c/θ ratios of 0.63 for **5-2a** and 0.74 for **5-4a** point to a significant degree of magnetic anisotropy, as might be expected from the crystal symmetry.[11] The appearance of the hysteresis loops, with $M_{rem} \sim \frac{1}{2}M_{sat}$, is also broadly consistent with that expected for a highly anisotropic uniaxial system.[24]

Presentation of the magnetic measurements for **5-2a** and **5-4a** would not be complete without a discussion of the dependence of the magnetic response of the materials on the nature of reducing agent used to generate them. As indicated in the Experimental section (**Section 5.8**), the magnetic parameters reported here (listed in **Table 5.4**) refer to samples prepared using TMPDA as reducing agent. In contrast, early magnetic data for **5-2a** were obtained from samples prepared using TDAE.[25] While the latter reagent afforded material that was analytically pure, its strong reducing properties led to more rapid nucleation and precipitation of the radicals. The resulting crystallites were smaller and, more importantly, also contained a greater number of structural defects which, in turn, affected the magnetic response. Thus, the slightly lower values for C (0.349 emu mol^{-1}) and M_{sat} (0.95 Nβ) for **5-2a** can be ascribed to the presence of a low concentration of diamagnetic dimers. In order to test this interpretation we explored the response of **5-4a** to changes in reductant, and to our satisfaction found the same dependency. A sample of **5-4a** prepared using TDAE provided lower C (0.340 emu mol^{-1}) and M_{sat} (0.94 Nβ) values.

We also point out that the coercive field H_c for **5-2a** listed in **Table 5.4** is smaller than that observed (590 Oe) when TDAE was used to generate the radical (**Figure 5.14a**). A similar trend has been found for **5-4a**; the H_c value (at 2K) of a sample prepared using TDAE was 2030 Oe, that is, larger than that of the TMPDA-produced material (1370 Oe, **Figure 5.14b**). The increased coercivity observed for the TDAE-produced samples is not unexpected. The defects that lead to a slight suppression in C and M_{sat} may also serve to pin domain boundaries and inhibit the reversal of magnetization, thereby increasing H_c.[24]

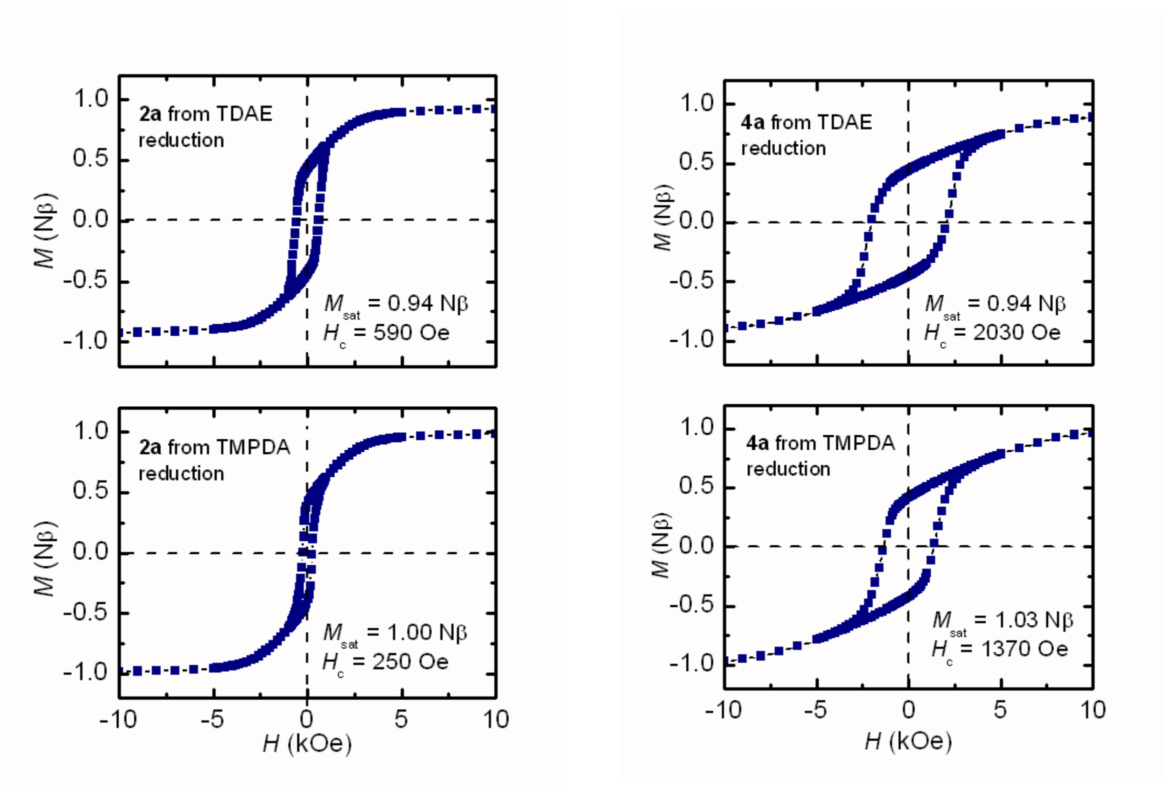

(a) (b)

Figure 5.14 (a) M versus H plots at 2 K for **5-2a** prepared using TDAE (top) and TMPDA (bottom); (b) M versus H plots at 2 K for **5-4a** prepared using TDAE (top) and TMPDA (bottom). The two plots in (a) and (b) illustrate the lowering of M_{sat} and the increase in H_c caused by diamagnetic defects introduced during a TDAE reduction.

5.8 Conclusions

For many years the development of molecular conductors and magnetic materials based on neutral radicals has evolved along separate, non-converging paths. Work on conductors has focused on (i) radicals which possess extensive spin delocalization, to lower the onsite Coulomb barrier U, and (ii) the incorporation of heavy heteroatoms (S) to increase intermolecular overlap and hence W. By contrast most magnetic materials have been built using light heteroatom radicals, in which spin density is more localized. In addition, steric bulk is often employed to suppress dimerization. This combination of spin localization, which increases U, and molecular bulk, which decreases W, militates against the use of these materials as molecular conductors.

Because of these apparently conflicting design criteria, the possibility that the unpaired electrons in molecular radicals might serve simultaneously as carriers of charge and spin has received limited consideration.[26,27] The resonance stabilized selenazyl radicals reported here demonstrate that multifunctionality, that is, bulk ferromagnetism and activated conductivity, can be generated using a single component molecular radical. While the T_c values of the present materials are still too low to allow measurements of conductivity in the ferromagnetic regime, it is possible that chemical and structural modifications of the present systems may lead to improvements in T_c and/or conductivity, so that field-dependent conductivity can be probed. The application of physical pressure should also increase both conductivity[28] and T_c.[29]

The importance of magnetic purity, that is, the need to optimize the reduction of the cations to the radicals so as to minimize structural defects, cannot be overstated. While such defects lead to relatively small departures in C and M_{sat} values from ideal behaviour, the variations in H_c are much larger.

5.9 Experimental Section

Please see **Appendix A** for general methods and procedures.

Preparation of 8-Chloro-4-ethyl-4*H*-bis[1,2,3]thiaselenazolo[4,5-b:5',4'-e]pyridin-2-ium Triflate [5-2a][OTf]. Compound [**5-1a**][OTf] (0.884 g, 2.00 mmol) and finely ground Se dioxide (0.666 g, 6.00 mmol) were added to a large glass pressure vessel along with 80 mL MeCN, and the mixture stirred and heated in an oil bath at 110 °C for 48 h. Analysis of the mixture at this time by ESI mass spectrometry showed complete and specific formation of [**5-2a**]$^+$. The flask was cooled to room temperature, and the dark green solution filtered through a glass Büchner funnel to remove a small amount of black precipitate. The filtrate was concentrated to 30 mL, cooled to room temperature for 1 h, then at -20 °C for 2 h. Red crystals of [**5-2a**][OTf] (0.704 g, 1.31 mmol, 65 %) were filtered off, washed with DCM and dried in air. The product was double recrystallized from MeCN as red needles; mp 294 - 246 °C. IR: 2254 (w, MeCN), 1453 (m), 1435 (s), 1282 (s), 1245 (vs), 1184 (w), 1155 (s), 1073 (w), 1026 (s), 1004 (w), 757 (w), 742 (s), 720 (w), 636 (s), 598 (m), 533 (w), 516 (m), 476 (w) cm^{-1}. Samples for elemental analysis were heated overnight at 78 °C/10^{-2} Torr to remove the MeCN solvate. Anal. Calcd for $C_8H_5ClF_3N_3O_3S_3Se_2$: C, 17.87; H, 0.94; N, 7.81 %. Found: C, 17.73; H, 0.87; N, 7.57 %.

Preparation of 8-Chloro-4-ethyl-4*H*-bis[1,2,3]selenathiazolo[4,5-*b*:5',4'-*e*]pyridin-2-ium Triflate, [5-3a][OTf]. Freshly prepared iodobenzene dichloride (1.42 g, 5.15 mmol) was added to a slurry of [**5-3**][OTf] (R_1 = Et, R_2 = H) (2.36 g, 4.69 mmol) in 300 mL MeCN and the reaction mixture heated to a gentle reflux for 1 h before being hot filtered to remove any insoluble material. The filtrate was concentrated to 100 mL and allowed to stand at room temperature for 16 h. Red crystals of crude [**5-3a**][OTf] were filtered off and washed with DCM; yield 1.77 g (3.29 mmol, 70 %). The product was purified by recrystallization from MeCN and HOAc to afford lustrous red needles; mp > 270 °C dec. IR: 1499 (m), 1446 (s), 1434 (s), 1356 (s), 1273 (m), 1242 (s), 1185 (m), 1169 (m), 1076 (m), 1027 (s), 997 (w), 881 (m), 841 (m), 810 (w), 790 (w), 655 (s), 637 (s), 597 (w), 573 (w), 551 (w), 517 (m) cm^{-1}. Anal. Calcd for $C_8H_5ClF_3N_3O_3S_3Se_2$: C, 17.87; H, 0.94; N, 7.81 %. Found: C, 17.90; H, 1.04; N, 7.91 %.

Preparation of 8-Chloro-4-ethyl-4*H*-bis[1,2,3]diselenazolo[4,5-*b*:5',4'-*e*]pyridin-2-ium Triflate, [5-4a][OTf] Finely ground selenium dioxide (0.900 g, 8.11 mmol) was added to a hot solution of [**5-3a**][OTf]

(1.31 g, 2.43 mmol) in 120 mL HOAc. The mixture was heated at reflux for 90 min, and then cooled slowly to room temperature. After 16 h crude [**5-4a**][OTf] was filtered off and washed with DCM; yield 0.850 g (1.35 mmol, 55 %). Dark purple needles were isolated by recrystallization from HOAc; mp > 255 °C dec. IR: 1417 (s), 1355 (s), 1280 (s), 1245 (s), 1224 (m), 1180 (w), 1156 (s), 1084 (w), 1062 (w), 1026 (s), 987 (w), 923 (w), 773 (w), 757 (m), 751 (w), 727 (m), 636 (s), 579 (s), 549 (m), 517 (s) cm^{-1}. Anal. Calcd for $C_8H_5ClF_3N_3O_3S_1Se_4$: C, 15.22; H, 0.80; N, 6.65 %. Found: C, 15.40; H, 0.68; N, 6.51 %.

Preparation of Radicals: Method 1. *Bulk material for conductivity and magnetic measurements*. Before use, all glassware was soaked overnight in dilute HNO_3, then washed with deionized water followed by distilled water, and finally oven dried at 100 °C overnight. Magnetic stirbars were glass-covered. Degassed solutions (3 freeze-pump-thaw cycles) of TMPDA (0.330 - 0.586 mmol) in 40 - 75 mL MeCN and [**5-2a -5-4a**][OTf] (0.317 - 0.558 mmol) in 120 - 150 mL MeCN were combined and after 30 min the gold-brown precipitate of **5-2a - 5-4a** was filtered off and washed 4 × 20 mL MeCN. **Method 2A**. *Diffusion H-cells for single crystal growth of **5-2a, 5-3a***. Degassed solutions (3 freeze-pump-thaw cycles) of OMFc (0.058 mmol) in 15 mL MeCN and [**5-2a**, **5-3a**][OTf] (0.055 mmol) in 15 mL MeCN were allowed to diffuse together slowly at room temperature over a period of 16 h. The solvent was decanted to leave metallic green/black needles of **5-2a**, **5-3a** suitable for X-ray work. **Method 2B**. *Electrocrystallization H-cells for single crystal growth of **5-4a***. The electrocrystallization work employed standard electrochemical H-cell techniques,[30] with samples of [**5-4a**][OTf] (20 mg) dissolved under nitrogen in 20 mL of MeCN containing 0.008 M [*n*-Bu_4N][PF_6] as supporting electrolyte. Currents ranged from 5 to 10 μA, with growth periods of 2 - 4 days.

Analytical Data for Radicals. 5-2a. Yield 88 % (Method 1), dec > 120 °C. IR: 1442 (s), 1409 (w), 1324 (m), 1228 (s), 1172 (m), 1082 (m), 1065 (m), 914 (w), 840 (s), 729 (s), 719 (m), 694 (s), 580 (m), 534 (w), 459 (m) cm^{-1}. Anal. Calcd for $C_7H_5ClN_3S_2Se_2$: C, 21.63; H, 1.30; N, 10.81 %. Found: C, 21.66; H, 1.26; N, 10.86 %. **5-3a.** Yield 86 % (Method 1), dec > 120 °C. IR: 1485 (w), 1441 (s), 1416 (s), 1352 (w), 1328 (w), 1315 (m), 1217 (s), 633 (s), 592 (s), 526 (m), 490 (m), 465 (s) cm^{-1}. Anal. Calcd for $C_7H_5ClN_3S_2Se_2$: C, 21.63; H, 1.30; N, 10.81 %. Found: C, 21.49; H, 1.31; N, 10.60 %. **5-4a.** Yield 85 % (Method 1), dec > 120 °C. IR: 1403 (w), 1316 (m), 1224 (s), 1167 (m), 1078 (w), 988 (m), 812 (m), 689 (s), 573 (m), 559 (w), 432 (w) cm^{-1}. Anal. Calcd for $C_7H_5ClN_3Se_4$: C, 17.43; H, 1.04; N, 8.71 %. Found: C, 17.17; H, 1.23; N, 8.66 %.

Chapter 6

Variations on a Tetragonal Theme

6.1 Introduction

The previous chapter presented the synthesis, characterization and solid state properties of a family of radicals **6-1**, **6-2**, **6-3** and **6-4** (R_1 = Et, R_2 = Cl). As we had hoped, X-ray crystallographic studies confirmed that all four radicals are isostrucutural, crystallizing in the space group $P\overline{4}2_1m$. Furthermore, the crystal structures consist of slipped π-stack arrays of undimerized radicals packed about $\overline{4}$ centers, and thus, this is the first example of a complete set (or family) of undimerized isostructural *bis*-DTA radials. Variable temperature conductivity (σ) measurements reveal an improvement in σ_{RT}, by two orders of magnitude, when Se occupies all chalcogen (E_1 and E_2) positions. Perhaps more importantly, the family of radicals demonstrate a rich diversity of magnetic properties. Variable temperature magnetic susceptibility measurements indicate that all four radicals exhibit S = ½ Curie-Weiss behaviour above 50 K. However, below 50 K the three Se-based radicals display magnetic ordering. Radical **6-3** (R_1 = Et, R_2 = Cl) undergoes a phase transition at 14 K to a weakly spin-canted antiferromagnetic state; radicals **6-2** (R_1 = Et, R_2 = Cl) and **6-4** (R_1 = Et, R_2 = Cl) order ferromagnetically, with Curie temperatures (T_c) of 12.8 K and 17.0 K respectively. The coercive fields H_c (measured at 2 K) of **6-2** (R_1 = Et, R_2 = Cl) (250 Oe) and **6-4** (R_1 = Et, R_2 = Cl) (1370 Oe) are much larger than those seen in conventional light atom organic ferromagnets.

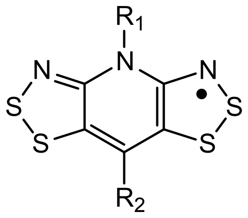

6-1

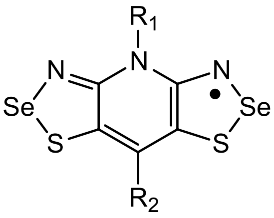

6-2

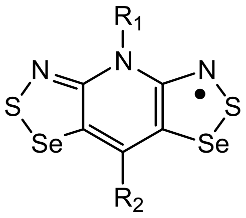

6-3

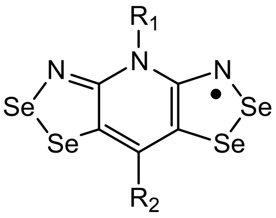

6-4

In order to explore the origin of the ferromagnetic response observed in **6-2** and **6-4** (R_1 = Et, R_2 = Cl) we sought to probe the effect on structure and transport properties of minor structural modifications of the molecular framework of **6-2** (R_1 = Et, R_2 = Cl). Our intent was that these changes be sufficiently small so as not to alter the tetragonal ($P\overline{4}2_1m$) space group and solid state packing pattern found for **6-2** (R_1 = Et, R_2 = Cl), hereafter termed **6-2a** (**Scheme 6.1**). At the same time, however, we hoped to induce changes in intermolecular contacts, and hence overlap and exchange interactions, that would lead to a change in magnetic behaviour. In essence, we wished to see if we could switch "on" and "off" the ferromagnetic ordering found for **6-2a** by molecular modification. To that end we synthesized and structurally characterized the series of radicals **6-2(b -e)** (**6-2d** has been reported in **Chapter 4; 6-2e** was prepared by my colleague and the synthesis will not be presented here), in which the R_1 and R_2 groups are similar in size to those seen in **6-2a** (**Scheme 6.1**). To our pleasure, X-ray structural determination verified that all four variants do indeed crystallize in the same tetragonal $P\overline{4}2_1m$ space group as **6-2a**. Furthermore, all four variants show room temperature conductivities σ(300 K) that are similar to that found for **6-2a** (near 10^{-4} S cm^{-1}). The magnetic response of the four variants is, however, very different. While **6-2d** and **6-2e** behave as ferromagnets, with T_cs and H_cs close to those found for **6-2a**, compounds **6-2b** and **6-2c** show no sign of bulk magnetic ordering, instead behaving as Curie-Weiss paramagnets with small antiferromagnetic Weiss constants (θ). Finally, it should be pointed out that **Chapter 6** is "work in progress" as the magnetic data for **6-2c** has just been received and incorporated into this manuscript.

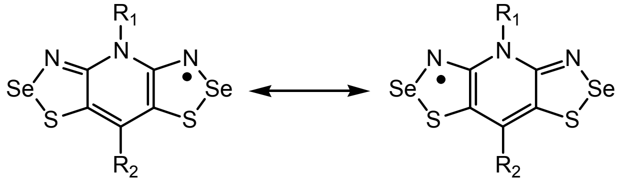

	6-2a	**6-2b**	**6-2c**	**6-2d**	**6-2e**
$\mathbf{R_1}$	Et	Pr	CH_2CF_3	Et	Et
$\mathbf{R_2}$	Cl	Cl	Cl	Me	Br

Scheme 6.1

6.2 Synthesis

Preparative routes to salts of the all-S framework were based on double Herz cyclization methods developed in our laboratory.[1,2] Thus, the triflate (trifluoromethanesulfonate) salts of [**6-1a,b,c**]$^+$ were obtained by reacting the zwitterion **6-5**[3] with an alkyl triflate R_1OTf (R_1 = Et, Pr, CH_2CF_3) as in **Scheme 6.2a** (compounds [**6-1a,b**][OTf] were prepared according to literature procedures).[1a] Compound [**6-1d**][OTf] (**Scheme 6.2b**) was prepared by heating sulfur monochloride with [**6-6**][OTf], itself made by the reaction of *N*-ethyl-2,6-dichloro-4-methylpyridinium triflate with ammonia gas (the complete synthesis is reported in **Section 4.2**).

Our initial approach for the generation of derivatives of **6-2** was based on the condensation of S-acetylated pyridinedithiols with selenium halides,[4] which provided an effective but somewhat lengthy preparative procedure. More recently we have taken advantage of chemistry developed thirty years ago[5] for the direct incorporation of Se into the 2-position of monofunctional 1,2,3-dithiazolylium (DTA) salts using SeO_2 in acetic acid at reflux.[6] The method is readily applicable to the present bifunctional systems, and allows for the introduction of Se into salts of [**6-1**]$^+$, thereby affording salts of [**6-2**]$^+$ in a single step (**Scheme 6.2c**). We have used this route previously,[7] and it works well for the preparation of [**6-2d**]$^+$, which is obtained after 90 min in refluxing HOAc (see **Section 4.2.2**). However, while this approach is simple and fast, when R_2 = Cl as in [**6-1a**,**b**,**c**]$^+$, the harsh reaction conditions originally prescribed lead to Se insertion which is not regiospecific (see **Section 4.2.2** for a discussion on SeO_2 and the regiospecificity of Se insertion).

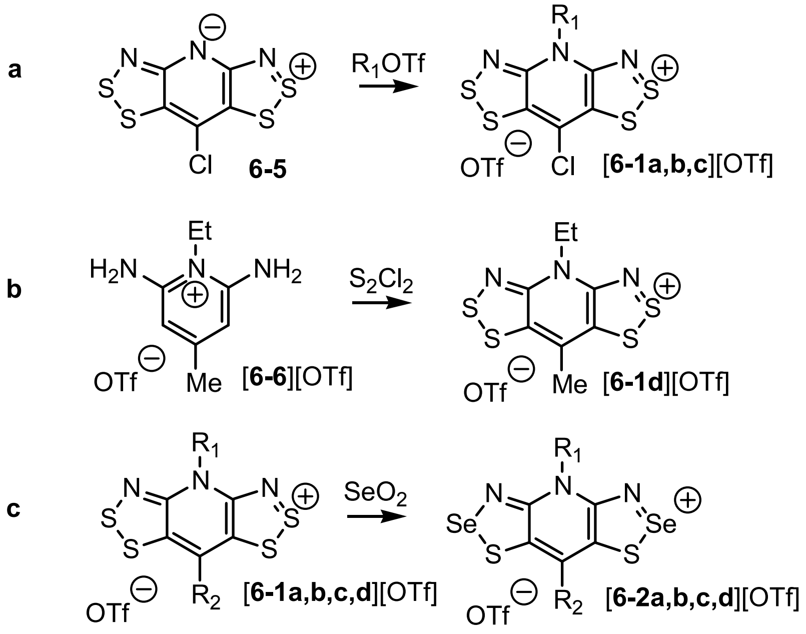

Scheme 6.2

Fortunately, full regiospecificity was eventually obtained for [**6-2a**,**b**,**c**]$^+$ by performing the SeO_2 insertion in acetonitrile (MeCN) at 110 °C in a pressure vessel. Progress of the reaction was monitored by ESI-MS, with complete conversion to (99% +) S_2Se_2 material being achieved in 48 - 72 h. Infrared analysis of the isolated triflates showed clean signatures for the presence of a single regioisomer, that is, [**6-2**][OTf]. Reduction of the salts [**6-2a** - **6-2d**][OTf] to the respective radicals required consideration of the relevant half-wave potentials $E_{½}$ (0/+1). Based on our experience with related systems, for those radicals with a halogen occupying the R_2-position, as in **6-2(a-c)**, the reduction could be effected with either octamethylferrocene (OMFc), hexamethylferrocene (HMFc) or *N*,*N*,*N*′,*N*′-tetramethyl-*p*-phenylenediamine (TMPDA),[8] but when R_2 = Me,[2] as in **6-2d**, only the more powerful reducing agent decamethylferrocene (DMFc) was used successfully (see **Appendix A** for a list of reducing agents).

6.3 Crystallography

As anticipated, the four new radicals **6-2(b-e)** are isostructural with **6-2a**, all crystallizing in the tetragonal space group $P\overline{4}2_1m$. Unit cell information and crystal metrics, derived from single crystal X-ray data collected at ambient temperature, are compiled in **Table 6.1**. Data sets were also collected at 100 K, and unit cell and structural information from these refinements are found in **Table 6.2**. At the molecular level, the crystal structures at both collection temperatures consist of undimerized radicals bisected by mirror planes; comparative views of the five radicals (at 298 K), showing atom numbering, are shown in **Figure 6.1**. The intramolecular distances and angles are typical for this class of heterocyclic radical, the internal Se_1-S_1, Se_1-N_1 and Se_1-C_2 bonds being slightly longer than in the corresponding cations. The difference can be ascribed to the antibonding nature of the radical SOMO, which is not occupied in the cation.[1a]

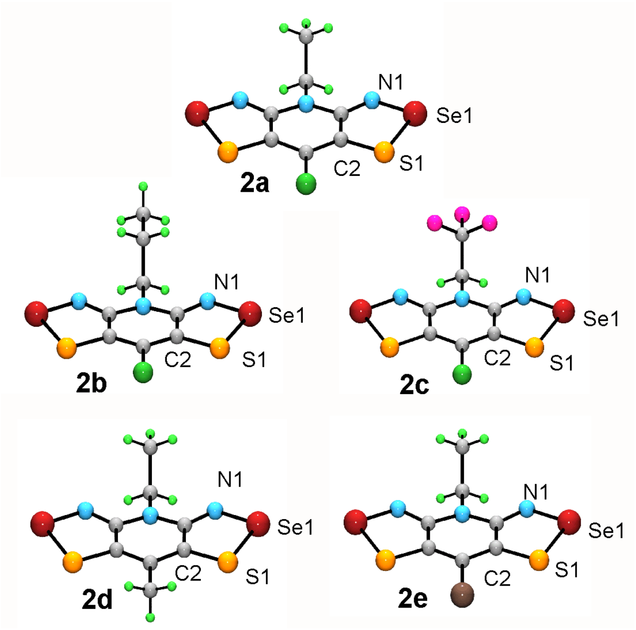

Figure 6.1 Molecular structures of **6-2** with atom numbering scheme.

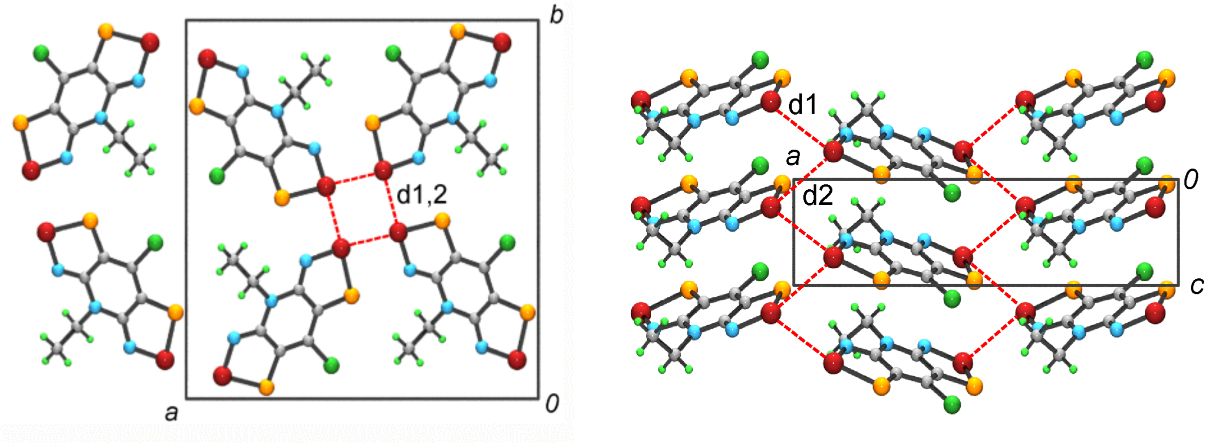

Figure 6.2 Unit cell drawings of **6-2a** (at 298 K), showing intermolecular Se1---Se1′contacts (dashed lines) as viewed along the *z*-direction (left) and along the *y*-direction (right).

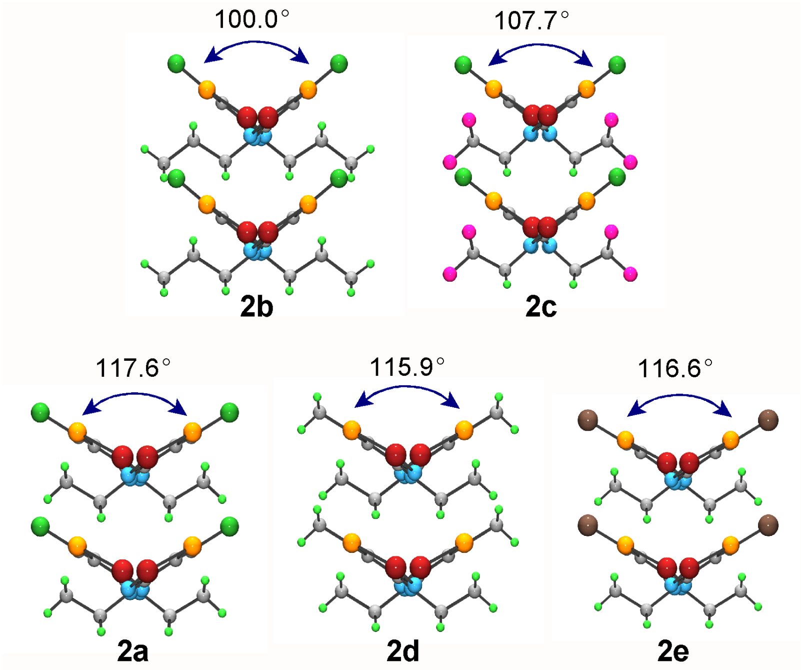

Figure 6.3 Cross-braced π-stacks, viewed parallel to {1,1,0}, with dihedral angle (2τ) between molecular planes (at 298 K).

Overall, the molecular packing of the 100 K structures are strikingly similar to that of the 298 K structures, and as expected, the contact distances d1 – d3, interplanar seperation δ, and inclination angle τ[1c] decrease slightly upon cooling (**Table 6.2**). While the crystal structures of the four radicals are essentially identical, there are subtle but important variations within the series which can be related to differences in transport properties. The radicals pack in slipped π-stack arrays running along the *z*-direction. The unit cell (at 298 K) of the parent radical **6-2a**, viewed down and perpendicular to the *z*-direction, is shown in **Figure 6.2**. The mean interplanar separations δ and the inclination angle τ of the mean molecular plane with respect to the stacking axis are listed in **Table 6.1** (298K) and **Table 6.2** (100 K). There are some significant variations in τ, which are visualized in **Figure 6.3**, which shows the cross-braced nature of adjacent π-stacks viewed parallel to {1, 1, 0}. These differences are associated with the steric size of the R_1 group. Thus in **6-2a**, **6-2d** and **6-2e**, where R_1 = Et, τ holds steady in the range 57.95(1)° - 58.83(1)° at 298 K. By contrast, in **6-2b** ($R_1 = C_3H_7$) and **6-2c** ($R_1 = CH_2CF_3$), the radicals tip more sharply to relieve steric congestion, so as to afford τ angles of 53.86(1)° and 50.00(1)° respectively.

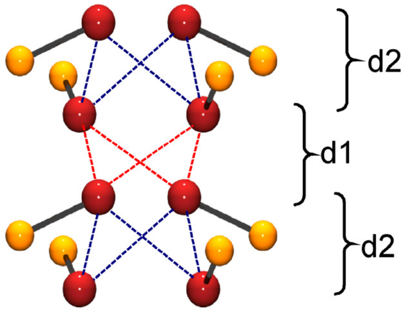

	298 K		100 K	
	d1 (Å)	d2 (Å)	d1 (Å)	d2 (Å)
6-2a	3.328(1)	3.459(1)	3.266(1)	3.397(1)
6-2b	3.490(1)	3.554(1)	3.443(1)	3.500(1)
6-2c	3.407(1)	3.630(1)	3.350(1)	3.589(1)
6-2d	3.343(1)	3.470(1)	3.306(1)	3.444(1)
6-2e	3.344(1)	3.490(1)	3.298(1)	3.453(1)

Figure 6.4 Alternation in contacts d1/d2 about consecutive $\overline{4}$ centers along *z* at 298K and 100 K.

Table 6.1 Crystallographic Data and Metrics for **6-2** at 298 K.

Radical	**6-2a**[a]	**6-2b**	**6-2c**	**6-2d**	**6-2e**
Formula	$C_7H_5ClN_3S_2Se_2$	$C_8H_7ClN_3S_4$	$C_7H_2ClF_3N_3S_4$	$C_8H_8N_3S_4$	$C_7H_5CBrN_3S_4$
M	388.63	402.66	442.61	368.21	433.09
a, Å	16.0334(8)	16.2209(8)	16.2612(8)	16.0088(17)	16.0885(7)
b, Å	16.0334(8)	16.2209(8)	16.2612(8)	16.0088(17)	16.0885(7)
c, Å	4.1090(4)	4.3831(4)	4.3882(4)	4.1385(9)	4.1339(3)
V, Å^3	1056.30(13)	1153.27(13)	1160.36(13)	1060.60(30)	1070.02(10)
ρ(calcd) g cm^{-1}	2.444	2.319	2.534	2.306	2.688
space group	$P\overline{4}2_1m$	$P\overline{4}2_1m$	$P\overline{4}2_1m$	$P\overline{4}2_1m$	$P\overline{4}2_1m$
Z	4	4	4	4	4
temp, K	298(2)	298(2)	298(2)	298(2)	298(2)
μ, mm^{-1}	7.61	6.98	6.98	7.33	11.00
λ, Å	0.71073	0.71073	0.71073	0.71073	0.71073
data/restr./par.	1150/0/76	1263/0/82	1296/12/91	1161/5/81	1166/0/76
sol. method	direct methods	direct methods	direct methods	direct methods	direct methods
R, R_w (on F^2)	0.0447, 0.1003	0.0230, 0.0482	0.0234, 0.0609	0.0337, 0.0793	0.0173, 0.0402
Se1-S1, Å	2.249(2)	2.243(1)	2.233(1)	2.233(1)	2.244(1)
Se1-N1, Å	1.805(6)	1.823(3)	1.824(4)	1.814(4)	1.820(3)
C2-S1, Å	1.733(7)	1.735(3)	1.736(4)	1.735(5)	1.740(3)
d1, Å	3.328(1)	3.490(1)	3.407(1)	3.343(1)	3.344(1)
d2, Å	3.459(1)	3.554(1)	3.630(1)	3.470(1)	3.490(1)
d3, Å	3.655(2)	3.620(1)	3.590(1)	3.655(1)	3.666(1)
δ, Å	3.516(7)	3.501(3)	3.544(5)	3.508(5)	3.517(3)
τ, deg	58.83(1)	50.00(1)	53.86(1)	57.95(1)	58.29(1)
deviation from plane, Å	0.087	0.075	0.0563	0.0891	0.093

[a] Data from reference 8a.

Table 6.2 Crystallographic Data and Metrics for Structures **6-2** at 100 K.

Radical	**6-2a**	**6-2b**	**6-2c**	**6-2d**	**6-2e**
Formula	$C_7H_5ClN_3S_2Se_2$	$C_8H_7ClN_3S_2Se_2$	$C_7H_2ClF_3N_3S_2Se_2$	$C_8H_8N_3S_2Se_2$	$C_7H_5CBrN_3S_2Se_2$
M	388.63	402.66	442.61	368.21	433.09
a, Å	15.9040(10)	1615.83(11)	16.2389(5)	16.0276(12)	16.0499(7)
b, Å	15.9040(10)	1615.83(11)	16.2389(5)	16.0276(12)	16.0499(7)
c, Å	4.0161(5)	4.3026(6)	4.2776(3)	4.0830(7)	4.0684(3)
V, Å^3	1015.49(16)	1123.37(19)	1128.01(9)	1048.9(2)	1048.02(10)
ρ(calcd), g cm^{-1}	2.542	2.381	2.606	2.332	2.745
space group	$P\bar{4}2_1m$	$P\bar{4}2_1m$	$P\bar{4}2_1m$	$P\bar{4}2_1m$	$P\bar{4}2_1m$
Z	4	4	4	4	4
temp, K	100(2)	100(2)	100(2)	100(2)	100(2)
μ, mm^{-1}	7.92	7.16	7.183	7.414	11.231
λ, Å	0.71073	0.71073	0.71073	0.71073	0.71073
data/restr./par.	1077/12/76	1214/12/82	1726/0/91	1111/0/77	1580/0/75
sol. method	direct methods	direct methods	direct methods	direct methods	direct methods
R, R_w (on F^2)	0.0371, 0.0717	0.0245, 0.0529	0.0134, 0.0351	0.0327, 0.0667	0.0315, 0.0729
Se1-S1, Å	2.2391(17)	2.2473(10)	2.2390(4)	2.2480(13)	2.2490(12)
Se1-N1, Å	1.8104(54)	1.8251(30)	1.8293(15)	1.8278(43)	1.8259(39)
C2-S1, Å	1.7290(60)	1.7396(37)	1.7357(16)	1.7542(50)	1.7418(43)
d1, Å	3.266(1)	3.443(1)	3.350(1)	3.306(1)	3.298(1)
d2, Å	3.397(1)	3.500(1)	3.589(1)	3.444(1)	3.453(1)
d3, Å	3.613(2)	3.589(1)	3.587(1)	3.648(1)	3.641(1)
δ, Å	3.450(2)	3.407(2)	3.465(1)	3.442(2)	3.439(2)
τ, deg	59.2(1)	52.4(1)	54.1(1)	57.5(1)	57.7(1)
deviation from plane, Å	0.096	0.0588	0.0455	0.0919	0.0746

Finally, the π-stacks are packed about the $\overline{4}$ centers which run along the *z*-direction, thereby generating the four-fold pinwheel-like clusters illustrated in **Figure 6.2**. These clusters are linked by intermolecular Se1---Se1′ contacts d1 and d2 which, when propagated along *z*-direction, generate an alternating sequence of Se_4 tetrahedra (**Figure 6.4**). In all five structures **6-2(a-e)** the values of d1 and d2 (**Table 6.1**, **Table 6.2** and **Figure 6.4**) are well within the van der Waals contact (3.8 Å) for two Se,[9] but within the group the three radicals with R_1 = Et (**6-2a**, **6-2d** and **6-2e**) are associated with d1 and d2 values that are significantly shorter than those seen in **6-2b** and **6-2c**, where more bulky R_1 groups (C_3H_7 and CH_2CF_3) are present.

6.4 Band Structures

In order to compare the extent of intermolecular electronic interactions in **6-2**, in particular the consequences of the variations in the presence of larger R_1 groups in **6-2b** and **6-2c**, we have performed Extend Hückel Theory (EHT) band structure calculations on all five crystal structures (using the ambient temperature coordinates). The results should be viewed with caution, as in strongly correlated systems such as these the tight-binding model fails to provide a proper description of the ground state. These failings notwithstanding, the EHT method can, within a closely related series of structures, provide a qualitative insight into trends in orbital interactions, and hence bandwidth *W*, which in this case we estimated in terms of the energetic spread (dispersion) of the four crystal orbitals (COs) arising from the interaction of the four SOMOs in the unit cell.

The results are illustrated in **Figure 6.5**, which shows plots of the four frontier COs plotted along the reciprocal space direction Γ(0, 0, 0) to Z (0, 0, ½). By virtue of the tetragonal symmetry, CO trends along this reciprocal space vector can be associated precisely with orbital interactions along the stacking axis in real space. The tetragonal symmetry also leads to the degeneracy (coincidence) of two of the COs, and in the case of **6-2a**, **6-2d** and **6-2e** there is an intruder orbital that falls in the same energy range. Overall the appearance of the dispersion curves is much the same. The bandwidth *W* (**Table 6.3**) of all five compounds is near 1 eV, a remarkably large value for a molecular compound, but in keeping with the tight crystal packing. Closer inspection, however, reveals some subtle differences. From the spread of the dispersion curves across the series it is apparent that the bandwidth *W* (**Table 6.3**) for compounds **6-2b** and **6-2c** is less than the other three compounds. This conclusion is consistent with the slightly longer intermolecular contacts observed for these two radicals. Their electronic structures are also slightly more 1-dimensional.

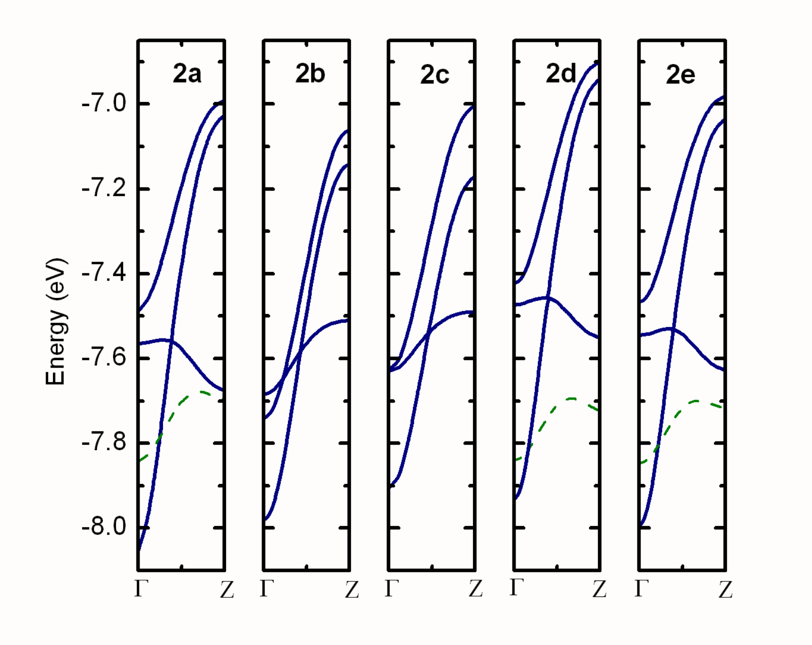

Figure 6.5 CO dispersion curves from Γ (0, 0, 0) to Z (0, 0, ½). Dashed green lines are intruder bands.

Table 6.3 Bandwidth, Conductivity and Magnetic Parameters for **6-2**(**a-e**).

	2a [a]	**2b**	**2c**	**2d**	**2e**
W (eV)	1.06	0.9	0.9	1.03	1.01
σ(300 K) (S cm^{-1})	1.0×10^{-4}	5.0×10^{-5}	2.0×10^{-5}	2.0×10^{-4}	1.2×10^{-4}
E_{act} (eV)	0.27	0.31	0.31	0.27	0.29
C (emu K mol^{-1})	0.369	0.383	0.33	0.391	0.394
θ (K)	20.3	−3.1	-1.0	18.4	21.0
T_c (K)	12.8	—	—	13.6	14.1
M_{sat} (Nβ) at 2 K	1.0	—	—	0.98	1.02
M_{rem} (Nβ) at 2 K	0.41	—	—	0.38	0.42
H_c (Oe) at 2 K	250	—	—	230	320

[a] Data from reference 8a.

6.5 Conductivity and Magnetic Measurements

The results of band structure calculations described above, led us to believe that the conductivity characteristics of the five radicals **6-2**(**a-e**) would be similar. The results of 4-probe variable temperature measurements, presented in **Figure 6.6** in the form of plots of log σ versus 1/*T*, confirm these expectations. Despite the high bandwidths found for these systems, their conductivity remains activated, with σ(300K) spanning a range from 10^{-5} S cm^{-1} to 10^{-4} S cm^{-1}. Within the series, however, the slightly lower conductivities and higher activation energies E_{act} for **6-2b** and **6-2c** (**Table 6.3**) are in accord with the reduced *W*s estimated for these two radicals.

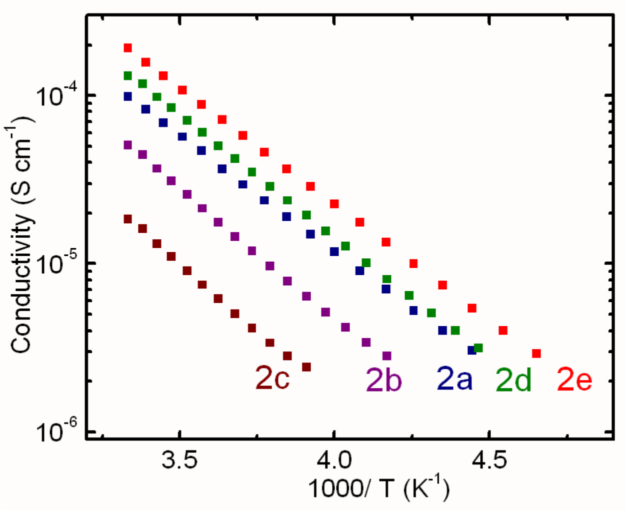

Figure 6.6 Log σ versus 1/T plots for **6-2(a-e)**. Derived activation energies are in **Table 6.3**.

Magnetic susceptibility measurements have been performed on **6-2(a-e)** over the temperature range 2 - 300 K. At temperatures above 50 K, the static susceptibility χ (corrected for diamagnetic contributions) of all five compounds is that expected for a S = ½ paramagnet; values of *C* and *θ* obtained from Curie-Weiss fits to the high temperature data are listed in **Table 6.3**. At temperatures below 50 K, the behaviour within the series diverges, and for presentation and discussion purposes it is convenient to separate the results into two groups, consisting of (i) those in which the ethyl group (R_1) of the parent radical has been changed, that is, **6-2b** and **6-2 c**, and (ii) those in which the R_2 substituent of **6-2a** has been modified, that is, **6-2d** and **6-2e**.

The effect of replacement of the R_1 ethyl group in **6-2a** by C_3H_7 (propyl, Pr; **6-2b**) and CH_2CF_3 (trifluoroethyl fEt; **6-2c**) substituent is dramatic. The transition to a ferromagnetically ordered state observed for **6-2a** is completely lost in the two more sterically encumbered variants. Plots of χT versus T at $H = 100$ Oe (**Figure 6.7**) are consistent with Curie-Weiss behaviour, with the value χT holding steady near 0.375 emu K mol^{-1}over the range 300-50 K, as expected for a $S = ½$ paramagnet. Below 50 K, χT drops sharply, indicative of the onset of weak antiferromagnetic exchange interactions. There was no indication, based on ZFC-FC experiments, of the presence of spin-canting in either of these two radicals.

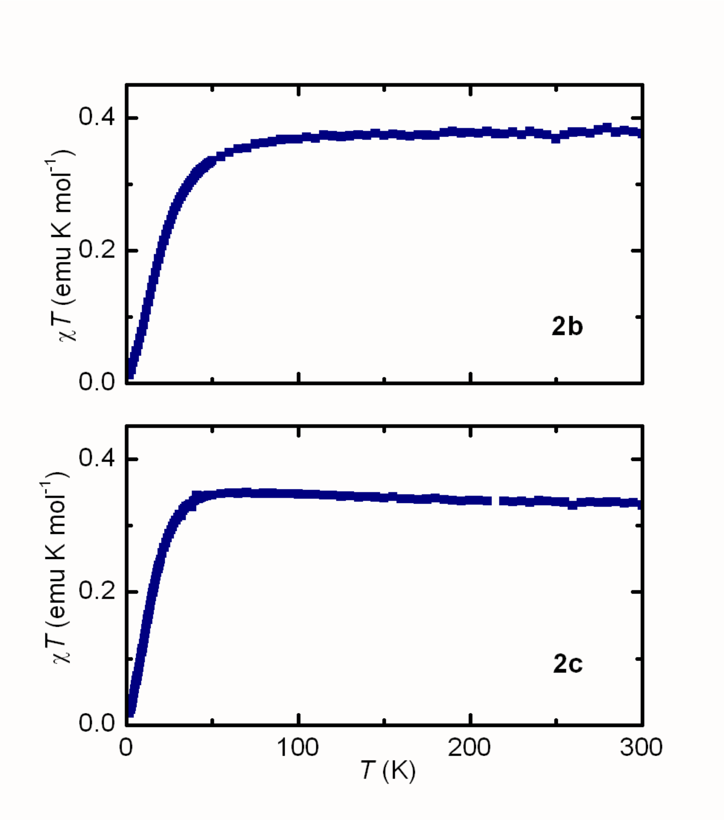

Figure 6.7 Plots of χT (field-cooled) versus temperature at $H = 100$ Oe for **6-2b** and **6-2c**.

In contrast to compounds **6-2b** and **6-2c**, where ferromagnetic ordering is lost, **6-2e** behaves in a manner very similar to both **6-2a** and **6-2d**. Radical **6-2e** shows a large, positive (ferromagnetic) Weiss constant (**Table 6.3**), with a value of χT (300 K) of 0.422 emu K mol^{-1}; plots of χT (field-cooled) versus T at $H = 100$ Oe reveal the same low temperature ferromagnetic surge seen for **6-2a,d**. As shown in **Figure 6.8**, χT starts to rise rapidly just below 20 K and reaches maximum value of 214 emu K mol^{-1} at 11 K for **6-2e**. These values are comparable to **6-2a** (183 emu K mol^{-1} at 10 K) and **6-2d** (181 emu K mol^{-1} at 10.5 K).

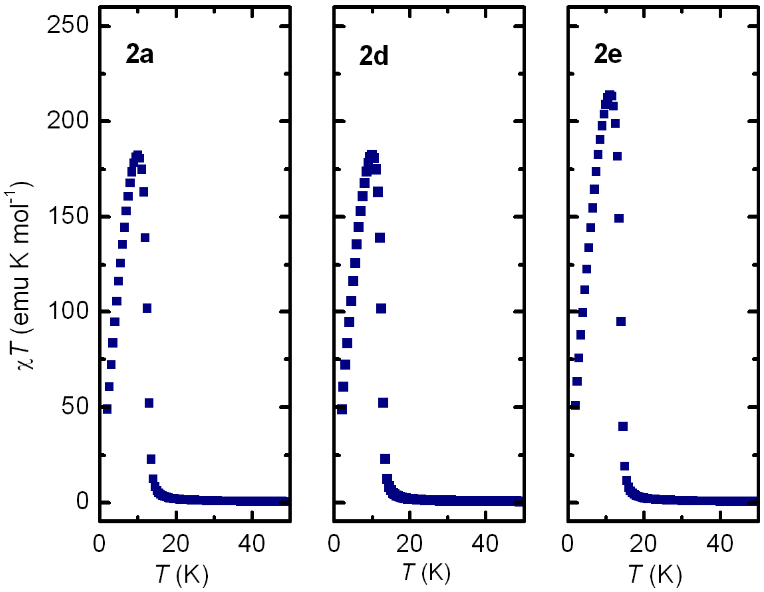

Figure 6.8 Plots of χT (field-cooled) versus temperature (2 - 50 K) at H = 100 Oe for **6-2a**, 6-**2d** and 6-**2e**.

Measurements of the field independent magnetization M_{sp} of **6-2e** provided additional evidence for the existence of a ferromagnetically ordered state, as found for **6-2a,d**, and also afforded a qualitative measure of the ordering temperature. As illustrated in **Figure 6.9**, M_{sp} decays rapidly with temperature, as thermal energy overcomes magnetic ordering, reaching a value of zero near 12.5 K (**6-2a**), 13.5 K (**6-2d**) and 14 K (**6-2e**), in accord with the point of maximum slope in the χT versus T plots described above. Back-extrapolation to T = 0 K afforded values of M_{sp}, the spontaneous magnetization at 0 K near 0.41 Nβ (**6-2a**), 0.39 Nβ (**6-2d**) and 0.41 Nβ (**6-2e**). Variable AC susceptibility measurements at different frequencies allowed us to pinpoint the ordering temperature T_c of **6-2e**. As shown in **Figure 6.10**, **6-2e** shows a sharp, well-defined maxima in the real (in-phase) χ' and imaginary (out-of-phase) χ'' components at 14.1 K, a value that is slightly higher than that found for **6-2a,d**. As in the case of **6-2a**, the invariance of T_c with changes in the cycling frequency (from 50 Hz to 5 kHz) establishes that all three materials are not spin glasses.

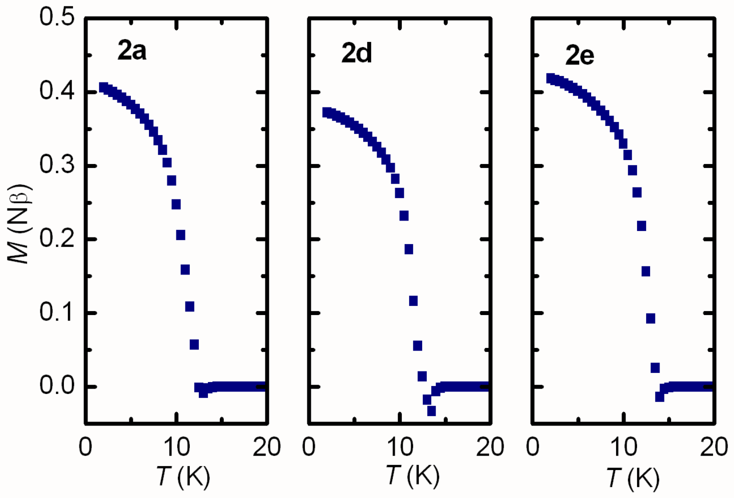

Figure 6.9 Field independent magnetization as a function of temperature for **6-2a**, **6-2d** and **6-2e**.

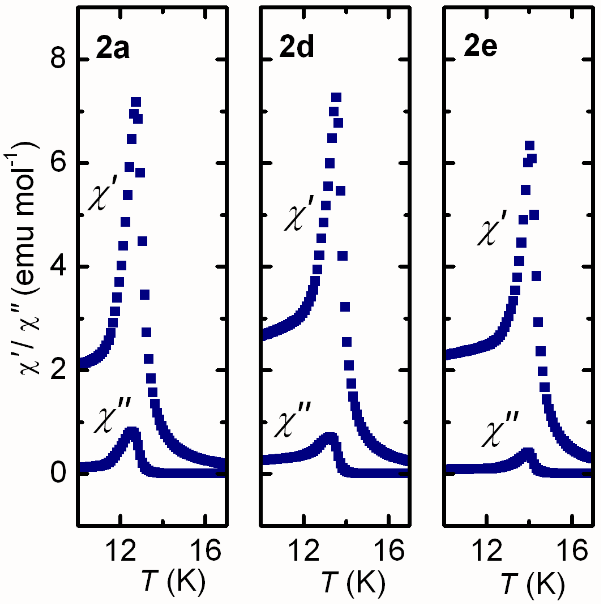

Figure 6.10 In-phase χ′ and out-of-phase χ″AC magnetic susceptibility (at 1 KHz) of **6-2a**, **6-2d** and **6-2e** as a function of temperature.

We also performed magnetization experiments as a function of field on **6-2e**. Here, M rises sharply with H, reaching (at 2 K) a maximum at $H = 10$ kOe, after which there is no further change in M with H (up to 55 kOe). The corresponding saturation magnetization value M_{sat} is 1.02 Nβ for **6-2e**, in good agreement with that expected ($M_{sat} = g\text{N}\beta S = 1$ Nβ) for a $S = ½$ with g nominally equal to 2. As in the case of **6-2a** and **6-2d**, reversal and cycling of the field sweep leads to hysteresis in the magnetization for **6-2e**. Plots of M versus H for all three compounds, from measurements taken at 2 K are shown in **Figure 6.11**. The remanent magnetization M_{rem} of the three compounds is virtually the same, the coercive field H_c (at 2K) ranges from 250 Oe in **6-2a**, to 230 Oe in **6-2d**, to 320 Oe in **6-2e**.

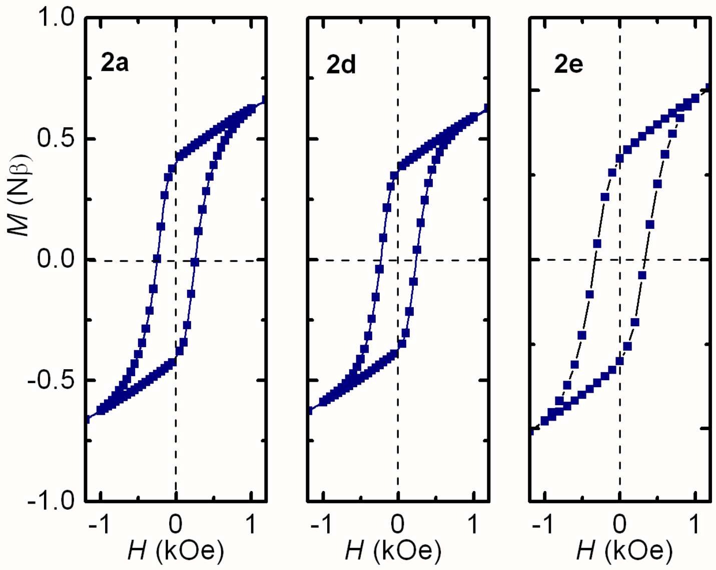

Figure 6.11 Magnetization of **2a**, **2d** and **2e** as a function of magnetic field at 2 K.

6.6 Discussion

The quest for stable radical materials capable of electrical conductivity has led us to investigate the *bis*-DTA system. The synthesis of this class of radical, although challenging, has netted great rewards when one looks at the physical properties of the material. Through resonance stabilization, disproportionation enthalpies and electrochemical cell potentials have been minimized, as compared to all other thiazyl (SN) radicals found in the literature. Furthermore, the versatility of the *bis*-DTA backbone allows for the synthetic modification of the R_1 and R_2 ligands, a factor which alters the packing of the radicals in the solid state. The previous chapter served a four-fold purpose, that is it (i) demonstrated that Se can be incorporated into any position of the *bis*-DTA backbone, again driving home the versatility of *bis*-DTAs, (ii) the generation of an isostructural set of radicals allows for a detailed analysis of the bulk properties with respect to Se position in the radical, (iii) Se increases the measured conductivity, a factor critical to the development of neutral radicals conductors, and (iv) the incorporation of Se into the *bis*-DTA framework can give rise to an interesting array of magnetic effects, and in particular ferromagnetism and weak ferromagnetism.

The work presented in this chapter focuses on the synthetic modification of the R_1 and R_2 substituents of **6-2**, where our intent was to make slight synthetic modifications to the periphery of the radical that would alter the intermolecular contacts within the solid, but still maintain the same space group configuration ($P\bar{4}2_1m$), *i.e.*, generate an isostructural set. Overall, we sought to probe the conductivity and magnetic susceptibility of these systems. To this end, three new radicals, **6-2b**, **6-2c**, and **6-2e**, have been synthesized and fully characterized, and as we had hoped, all three radicals crystallize in the $P\bar{4}2_1m$ space group. Collectively, **6-2b**, **6-2c**, and **6-2e** along with **6-2a** (initially reported in **Chapter 5**) and **6-2d** (initially reported in **Chapter 4**) form an isostructural series of radicals that only vary by the nature of the R_1 and R_2 substituent. However, it is clear that the set of five radicals can be further subdivided into two groups: **6-2a**, **6-2d**, and **6-2e** (hereafter termed **Group 1**) and **6-2c** and **6-2d** (hereafter termed **Group 2**). Variable temperature conductivity measurements performed on the isostructural series demonstrate room temperature conductivities and activation energies on the order of 10^{-4} S cm^{-1} and 0.29 eV for **Group 1** and 10^{-5} S cm^{-1} and 0.31 eV for **Group 2**. We believe these results can be rationalized by the distance of the Se---Se′ contacts about the $\bar{4}$ centre, where the contacts in **Group 1** are significantly shorter than those of **Group 2** (**Table 6.1 and 6.2**); bandwidth (W) calculations also agree with this interpretation, as the radicals in **Group 1** have $W \geq 1.0$ eV and the radicals belonging to **Group 2** have $W = 0.90$ eV. However, it is the magnetic susceptibilities of each radical at temperatures below 50 K that clearly defines each grouping.

All three radicals belonging to **Group 1** give rise to ferromagnetic ordering, with Curie temperatures (T_c) of 12.8 K, 13.6 K and 14.1 K for **6-2a**, **6-2d**, and **6-2e** consecutively. Furthermore, all three radicals exhibit magnetic coersivities H_c (at 2 K) of 250 Oe, 230 Oe and 320 Oe for **6-2a**, **6-2d**, and **6-2e**. In contrast, **Group 2** radicals do not display ferromagnetic ordering at low temperatures, but rather demonstrates Curie-Weiss behaviour with small Weiss constants (θ) of -3.0 K for **6-2b** and -1.0 K for **6-2c**. Thus, through the modification of R_1, we have succeeded in "switching off" the ferromagnetic interactions that are observed for **Group 1** radicals. Clearly, the steric bulk of the $R_1 = C_3H_7$ (Pr) and CH_2CF_3 (fEt) ligands served to increase the Se---Se′ contact distances that form around the $\overline{4}$ centre. Furthermore, both R_1 groups appear to decrease the inclination angle τ (where $\tau = 90°$ describes superimposed stacks of radicals and $\tau < 90°$ describes the degree of "slippage" between two radicals with respect to the stacking (z) axis) as compared to **Group 1** radicals (**Figure 6.12**, **Table 6.1** and **6.2**).

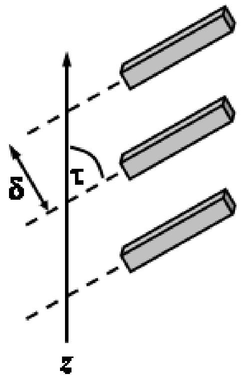

Figure 6.12 Definition of δ and τ for a stack of π-radicals (represented as blocks) along the z-axis.

It is clear that the symmetry operators afforded by the space group $P\overline{4}2_1m$ act to *spatially orient* the radicals into conformations that permit ferromagnetic exchange; however, crystallization in this space group is not the only requirement for long range ferromagnetic order to ensue, as small variations within the structure, *i.e.*, the increase of the bulky R_1 ligands, can have a large effect on the magnetic susceptibility of the bulk material. As already stated above, we have found that the contact distances d1 - d3 in **Group 1** radicals are significantly shorter than those of **Group 2** (**Table 6.1 and 6.2**). These distances, which are all well within the van der Waals distances for Se---Se′(3.8 Å) and Se---S′ (3.6 Å) contacts,[9] will effect the magnitude of the radical SOMO interactions, and this may lead to an increase/decrease in the magnitude of the magnetic exchange between radicals in the solid. Furthermore, the values of τ, which are roughly 58°

(at 298 K) for radicals belonging to **Group 1**, differ significantly from those of **Group 2** (50.0° and 53.8° for **6-2b** and **6-2c** respectively). Upon cooling to 100 K, the distances of d1 - d3 as well as δ decrease, as a result of thermal contraction (the crystal symmetry is still maintained), whereas τ increases in **6-2a**, **6-2b** and **6-2c** and decreases in **6-2d** and **6-2e**. Thus, while cooling the single crystal results in decreased intermolecular contacts, τ varies within each Group.

But why are radicals **5-2a**, **5-2d** and **5-2e** ferromagnetic at low temperatures, and furthermore, why is the ferromagnetism "turned off" when R_1 = Pr or fEt? At the present time, these questions cannot be answered; however, a few suggestions can be offered. First, developing a complete understanding of the ferromagnetic origins in **Group 1** radicals will, in no doubt, require a theoretical chemist to carefully model the radical system. Furthermore, due to the variation in d1 - d3, δ and τ upon cooling, it will be necessary to obtain single crystal X-ray data of the radical at (or below) T_c in order to probe the exact structure-property relationship. In the literature, there are many models that one could attempt to apply to this system, but one of the most recognized models is the McConnell I mechanism, where McConnell stated that the interaction of positive spin density and negative spin density of two π-type radicals could lead to ferromagnetic exchange.[10] Rawson points out, however, that in many known cases of π-type organic ferromagnets, there are few short intermolecular contacts between regions of positive (or negative) spin densities.[11] A prime example is the nitronyl nitroxide class, where electron spin density resides primarily on the NO appendages and although ferromagnetic ordering at low temperatures has been observed, there are few contacts within the sum of the van der Waals radii for N---O′ and O---O′ in the solid state.[12] In contrast, *bis*-DTAs and Se-containing analogues give rise to radicals with delocalized spin density throughout the radical backbone and close intermolecular contacts (within van der Waals distances) and therefore, neighbouring SOMOs can interact (*i.e.*, overlap) in the solid state. Thus, the McConnell model could be probed for these systems.

However, it is likely both the magnitude and geometry of the interacting radical SOMOs that dictates the magnetic exchange in these radicals and it may be advantageous to probe the exchange energies of SOMO overlap between nearest neighbours. This approach has been suggested by others,[13] and applied to molecular radicals with some degree of success by Novoa and coworkers.[14] For example, if there is nonorthogonal SOMO overlap between two neighbours, the magnetic exchange would be antiferromagnetic in nature. In contrast, if there is orthogonal overlap between SOMOs, there is the potential for ferromagnetic exchange. Rawson has applied this idea to dithiadizolyl radicals (DTDAs),[11,15] where the magnetic exchange energies were probed by investigating the nature of the SOMO overlap between two DTDA radicals. In these studies, Rawson illustrated that orthogonal overlap of neighbouring SOMOs gives rise to ferromagnetic exchange energies.

In the case of **5-2a**, **5-2d** and **5-2e**, at 100 K there are three sets of radical geometries with intermolecular contacts well within the van der Waals distances for two Se atoms, that is (i) radicals within the π-stack, oriented along the [0,0,1] direction (**Figure 6.13a**), (ii) the radicals having the close contacts d 1- d3 (**Figure 6.13b**), and (iii) the radicals on the {1,1,0} plane (**Figure 6.13c**).

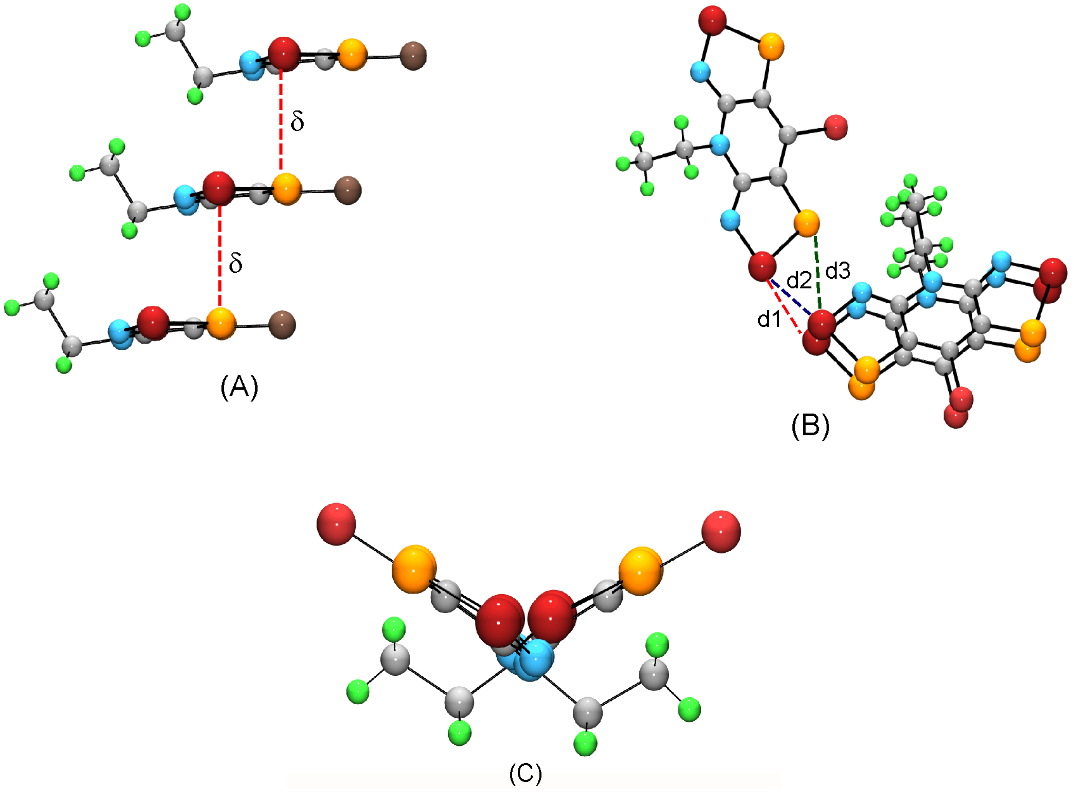

Figure 6.13 Illustration of **6-2e** radicals (a) viewed parallel to [0,0,1], (b) with d1- d3 contacts and (c) parallel to {1,1,0} with dihedral angle (2τ) between molecular planes. Dashed lines represent intermolecular interactions within the van der Waals contact distances.

Clearly, probing the magnetic exchange pathways between neighbouring radicals in **Figure 6.13** will not predict bulk ferromagnetism, but will give us an understanding of nearest neighbour coupling. Furthermore, *ab initio* calculations of each exchange pathways will lead to a better understanding of the dimensionality afforded by the magnetic pathways and may provide a correlation between *ab initio* calculations and the observation of bulk ferromagnetism. It would also be advantageous to undertake *ab initio* calculations where (i) the distances d1 - d3 and δ are incrementally increased/decreased and (ii) where τ is varied in a stepwise fashion. Increasing d1 - d3 and δ should decrease the exchange energy (but not the sign) whereas changes in τ may result in a change in both the sign and magnitude of the exchange energy.

6.7 Conclusion and Future Work

The development of neutral radical conductors faces two main design challenges, that is, to decrease the onsite Coulomb repulsion *U* and increase the intermolecular bandwidth *W*. The neutral radicals presented in this thesis, and in particular Se-containing *bis*-DTAs, address both of these issues directly. New synthetic technologies have allowed for (i) the incorporation of Se into all positions of the *bis*-DTA ring, and (ii) the modification of R_1 and R_2 substituents; both have led to a vast array of Oakley radicals that have been studied. Calculated disproportionation enthalpies and measured electrochemical cell potentials are lower than all other thiazyl (SN) and selazyl (SeN) based radicals to date, and the incorporation of Se into the *bis*-DTA backbone has lead to solid state *W*s greater than 1 eV - values that are far superior to those of previous studied radical materials. Furthermore, we have also discovered that the incorporation of the heavy atom Se into many of our radicals affords an unexpected, yet warmly welcomed, array of bulk magnetic properties such as ferromagnetism and weak ferromagnetism.

The generation of isostructural sets will continue to play a large role in research, as it has allowed us to directly compare the effect of Se incorporation/position in our radicals, and from these studies it is clear that replacement of S by Se has the desired effect of increasing the conductivity of the bulk material (by up to 3 orders of magnitude) as well as enhance the magnetic properties of the bulk material. We have also begun to systematically study the effect of R_1 and R_2 substituents on the magnetic properties of the bulk radical. Clearly, the investigation of the magnetic effects afforded by the incorporation of heavy atoms into *bis*-DTAs and modification of R_1 and R_2 substituents is in its infancy. However, this work has opened the door to a new class of multifunctional Oakley radical - one that displays both ferromagnetism and enhanced conductivity. Perhaps this work will lead to SeN radicals that display properties such as magnetoresistance or itinerant magnetism - I am eager to see what is to come.

6.8 Experimental Section

Please see **Appendix A** for general methods and procedures.

Preparation of 8-Chloro-4-trifluoroethyl-4*H*-bis[1,2,3]dithiazolo[4,5-b:5',4'-e]pyridin-2-ium Triflate [6-1c][OTf]. Neat 2,2,2-trifluoroethyl triflate (3.5 mL, 24.0 mmol) was added to a stirred slurry of **6-5** (2.38 g, 8.95 mmol) in 25 mL DCE in a small glass pressure vessel. The vessel was sealed and the mixture was heated in an oil bath at 100 °C for 40 h. The reaction mixture was cooled to room temperature and crude [**6-1c**][OTf] was filtered off as dark red solid, washed with 5 x 20 mL DCE and dried in air; yield 3.63 g (7.29 mmol, 81 %). Recrystallization from MeCN afforded copper colored platlets; mp > 300 °C dec. IR: 1520 (w), 1497 (s), 1438 (s), 1365 (s), 1274 (s), 1240 (vs), 1169 (s), 1108 (m), 1027 (s), 1008 (w), 931 (w), 866 (w), 841 (w), 831 (w), 767 (vs), 716 (w), 689 (w), 676 (w), 669 (s), 640 (s), 574 (w), 539 (w), 516 (m), 479 (s) cm^{-1}. Anal. Calcd. for $C_8H_2ClF_6N_3O_3S_5$: C, 19.30; H, 0.40; N, 8.44 %. Found: C, 19.55; H, 0.41; N, 8.67 %.

Preparation of Bis[1,2,3]thiaselenazolo[4,5-b:5',4'-e]pyridin-2-ium Triflates [6-2b,c][OTf]. Compound [**6-1b,c**][OTf] (2.00 mmol) and finely ground selenium dioxide (0.666 g, 6.00 mmol) were added to a large glass pressure vessel along with 80 mL MeCN, and the mixture stirred and heated in an oil bath at 110 °C for 48 - 72 h. The reaction was continued until analysis of the mixture by ESI mass spectrometry showed complete and specific formation of [**6-2**]$^+$. The flask was cooled to room temperature, and the dark green solution filtered through a glass Büchner funnel to remove a small amount of black precipitate. The filtrate was concentrated to 30 mL, cooled to room temperature for 1 h, then at -20 °C for 2 h. Red crystals of [**6-2b,c**][OTf] were filtered off, washed with DCM and dried in air. The product was double recrystallized from MeCN and/or HOAc as red needles.

Analytical Data for Salts [6-2b,c][OTf]. [**6-2b**][OTf]: Yield 64 %, mp 260-2 °C. IR: 2257 (w, MeCN), 1437 (s), 1288 (s), 1240 (s), 1218 (s), 1180 (w), 1155 (s), 1147 (s), 1082 (w), 1027 (s), 972 (w), 754 (w), 735 (w), 719 (w), 637 (s), 595 (m), 571 (w), 551 (w), 516 (w), 476 (w) cm^{-1}. Anal. Calcd. for $C_9H_7ClF_3N_3O_3S_3Se_2$: C: 19.59, H: 1.28, N: 7.62 %. Found: C: 19.43, H: 1.10, N: 7.68 %. [**6-2c**][OTf]: Yield 70 %, mp > 300 °C dec. IR: 2253 (w, MeCN), 1483 (s), 1286 (s), 1261 (s), 1238 (s), 1220 (s), 1189 (w), 1171 (s), 1147 (s), 1094 (s), 1024 (s), 997 (m), 842 (w), 829 (m), 758 (m), 748 (s), 719 (s), 684 (m), 638 (s), 611 (m), 593 (m), 573 (w), 540 (w), 515 (w), 474 (w) cm^{-1}. Anal. Calcd. for $C_8H_2ClF_6N_3O_3S_3Se_2$: C, 16.24; H, 0.34; N, 7.10 %. Found: C, 16.41; H, 0.72; N, 7.23 %. **Preparation of Radicals 6-2b ,c: Method 1.** *Bulk material for conductivity and magnetic measurements*. Before use, all glassware was soaked overnight in dilute HNO_3, then washed with deionized water followed by distilled water, and finally oven dried at 100 °C overnight. Magnetic stirbars were glass-covered. Degassed solutions (3 freeze-pump-thaw cycles) of reducing agent (0.571 - 1.01 mmol) (**6-2b**: DMFc, **6-2c**: OMFc) in 40 - 125 mL MeCN and [**6-2b,c**][OTf] (0.429 - 0.580 mmol) in 90 - 150 mL MeCN were combined and after 30 m the gold-brown precipitate of **6-2b,c** was filtered off and washed 4 × 20 mL MeCN. **Method 2**. *Diffusion H-cells for single crystal growth*. Degassed solutions (3 freeze-pump-thaw cycles) of reducing agent (0.056 - 0.085 mmol) (**6-2b,c**: OMFc) in 15 mL MeCN and [**6-2b,c**][OTf] (0.038 - 0.054 mmol) in 15 mL MeCN were allowed to diffuse together slowly at room temperature over a period of 16 h. The solvent was decanted to leave metallic green/black needles of **6-2b,c** suitable for X-ray work.

Analytical Data for Radicals 6-2b,c by Method 1. 6-2b. Yield 89 %, mp > 120 °C dec. IR: 1410 (m), 1319 (s), 1296 (w), 1279 (m), 1223 (s), 1176 (w), 1075 (s), 965 (s), 906 (w), 890 (m), 815 (m), 730 (s), 696 (s), 615 (m), 577 (m), 534 (m), 502 (w), 460 (m) cm^{-1}. Anal. Calcd. for $C_8H_7ClN_3S_2Se_2$: C, 23.86; H, 1.75; N, 10.44 %. Found: C, 24.00; H, 1.66; N, 10.68 %. **6-2c**. Yield 68 %, mp > 120 °C dec. IR: 1405 (m), 1322 (s), 1251 (s), 1228 (w), 1184 (s), 1165 (s), 1090 (s), 984 (m), 836 (m), 815 (w), 734 (m), 697 (s), 680 (w), 613 (m), 572 (w), 541 (w), 529 (w), 460 (w) cm^{-1}. Anal. Calcd. for $C_7H_2ClF_3N_3S_2Se_2$: C, 19.00; H, 0.46; N, 9.46 %. Found: C, 19.25; H, 0.33;N, 9.68 %.

Appendix A

A.1 Procedures

A.1.1 General Procedures

Many of the reactions and manipulations were performed under an inert atmosphere of nitrogen. Those reactions carried out in solution were handled by standard or modified Schlenk techniques using a double-manifold glass vacuum line (nitrogen / vacuum) with an Edwards E2M series rotary vacuum pump. Air sensitive solids were handled and stored in a nitrogen-filled Braun MB-150M drybox.

A.2.1 H-cell Crystallizaton

For materials which are highly insoluble, *i.e.*, recrystallization is not an option, H-cell techniques are sometimes used to grow crystals of analytical grade. A typical H-cell apparatus is illustrated in **Figure A.1**.[1] In the experiment, two solutions are allowed to diffuse through a frit, resulting in crystal growth of the desired compound at the interface of the two solutions.

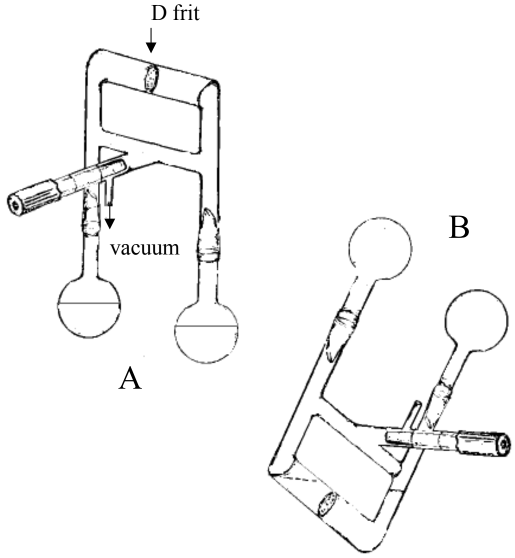

Figure A.1 H-cell apparatus used for crystal growth.

These experiments are especially useful for the preparation of air or moisture sensitive materials, *i.e.*, neutral radicals, as a thorough degassing of the solvents is possible. Two solutions containing each reactant are placed in each of the round bottom flasks and the cell is oriented as shown in A. The solutions are put through a freeze-pump-thaw cycle five times to ensure that all oxygen has been removed from the vessel. The apparatus is flooded with an inert gas (argon or nitrogen) and then tipped, slightly askew, to allow the two solutions to combine, one running through the frit into the other (B). The result is crystal growth of the product on the frit.

A.2 Techniques

A.2.1 Density Functional Theory

DFT calculations were run on a PC workstation using the B3LYP method available in the Gaussian 98W[2] and Gaussian 03W[3] suit of programs. Geometries were optimized using a 6-31G(d,p) basis set, within appropriate symmetry constraints.

A.2.2 NMR Spectra

^{1}H NMR spectra were collected on a Bruker Avance 300 MHZ NMR spectrometer.

A.2.3 Infrared Spectral Analysis

Infrared spectra were recorded (at 2cm^{-1} resolution) as Nujol mulls or neat liquids on KBr plates, on a Nicolet Avatar 320 FT infrared spectrometer.

A.2.4 Mass Spectrometry

Low resolution mass spectra (70 eV, EI, DEI and CI, DCI) were run on the following machines: a Finnigan 4500 quadrupole mass spectrometer at the McMaster Regional Centre for Mass Spectrometry, and either a Micromass Q-TOF Ultima Global LC/MS/MS system of a JEOL HX110 double focusing mass spectrometer at the University of Waterloo.

A.2.5 Cyclic Voltammetry

Cyclic voltammetry was performed on dry acetonitrile or dichloroethane solutions containing 0.1 M tetra-*n*-butylammonium hexafluorophosphate. A PINE Bipotentiostat, Model AFCBP1 was used. Scan rates of 50 - 100 mV s^{-1} were employed. Potentials were scanned from -2.5 to 2.0 V with respect to the quasireference electrode in a single compartment cell fitted with Pt electrodes and referenced to the ferrocenium / ferrocene couple at 0.38 V *vs*. SCE in CH_3CN (0.48 V *vs.* SCE in CH_2Cl_2).[4]

A.2.6 EPR Spectra

The X-band EPR spectra were recorded on methylene chloride (or toluene when stated) solutions of the radical at ambient temperature using a Bruker EMX spectrometer. Hyperfine coupling constants were obtained by spectral simulation using Simfonia[5] and WinSim.

A.2.7 Elemental Analysis

Elemental analyses were performed by MHW Laboratories, Pheonix, AZ.

A.2.8 Magnetic Susceptibility Measurements

Magnetic susceptibilities were measured on a George Associates Faraday balance operating at 0.5 T (University of California, Riverside), DC magnetic susceptibility measurements were performed on a Quantum Design MPMS SQUID magnetometers (University of Victoria, Memorial University of Newfoundland and McMaster University). AC susceptibility measurements were performed on an Oxford Instruments MagLab EXA (McMaster).

A.2.9 X-ray Crystallography

Single crystal X-ray data were collected at ambient temperature (and 100 K when stated) using phi and omega scans with a (i) Bruker APEX I CCD detector on a D8 3-circle goniometer (University of Waterloo), (ii) Bruker P4/CCD diffractometer (McMaster University, University of Louisville) and (iii) Bruker APEX II CCD detector on a D8 3-circle goniometer (McMaster University) with Kα (λ = 0.71073

Å) radiation. Single crystal data were also collected on a Bruker SMART 6000 CCD on a D8 3-circle goniometer and a parallel focus Cu Kα (λ = 1.54178 Å) with a rotating anode generator. All data were reduced using Bruker's SMART program and integrated using Bruker's SAINT software.[6] or by the APEX II software package. The structures were solved by direct methods using SHELXS-90[7] and refined by least-squares methods on F^2 using SHELXL-97[8] incorporated in the SHELXTL suite of programs.[9] Agreement indices are calculated as followed:

$R = [\Sigma||F_o| - |F_c||]/[\Sigma|F_o|]$ for $I > 2\,\sigma(I)$; $R_w = \{[\Sigma w||F_o|^2 - |F_c|^2|^2]/[\Sigma(w|F_o|^4)]\}^{1/2}$.

Powder data were collected on a X-ray powder diffractometer with a position sensitive detector (INEL) at ambient temperature using Cu $K\alpha_1$ radiation (λ = 1.5406 Å). All powder data were indexed using the software package Crysfire[10] and employed the indexing software Taup[11] and Dicvol91.[12] All *ab initio* solutions were carried out with FOX[13] and Rietveld methods[14] *via* the GSAS software package.[15]

A.2.10 Conductivity Measurements

Temperature dependent conductivity measurements were performed on pressed pellet samples using a four-probe method. A home-made device was used to measure the voltage drop under dynamic vacuum. Silver paint was used to apply the electrical contacts.

A.2.11 Band Calculations

Band electronic structure calculations were performed with the EHMACC suite of programs[16] using the Coulomb parameters of Baasch, Viste and Gray[17] and a quasi-split valence basis set adapted from Clementi and Roetti;[18] numerical values are tabulated elsewhere.[19] The off-diagonal elements of the Hamiltonian matrix were calculated with the standard weighting formula.[20] Atomic positions were taken from the ambient temperature crystallographic data.

A.3 Source of Starting Materials

A.3.1 Purchased Chemicals that Were Used as Received

1-aminonaphthalene	Aldrich
2,6-diaminopyridine	Aldrich
2-naphthol	Aldrich
acetic acid, glacial	Fisher
acetic anhydride, reagent grade	Fisher
ammonia gas	Matheson
ammonium hydroxide	Fisher
ammonium thiocyanate	Fisher
bromine	Fisher
calcium hydride	Fisher
carbon disulfide	Fisher
chlorobenzene	Fisher
chloroform -*d*	Isotec
chlorine gas	Matheson
decamethylferrocene	Aldrich/Alfa Aesar
diethyl ether	Fisher
ethanol, 95%	Fisher
ethyl acetate	Fisher
ethyl triflate, 99%	Aldrich
ferrocene	Aldrich
gallium trichloride, anhydrous beads, -10 mesh, 99.99%	Aldrich
heptane	Fisher
hexane	Fisher
hydrochloric acid, 12 M	Fisher
methanol	Fisher
methyl triflate, 99%	Aldrich

nitric acid	Fisher
nitrogen gas	In-house supply
nitrosonium tetrafluoroborate	Fisher
octamethylferrocene	Aldrich
phosphorous oxychloride	Aldrich
potassium selenocyanate	Aldrich
potassium thiocyanate	Fisher
Proton Sponge	Aldrich
pyridine	Fisher
selenium powder, -100 mesh, 99.5+ %	Aldrich
selenium dioxide	Aldrich
sodium	BDH Labs
sodium bisulfite	Fisher
sodium dithionite	Aldrich
sodium hydroxide, pellets, 97.0 %	Aldrich
sodium sulfide nonahydrate	Aldrich
sulfur monochloride	Aldrich
n-tetrabutylammonium hexafluorophosphate	Fisher
tetrakisdimethyl-aminoethylene	Aldrich
N,N,N′,N′-tetramethyl-*p*-phenylenediamine	Aldrich
thionyl chloride	Acros
triethylamine, 99 %	Aldrich
triflic acid	Aldrich
trimethylsilylazide	Aldrich
triphenyl antimony	Aldrich

A.3.2 Solvents Purified Prior to Use

acetonitrile (Caledon) - distilled from P_2O_5 or CaH_2

chlorobenzene (Fisher) - distilled from P_2O_5

dichloroethane, 1,2- (Fisher) - distilled from P_2O_5

methylene chloride (Fisher) - distilled from P_2O_5

tetrahydrofuran (Caledon) - distilled from lithium aluminum hydride

toluene (Fisher) - distilled from sodium

A.3.3 Commonly Used Chemicals Synthesized "In House"

A.3.3.1 Iodobenzene Dichloride

Chlorine gas was passed over a chilled solution of iodobenzene (4.50 g, 22.0 mmol) in 45 mL DCE for 15 min, yielding a yellow precipitate. The resulting solution was then stirred for an additional 15 min on ice, and 30 min at RT to remove excess chlorine gas. The product was collected by filtration, washed with copious amounts of DCM, and dried; yield 4.05g (14.7 mmol, 67%). This air-sensitive solid was stored at -20 °C and used within 48 h.

A.3.3.2 Selenium Tetrachloride

Selenium powder (22.0 g, 0.28 mol) was slurried in 250 mL of dry MeCN, cooled on ice. Chlorine gas was passed over, but not into, the slurry eventually yielding a white precipitate. The product was collected by filtration, washed with copious amounts of MeCN, and dried *in vacuo*; yield 50 - 55 g (81 - 89 %). This air-sensitive solid was stored in the dry box and was stable for over a year.

A.4 Half-Wave Potentials of Reducing Agents

Table A.1 Half-Wave Potential of Reducing Agents.

Reducing Agent	$E_{½}$ (0/+1), $E_{½}$ (+1/+2)	
	This work [a]	Literature [b]
Ferrocene	0.380	0.380[21]
Dimethylferrocene	0.263	0.241, 0.30[22]
Hexamethylferrocene	0.056	0.04[23]
Octamethylferrocene	−0.038	0.01, −0.02[24]
Decamethylferrocene	−0.131	−0.124[25]
Tetramethyl-*p*-phenylenediamine	0.094, 0.692	0.10, 0.67[26]
Tetrakisdimethylaminoethylene	−0.600 (2e^-)	−0.61, −0.78[27]
		−0.62 (2e^- DMF)

[a] Volts *vs* SCE, anhydrous MeCN, Pt electrodes, 0.1 *M* *n*-Bu_4N^+ PF_6^-. [b] See cited reference for experimental conditions, potentials have been normalized to SCE.

A.5 Room Temperature Conductivities of Benchmark Compounds

Table A.2 Room Temperature Conductivities of Benchmark Compounds.

Compound	**σ_{RT} (S cm^{-1})**	**Type**
Ag, Au, Cu	10^6	Metal
Bi	10^4	Metal
[TTF][TCNQ]	10^3	Metal
TMTSF superconductors	10^3	Metal
[TTF][Br]0.7	10^2	Metal
PbS, Te	10^2	Metal
ET superconductors	10^0 - 10^1	Semiconductor
[Perylene][Br]	10^{-1}	Semiconductor
Ge	5×10^{-2}	Semiconductor
Si	5×10^{-6}	Semiconductor
Se, AgCl	10^{-8}	Semiconductor
[TTF][Br]	10^{-10}	Insulator
TTF	10^{-12}	Insulator
glass	10^{-14} - 10^{-13}	Insulator

References

References for Chapter 1

1 (a) Tanko, J. M. *Annu. Rep. Prog. Chem. Sect. B.*, **2006**, *102*, 247, (b) Aldabbagh, F; Bowman, W. R.; Storey, J. D. M. *Investigation of Organic Reactions and Their Mechanisms*, Blackwell Publishing, Oxford, **2006**.

2 Grindnev, A. A.; Ittel, S. D. *Chem. Rev.*, **2001**, *101*, 3611.

3 Rosen, G. M.; Tsai, P.; Pou, S. *Chem. Rev.*, **2002**, *102*, 1191.

4 Baird, M. C. Chem. Rev., **1988**, *88*, 1217.

5 Thatcher, W. B. *Diradicals*, Wiley, New York, **1982**.

6 (a) Weindruch, R. *Sci. Am.*, **1996**, *274*, 46. (b) Henig, R. M. *Scientific American Presents*, **2000**, *Summer*, 30. (c) Moussa, B. H. Y.; Riederer, P. *Sci. Am.*, **1997**, *276*, 52.

7 Power, P. P. *Chem. Rev.***, 2003**, *103*, 789.

8 Gomberg, M. *J. Am. Chem. Soc.*, **1900**, *22*, 757.

9 (a) Neuman, W. P.; Uzick, W.; Zarkadis, A. K. *J. Am. Chem. Soc.*, **1986**, *108*, 3762. (b) McBride, J. M. *Tetrahedron*, **1974**, *30*, 2009. (c) Kahr, B.; Vanengen, D.; Gopalan, P. *Chem. Mater.*, **1993**, *5*, 729. (d) Neuman, W. P.; Penenory, A.; Stewen, U.; Lehnig, M. *J. Am. Chem. Soc.*, **1989**, *111*, 5845.

10 Sabacky, M. J.; Johnson, C. S.; Smith, R. G.; Gutowsky, H. S.; Martin, J. C. *J. Am. Chem. Soc.*, **1967**, *89*, 2054.

11 Jang, S. H.; Gopalan, P.; Jackson, J. E.; Kahr, B. *Angew. Chem., Int. Ed. Engl.*, **1994**, *33*, 775.

12 Sitzmann, H.; Bock, H.; Boese, R.; Dezember, T.; Havlas, Z.; Kaim, W.; Moscherosch, M.; Zanathy, L. *J. Am. Chem. Soc.*, **1993**, *115*, 12003.

13 Goto, K.; Kubo, T.; Yamamoto, K.; Nakasuji, K.; Sato, K.; Shiomi, D.; Takeji, T.; Kubota, M.; Kobayashi, T.; Yakusi, K.; Ouyang, J. *J. Am. Chem. Soc.*, **1999**, *121*, 1619.

14 (a) Coppinger, G. M. *J. Am. Chem. Soc.*, **1957**, *79*, 501. (b) Dietz, F.; Tyutyulkox, N.; Baumgarten, M. *J. Phys. Chem. B*, **1998**, *102*, 3912.

15 Kuhn, R.; Trischmann, H. *Angew. Chem., Int. Ed. Engl.*, **1963**, *3*, 155.

16 Neugebauer, F. A.; Umminger, I. *Chem. Ber.*, **1980**, *113*, 1205.

17 Rozanstev, E. G. *Free Nitroxyl Radicals*, Plenum, New York, **1970**.

18 Caneschi, A.; Gatteschi, D.; Rey, P. *Prog. Inorg. Chem.*, **1991**, *39*, 331.

19 (a) Pandey, K. K.; Raju, D. K. M.; Nigam, H. L.; Agarwala, U. C. *Proc. Indian Nat. Sci. Acad.*, **1982**, *48A*, 16. (b) Pandey, K. K. *Prog. Inorg. Chem.*, **1992**, *40*, 445.

20 (a) Burt, F.P.; *J. Chem. Soc.*, **1910**, 1171. (b) Walatka, V.V.; Labes, M. M. *Phys. Rev. Lett.*, **1973**, *31*, 1139. (c) Labes, M. M.; Love, P.; Nichols, L. F. *Chem. Rev.*, **1979**, *79*, 1. (d) Cohen, M. J.; Garito, A. F.; Heeger, A. J.; MacDiarmid, A. G.; Mikulski, C. M.; Saran, M. S.; Kleppinger, J. *J. Am. Chem. Soc.*, **1976**, *98*, 3844. (e) Greene, R. L.; Street, G. B.; Suter, L. J. *Phys. Rev. Lett.*, **1975**, *34*, 577.

21 Oakley, R. T. *Prog. Inorg. Chem.*, **1988**, *36*, 299.

22 Milulski, C. M.; Russo, P. J.; Soran, M. S.; MacDiarmid, A. G.; Farito, A. F.; Heegler, A. J. *J. Am. Chem. Soc.*, **1975**, *97*, 6358.

23 (a) Villena-Blanco, M.; Jolly, W. L. *Inorg. Synth.*, **1967**, *9*, 98. (b) Maaninen, A.; Siivari, J.; Laitinen, R. S.; Chivers, T. *Inorg. Synth.*, **2002**, *33*, 196.

24 (a) Cordes, A. W.; Hayes. P. J.; Josephy, P. D.; Koenig, H.; Oakley, R. T.; Pennington, W. T. *J. Chem. Soc., Chem. Commun.*, **1984**, 1021. (b) Hayes. P. J.; Oakley, R. T.; Cordes, A. W.; Pennington, W. T. *J. Am. Chem. Soc.*, **1985**, *107*, 1346.

25 Herler, S.; Mayer, P.; Noth, H.; Schulz, A.; Suter, M.; Vogt, M. *Angew. Chem., Int. Ed. Engl.*, **2001**, *40*, 3173.

26 (a) Fairhurst, S. A.; Preston, K. F.; Sutcliffe, L. H. *Can. J. Chem.*, **1984**, *62*, 1124. (b) Johnson, K. M.; Preston, K. F.; Sutcliffe, L. H. *Mag. Reson. Chem.*, **1988**, *26*, 1015. (c) Gillespie, R. J.; Kent, J. P.; Sawyer, J. F. *Inorg. Chem.*, **1981**, *20*, 3784.

27 (a) Cordes, A. W.; Haddon, R. C.; MacKinnon, C. D.; Oakley, R. T.; Patenaude, G. W.; Reed, R. W.; Rietveld, T.; Vajda, K. E. *Inorg. Chem.*, **1996**, *35*, 7626. (b) Andrew, M. P.; Cordes, A. W.; Douglas, D. C.; Flemming, R. M.; Glarum, S. H.; Haddon, R. C.; Marsh, P.; Oakley, R. T.; Palstra, T. T. M.; Schneemeyer, L. F.; Trucks, G. W.; Tycko, R.; Waszczak, J. V.; Young, K. M.; Zimmerman, N. M. *J. Am. Chem. Soc.*, **1991**, *113*, 3559. (c) Cordes, A. W.; Haddon, R. C.; Hicks, R. G.; Kennepohl, D. K.; Oakley, R. T.; Palstra, T. T. M.; Schneemeyer, L. F.; Scott, S. R.; Waszczak, J. V. *Chem. Mater.*, **1993**, *5*, 820. (d) Cordes, A. W.; Haddon, R. C.; Oakley, R. T.; Schneemeyer, L. F.; Waszczak, J. V.; Young, K. M.; Zimmerman, N. M. *J. Am. Chem. Soc.*, **1991**, *113*, 582. (e) Cordes, A. W.; Haddon, R. C.; Hicks, R. G.; Oakley, R. T.; Palstra, T. T. M.; Schneemeyer, L. F.; Waszczak, J. V. *J. Am. Chem. Soc.*, **1992**, *114*, 1729. (f) Bryan, C. D.; Cordes, A. W.; Goddard, J. D.; Haddon, R. C.; Hicks, R. G.; MacKinnon, C. D.; Mawhinney, R. C.; Oakley, R. T.; Palstra, T. T. M.; Perel, A. S. *J. Am. Chem. Soc.*, **1996**, *118*, 330.

28 Vegas, A.; Perezsalazar, A.; Banister, A. J.; Hey, R. G. *J. Chem. Soc., Chem. Commun.*, **1980**, 1812.

29 Fairhurst, S. A.; Johnson, K. M.; Sutcliffe, L. H.; Preston, K. F.; Banister, A. J.; Hauptman, Z. V.; Passmore, J. *J. Chem. Soc., Dalton Trans.*, **1986**, 1465.

30 (a) Wolmershäuser, G.; Kraft, G. *Chem. Ber.*, **1990**, *123*, 881. (b) Du, H.; Haddon, R. C.; Krossing, I.; Passmore, J.; Rawson, J. M.; Schriver, M. J. *Chem. Commun.*, **2002**, 1836. (c) Brownridge, S.; Du, H. B.; Fairhurst, S. A.; Haddon, R. C.; Oberhammer, H.; Parsons, S.; Passmore, J.; Schriver, M. J.; Sutcliffe, L. H.; Westwood, N. P. C. *J. Chem. Soc., Dalton Trans.*, **2000**, 3365. (d) Awere, E. G.; Burford, N.; Mailer, C.; Passmore, J.; Schriver, M. J.; White, P. S.; Banister, A. J.; Oberhammer, H.; Sutcliffe, L. H. *J. Chem. Soc., Chem Commun.*, **1987**, 66. (e) Awere, E. G.; Burford, N.; Haddon, R. C.; Parsons, S.; Passmore, J.; Waszczak, V.; White, P. S. *Inorg. Chem.*, **1990**, *29*, 4821.

31 Barclay, T. M.; Cordes, A. W.; George, N. A.; Haddon, R. C.; Oakley, R. T.; Palstra, T. T. M.; Patenaude, G. W.; Reed, R. W.; Richardson, J. F.; Zhang, H. Z. *Chem. Commun.*, **1997**, 873.

32 Barclay, T. M.; Cordes, A. W.; George, N. A.; Haddon, R. C.; Itkis, M. E.; Mashuta, M. S.; Oakley, R. T.; Patenaude, G. W.; Reed, R. W.; Richardson, J. F.; Zhang, H. Z. *J. Am. Chem. Soc.*, **1998**, *120*, 352.

33 (a) Wolmershauser, G.; Johann, R. *Angew. Chem., Int. Ed. Engl.*, **1989**, *28*, 920. (b) Fujita, W.; Awaga, K. *Science*, **1999**, *286*, 261. (c) McManus, G. D.; Rawson, J. M.; Feeder, N.; van Duijn, J.; McInnes, E. J. L.; Novoa, J. J.; Burriel, R.; Palacio, F.; Oliete, J. *J. Mater. Chem.*, **2001**, *11*, 1992.

34 (a) Heckmann, G.; Johann, R.; Kraft, G.; Wolmershäuser, G. *Synth. Met.*, **1991**, *43*, 3287. (b) Brusso, J. L.; Clements, O. P.; Haddon, R. C.; Itkis, M. E.; Leitch, A. A.; Oakley, R. T.; Reed, R. W.; Richardson, J. F. *J. Am. Chem. Soc.*, **2004**, *126*, 8256. (c) Brusso, J. L.; Clements, O. P.; Haddon, R. C.; Itkis, M. E.; Leitch, A. A.; Oakley, R. T.; Reed, R. W.; Richardson, J. F. *J. Am. Chem. Soc.*, **2004**, *126*, 14692.

35 (a) Gutlich, P.; Hauser, A.; Spiering, H. *Angew. Chem., Int. Ed. Engl.*, **1994**, *33*, 3024. (b) Kahn, O.; Martinez, C. J. *Science*, **1998**, *279*, 44.

36 (a) Preston, K. F.; Sutcliffe, L. H. *Mag. Reson. Chem.*, **1990**, *28*, 189. (b) Mayer, R.; Domschke, G.; Bleisch, S. *Tetrahedron Lett.*, **1978**, 4003. (c) Mayer, R.; Domschke, G.; Bleisch, S.; Bartl, A; Stăsko, A. *Z. Chem.* **1981**, *21*, 146. (d) Mayer, R.; Domschke, G.; Bleisch, S.; Fabian, J.; Bartl, A.; Stăsko, A. *Collect. Czech. Chem. Commun.,* **1984**, *49*, 684. (e) Mayer, R.; Bleisch, S.; Domschke, G.; Tkáč, A.; Stăsko, A. *Org. Magn. Reson.*, **1979**, *12*, 532. (f) Harrison, S. R.; Pilkington, R. S.; Sutcliffe, L. H. *J. Chem. Soc., Faraday Trans. 1*, **1984**, *80*, 669.

37 Barclay, T. M.; Cordes, A. W.; Haddon, R. C.; Itkis, M. E.; Oakley, R. T.; Reed, R. W.; Zhang, H. Z. *J. Am. Chem. Soc.*, **1999**, *121*, 969.

38 Cordes, A. W.; Mingie, J. R.; Oakley, R. T.; Reed, R. W.; Zhang, H. *Can. J. Chem.*, **2001**, *79*, 1352.

39 Barclay, T. M.; Beer, L.; Cordes, A. W.; Oakley, R. T.; Preuss, K. E.; Taylor, N. J.; Reed, R. W. *Chem. Commun.*, **1999**, 531.

40 Beer, L.; Cordes, A. W.; Haddon, R. C.; Itkis, M. E.; Oakley, R. T.; Reed, R. W.; Robertson, C. M. *Chem. Commun.*, **2002**, 1872.

41 (a) Beer, L.; Brusso, J. L.; Haddon, R. C.; Itkis, M. E.; Kirschbaum, K.; MacGreggor, D. S.; Oakley, R. T.; Pinkerton, A. A.; Reed, R. W. *J. Am. Chem. Soc.*, **2002**, *124*, 9498. (b) Beer, L.; Britten, J. F.; Brusso, J. L.; Cordes, A. W.; Haddon, R. C.; Itkis, M. E.; MacGreggor, D. S.; Oakley, R. T.; Reed, R. W.; Robertson, C. M. *J. Am. Chem. Soc.*, **2003**, *125*, 14394. (c) Beer, L.; Brusso, J. L.; Cordes, A. W.; Godde, E.; Haddon, R. C.; Itkis, M. E.; Oakley, R. T.; Reed, R. W. *Chem. Commun.*, **2002**, 2562. (d) Beer, L.; Britten, J. F.; Clements, O. P.; Haddon, R. C.; Itkis, M. E.; Matkovich, K. M.; Oakley, R. T.; Reed, R. W. *Chem. Mater.*, **2004**, *16*, 1564. (e) Leitch, A. A.; Reed, R. W.; Robertson, C. M.; Britten, J. F.; Yu, X.; Secco, R. A.; Oakley, R. T. *J. Am. Chem. Soc.*, **2007**, *129*, 7903.

42 (a) Awaga, K.; Sugano, T.; Kinoshita, M. *Bull. Chem. Soc. Jpn.*, **1986**, *58*, 1886. (b) Barth, T.; Kanellakopulos, B.; Krieger, C.; Neugebauer, F. A. *J. Chem. Soc., Chem. Commun.*, **1993**, 1626.

43 Leitch, A. L.; McKenzie, C. E.; Oakley, R. T.; Reed, R. W.; Richardson, J. F.; Sawyer, L. D. *Chem. Commun.*, **2006**, 1088.

44 See **Table A.2** in **Appendix A** for a table containing the room temperature conductivities of benchmark compounds/elements.

45 McCoy, H. N.; Moore, W. C. *J. Am. Chem. Soc.*, **1911**, *33*, 273.

46 Kraus, H. J. *J. Am. Chem. Soc.*, **1913**, *34*, 1732.

47 (a) Little, W. A. *Phys. Rev.*, **1964**, 1416. (b) Little, W. A. *Sci. Am.*, **1965**, *212*, 21.

48 (a) Bendikov, M.; Wudl, F.; Perepichka, D. F. *Chem. Rev.*, **2004**, *104*, 4891. (b) Jérome, D. *Chem. Rev.* **2004**, *104*, 5565. (c) Geiser, U.; Schlueter, J. A. *Chem. Rev.*, **2004**, *104*, 5203. (d) Yamada, J.; Akutsu, H.; Nishikawa, H.; Kikuchi, K. *Chem. Rev.*, **2004**, *104*, 5057. (e) Saito, G.; Yoshida, Y. *Bull. Chem. Soc. Jpn.*, **2007**, *80*, 1.

49 Kobayashi, A.; Fujiwara, E.; Kobayashi, H. *Chem. Rev.*, **2004**, *104*, 5243.

50 Wudl, F.; Smith, G. M.; Hufnagel, E. J. *J. Chem. Soc., Chem. Commun.*, **1970**, 1453.

51 Melby, L. R.; Harder, R. J.; Hertler, W. R.; Mahler, W.; Benson, R. E.; Mochel, W. E. *J. Am. Chem. Soc.*, **1962**, *84*, 3374.

52 (a) Ferraris, J.; Cowan, D. O.; Walatka, V. V.; Perlstein, J. H. *J. Am. Chem. Soc.*, **1973**, *95*, 948. (b) Coleman, L. B.; Cohen, M. J.; Sandman, D. J.; Yamagishi, F. G.; Garito, A. F.; Heeger, A. J. *Solid State Commun.*, **1973**, *12*, 1125. (c) Torrance, J. B. *Acc. Chem. Res.*, **1979**, *12*, 79.

53 (a) Williams, J. M.; Emge, T. J.; Wang, H. H.; Benzo, M. A.; Copps, P. T.; Hall, L. N.; Carlson, K. D.; Crabtree, G. W. *Inorg. Chem.*, **1984**, *23*, 2558. (b) Williams, J. M.; Wang, H. H.; Benzo, M. A.; Emge, T. J.; Sowa, L. M.; Copps, P. T.; Behroozi, G.; Hall, L. N.; Carlson, K. D.; Crabtree, G. W. *Inorg. Chem.*, **1984**, *23*, 3839. (c) Wang, H. H.; Benzo, M. A.; Geiser, U.; Firestone, M. A.; Webb, K. S.; Nunez, L.; Crabtree, G. W.; Carlson, K. D.; Williams, J. M.; Azevedo, L. J.; Kwak, J. F.;

Schirber, J. E. *Inorg. Chem.*, **1985**, *24*, 2465.

54 (a) Bechgaard, K.; Jacobsen, C. S.; Mortensen, K.; Pedersen, H. J.; Thorup, N. *Solid State Commun.*, **1980**, *33*, 1119. (b) Jacobsen, C. S.; Mortensen, K.; Thorup, N.; Tanner, D. B.; Weger, M.; Bechgaard, K. *Chem. Scr.*, **1981**, *17*, 103. (c) Torrance, J. B.; Pedersen, H. J.; Bechgaard, K. *Phys. Rev. Lett.*, **1982**, *49*, 881. (d) Bechgaard, K.; Carneiro, K.; Eg, O.; Olsen, M.; Rasmussen, F. B. *Mol. Cryst. Liq. Cryst.*, **1982**, *79*, 271. (e) Guy, D. R. P.; Boebinger, G. S.; Marseglia, E. A.; Friend, R. H.; Bechgaard, K. *J. Phys. C: Solid State Phys.*, **1983**, *16*, 691.

55 Miller, J. S. *Ann. N. Y. Acad. Sci.*, **1978**, *313*, 25.

56 (a) Tanaka, H.; Okano, Y.; Kobayashi, H.; Suzuki, W.; Kobayashi, A. *Science*, **2001**, *291*, 285. (b) Tanaka, H.; Tokumoto, M.; Ishibashi, S.; Graf, D.; Choi, E. S.; Brooks, J. S.; Yasuzuka, S.; Okano, Y.; Kobayashi, H.; Kobayashi, A. *J. Am. Chem. Soc.*, **2004**, *126*, 10518. (c) Kobayashi, A.; Sasa, M.; Suzuki, W.; Fujiwara, E.; Tanaka, H.; Tokumoto, M.; Okano, Y.; Fujiwara, H.; Kobayashi, H. *J. Am. Chem. Soc.*, **2004**, *126*, 426.

57 (a) Haddon, R. C. *Nature*, **1975**, *256*, 394. (b) Haddon, R. C. *Aust. J. Chem.*, **1975**, *28*, 2333. (c) Haddon, R. C. *Aust. J. Chem.*, **1975**, *28*, 2343.

58 (a) Mott, N. F. *Proc. Phys. Soc., London Sect. A*, **1949**, *62*, 416. (b) Austin, I. G.; Mott, N. F. *Science*, **1970**, *168*, 71.

59 For an excellent example, see: Cox, P. A. *The Electronic Structure and Chemistry of Solids*; Oxford University Press: Oxford, 1987.

60 (a) Cordes, A. W.; Haddon, R. C.; Oakley, R. T. *Phosphorus, Sulfur, Silicon and Related Elements*, **2004**, *179*, 673. (b) Kaszynski, P. *J. Phys. Chem. A*, **2001**, *105*, 7626. (c) Boeré, R. T.; Roemmele, T. L. *Coord. Chem. Rev.*, **2000**, *210*, 369. (d) Kaszynski, P. *J. Phys. Chem. A*, **2001**, *105*, 7615.

61 Peierls, R. E. *Quantum Theory of Solids*; Oxford Press: London, 1955.

62 Sogo, P. B.; Nakazaki, M.; Calvin, M. J. *J. Chem. Phys.*, **1957**, *26*, 1343.

63 Haddon, R.C. *J. Org. Chem.*, **1987**, *52*, 711.

64 Koutentis, P. A.; Chen, Y.; Cao, Y.; Best, T. P.; Itkis, M. E.; Beer, L; Oakley, R. T.; Cordes, A. W.; Brock, C. P.; Haddon, R. C. *J. Am. Chem. Soc.*, **2001**, *123*, 3864.

65 Koutentis, P. A.; Haddon, R. C.; Oakley, R. T.; Cordes, A. W.; Brock, C. P. *Acta. Crystallogr.*, **2001**, *B57*, 680.

66 Beer, L.; Mandal, S. K.; Reed, R. W.; Oakley, R. T.; Tham, F. S.; Donnanieu, B.; Haddon, R. C. *Cryst. Growth Des.*, **2007**, *7*, 802.

67 Mandal, S. K.; Itkis, M. E.; Chi, X.; Samanta, S.; Lidsky, D.; Reed, R. W.; Oakley, R. T.; Tham, F. S.; Haddon, R. C. *J. Am. Chem. Soc.*, **2005**, *127*, 8185.

68 Chi, X.; Itkis, M. E.; Kirschbaum, K.; Pinkerton, A. A.; Oakley, R. T.; Cordes, A. W.; Haddon, R. C. *J. Am. Chem. Soc.*, **2001**, *123*, 4041.

69 Liao, P.; Itkis, M. E.; Oakley, R. T.; Tham, F. S.; Haddon, R. C. *J. Am. Chem. Soc.*, **2004**, *126*, 14297.

70 (a) Chi, X.; Itkis, M. E.; Patrick, B. O.; Barclay, T. M.; Reed, R. W.; Oakley, R. T.; Cordes, A. W.; Haddon, R. C. *J. Am. Chem. Soc.*, **1999**, *121*, 10395. (b) Pal, S. K.; Itkis, M. E.; Reed, R. W.; Oakley, R. T.; Cordes, A. W.; Tham, F. S.; Siegrist, T.; Haddon, R. C. *J. Am. Chem. Soc.*, **2004**, *126*, 1478.

71 Pal, S. K.; Itkis, M. E.; Tham, F. S.; Reed, R. W.; Oakley, R. T.; Haddon, R. C. *J. Am. Chem. Soc.*, **2008**, *130*, 3942.

72 Pal, S. K.; Itkis, M. E.; Tham, F. S.; Reed, R. W.; Oakley, R. T.; Haddon, R. C. *Science*, **2005**, *309*, 281.

73 Mandal, S. K.; Samanta, S.; Itkis, M. E.; Jensen, D. W.; Reed, R. W.; Oakley, R. T.; Tham, F. S.; Donnadieu, B.; Haddon, R. C. *J. Am. Chem. Soc.*, **2006**, *128*, 1982.

74 Pauling, L. *Nature*, **1948**, *161*, 1019.

75 (a) Burt, F. P. *J. Am. Chem. Soc.*, **1910**, 1171. (b) Walatka, V. V.; Labes, M. M.; Perlstien, J. H. *Phys. Rev. Lett.*, **1973**, *31*, 1139. (c) Green, R. L.; Street, G. B.; Suter, L. J. *Phys. Rev. Lett.*, **1975**, *34*, 577.

76 (a) Bryan, C. D.; Cordes, A. W.; Fleming, R. M.; George, N. A.; Glarum, S. H.; Haddon, R. C.; Oakley, R. T.; Palstra, T. T. M.; Perel, A. S.; Schneemeyer, L. F.; Waszcak, J. V. *Nature*, **1993**, *365*, 821. (b) Bryan, C. D.; Cordes, A. W.; Haddon, R. C.; Hicks, R. G.; Kennepohl, D. K.; MacKinnon, C. D.; Oakley, R. T.; Palstra, T. T. M.; Perel, A. S.; Scott, S. R.; Schneemeyer, L. F.; Waszcak, J. V. *J. Am. Chem. Soc.*, **1994**, *116*, 1205. (c) Cordes, A. W.; Haddon, R. C.; Oakley, R. T. *Adv. Mater.*, **1994**, *6*, 508. (d) Bryan, C. D.; Cordes, A. W.; Fleming, R. M.; George, N. A.; Glarum, S. H.; Haddon, R. C.; MacKinnon, C. D.; Oakley, R. T.; Palstra, T. T. M.; Perel, A. S.; Schneemeyer, L. F.; Waszcak, J. V. *J. Am. Chem. Soc.*, **1995**, *117*, 6880. (e) Bryan, C. D.; Cordes, A. W.; George, N. A.; Haddon, R. C.; MacKinnon, C. D.; Oakley, R. T.; Palstra, T. T. M.; Perel, A. S. *Chem. Mater.*, **1996**, *8*, 762.

77 Carlin, R. *Magnetochemistry*, Springer-Verlag, Berlin, **1986**.

78 Coronado, E.; Day, P. *Chem. Rev.*, **2004**, *104*, 5419.

79 Fujita, W.; Awaga, K. *Chem. Phys. Lett.*, **2002**, *357*, 385.

80 Allemand, P. M.; Khemani, K. C.; Koch, A.; Wudl, F.; Holczer, K.; Donovan, S.; Gruner, G.; Thompson, J. D. *Science*, **1991**, *253*, 301.

81 Kinoshita, M.; Turek, P.; Tamura, M.; Nozawa, K.; Shiomi, D.; Nakazawa, Y.; Ishikawa, M.; Takahashi, M.; Awaga, K.; Inabe, T.; Maruyama, Y. *Chem. Lett.*, **1991**, 1225.

82 Chiarelli, R.; Rassat, A.; Rey, P. *J. Chem. Soc., Chem. Commun.*, **1992**, 1081. (b) Chiarelli, R.; Novak, M. N.; Rassat, A.; Tholence, J. L. *Nature*, **1993**, *363*, 147.

83 Alberola, A.; Less, R. J.; Pask, C. M.; Rawson, J. M.; Palacio, F.; Oliete, P.; Paulsen, C.; Yamaguchi, A.; Farley, R. D.; Murphy, D. M. *Angew. Chem. Int. Ed.,* **2003**, *42*, 4782.

84 Banister, A. J.; Bricklebank, N.; Lavender, I.; Rawson, J. M.; Gregory, C. I.; Tanner, B. K.; Clegg, W.; Elsegood, M. R. J.; Palacio, F. *Angew. Chem. Int. Ed.,* **1996**, *35*, 2533.

85 (a) Wolf, S. A.; Awschalom, D. D.; Buhrman, R. A.; Daughton, J. M.; von Molnár, S.; Roukes, M. L.; Chtchelkanova, A. Y.; Trege, B. D. M. *Science*, **2001**, *294*, 1488. (b) Prinz, G. A. *Science*, **1998**, *282*, 1660. (c) Naber, W. J. M.; Faez, S.; van der Wiel, W. G. *J. Phys. D: Appl. Phys.*, **2007**, *40*, R205.

86 (a) Coronado, E.; Day, P. *Chem. Rev.*, **2004**, *104*, 5419. (b) Coronado, E.; Giménez-Saiz, C.; Gómez-García, C. J. *Coord. Chem. Rev.*, **2005**, *249*, 1776. (c) Coronado, E.; Galán-Mascarós, J. R. *J. Mater. Chem*., **2005**, *15*, 66.

87 (a) Coronado, E.; Galán-Mascarós, J. R.; Gómez-García, C. J.; Laukhin, V. *Nature,* **2000**, *408*, 447. (b) Figure 1.9 has been reproduced from reference 84a.

88 Bondi, A. *J. Phys Chem*., **1964**, *68*, 441.

89 (a) Rawson, J. M.; Luzon, J.; Palacio, F. *Coord. Chem. Rev.*, **2005**, *249*, 2631. (b) Luzon, J.; Campo, J.; Palacio, F.; McIntyre, G. J.; Rawson, J. M. *Polyhedron*, **2005**, *24*, 2579.

References for Chapter 2

1 (a) Beer, L.; Brusso, J. L.; Haddon, R. C.; Itkis, M. E.; Kirschbaum, K.; MacGreggor, D. S.; Oakley, R. T.; Pinkerton, A. A.; Reed, R. W. *J. Am. Chem. Soc.*, **2002**, *124*, 9498. (b) Beer, L.; Britten, J. F.; Brusso, J. L.; Cordes, A. W.; Haddon, R. C.; Itkis, M. E.; MacGreggor, D. S.; Oakley, R. T.; Reed, R. W.; Robertson, C. M. *J. Am. Chem. Soc.*, **2003**, *125*, 14394. (c) Beer, L.; Brusso, J. L.; Cordes, A. W.; Godde, E.; Haddon, R. C.; Itkis, M. E.; Oakley, R. T.; Reed, R. W. *Chem. Commun.*, **2002**, 2562. (d) Beer, L.; Britten, J. F.; Clements, O. P.; Haddon, R. C.; Itkis, M. E.; Matkovich, K. M.; Oakley, R. T.; Reed, R. W. *Chem. Mater.*, **2004**, *16*, 1564.

2 Oakley, R. T.; Reed, R. W.; Cordes, A. W.; Craig, S. L.; Graham, S. B. *J. Am. Chem. Soc.*, **1987**, *109*, 7745.

3 (a) Belluz, P. Del Bel; Cordes, A. W.; Kristof, E. M.; Kristof, P. V.; Liblong, S. W.; Oakley, R. T. *J. Am. Chem. Soc.*, **1989**, *111*, 9276. (b) Cordes, A. W.; Haddon, R. C.; Oakley, R. T.; Schneemeyer, L. F.; Waszczak, J. A.; Young, K. M.; Zimmerman, N. M. *J. Am. Chem. Soc.*, **1991**, *113*, 582. (c) Andrews, M. P.; Cordes, A. W.; Douglass, D. C.; Fleming, R. M.; Glarum, S. H.; Haddon, R. C.; Marsh, P.; Oakley, R. T.; Palstra, T. T. M.; Schneemeyer, L. F.; Trucks, G. W.; Tycko, R. R.; Waszczak, J. V.; Warren, W. W.; Young, K. M.; Zimmerman, N. M. *J. Am. Chem. Soc.*, **1991**, *113*, 3559. (d) Cordes, A. W.; Haddon, R. C.; Hicks, R. G.; Oakley, R. T.; Palstra, T. T. M.; Schneemeyer, L. F.; Waszczak, J. V. *J. Am. Chem. Soc.*, **1992**, *114*, 1729. (e) Cordes, A. W.; Haddon, R. C.; Hicks, R. G.; Oakley, R. T.; Palstra, T. T. M. *Inorg. Chem.*, **1992**, *31*, 1802. (f) Cordes, A. W.; Glarum, S. H.; Haddon, R. C.; Hallford, R.; Hicks, R. G.; Kennepohl, D. K.; Oakley, R. T.; Palstra, T. T. M.; Scott, S. R. *J. Chem. Soc., Chem. Commun.*, **1992**, 1265. (g) Davis, W. M.; Hicks, R. G.; Oakley, R. T.; Zhao, B.; Taylor, N. J. *Can. J. Chem.*, **1993**, *71*, 180. (h) Cordes, A. W.; Haddon, R. C.; Hicks, R. G.; Kennepohl, D. K.; Oakley, R. T.; Palstra, T. T. M.; Schneemeyer, L. F.; Scott, S. R.; Waszczak, J. V. *Chem. Mater.*, **1993**, *5*, 820. (i) Cordes, A. W.; Bryan, C. D.; Davis, W. M.; de Laat, S. H.; Glarum, S. H.; Goddard, J. D.; Haddon, R. C.; Hicks, R. G.; Kennepohl, D. K.; Oakley, R. T.; Scott, S. R.; Werswood, N. P. C. *J. Am. Chem. Soc.*, **1993**, *115*, 7232. (j) Bryan, C. D.; Cordes, A. W.; Haddon, R. C.; Hicks, R. G.; Oakley, R. T.; Palstra, T. T. M.; Perel, A. S.; Scott, S. R. *Chem. Mater.*, **1994**, *6*, 508. (k) Bryan, C. D.; Cordes, A. W.; Oakley, R. T.; Spence, R. E. v. H. *Acta Crystallogr.*, **1995**, *C51*, 2402. (l) Beer, L.; Cordes, A. W.; Myles, D. J. T.; Oakley , R. T.; Taylor, N. J. *Cryst. Eng. Chem.*, **2000**, *2*, 89. (m) Britten, J. F.; Clements, O. P., Cordes, A. W.; Haddon, R. C.; Oakley, R. T.; Richardson, J. F. *Inorg. Chem.*, **2001**, *40*, 6820.

4 Oakley, R. T.; Reed, R. W.; Robertson, C. M.; Richardson, J. F. *Inorg. Chem.*, **2005**, *44*, 1837.

5 Robertson, C. M. **2004**. *Synthesis and solid state investigation of sulphur nitrogen selenium heterocycles.* University of Waterloo, MSc thesis.

6 Warburton, W. K. *Chem Rev.*, **1957**, *57*, 1011.

7 Antonello, S.; Benassi, R.; Gavioli, G.; Taddei, F.; Maran, F. *J. Am. Chem. Soc.*, **2002**, *124*, 7529.

8 Barclay, T. M.; Cordes, A. W.; Goddard, J. D.; Mawhinney, R. C.; Oakley, R. T.; Preuss, K. E.; Reed, R. W. *J. Am. Chem. Soc.*, **1997**, *119*, 12136.

9 (a) Haddon, R. C. *Nature,* **1975**, *256*, 394. (b) Haddon, R. C. *Aust. J. Chem*., **1975**, *28*, 2333. (c) Haddon, R. C. *Aust. J. Chem*., **1975**, *28*, 2343.

10 Kaszynski, P. *J. Phys. Chem. A*, **2001**, *105*, 7626.

11 Boeré, R. T.; Roemmele, T. L. *Coord. Chem. Rev.,* **2000**, *210*, 369.

12 Kaszynski, P. *J. Phys. Chem. A*, **2001**, *105*, 7615.

13 (a) Oakley, R. T.; Reed, R. W.; Cordes, A. W.; Craig, S. L.; Graham, J. B. *J. Am. Chem. Soc*., **1987**, *109*, 7745. (b) Bestari, K.; Cordes, A. W.; Oakley, R. T.; Young, K. M. *J. Am. Chem. Soc*., **1990**, *112*, 2249.

14 Bryan, C. D.; Cordes, A. W.; Fleming, R. M.; George, N. A.; Glarum, S. H.; Haddon, R. C.; MacKinnon, C. D.; Oakley, R. T.; Palstra, T. T. M.; Perel, A. S. *J. Am. Chem. Soc.*, **1995**, *117*, 6880.

15 Maaninen, A.; Konu, J.; Laitinen, R.; Chivers, T.; Schatte, G.; Pietikäinen, J.; Ahlgren, M. *Inorg. Chem*., **2001**, *40*, 3539.

16 Dutton, J. L.; Tuononen, H. M.; Jennings, M. C.; Ragogna, P. J. *J. Am. Chem. Soc.*, **2006**, *128*, 12624.

17 Beer, L.; Cordes, A. W.; Haddon, R. C.; Itkis, M. E.; Oakley, R. T.; Reed, R. W.; Robertson, C. M. *Chem. Commun*., **2002**, 1872.

18 Barclay, T. M.; Beer, L.; Cordes, A. W.; Oakley, R. T.; Preuss, K. E.; Taylor, N. J.; Reed, R. W. *Chem. Commun*.,**1999**, 531.

19 Barclay, T. M.; Cordes, A. W.; Haddon, R. C.; Itkis, M. E.; Oakley, R. T.; Reed, R. W.; Zhang, H. *J. Am. Chem. Soc.*, **1999**, *121*, 969.

20 Barclay, T. M.; Cordes, A. W.; George, N. A.; Haddon, R. C.; Oakley, R. T.; Patenaude, G. W.; Reed, R. W.; Zhang, H. *J. Chem. Soc., Chem. Commun*., **1997**, 873.

21 Dunitz, J. D.; Brock, C. P. *Acta Crystallogr*., **1982**, *38B*, 2218.

22 Brock, C. P.; Dunitz, J. D. *Acta Crystallogr*., **1990**, *46B*, 795.

23 (a) Gavezzotti, A.; Desiraju, G. R. *Acta Crystallogr*., **1988**, *44B*, 427. (b) Hobza, H.; Selzle, H. L.; Schlag, E. W. *J. Am. Chem. Soc.,* **1994**, *116*, 3500. (c) Podeszwa, R.; Bukowski, R.; Szalewicz, K. *J. Phys Chem. A*, **2006**, *110*, 10345.

24 Bondi, A. *J. Phys. Chem*., **1964**, *68*, 441.

25 Koutentis, P. A.; Rees, C. W. *J. Chem. Soc., Perkin Trans, 1*, **1999**, 111.

26 Kobayashi, H.; Okanoa, K.; Fujiwara, H.; Tanaka, H.; Tokumoto, M.; Suzuki, W.; Fujiwara, E.; Kobayashi, A. *Proceedings of the NATO Advanced Study Institute on Organic Conductors, Superconductors and Magnets: From Synthesis to Molecular Electronics*, Eds. L. Ouahab and E. Yagubskii, Kluwer Academic Publishers, 2004, pps 81-98.

27 Akulin, Yu. I.; Gel'mont, M. M.; Strelets, B. Kh.; Efros, L. S. *Khimiya Geterotsiklicheskikh Soedinenii,* **1978**, 912.

28 Seeboth, H. *Angew. Chem., Int. Ed. Engl.*, **1967**, *6*, 307.

References for Chapter 3

1 Brusso, J. L.; Derakhshan, S.; Itkis, M. E.; Kleinke, H.; Haddon, R. C.; Oakley, R. T.; Reed, R. W.; Richardson, J. F.; Robertson, C. M.; Thompson, L. K. *Inorg. Chem*., **2006**, *45*, 10958.

2 (a) Beer, L.; Brusso, J. L.; Haddon, R. C.; Itkis, M. E.; Leitch, A. A.; Oakley, R. T.; Reed, R. W.; Richardson, J. F. *Chem. Commun*., **2005**, 1543. (b) Beer, L.; Brusso, J. L.; Haddon, R. C.; Itkis, M. E.; Kleinke, H.; Leitch, A. A.; Oakley, R. T.; Reed, R. W.; Richardson, J. F.; Secco, R. A.; Yu, X. *J. Am. Chem. Soc.,* **2005**, *127*, 18159.

3 Beer, L.; Britten, J. F.; Clements, O. P.; Haddon, R. C.; Itkis, M. E.; Matkovich, K. M.; Oakley, R. T.; Reed, R. W. *Chem. Mater*., **2004**, *16*, 1564.

4 Beer, L.; Brusso, J. L.; Haddon, R. C.; Itkis, M. E.; Oakley, R. T.; Reed, R. W.; Richardson, J. F.; Secco, R. A.; Yu, X. *Chem. Commun*., **2005**, 5745.

5 (a) Akulin, Y. I.; Gel'mont, M. M.; Strelets, B. Kh.; Efros, L. S. *Khim. Geterotsikl. Soedin*., **1978**, 912. (b) A similar approach has been used to incorporate selenium into dithiadiazolylium salts. For example, see: Less, R. J.; Rawson, J. M.; Jones, M. *Polyhedron*, **2001**, *20*, 523.

6 Taupin, D. *J. Appl. Cryst*., **1973**, *6*, 380.

7 Shirley, R. Crysfire 2002 v9.45.26y, Surrey, England.

8 Nicolin, V. F.; Cerny, R. *J. Appl. Cryst*., **2002**, *35*, 734.

9 Rietveld, H. M. *J. Appl. Crystallog*., **1969**, *2*, 65.

10 Larson, A. C.; Von Dreele, R. B. Report No. LA-UR-86-748; Los Alamos National Laboratory, Los Alamos, NM, 1987.

11 Brusso, J. L.; Cvrkalj, K.; Leitch, A. A.; Oakley, R. T.; Reed, R. W.; Robertson, C. M. *J. Am. Chem. Soc*., **2006**, *128*, 15080.

12 Werner, P. -E.; Eriksson, L.; Westdahl, M. *J. Appl. Cryst*., **1985**, *18*, 367.

13 Beer, L.; Britten, J. F.; Brusso, J. L.; Cordes, A. W.; Haddon, R. C.; Itkis, M. E.; MacGreggor, D. S.; Oakley, R. T.; Reed, R. W.; Robertson, C. M. *J. Am. Chem. Soc*., **2003**, *125*, 14394.

14 Leitch, A. A.; Reed, R. W.; Robertson, C. M.; Britten, J. F.; Yu, X.; Secco, R. A.; Oakley, R. T. *J. Am. Chem. Soc*., **2007**, *129*, 7903.

15 ABABAB refers to the alternation of the radical orientation in the π-stack such that the steric interaction of the bulky R_1 group is minimized within the π-stack.

16 Estimated from Pascal's constants. Carlin, R. L. *Magnetochemistry*; Springer-Verlag: New York, 1986.

17 Bondi, A. J. *Phys. Chem*., **1964**, *68*, 441.

18 Alberola, A,; Clements, O. P.; Collis, R. J.; Cubbitt, L.; Grant, C. M.; Less, R. J.; Oakley, R. T.; Rawson, J. M.; Reed, R. W.; Robertson, C. M. *Cryst. Growth Des.*, **2008**, *8*, 155.

19 Parsons, S. *Acta Cryst.*, **2003**, *D59*, 1995.

20 Sheldrick, G. M. SHELXL-97. Program for the Refinement of Crystal Structures, University of Gottingen, Gottingen, Germany, 1997.

21 (a) Barclay, T. M.; Cordes, A. W.; George, N. A.; Haddon, R. C.; Itkis, M. E.; Mashuta, M. S.; Oakley, R. T.; Patenaude, G. W.; Reed, R. W.; Richardson, J. F.; Zhang, H. Z. *J. Am. Chem. Soc.*, **1998**, *120*, 352. (b) Wolmershauser, G.; Johann, R. *Angew. Chem., Int. Ed. Engl.*, **1989**, *28*, 920. (c) Fujita, W.; Awaga, K. *Science*, **1999**, *286*, 261. (d) McManus, G. D.; Rawson, J. M.; Feeder, N.; van Duijn, J.; McInnes, E. J. L.; Novoa, J. J.; Burriel, R.; Palacio, F.; Oliete, J. *J. Mater. Chem.*, **2001**, *11*, 1992. (e) Heckmann, G.; Johann, R.; Kraft, G.; Wolmershäuser, G. *Synth. Met.*, **1991**, *43*, 3287. (f) Brusso, J. L.; Clements, O. P.; Haddon, R. C.; Itkis, M. E.; Leitch, A. A.; Oakley, R. T.; Reed, R. W.; Richardson, J. F. *J. Am. Chem. Soc.*, **2004**, *126*, 8256. (g) Brusso, J. L.; Clements, O. P.; Haddon, R. C.; Itkis, M. E.; Leitch, A. A.; Oakley, R. T.; Reed, R. W.; Richardson, J. F. *J. Am. Chem. Soc.*, **2004**, *126*, 14692.

22 Giacovazzo, C. *Fundamentals of Crystallography*; Oxford University Press: Oxford, 1992.

23 Stout, G. H.; Jensen, L. H. *X-ray structure determination* (2nd ed.); John Wiley & Sons, Inc: New York, 1989.

24 Dauter, Z. *Acta Cryst.*, **2003**, *D59*, 2004.

References for Chapter 4

1 Brusso, J. L.; Derakhshan, S.; Itkis, M. E.; Kleinke, H.; Haddon, R. C.; Oakley, R. T.; Reed, R. W.; Richardson, J. F.; Robertson, C. M.; Thompson, L. K. *Inorg. Chem*., **2006**, *45*, 10958.

2 Brusso, J. L.; Cvrkalj, K.; Leitch, A. A.; Oakley, R. T.; Reed, R. W.; Robertson, C. M. *J. Am. Chem. Soc*., **2006**, *128*, 15080.

3 Alberola, A.; Clements, O. P.; Collis, R. J.; Cubbitt, L.; Grant, C. M.; Less, R. J.; Oakley, R. T.; Rawson, J. M.; Reed, R. W.; Robertson, C. M. *Cryst. Growth Des.*, **2008**, *8*, 155.

4 Leitch, A. A.; Reed, R. W.; Robertson, C. M.; Britten, J. F.; Yu, X.; Secco, R. A.; Oakley, R. T. *J. Am. Chem. Soc*., **2007**, *129*, 7903.

5 Beer, L.; Brusso, J. L.; Haddon, R. C.; Itkis, M. E.; Oakley, R. T.; Reed, R. W.; Richardson, J. F.; Secco, R. A.; Yu, X. *Chem. Commun*., **2005**, 5745.

6 Beer, L.; Britten, J. F.; Clements, O. P.; Haddon, R. C.; Itkis, M. E.; Matkovich, K. M.; Oakley, R. T.; Reed, R. W. *Chem. Mater*., **2004**, *16*, 1564.

7 Beer, L.; Brusso, J. L.; Cordes, A. W.; Haddon, R. C.; Itkis, M. E.; Kirschbaum, K.; MacGregor, D. S.; Oakley, R. T.; Pinkerton, A. A.; Reed, R. W. *J. Am. Chem. Soc*., **2002**, *124*, 9498.

8 (a) Cope, A. C.; Hofmann, C. M.; Wyckoff, C.; Hardenbergh, E. J. *J. Am. Chem. Soc.*, **1941**, *63*, 3452. (b) Ames, D. E.; Bowmann, R. E.; Grey, T. F. *J. Chem. Soc.*, **1953**, 3008.

9 Rokach, J.; Hamel, P.; Hunter, N. R.; Rooney, C. S.; Anderson, P. S.; Cragoe, E. J. Jr.; Mandel, L. R. *J. Med. Chem.*, **1979**, *22*, 237.

10 (a) Akulin, Y. I.; Gel'mont, M. M.; Strelets, B. Kh.; Efros, L. S. *Khim. Geterotsikl. Soedin*., **1978**, 912. (b) A similar approach has been used to incorporate selenium into dithiadiazolylium salts. For example, see: Less, R. J.; Rawson, J. M.; Jones, M. *Polyhedron*, **2001**, *20*, 523.

11 Boeré, R. T.; Roemmele, T. L. *Coord. Chem. Rev.*, **2000**, *210*, 369.

12 Antonello, S.; Benassi, R.; Gavioli, G.; Taddei, F.; Maran, F. *J. Am. Chem. Soc*., **2002**, *124*, 7529.

13 Barclay, T. M.; Cordes, A. W.; Goddard, J. D.; Mawhinney, R. C.; Oakley, R. T.; Preuss, K. E.; Reed, R. W. *J. Am. Chem. Soc.,* **1997***, 119*, 12136.

14 Beer, L.; Britten, J. F.; Brusso, J. L.; Cordes, A. W.; Haddon, R. C.; Itkis, M. E.; MacGreggor, D. S.; Oakley, R. T.; Reed, R. W.; Robertson, C. M. *J. Am. Chem. Soc.*, **2003**, *125*, 14394.

15 Boultif, A.; Louer, D. *J. Appl. Cryst.*, **1991**, *24*, 987.

16 Shirley, R. Crysfire 2002 v9.45.26y, Surrey, England.

17 Bondi, A. *J. Phys. Chem.*, **1964**, *68*, 441.

18 Nicolin, V. F.; Cerny, R. *J. Appl. Cryst.*, **2002**, *35*, 734.

19 Rietveld, H. M. *J. Appl. Crystallog.*, **1969**, *2*, 65.

20 Larson, A. C.; Von Dreele, R. B. Report No. LA-UR-86-748; Los Alamos National Laboratory, Los Alamos, NM, 1987.

21 (a) Finger, L. W.; Cox, D. E.; Jephcoat, A. P. *J. Appl. Cryst.*, **1994**, *27*, 892. (b) Cheary, R. W.; Coelho, A. A. *J. Appl. Cryst.*, **1998**, *31*, 851.

22 (a) Cozzolino, A. F.; Britten, J. F.; Vargas-Baca, I. *Cryst. Growth Des.*, **2006**, *6*, 181. (b) Cozzolino, A. F.; Vargas-Baca, I.; Mansour, S.; Mahmoudkhani, A. H. *J. Am. Chem Soc.*, **2005**, *127*, 3184.

23 Carlin, R. L. *Magnetochemistry*; Springer-Verlag: New York, 1986.

References for Chapter 5

1 (a) Beer, L.; Brusso, J. L.; Cordes, A. W.; Haddon, R. C.; Itkis, M. E.; Kirschbaum, K.; MacGregor, D. S.; Oakley, R. T.; Pinkerton, A. A.; Reed, R. W. *J. Am. Chem. Soc.*, **2002**, *124*, 9498. (b) Beer, L.; Brusso, L. J.; Cordes, A. W.; Haddon, R. C.; Godde, E.; Itkis, M. E.; Oakley, R. T.; Reed, R. W. *Chem. Commun.*, **2002**, 2562. (c) Beer, L.; Britten, J. F.; Brusso, J. L.; Cordes, A. W.; Haddon, R. C.; Itkis, M. E.; MacGregor, D. S.; Oakley, R. T.; Reed, R. W.; Robertson, C. M. *J. Am. Chem. Soc.*, **2003**, *125*, 14394.

2 (a) Beer, L.; Brusso, J. L.; Haddon, R. C.; Itkis, M. E.; Leitch, A. A.; Oakley, R. T.; Reed, R. W.; Richardson, J. F. *Chem. Commun.*, **2005**, 1543. (b) Beer, L.; Brusso, J. L.; Haddon, R. C.; Itkis, M. E.; Kleinke, H.; Leitch, A. A.; Oakley, R. T.; Reed, R. W.; Richardson, J. F.; Secco, R. A.; Yu, X. *J. Am. Chem. Soc.,* **2005**, *127*, 18159.

3 Akulin, Y. I.; Gel'mont, M. M.; Strelets, B. Kh.; Efros, L. S. *Khim. Geterotsikl. Soedin.*, **1978**, 912.

4 A similar approach has been used to incorporate Se into dithiadiazolylium salts. For example, see: Less, R. J.; Rawson, J. M.; Jones, M. *Polyhedron*, **2001**, *20*, 523.

5 Brusso, J. L.; Derakhshan, S.; Itkis, M. E.; Kleinke, H.; Haddon, R. C.; Oakley, R. T.; Reed, R. W.; Richardson, J. F.; Robertson, C. M.; Thompson, L. K. *Inorg. Chem.*, **2006**, *45*, 10958.

6 Leitch, A. A.; Brusso, J. L.; Cvrkalj, K.; Reed, R. W.; Robertson, C. M.; Dube, P. A.; Oakley, R. T. *Chem. Commun.*, **2007**, 3368.

7 See **Appendix A** for a table of half-wave potentials of the reducing agents used in this work.

8 (a) Cordes, A. W.; Mingie, J. R.; Oakley, R. T.; Reed, R. W.; Zhang, H. *Can. J. Chem.*, **2001**, *79*, 1352. (b) Beer, L.; Cordes, A. W.; Haddon, R. C.; Itkis, M. E.; Oakley, R. T.; Reed, R. W.; Robertson, C. M. *Chem. Commun.*, **2002**, 1872. (c) Oakley, R. T.; Reed, R. W.; Robertson, C. M.; Richardson, J. F. *Inorg. Chem.*, **2005**, *44*, 1837.

9 Bondi, A. *J. Phys. Chem.*, **1964**, *68*, 441.

10 (a) Cozzolino, A. F.; Britten, J. F.; Vargas-Baca, I. *Cryst. Growth Des.*, **2006**, *6*, 181. (b) Cozzolino, A. F.; Vargas-Baca, I.; Mansour, S.; Mahmoudkhani, A. H. *J. Am. Chem Soc.*, **2005**, *127*, 3184.

11 Carlin, R. L. *Magnetochemistry*; Springer-Verlag: New York, 1986.

12 Leitch, A. A.; Brusso, J. L.; Cvrkalj, K.; Reed, R. W.; Robertson, C. M.; Dube, P. A.; Oakley, R. T. *Chem. Commun.*, **2007**, 3368.

13 Spin-orbit effects raise the isotropic *g*-values of **5-2a** and **5-4a** (**Table 5.4**) above the free-electron mark of 2.0023, as a result of which the observation of M_{sat} (= gSNβ) slightly greater than 1.0 Nβ for **5-4a** is not unexpected.

14 (a) Cordes, A. W.; Haddon, R. C.; Oakley, R. T. *Adv. Mater.*, **1994**, *6*, 798. (b) Cordes, A. W.; Haddon, R. C.; Oakley, R. T. *The Chemistry of Inorganic Ring Systems*; Elsevier: Amsterdam: Ed. R. Steudel, p. 295, 1992. (c) Beer, L.; Cordes, A. W.; Myles, D. J. T.; Oakley, R. T.; Taylor, N. J.

Cryst. Eng. Chem., **2000**, *2*, 109. (d) Rawson, J. M.; Alberola, A.; Whalley, A. *J. Mater. Chem.*, **2006**, *16*, 2560.

15 Cordes, A. W.; Haddon, R. C.; Oakley, R. T. *Phosphorus, Sulfur, Silicon, Relat. Elem.*, **2004**, *179*, 673.

16 (a) Kinoshita, M.; Turek, P.; Tamura, M.; Nozawa, K.; Shiomi, D.; Nakazawa, Y.; Ishikawa, M.; Takahashi, M.; Awaga, K.; Inabe, T.; Maruyama, Y. *Chem. Lett.*, **1991**, 1225. (b) Chiarelli, R.; Novak, M. N.; Rassat, A.; Tholence, J. L. *Nature*, **1993**, *363*, 147. (c) Mito, M.; Nakano, H.; Kawae, T.; Hitaka, M.; Takagi, S.; Deguchi, H.; Suzuki, K.; Mukai, K.; Takeda, K. *J. Phys. Soc. Jpn.*, **1997**, *66*, 2147. (d) Alberola, A.; Less, R. J.; Pask, C. M.; Rawson, J. M.; Palacio, F.; Oliete, P.; Paulsen, C.; Yamaguchi, A.; Farley, R. D.; Murphy, D. M. *Angew. Chem. Int. Ed.,* **2003**, *42*, 4782.

17 Mito, M.; Nakano, H.; Kawae, T.; Hitaka, M.; Takagi, S.; Deguchi, H.; Suzuki, K.; Mukai, K.; Takeda, K. *J. Phys. Soc. Jpn.*, **1997**, *66*, 2147.

18 Banister, A. J.; Bricklebank, N.; Lavender, I.; Rawson, J. M.; Gregory, C. I.; Tanner, B. K.; Clegg, W.; Elsegood, M. R. J.; Palacio, F. *Angew. Chem. Int. Ed.,* **1996**, *35*, 2533.

19 Feeder, N.; Less, R. J.; Rawson, J. M.; Oliete, P.; Palacio, F. *Chem. Commun.*, **2000**, 2449.

20 García, F.; Less, R. J.; Naseri, V.; McPartlin, M.; Rawson, J. M.; Wright, D. S. *Angew. Chem. Int. Ed.,* **2007**, *46*, 7827.

21 Dzyaloshinsky, I. *J. Phys. Solids*, **1958**, *4*, 241. (b) Moriya, T. *Phys. Rev.*, **1960**, *120*, 91.

22 Allemand, P. M.; Khemani, K. C.; Koch, A.; Wudl, F.; Holczer, K.; Donovan, S.; Gruner, G.; Thompson, J. D. *Science*, **1991**, *253*, 301.

23 Fujita, W; Awaga, K. *Chem. Phys. Lett.*, **2004**, *388*, 186.

24 (a) Chikazume, S. *Physics of Magnetism*; John-Wiley: New York, 1964. (b) Bertotti, G. *Hysteresis in Magnetism*; Academic Press: New York, 1998.

25 Robertson, C. M.; Myles, D. J. T.; Leitch, A. A.; Reed, R. W.; Dooley, D. M.; Frank, N. L.; Dube, P. A.; Thompson, L. K.; Oakley, R. T. *J. Am. Chem. Soc.*, **2007**, *129*, 12688.

26 Dooley, B. M.; Bowles, S. E.; Storr, T.; Frank, N. L. *Org. Lett.*, **2007**, *9*, 4781.

27 (a) Prigodin, V. N.; Raju, N. P.; Pokhondnya, K. I.; Miller, J. S.; Epstein, A. J. *Adv. Mater.,* **2002**, *14*, 1230. (b) Blundell, S. J.; Pratt, F. L. *J. Phys.: Condens. Matter.*, **2004**, *16*, R771.

28 Beer, L.; Brusso, J. L.; Haddon, R. C.; Itkis, M. E.; Oakley, R. T.; Reed, R. W.; Richardson, J. F.; Secco, R. A.; Yu, X. *Chem. Commun.*, **2005**, 5745.

29 (a) Mito, M.; Kawae, T.; Takeda, K.; Takagi, S.; Matsushita, Y.; Deguchi, H.; Rawson, J. M.; Palacio, F. *Polyhedron*, **2001**, *20*, 1509. (b) Mito, M.; Fujino, M.; Deguchi, H.; Takagi, S.; Fujita, W.; Awaga, K. *Polyhedron*, **2005**, *24*, 2501.

30 (a) Ferraro, J. R.; Williams, J. M. *Introduction to Synthetic Electrical Conductors*; Academic Press: New York, 1987; p 25. (b) Stephens, D. A.; Rehan, A. E.; Compton, S. J.; Barkhau, R. A.; Williams, J. M. *Inorg. Synth*., **1986**, *24*, 135.

References for Chapter 6

1 (a) Beer, L.; Brusso, J. L.; Cordes, A. W.; Haddon, R. C.; Itkis, M. E.; Kirschbaum, K.; MacGregor, D. S.; Oakley, R. T.; Pinkerton, A. A.; Reed, R. W. *J. Am. Chem. Soc.*, **2002**, *124*, 9498. (b) Beer, L.; Brusso, L. J.; Cordes, A. W.; Haddon, R. C.; Godde, E.; Itkis, M. E.; Oakley, R. T.; Reed, R. W. *Chem. Commun.,* **2002**, 2562. (c) Beer, L.; Britten, J. F.; Brusso, J. L.; Cordes, A. W.; Haddon, R. C.; Itkis, M. E.; MacGregor, D. S.; Oakley, R. T.; Reed, R. W.; Robertson, C. M. *J. Am. Chem. Soc.*, **2003**, *125*, 14394.

2 Beer, L.; Britten, J. F.; Clements, O. P.; Haddon, R. C.; Itkis, M. E.; Matkovich, K. M.; Oakley, R. T.; Reed, R. W. *Chem. Mater.*, **2004**, *16*, 1564.

3 Beer, L.; Cordes, A. W.; Oakley, R. T.; Mingie, J. R.; Preuss, K. E.; Taylor, N. J. *J. Am. Chem. Soc.*, **2000**, *122*, 7602.

4 (a) Beer, L.; Brusso, J. L.; Haddon, R. C.; Itkis, M. E.; Leitch, A. A.; Oakley, R. T.; Reed, R. W.; Richardson, J. F. *Chem. Commun.*, **2005**, 1543. (b) Beer, L.; Brusso, J. L.; Haddon, R. C.; Itkis, M. E.; Kleinke, H.; Leitch, A. A.; Oakley, R. T.; Reed, R. W.; Richardson, J. F.; Secco, R. A.; Yu, X. *J. Am. Chem. Soc.,* **2005**, *127*, 18159.

5 Akulin, Y. I.; Gel'mont, M. M.; Strelets, B. Kh.; Efros, L. S. *Khim. Geterotsikl. Soedin.*, **1978**, 912.

6 A similar approach has been used to incorporate selenium into dithiadiazolylium salts. For example, see: Less, R. J.; Rawson, J. M.; Jones, M. *Polyhedron*, **2001**, *20*, 523.

7 (a) Brusso, J. L.; Derakhshan, S.; Itkis, M. E.; Kleinke, H.; Haddon, R. C.; Oakley, R. T.; Reed, R. W.; Richardson, J. F.; Robertson, C. M.; Thompson, L. K. *Inorg. Chem*., **2006**, *45*, 10958. (b) Beer, L.; Brusso, J. L.; Haddon, R. C.; Itkis, M. E.; Oakley, R. T.; Reed, R. W.; Richardson, J. F.; Secco, R. A.; Yu, X. *Chem. Commun.*, **2005**, 5745.

8 (a) Robertson, C. M.; Myles, D. J. T.; Leitch, A. A.; Reed, R. W.; Dooley, B. M.; Frank, N. L.; Dube, P. A.; Thompson, L. K.; Oakley, R. T. *J. Am. Chem. Soc.*, **2007**, *129*, 12688. (b) Robertson, C. M.; Leitch, A. A.; Reed, R. W.; Dube, P. A.; Oakley, R. T. *J. Am. Chem. Soc.*, Submitted for publication, February 2008.

9 Bondi, A. *J. Phys. Chem.*, **1964**, *68*, 441.

10 McConnell, H. M. *J. Chem. Phys.*, **1963**, 1910.

11 Rawson, J. M.; Luzon, J.; Palacio, F. *Coord. Chem. Rev.*, **2005**, *249*, 2631.

12 Novoa, J. J.; Deumal, M. *Struct. Bonding*, **2001**, *100*, 33.

13 (a) Kahn, O.; Galy, J.; Journaux, Y.; Jaud, J.; Morgenstern-Badarau, I. *J. Am. Chem. Soc.*, **1982**, *104*, 2165. (b) Verdaguer, M. *Polyhedron*, **2001**, *20*, 1115. (c) Kollmar, C.; Kahn, O. *Acc. Chem. Res.*, **1993**, *26*, 259. (d) Miller, J. S.; Epstein, A. J. *Angew. Chem. Int. Ed. Engl.*, **1994**, *33*, 385.

14 (a) Jornet, J.; Deumal, M.; Ribal-Arino, J.; Bearpark, M. J.; Robb, M. A.; Hicks, R. G.; Novoa, J. J. *Chem. Eur. J.*, **2006**, *12*, 3995. (b) Deumal, M.; Mota, F.; Bearpark, M. J.; Robb, M. A.; Novoa,

J. J. *Mol. Phys.*, **2006**, *104*, 857.

15 Luzon, J.; Campo, J.; Palacio, F.; McIntyre, G. J.; Rawson, J. M. *Polyhedron*, **2005**, *24*, 2579.

References for Appendix A

1 Bestari, K. **1992**. Guelph University, PhD thesis.

2 Frisch, M. J.; Trucks, G. W.; Schlegel, H. B.; Scuseria, G. E.; Robb, M. A.; Cheeseman, J. R.; Zakrzewski, V. G.; Montgomery Jr., J. A.; Stratmann, R. E.; Burant, J. C.; Dapprich, S.; Millam, J. M.; Daniels, A. D.; Kudin, K. N.; Strain, M. C.; Farkas, O.; Tomasi, J.; Barons, V.; Cossi, M.; Cammi, R.; Mennucci, B.; Pomelli, C.; Adamo, C.; Clifford, S.; Ochterski, J.; Petersson, G. A.; Ayala, P. Y.; Cui, Q.; Morokuma, K.; Malick, D. K.; Rabuck, A. D.; Raghavachari, K.; Foreman, J. B.; Cioslowski, J.; Ortiz, J. V.; Stefanov, B. B.; Liu, G.; Fox, D. J.; Keith, T.; Al-Laham, M. A.; Peng, C. Y.; Nanayakkara, A.; Wong, M. W.; Andres, J. L.; Gonzalez, C.; Head-Gordon, M.; Repogle, E. S.; Pople, J. A. *Gaussian 98*, Revision A:6. Gaussian, Inc.: Pittsburg, PA, **1998**.

3 Frisch, M. J.; Trucks, G. W.; Schlegel, H. B.; Scuseria, G. E.; Robb, M. A.; Cheeseman, J. R.; Montgomery, Jr., J. A.; Vreven, T.; Kudin, K. N.; Burant, J. C.; Millam, J. M.; Iyengar, S. S.; Tomasi, J.; Barone, V.; Mennucci, B.; Cossi, M.; Scalmani, G.; Rega, N.; Petersson, G. A.; Nakatsuji, H.; Hada, M.; Ehara, M.; Toyota, K.; Fukuda, R.; Hasegawa, J.; Ishida, M.; Nakajima, T.; Honda, Y.; Kitao, O.; Nakai, H.; Klene, M.; Li, X.; Knox, J. E.; Hratchian, H. P.; Cross, J. B.; Adamo, C.; Jaramillo, J.; Gomperts, R.; Stratmann, R. E.; Yazyev, O.; Austin, A. J.; Cammi, R.; Pomelli, C.; Ochterski, J. W.; Ayala, P. Y.; Morokuma, K.; Voth, G. A.; Salvador, P.; Dannenberg, J. J.; Zakrzewski, V. G.; Dapprich, S.; Daniels, A. D.; Strain, M. C.; Farkas, O.; Malick, D. K.; Rabuck, A. D.; Raghavachari, K.; Foresman, J. B.; Ortiz, J. V.; Cui, Q.; Baboul, A. G.; Clifford, S.; Cioslowski, J.; Stefanov, B. B.; Liu, G.; Liashenko, A.; Piskorz, P.; Komaromi, I.; Martin, R. L.; Fox, D. J.; Keith, T.; Al-Laham, M. A.; Peng, C. Y.; Nanayakkara, A.; Challacombe, M.; Gill, P. M. W.; Johnson, B.; Chen, W.; Wong, M. W.; Gonzalez, C.; Pople, J. A. *Gaussian 03*, Revision C.02. Gaussian Inc.: Wallingford, CT, **2004**.

4 Boeré, R. T.; Moock, K. H.; Parvez, M. Z.; *Anorg. Allg. Chem.*, **1994**, *620*, 1589.

5 WinEPR Simfonia, Bruker Instruments, Inc., Billerica, MA.

6 SAINT, version 6.22 Bruker Advanced X-ray Solutions, Inc., Madison, WI, 2001.

7 Sheldrick, G. M. SHELXS-90. *Acta Crystallogr. A* **1990**, *46*, 467.

8 Sheldrick, G. M. SHELXL-97. Program for the Refinement of Crystal Structures, University of Gottingen, Gottingen, Germany, 1997.

9 SHELXTL, VERSION 6.12 Program Library for Structure Solution and Molecular Graphics, Bruker Advanced X-ray Solutions, Inc., Madison, WI, 2001.

10 Shirley, R. Crysfire 2002 v9.45.26y, Surrey, England.

11 Taupin, D. *J. Appl. Cryst.*, **1973**, *6*, 380.

12 Boultif, A.; Louer, D. *J. Appl. Cryst.*, **1991**, *24*, 987.

13 Nicolin, V. F.; Cerny, R. *J. Appl. Cryst.*, **2002**, *35*, 734.

14 Rietveld, H. M. *J. Appl. Crystallog.*, **1969**, *2*, 65.

15 Larson, A. C.; Von Dreele, R. B. Report No. LA-UR-86-748; Los Alamos National Laboratory, Los Alamos, NM, 1987.

16 EHMACC, Quantum Chemistry Program Exchange, program number 571.

17 Basch, H.; Viste, A.; Gray, H. B. *Theor. Chim. Acta* **1965**, *3*, 458.

18 Clementi, E.; Roetti, C. *At. Data. Nucl. Data Tables* **1974**, *14*, 177.

19 Cordes, A. W.; Haddon, R. C.; Oakley, R. T.; Schneemeyer, L. F.; Waszczak, J. V.; Young, K. M.; Zimmerman, N. M. *J. Am. Chem. Soc.* **1991**, *113*, 582. (b) Andrews, M. P., *et al.*; *J. Am. Chem. Soc.* **1991**, *113*, 3559.

20 Ammeter, J. H.; Bürgi, H. B.; Thibeault, J. C.; Hoffmann, R. *J. Am. Chem. Soc.* **1978**, *100*, 3686.

21 Boeré , R. T.; Roemmele, T. L. *Coord. Chem Rev*., **2000**, *210*, 369.

22 (a) Hoh, G. L. J.; McEwen, W. E.; Kleinberg, J. *J. Am. Chem. Soc*., **1961**, *83*, 3949. (b)Lemoine, P.; Gross, M.; Braunstein, P.; Mathey, F.; Deschamps, B.; Nelson, J. H. Organometallics, **1984**, *3,* 1303.

23 Zürcher, S.; Petrig, J.; Perseghini, M.; Gramlich, V.; Wörle, M.; von Arx, D.; Togni, A. *Hel. Chim. Acta.,* **1999**, *82,* 1324.

24 (a) Zou, C.; Wrighton, M. S. *J. Am. Chem. Soc.,* **1990**, *112*, 7578. (b) Hobi, M.; Ruppert, O.; Gramlich, V.; Togni, A. *Organometallics*, **1997**, *16*, 1384.

25 Noviandri, I.; Brown, K. N.; Flemming, D. S.; Gulyas, P. T.; Lay, P.A.; Masters, A. F.; Phillips, L. *J. Phys. Chem. B*, **1999**, *103*, 6713.

26 Suzuki, T.; Tsuji, T.; Okubo, T.; Okada, A.; Obana, Y.; Fukushima, T.; Miyashi, T.; Yamashita, Y. *J. Org. Chem*., **2001**, *66,* 8954.

27 (a) Burkholder, C.; Dolbier, W. R.; Medebielle, M. *J. Org. Chem*., **1998**, *63*, 5385. (b) Loss, S.; Magistrato, A.; Cataldo, L.; Hoffmann, S.; Geoffroy, M.; Roethlisberger, U.; Gruetzmacher, H.; *Angew. Chem. Int. Ed.*, **2001**, *40*, 723.